Condition Monitoring Techniques for Wind Turbines

Christopher James Crabtree

A thesis presented for the degree of
Doctor of Philosophy

Durham University
United Kingdom

February 2011

Dedicated to

Ellen and my family

Condition Monitoring Techniques for Wind Turbines

Christopher James Crabtree

Submitted for the degree of Doctor of Philosophy
February 2011

Abstract

This thesis focuses on practical condition monitoring of wind turbines. With offshore wind playing an increasing part in UK electricity generation, prompt fault detection leading to preventative maintenance is gaining in importance. This work describes the development of a condition monitoring test rig and the innovation and application of signal processing techniques for the detection of faults in non-stationary signals. Work is supported throughout by information from wind turbine operators and their experiences of variable speed, variable load wind turbines in the field.

Experimental work is carried out on a condition monitoring test rig comprising a wound rotor induction generator, gearbox and DC driving motor. The test rig operates at variable speed and allows the implementation of a number of fault-like conditions including rotor electrical asymmetry, shaft mass unbalance and gear tooth failure. Test rig instrumentation was significantly developed during this research and both electrical and mechanical condition signals are monitored.

A signal processing algorithm was developed based on experience with analysis techniques and their relationship with the characteristics of a wind turbine. The algorithm is based on Fourier analysis and allows the analysis of fault-related speed-dependent frequencies within non-stationary signals such as those encountered on a wind turbine.

The detection of different faults is discussed and conclusions drawn on the applicability of frequency tracking algorithms. The newly developed algorithm is compared with a published method to establish its advantages and limitations.

Declaration

No part of this thesis has been submitted elsewhere for any other degree or qualification. The content of this thesis is all my own work unless referenced to the contrary in the text.

Acknowledgements

Over the three years from December 2007, many people have assisted me in completing the work describes in this thesis and I am grateful to them all.

In particular:

- My PhD supervisor, Prof. Peter Tavner, whose academic guidance and encouragement has been a constant source of motivation.
- Prof. Li Ran for suggesting the signal processing concept that has been developed in Chapter 5.
- The Supergen Wind Energy Technologies Consortium and the EPSRC who funded this work.
- The technicians at Durham. Particularly, Paul Jarvis and David Jones whose expertise, skills and knowledge have been essential in allowing the practical aspects of this work to be realised and achieved. Also, Ian Hutchinson, Ian Garrett and Neil Clarey for their support in the design and implementation of test rig instrumentation.
- Wenxian Yang, Michael Wilkinson and many others both within and outside Durham University who have provided important academic and industrial knowledge.
- David Futter, Neil Brinkworth of E.ON Engineering, Ratcliffe-on-Soar for sharing and discussing data and knowledge.
- Ashley Crowther and Nathan Wilson of Romax Technology for their advice on the development of the test rig.
- All those, past and present, from The New and Renewable Energy Group who have provided an excellent working atmosphere.

Contents

Nomenclature

A	Amplitude modulation constant (Chapter 4)
A	Fault frequency component amplitude (Chapter 5)
A_c , A_m	General amplitude modulation constants of signal and modulation function
c	Wavelet scaling constant
$c(t)$	Function under amplitude modulation
$CWT(c, \tau)$	Continuous wavelet transform of signal $s(t)$
$d(t)$	Shaft absolute displacement, mm
e	Residual specific unbalance, mm
e_{per}	Permissible residual specific unbalance, mm
E	Maximum wavelet scale parameter or component amplitude within scale/frequency window
f	Supply (stator) fundamental frequency, Hz (Chapter 4) (see f_{se})
f_c	Central frequency of interest, Hz
$\hat{f}_{frm}$	Rotational frequency of fault with respect to field, Hz
f_{ind}^{k}	Induction machine spectral component with index k, Hz
f_{lower}	Lower frequency of analysis window, Hz
f_{rm}	Shaft/rotor rotational frequency, Hz
$\hat{f}_{rm}$	Shaft rotational frequency with respect to field, Hz

f_s	Synchronous (field) frequency, Hz
f_{se}	Supply (stator) fundamental frequency, Hz
f_{upper} , f_{lower}	Upper and lower frequencies of analysis window, Hz
f_w	Analysis frequency window width, Hz
Δf	Frequency interval (spectral line spacing), Hz
F_{C_1} , F_{C_2}, F_{C_3}	Centrifugal force (blades 1, 2, 3), N
F_{C_R}	Centrifugal force resulting from mass unbalance, N
G	Balance quality grade, mm/s
$h(t)$	Shaft horizontal displacement, mm
$H(\omega)$	Fourier transform of mother wavelet, $\Psi(t)$
I	Turbulence intensity, %
IDFT_{local}	Iterative localised discrete Fourier transform
j	$\sqrt{-1}$
j	Supply voltage harmonic order constant (Chapter 4)
k	Air-gap field space harmonic constant (Chapter 4)
k	Harmonic multiple of frequency interval (Chapter 5)
k_{min} , k_{max}	Lower and upper harmonic multiples (see f_{lower} , f_{upper})
l	Supply time harmonic constant
m	Unbalance mass, kg
m_1, m_2, m_3	Blade mass (blades 1, 2, 3), kg
m_R	Equivalent unbalance mass, kg
$m(t)$	Amplitude modulation function

M	Rotor mass, kg
n	Time interval multiple (Chapter 5)
N	Signal length, samples (Chapter 5)
N	Gear ratio (Chapter 6)
p	Induction machine pole pairs
P_E	Electrical power, W
r	Number of shaft revolutions
r_1, r_2, r_3	Blade centre of mass (blades 1, 2, 3), m
r_R	Equivalent unbalance mass radius, m
$r(t)$	Rotor side waveform function
R_{1_H} , R_{2_H}, R_{3_H}	Healthy rotor phase resistances (1, 2 and 3), Ω
R_{1_f}	Induction machine faulted phase resistance (phase 1), Ω
R_{B_1} , R_{B_2}, R_{B_3}	Induction machine brush gear resistances (1, 2 and 3), Ω
R_{E_1} , R_{E_2}, R_{E_3}	Induction machine external phase resistance (1, 2 and 3), Ω
R_f	Additional fault resistance, Ω
R_{R_1} , R_{R_2}, R_{R_3}	Induction machine rotor phase winding resistances (1, 2 and 3), Ω
δR	Absolute rotor asymmetry, Ω
ΔR	Percentage rotor resistive asymmetry, %
s	Induction machine fractional slip
$s(t)$	Stator side waveform function (Chapter 4)
$s(t)$	Continuous time domain signal (Chapter 5)

$s(nT)$	Discrete time domain signal
$S(f)$	Continuous Fourier transform function
$S^*(f)$	Generalised discrete Fourier transform function
$S^*(k\Delta T)$	Discrete Fourier transform function (defined spectral line spacing)
t	Time, s
T	Sampling period, s
T_A	Analysis (processing) time, s
T_{LSS}	Low speed shaft torque, Nm
T_S	Total processed signal length, s
$\bar{U}$	Mean wind speed, m/s
$v(t)$	Shaft vertical displacement, mm
$y(t)$	General function resulting from amplitude modulation
$\bar{Y}$	Sample mean speed, rpm
$\theta_1, \theta_2, \theta_3$	Phasor angles (phases 1, 2, 3), radians
σ	Standard deviation of wind speed, m/s
τ	Continuous wavelet transform constant of translation
$\Psi(t)$	Mother wavelet function
ω	Rotational speed, rad/s
ω_{HSS}	High speed shaft speed, rad/s
ω_0	Centre frequency of mother wavelet

1 Introduction

"Blow, blow, thou winter wind,
Thou art not so unkind
As man's ingratitude"

'As You Like It', Act II, Scene vii
William Shakespeare

William Shakespeare's reference to man's ingratitude is probably more relevant now than it was when published in 1623. Whether or not he is referring to the wind itself could no doubt be the subject of a much heated literary debate however it could certainly be argued that, if written today, the quotation could easily apply to man's current worries about climate change and security of energy supply.

As concerns over climate change and energy security increase there is growing interest in renewable energy systems. Wind turbines (WT) in particular have been earmarked to play an important role in the generation of cleaner energy in the UK, the technology having proved itself over the last 20 years. WT technology is a rapidly developing sector of industry and large turbines up to 6MW are being constructed both onshore and offshore. The benefits of moving to the offshore environment are apparent from improved wind conditions. However there is a price to pay in terms of a harsher operating environment and reduced accessibility.

This chapter briefly introduces the fundamental concerns about climate change and energy security, explaining our growing interest in renewable energy systems and wind energy. This is followed by a short discussion of WT reliability and the resulting interest in effective condition monitoring (CM). A sub-section is also included introducing the Supergen Wind Energy Technologies Consortium and the position of this thesis within the Consortium. Finally an outline of the thesis is given at the end of the chapter with a presentation of its original contribution.

1.1 Climate Change and Energy Security

Over recent years there has been increasing concern over the threat of climate change and the effect that mankind is having on the environment though our methods of electricity generation and our increasing level of energy consumption. This topic is discussed in many publications and theses and so will only be summarised briefly in this work.

Figure 1 [1] shows historical levels of CO_2 in the atmosphere over the last 1000 years. It is clear that there has been a significant increase in the atmospheric concentration of CO_2, particularly since the year 1769; the year James Watt patented his efficient steam engine. With this invention the Industrial Revolution began in earnest and coal was being extracted from the ground at a previously unseen rate. Between 1769 and 1800 Britain's annual coal production doubled and over the next 30 years doubled once more [2], a trend which has continued or worsened in recent years.

The annual production of UK and world coal in giga-tons of CO_2 is shown in Figure 2. If we directly compare Figure 1 for atmospheric CO_2 concentrations and Figure 2 for annual production of coal it becomes difficult to deny that industrialisation has most likely had an effect on CO_2 levels and other greenhouse gases.

The Intergovernmental Panel on Climate Change notes the changing world temperature as a result of global warming from greenhouse gasses. Their fourth assessment report in 2007 [3] states that the average global surface temperature has risen by 0.74°C in the 100 years between 1906 and 2005 with an increasing rate of warming occurring in the last 25 years. The report also highlights the fact that 11 of the 12 warmest recorded years occurred within a 12 year period from 1995 to 2006.

However, despite evidence as presented by climate scientists, climate change has proven to be a subject of much debate over the years and the issue is often seen by sceptics as a natural, periodic change and not a result of the intervention of mankind.

One fact which must be considered, regardless of individual opinion on climate change, is the level of depletion of fossil fuels. Security of fossil fuel supply is gaining greater publicity as the availability of fuels forces domestic electricity and gas bills higher. Questions should perhaps be being asked about how long we can sustain our current way of living and what action can now be taken to help the situation. On this basis one of the greatest aspects to be addressed is that of UK electricity supply.

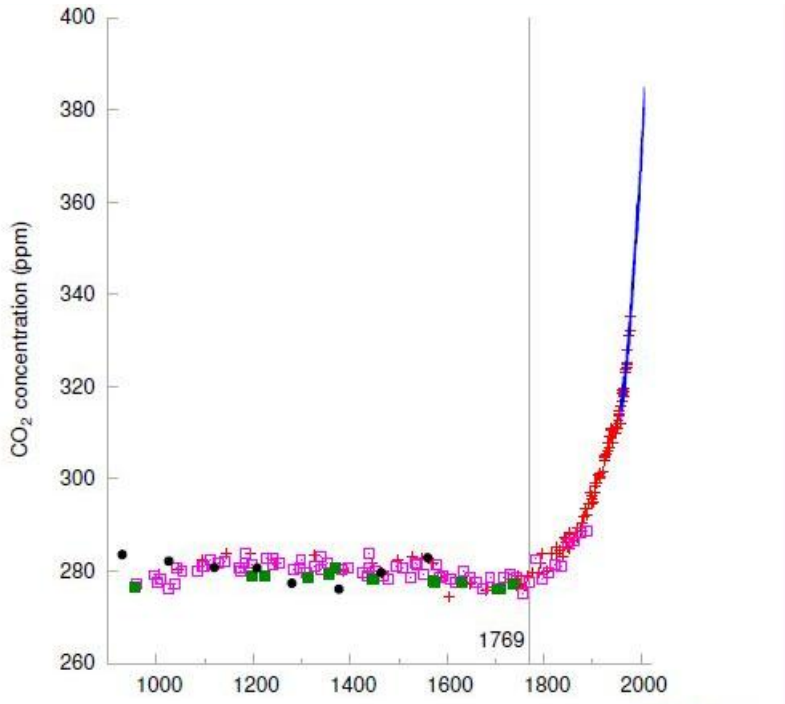

Figure 1: Atmospheric CO_2 concentration over 1000 years [1]

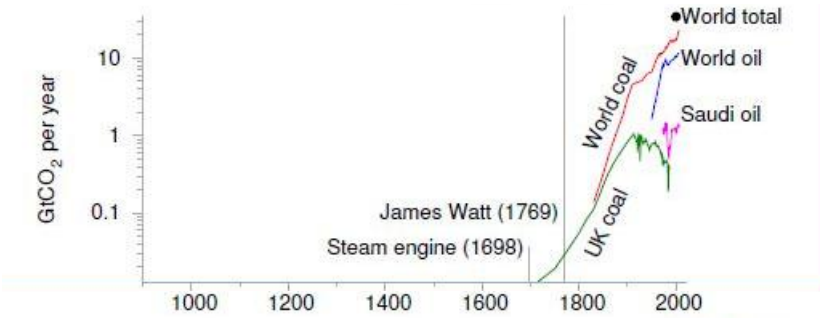

Figure 2: Coal extracted in $GtCO_2$ per year [1]

1.2 UK Electricity Supply and the Role of Wind Energy

The UK electricity demand since 1980 is shown in Figure 3, from the UK Department of Energy and Climate Change (DECC) [4]. With concern about climate change, levels of CO_2 and the development of cleaner generating technologies, there has been a significant shift away from coal over the last three decades. Although the greatest move has been towards gas as our primary energy source there has been a large increase in the electricity capacity generated from renewable sources. Figure 4, based on data from the UK Department for Business, Enterprise and Regulatory Reform (BERR), illustrates the changing make up of UK electricity generation and shows a clear

increase from 3% of supply from hydro and other fuels to 6% [5] with 2% being generated by wind. However, this is still a very small part of total UK capacity.

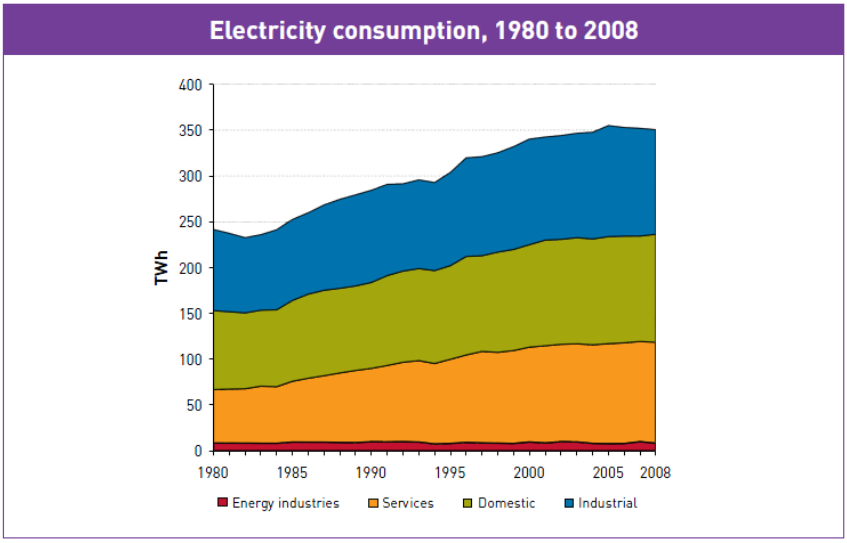

Figure 3: UK electricity consumption from 1980 to 2008 [4]

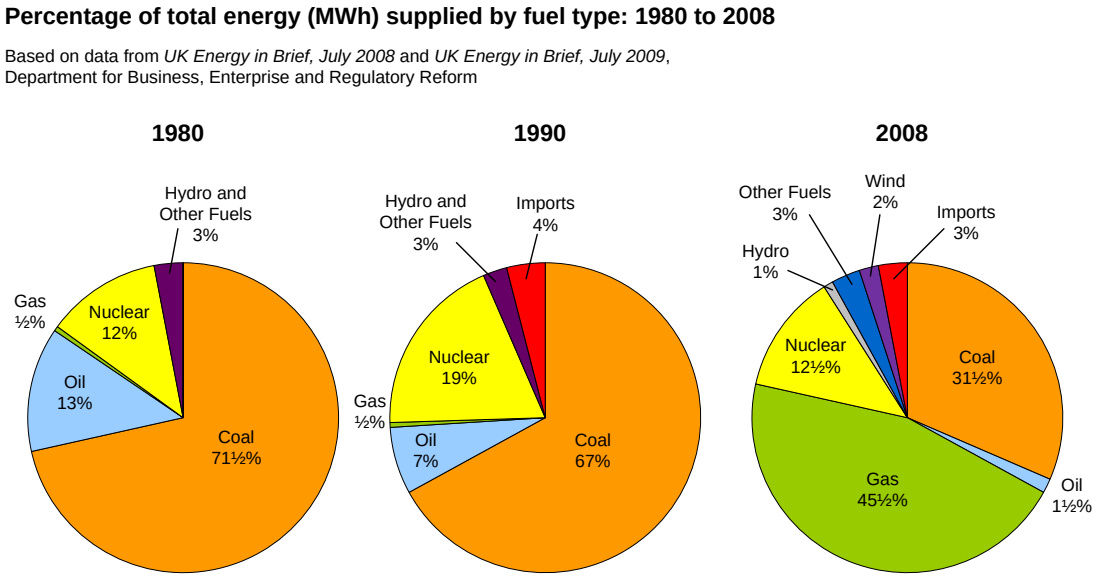

Figure 4: Electrical energy supplied by fuel type, 1980 to 2008

Until recently the UK government's target for CO_2 emissions was a 60% reduction on 1990 levels by 2050 however the Climate Change and Energy Secretary announced in October 2008 [6] a new target for an 80% reduction by the middle of the century. This is a significant overall target which will require a large increase in the use of renewable energy sources as well as the development of clean coal, nuclear and

other facilities in order for it to be achieved. In response to this, the UK government set a target to generate 10% of electricity from renewable sources by 2010 with aspiration towards 20% of capacity by 2015 [7] and it is likely that electricity generation from wind energy will play a significant part in this. Figure 5 shows the increase in WT capacity over the last 14 years as given by BERR [8] and the British Wind Energy Association (BWEA). It is clear that this trend of increasing capacity is set to continue into the future as technologies improve and develop. According to the BWEA UK Wind Energy Database (UKWED) [9] there are more than 3100 WTs installed in the UK with a capacity of over 5.1GW. The BWEA claims that this is enough to power 2.8 million homes and displace 5.8 million tonnes of CO_2 per year [9]. At the time of writing the BWEA UKWED states that 2.2GW of WT capacity is currently under construction in the UK with a further 15.7GW either consented (6.1GW) or in planning stages (9.6GW).

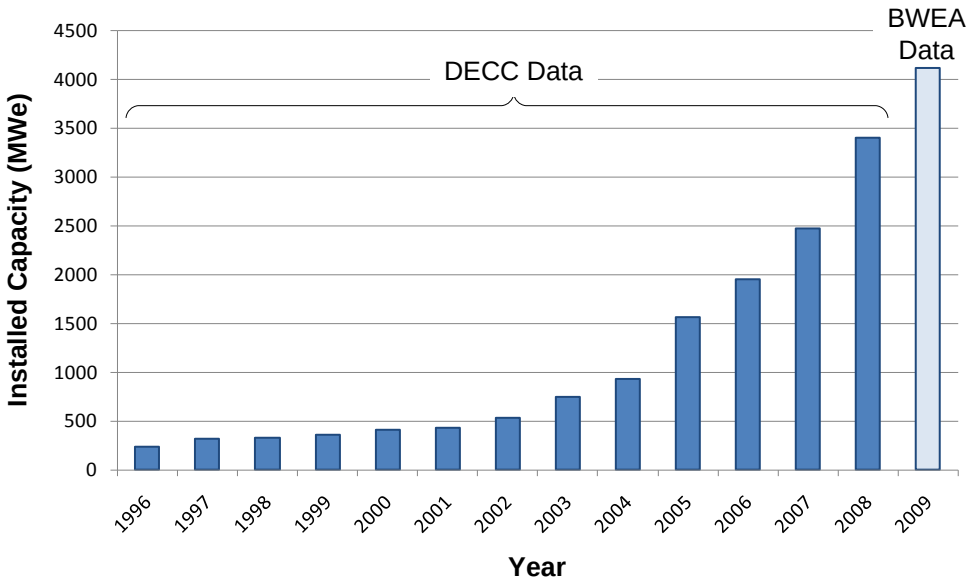

Figure 5: Total operational UK wind generation capacity 1996 to 2009 based on data from [8]and [9]

Despite suggestions from many critics that tens of thousands of WTs would be required to reach the target of 10% of electricity from wind, the BWEA claims that an 8% target could be reached by 2010 with around 3500 additional turbines; 2000 onshore and 1500 offshore [10]. As WT technology develops this figure should decrease. Figure 6 shows how turbine size and power has increased from early designs with the largest commercial turbine currently in operation being the Enercon E-126. This is a direct drive turbine with a rotor diameter of 126 metres and is rated at 7MW.

Building further on this, the WT manufacturer Clipper Windpower is developing a 10MW Turbine, known as the Britannia Project, specifically designed for the offshore environment [11].

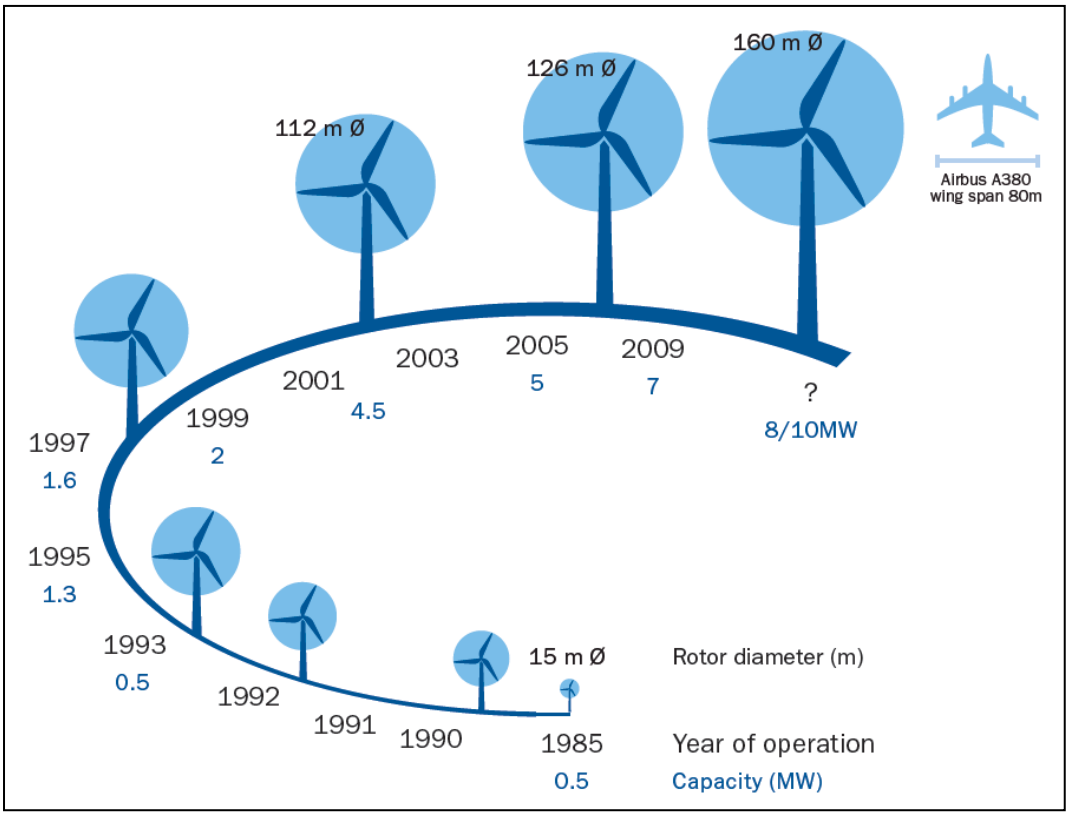

Figure 6: Growth in size of commercial wind designs [12]

1.3 Reliability of Wind Turbines

1.3.1 Introduction to Reliability

As seen in Figure 6, the physical size and electrical rating of WTs is increasing as technologies develop. Coupled with this, there is also a significant move towards offshore wind energy where planning considerations and public objection are less of an issue for developers. Furthermore, the main drive towards offshore wind farms is the increased wind resource. Figure 7 shows a wind speed chart for the UK illustrating the much greater wind resource available in certain offshore environments.

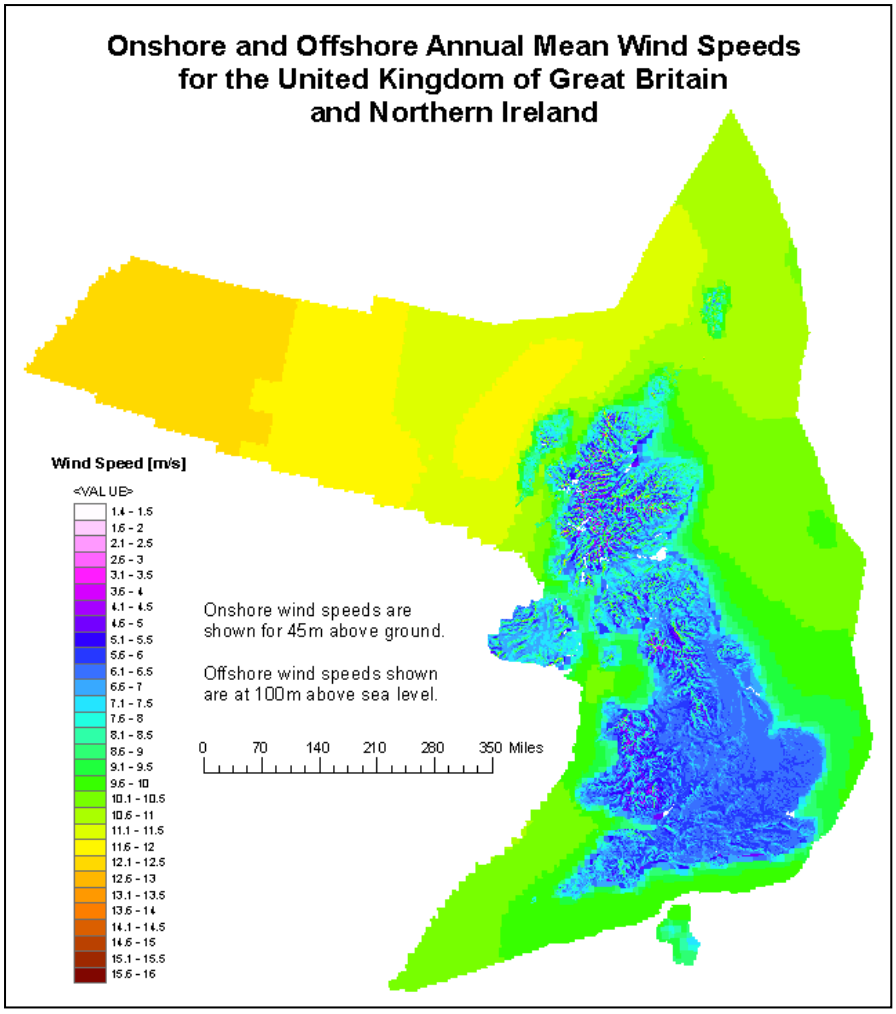

Figure 7: Annual mean wind speeds for the UK

However, the move to offshore environments highlights significant issues as regards turbine maintenance. Firstly, increased wind speeds will lead to not only higher capacity factors than for onshore turbines but also much greater mechanical loading of machine components. Secondly, the offshore environment reduces accessibility for maintenance. When onshore, small component failures are relatively simple to solve with an engineer able to visit the turbine and perform a maintenance action with minimal interference from environmental conditions. Once offshore, each small turbine failure could carry a very high cost not only in terms of components purchased but also in accessibility and personnel costs which can amount to €1000 per man-day [13]. In addition, poor weather could in fact mean that access is impossible during some periods of the year, for example over winter. In this case the very smallest of turbine component failures could lead to large downtimes and large resultant losses from prolonged periods of no generation. These issues have led to various studies being carried out to examine the reliability of WTs.

1.3.2 Reliability Studies and Results

Several quantitative studies of WT reliability have been carried out over recent years using publically available data. Work by Tavner et al. [14] demonstrated onshore failure rates of around 1-3 failures per turbine per year using data from Germany and Denmark. Bearing in mind concerns about accessibility and possible long periods of no generation resulting from this it would be reasonable to say that this failure rate is unacceptably high for cost effective offshore generation. Furthermore, the offshore environment is more likely to increase the number of failures so it would be expected that the initial failure rate could be higher still. This is commented on in a later paper [15] which suggests that a maximum failure rate of 0.5 failures per turbine per year would be required offshore in order to allow planned maintenance visits to occur no more than once each year.

A study by Spinato et al. [15] carried out a failure analysis based on turbine type as specified in the LWK data for onshore WTs, the result of which is shown by Figure 8. It is apparent that there is a general trend of increasing failure rate with turbine rating. This causes concern with regard to the move to offshore locations. To justify offshore installation costs and to increase energy production, ratings for offshore WTs are increasing, the largest proposed turbine currently rated at 10MW [11]. Based on Figure 8 we can assume that it will be difficult to decrease the initial failure rate as turbines continue to grow in capacity.

The study also carried out analysis for the reliability of drive train subassemblies. Figure 9 from [16] shows the failure frequency and downtime for two surveys of operational onshore WTs. When looking at the failure frequency we naturally assume that the worst contributors to WT downtime are the electrical system and electrical control areas with the mechanical subassemblies, gearbox, generator and blades, having a low impact. However, once the downtime per failure has been taken into account the gearbox, generator and blades become the most damaging in terms of lost operational hours.

These analyses were carried out for onshore turbines so it would be expected that the combination of decreased reliability and increased downtime per failure, resulting from restricted access, would very quickly make offshore wind an expensive and unattractive option. According to [17], 75% of onshore WT failures cause 5% of downtime while only 25% of failures cause 95% of downtime. Work by Tavner et al. [18] notes that the 75% of failures, where downtime is normally short, will have a

significant effect in the move to offshore wind as quick repairs will not be possible due to access issues.

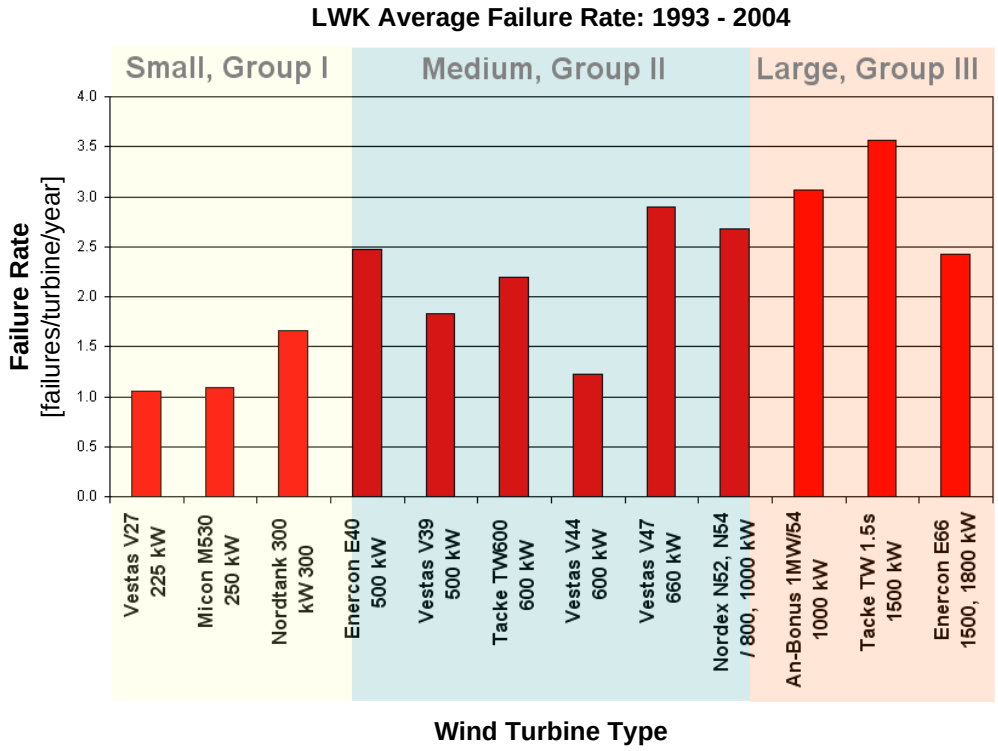

Figure 8: Failure rates of different WT models by turbine capacity [15]

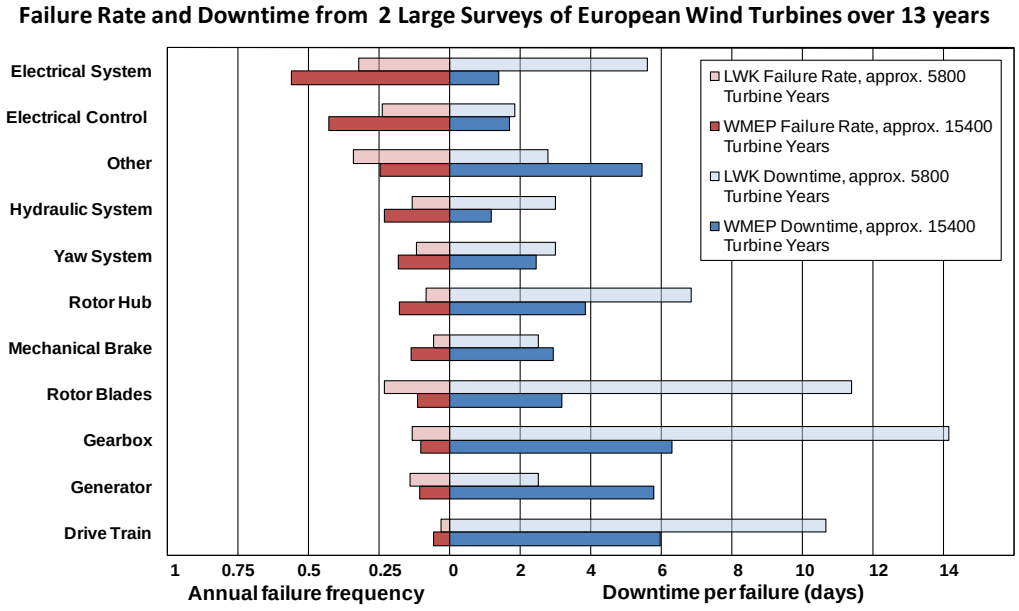

Figure 9: WT sub-assembly failure rate and downtime per failure for two surveys including over 20000 turbine years of data as published in [16]

Another study of subassembly reliability was carried out by Alewine on WT generators [19]. Figure 10 shows the results of this analysis alongside a reliability analysis of other rotating machines by Tavner [20]. It can be seen that, especially in WTs, rotor related faults and slip rings contribute significantly to total generator failures, particularly in small and medium WT generators, although bearing faults are dominant.

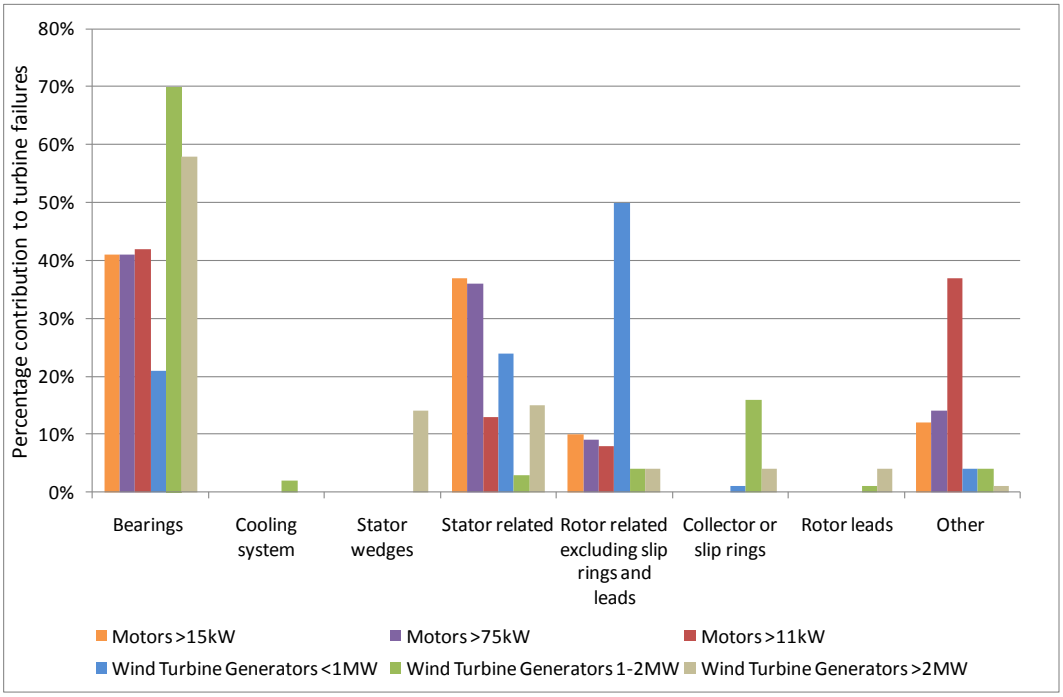

Figure 10: Comparison of failure contribution of WT generator components according to [19] and [20]

1.3.3 Summary

As a result of accessibility issues offshore it seems apparent that the number of site visits per year should be kept to a minimum to keep costs down however this will not be possible if failure rates remain high. In order to prevent catastrophic failure and reduce resulting downtime there must be suitable methods for detecting incipient faults in WT subassemblies well in advance of failure. This would allow the operator to incorporate any maintenance actions into a planned site visit and should negate the need for unplanned maintenance.

This will be the role of CM within the wind industry.

1.4 The Supergen Wind Energy Technologies Consortium

This research has been funded by a UK EPSRC doctoral training award as part of the Supergen Wind Energy Technologies Consortium, EP/D034560/1 [21].

The first of thirteen Supergen Consortia was launched by the EPSRC in November 2003 in response to the targets and objectives set out in the 2003 Energy White Paper. The Consortia were constructed so as to engage the user and stakeholder community with academic institutions and to enable greater interaction and dissemination of information between academic and industrial players. This structure was designed to increase the potential for the generation of ideas and allow for step changes in tackling challenges rather than incremental progress.

The Supergen Wind Energy Technologies Consortium is a diverse research body consisting of academic and industrial partners led by the University of Strathclyde and Durham University. The overall objective of the Consortium is "to undertake research to improve the cost-effective reliability and availability of existing and future large-scale WT systems in the UK". This is enabled through the division of research into four distinct themes:

- Theme W –Base-lining WT performance;
- Theme X – Drive-train loads and monitoring;
- Theme Y – Structural loads and materials, and;
- Theme Z – Environmental issues.

This thesis is written under the CM aspect of Theme X. Throughout this thesis, the author had the opportunity to work with a number of academic and industrial partners involved in Theme X including:

- The University of Manchester
- Loughborough University
- The University of Strathclyde
- E.ON Engineering Ltd.
- Romax Technology Ltd.

During the preparation of this thesis, there was a large amount of collaborative work and discussion with the Supergen Wind Energy Technologies Consortium industrial partners, primarily E.ON Engineering Ltd and Romax Technology Ltd.

E.ON Engineering [22], based at Ratcliffe-on-Soar fossil-fired, thermal power station near Nottingham, are responsible for CM conventional plant at power stations. As E.ON acquired wind farms into their generation portfolio, the Condition Monitoring Group at E.ON Engineering became involved in WT CM alongside monitoring conventional plant.

Their contribution has been significant through the provision of expert knowledge and information on WT CM from David Futter, Neil Brinkworth and Ian Mayes. E.ON Engineering has also allowed Durham University to examine data from their WT population so we could learn some of the practicalities and issues that have to be understood for practical CM to be successful.

Romax Technology [23] is a world leading drive train technical consultancy with over 20 years experience in the design of gearboxes, bearings and drive trains. The company's original products were based on the automotive industry but they have since expanded rapidly into the design and analysis of WT drive trains and gearboxes.

Discussion and work with Romax Technology has led to a much greater understanding of the dynamics of the Durham test rig as well giving the opportunity to learn from their modelling expertise. In particular, interaction with Ashley Crowther and Nathan Wilson has provided many points for thought as well as answers resulting from their experience in design and modelling.

Both E.ON Engineering and Romax Technology have played an important part in this work and we have been glad to have had the opportunity to learn from those working in the field and discuss and impart out own opinions and findings with two leading industrial partners.

1.5 Structure of the Thesis

This thesis is structured to reflect the direction, progress and results of research since December 2007. As such, it is divided into chapters based on different areas of research.

This introduction, Chapter 1, has briefly discussed the basis for interest in wind power and introduced the reader to WT reliability. In Chapter 2, this is taken forward with a review and discussion of CM techniques based on experiences and development of systems over time.

Chapter 3 then discusses practical wind farm CM based on collaborative work with an industrial partner. This section examines the practicalities and problems of monitoring WTs and how this has been overcome to an extent by the Condition Monitoring Group and their chosen monitoring systems.

In Chapter 4, the focus moves from background literature and examples in the field to describe CM research methods at Durham University. This includes detailed information on and justification for a CM test rig and the work which has been completed to ensure a worthwhile and advantageous experimental system. This chapter also leads to the theory of faults in electrical machines and drive trains, and the derivation of fundamental fault equations for various fault-like conditions including a selection of electrical and mechanical faults used in this thesis.

In Chapter 5 the analytical methods relevant to this thesis are described. This includes the comparison of spectral analysis methods and their application to the WT environment, including a previously published wavelet-based frequency tracking algorithm. Finally in Chapter 5, a Fourier-based algorithm for the analysis of WT CM signals is proposed and introduced mathematically.

Chapter 6 contains the results of test rig experimentation including the analysis of signals using the new Fourier-based algorithm. Results from rotor electrical asymmetry, shaft mass unbalance and gear tooth damage are presented for discussion. The Fourier-based algorithm is compared with the previously published wavelet-based method to aid discussion of its advantages and disadvantages.

Finally, Chapter 7 draws conclusions from this research. It also proposes possibilities for further research based on experiences from this project.

There are a number of appendices containing information and results, published and submitted papers in which the author has been involved, detailed test rig specifications not included in the main body of this text and enlarged figures for reference. There is also an expanded selection of results from Chapter 6.

Each Chapter concludes with a list of its references with reference numbers continuous throughout the thesis.

1.6 Original Contribution

Over the last few years, condition monitoring systems (CMS) have become a commonplace feature of WTs. In fact, all new WTs are fitted with some form of CMS by either the manufacturer or user. These systems have advanced significantly over recent years and a wider variety of signal processing techniques have been incorporated into both hardware and software.

However, as will be shown in Chapters 2 and 3, many commercially available CMSs are still highly dependent on the basic Fourier transform as applied in industries where stationary conditions are standard. For WTs, the situation is somewhat different with variable load and variable speed conditions being unavoidable features. While some effort has been made to adapt systems to their new environment, there is still a large degree of manual analysis required to interpret results.

Put simply, the original contribution of this thesis is the development of a potential method for the automation of CM. This is based on the understanding of signal processing techniques, the non-stationary operating conditions of WTs and faults themselves. This thesis describes the progressive process of algorithm development and testing through the use of industrial information and knowledge; data from a test rig and operational WTs; and reliability and failure data.

The case study of CM in industry and the use of both test rig and industrial data is also a significant contribution as the volume of publicly available industrial data and information on the subject of CM and the practicalities of its application is severely limited.

To summarise, the author contends that the collection of all these different items into a single piece of research in order to aid the development of an applicable and realisable signal processing algorithm stands as an important contribution to the, as yet, small body of information available to the wider CM and renewable energy community.

1.7 References

[1] MacKay, D.J.C., Sustainable Energy – without the hot air, UIT Cambridge, p. 9, 2009.

[2] MacKay, D.J.C., Sustainable Energy – without the hot air, UIT Cambridge, p. 6, 2009.

[3] IPCC, Climate Change 2007: The Physical Science Basis. Contribution of Working Group I to the Fourth Assessment Report of the Intergovernmental Panel on Climate Change, Solomon, S., Qin, D., Manning, M., Chen, Z., Marquis, M., Averyt, K.B., Tignor, M., Miller, H.L. (eds.), Cambridge University Press, Cambridge, United Kingdom and New York, NY, USA, 2007.

[4] Digest of UK Energy Statistics, Department of Energy and Climate Change (DECC), July 2009.

[5] UK Energy in Brief, Department for Business, Enterprise and Regulatory Reform, July 2008.

[6] Tougher climate target unveiled, http://news.bbc.co.uk/1/hi/uk_politics/7673748.stm, 16th October 2008, last accessed 11th February 2010.

[7] Meeting The Energy Challenge: A White Paper on Energy, Department for Trade and Industry, May 2007, Crown copyright 2007.

[8] Capacity of, and electricity generated from, renewable sources (DUKES 7.4), Digest of United Kingdom Energy Statistics, Department of Energy and Climate Change, July 2009.

[9] British Wind Energy Association, UK Wind Energy Database, www.bwea.com/ukwed/index.asp, last accessed 8th November 2010.

[10] British Wind Energy Association, Top Myths about Wind Energy, www.bwea.com/energy/myths.html, last accessed 11th February 2010.

[11] Clipper Leads on Technology and Size as it Develops the Britannia Offshore Wind Turbine, www.clipperwind.com/pr_100807.html, last accessed 8th October 2007.

[12] European Wind Energy Association, Wind Energy Factsheets, 10, 2010.

[13] Nilsson, J., Bertling, L., *Maintenance Management of Wind Power Systems Using Condition Monitoring Systems – Life Cycle Cost Analysis for Two Case Studies*, IEEE Trans., Energy Conversion, Vol. 22, Iss. 1, pp. 223-229, 2007.

[14] Tavner, P. J., Xiang, J., Spinato, F., Reliability analysis for Wind Turbines, Wind Energy, Vol. 10, Iss.. 1, pp. 1-18, 2007.

[15] Spinato, F., Tavner, P. J., van Bussel, G. J. W., Koutoulakos, E., Reliability of wind turbine subassemblies, IET Renewable Power Generation, Vol. 3, Iss. 4, pp. 1-15, 2009.

[16] Crabtree, C.J., Feng, Y., Tavner, P.J., *Detecting Incipient Wind Turbine Gearbox Failure: A Signal Analysis Method for Online Condition Monitoring*, Scientific Track Proceedings, European Wind Energy Conference 2010, Warsaw, Poland, 2010.

[17] Faulstich, S., Lyding, P., Hahn, B., *Electrical subassemblies of wind turbines – a substantial risk for the availability*, Proc. European Wind Energy Conference 2010, Warsaw, Poland, 2010.

[18] Tavner, P. J., Faulstich, S., Hahn, B., van Bussel, G. J. W., *Reliability & Availability of Wind Turbine Electrical & Electronic Components*, European Power Electronics Journal, accepted for publication, 2011.

[19] Alewine, K., *Wind Turbine Generator Failure Modes Analysis and Occurrence*, Windpower 2010, Dallas, Texas, May 2010.

[20] Tavner, P. J., *Review of Condition Monitoring of Rotating Electrical Machines*, IET Electric Power Applications, Vol. 2, No. 4, pp. 215-247, 2008.

[21] Supergen Wind, www.supergen-wind.org.uk, last accessed 10th March 2010.

[22] E.ON UK – E.ON Engineering Ltd, http://www.eon-uk.com/about/eonengineering.aspx, last accessed 27th May 2010.

[23] Romax Technology Ltd - World leading driveline engineering consultants, http://www.romaxtech.com, last accessed 27th May 2010.

2 Monitoring of Wind Turbines

"I have only one eye; I have a right to be blind sometimes... I really do not see the signal!"

Vice Admiral Horatio Lord Nelson
1758 – 1805

As has been noted in the summary of reliability data in §1.3.3, the detection of WT faults, particularly offshore, is gaining greater importance. This idea of successfully detecting incipient faults before they develop into failures has led to the development of a large number of WT CMSs [24][25]. Many of these systems are based on concepts already used in other rotating machine industries and the adaptation of systems to suit the WT environment. A survey of commercially available CMSs was carried out early in Phase 1 of the Supergen Wind Energy Technologies Consortium [24]. The survey was then added to continuously until early 2009. However, with the development of more systems and increasing industrial interest, a new survey was produced by this author. This survey [25] provides an up to date, at the time of writing, insight into the current state of the art of CM and shows the range of systems currently available to WT manufacturers and operators.

This chapter begins by defining various terms used throughout this thesis to describe the relationship between manufacturers, owners, operators, monitoring engineers, and maintenance managers and staff. This is followed by a discussion of the overall architecture, such as it is, for monitoring of WTs as a whole and the position of CM and diagnosis systems within the structure. The survey of CM and diagnosis systems is summarised to show the current position of the industry before conclusions are drawn about current systems and the future direction of CM.

2.1 Definitions

The structure of ownership and management of WTs, their warranties and any data recorded from them is not always clear so the format used throughout this thesis is presented here.

2.1.1 Original Equipment Manufacturer

The Original Equipment Manufacturer (OEM) is the company who designed, constructed and supplied the WT. In some cases there may be several OEMs for a particular turbine where, for example, the gearbox is manufactured under contract by another company. In this case it is assumed that there is a single WT OEM.

The OEM supplies a warranty with their WT and this generally includes all maintenance and monitoring functions during a certain period, normally 2-5 years. However, this comes at a price to the Owner Operator, who will be defined later, in that the OEM is normally reluctant to have any monitoring system fitted other than their own, and owns any data recorded during the warranty period. This means that the Owner Operator loses valuable information that may be useful after the warranty period when they begin monitoring the turbine themselves. After the warranty period, monitoring and maintenance responsibilities fall to the Owner Operator.

2.1.2 Owner Operator

This is the company or group that owns the turbine and is responsible for its operation. During the warranty period the Owner Operator has little to do with the turbine itself apart from wanting to ensure that it is operational and generating saleable energy. However, as stated, maintenance aspects during the warranty period fall to the OEM [26]. Later in this thesis, the term Owner Operator will be abbreviated for conciseness to Operator, although the full term will be used throughout these definitions. On occasion, the Owner and Operator may be different however it is assumed here that they are the same.

After the warranty period the Owner Operator becomes responsible for all monitoring and maintenance unless they pursue an extended maintenance contract with the OEM [26]. This is only likely to happen with small, local consortia owning few turbines. Large Owner Operators may install their own monitoring or data acquisition systems after the warranty to bring systems into line with their own requirements. In the case of large Owner Operators, the monitoring of turbines may fall to a group within the company or to an external monitoring contractor, for example SKF, since the main concern of the Owner Operator is not the details of a particular turbine but that their turbine fleet is healthy and generating energy.

2.1.3 Operations Staff

While this area may be quite broad, our main consideration is CM engineers or those who will make diagnoses and recommendations regarding WT condition. Operations Staff may be either a group within the Owner Operator structure or an external monitoring contractor, depending on the experience or expertise of the Owner Operator. Operations Staff working as a group within an Owner Operator are referred to as the Operations Group in this thesis.

Operations Staff are responsible for CM and fault diagnosis and will generally be monitoring engineers with some expertise in the field. Operations Staff responsible for monitoring and diagnosis will have expertise in machines and signal processing in order to examine time series data, spectra or results from other analyses and relate them successfully to components and sub-assemblies within the WT.

Once a fault has been detected and a diagnosis made, Operations staff will inform Maintenance Management Staff of their findings. In particular, they may make recommendations concerning the severity of the fault, the best course of action and the urgency of the problem.

2.1.4 Maintenance Management Staff

Maintenance Management Staff may either be a group within the Owner Operator or be an external contractor. This can be combined with an external contract for Operations Staff.

There are several tasks covered by WT Maintenance Management Staff, introduced in [27]. Firstly, they manage a general maintenance strategy for the Owner Operator's WTs such as an annual visit to the turbines to check oil, replace worn parts and carry out other smaller, less critical tasks. Secondly, Maintenance Management Staff coordinate condition-based maintenance based on recommendations from Operations Staff. This may either be an immediate response, shutting down a turbine to perform maintenance, or the decision to carry out maintenance after a certain time period based on CM and diagnoses from Operations Staff. Thirdly, a reactive maintenance strategy, while undesirable, may sometimes be required in the case of unpredicted, catastrophic failure of a turbine or component.

2.1.5 Maintenance Staff

Maintenance Staff, or Technicians, will be either part of the Owner Operator company structure or an external contractor and will act under instruction from Maintenance Management Staff. In the case of certain components, for example the gearbox, the Maintenance Staff employed may be from the component OEM. The job of maintenance staff is to examine a component on site and carry out maintenance as required.

2.2 Monitoring Structure

A WT Owner Operator is likely to want CM carrying out for a variety of different operational reasons, listed below.

- To obtain commercially important information such as confirmation that the turbine is operating and the amount of energy being generated.
- To confirm the health of the overall WT structure and its safety.
- To detect subassembly faults or failures through alarms systems.
- To find the exact nature and location of any fault or failure and schedule maintenance.

Conveniently each of these four points can be answered by splitting turbine monitoring into four classes of system. These are summarised by Figure 11 showing them and their approximate data rates that need to be transferred to the operator or, in some cases, the monitoring engineer. This overall architecture is beginning to be found in a larger number of WTs and is likely to be essential in the offshore environment.

While there are four classes of monitoring system described, they are considered in three sections due to the level of interaction between CM and diagnosis. The reasons for this are discussed.

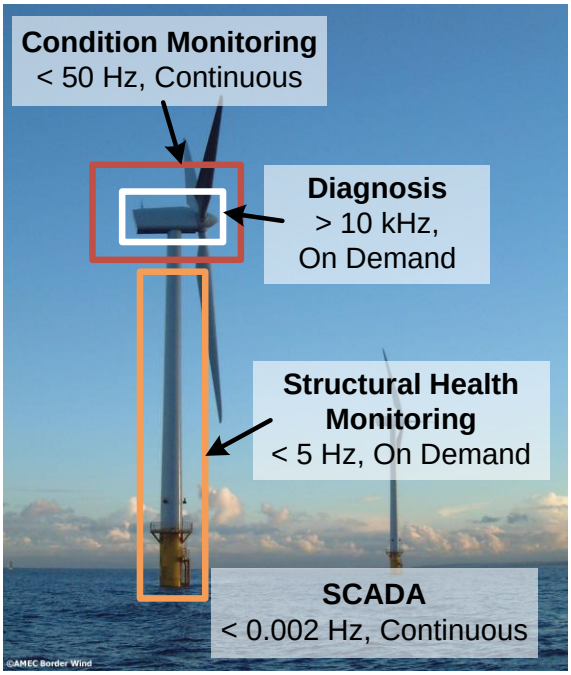

Figure 11: Structural health and condition monitoring of a wind turbine

2.2.1 Supervisory Control and Data Acquisition

The first class of system is the Supervisory Control and Data Acquisition (SCADA) system. This type of system is required on all modern WTs to monitor energy generated and confirm the operation of the turbine, measurements that are generally recorded in the turbine's controller. The data is also used by the OEM to provide useful information during the warranty period. While measurements are often recorded using high frequency sampling, they are averaged over time and a single 5-10 minute averaged value [28] is transmitted back to the operator. The SCADA system also triggers alarms as and when they occur. However, SCADA systems have developed to also provide alarms for malfunctions of the WT. According to Zaher et al. [29], 10 minute averaged signals often monitored in more recent SCADA systems include:

- Active power output (and standard deviation over 10 min interval);
- Anemometer-measured wind speed (and standard deviation over 10 min interval);
- Gearbox bearing temperatures;
- Gearbox lubrication oil temperature;
- Generator winding temperature;
- Generator bearing temperatures;
- Power factor;

- Reactive power;
- Phase currents, and;
- Nacelle temperature (1 hour average).

These SCADA systems are able to transmit alarms to the operator but are not currently able to provide detailed information on the health of a turbine. However, more recent SCADA systems are increasingly able to provide alarm signals based on time domain amplitude of temperature transducers [28] and on measurements from drive train vibration transducers. The alarms are generally based on the average or peak value for vibration during the 5-10 minute period.

Research is being carried out into the CM of WTs through SCADA analysis in the EU FP7 project ReliaWind [30]. The research consortium consists of a number of University partners alongside industrial consultants and WT manufacturers.

2.2.2 Structural Health Monitoring

The second class of system covers the area of structural health monitoring (SHM). These systems aim to determine the integrity of the WT tower, structure and foundations for faults driven by blade-passing frequencies, through low frequency sampling, below 5Hz, of accelerometers and similar low frequency transducers. Other monitoring technologies increasingly found for structural health monitoring of blades include fibre optic stain measurement and acoustic emission sensing. Acoustic emission sensing has not found great interest in the wind industry up to now because of its expense and equipment complexity, whereas fibre optic measurement systems have gained interest as will be discussed later in this chapter.

While structural health monitoring systems could be presented as a separate section in this thesis, it is clear that the monitoring of WT blades should be classed as CM, despite being carried out in a different fashion from rotating machinery CM. Therefore, structural health monitoring systems are grouped in with CMSs from this point forward.

2.2.3 Condition Monitoring and Diagnosis

The third and fourth classes of system are the two areas of CM and diagnosis. These are considered together as, for WT monitoring to be most effectively carried out, interaction of the CM and diagnosis systems is required. As will be shown, the two

classes of system consist of similar transducer inputs but with different internal functions and outputs.

CM itself may be considered as a broad method for determining the overall operational health of the WT. The key function of a successful CMS should be firstly to provide a reliable indication of the presence of a fault within the WT system and secondly to indicate the location and severity of the situation. This second point is important as the severity of the fault will be the trigger for further, more detailed investigation by monitoring engineers with the aim of diagnosing the fault. This point is the link between CM and diagnostic systems where CM leads to diagnosis.

The turbine Operator may not necessarily be interested in the early signals from the CMS. These signals are most useful to a monitoring engineer with many turbines to prioritise in terms of fault severity. The Operator's main interest is that alarms are reliable so that they can take confident action with regard to limiting power or shutting down a turbine to avoid serious or dangerous failure. The Operator, as opposed to the monitoring engineer, will not have a central interest in the exact nature of faults, according to discussions with industrial partners. A CM engineer is interested in alarms well in advance of failure in order to observe the progress of a fault from an early stage and plan for remedial action with the Operator. As the number of turbines increases, reliable CM alarms will be essential to direct monitoring engineers in the prioritisation of faults and WTs within an increasingly large WT population.

Since the main requirement is to provide alarms with a high degree of confidence, CM signals need not necessarily be output to the monitoring database on a high frequency basis and the system can carry out the required analysis on an intermittent basis.

Once an alarm has been triggered by the CMS, a diagnostic process could be activated automatically to give an initial indication of the fault. The monitoring engineer could then begin high frequency analysis in order to identify the exact location and nature of the fault. With these aims in mind, a suitable system configuration is required where the system provides enough data for reliable monitoring but not so much as to flood the monitoring engineer or data transmission network with excess information.

To conclude on CM and diagnosis, Figure 12 gives an indication of the three main subassemblies of a WTs which may require CM and diagnosis based on reliability data such as that given in §1.3.2.

While each of these subassemblies are shown as separate entities it is likely that a good CMS will blur the boundaries between them depending on available signals, to provide reliable alarms with a high degree of confidence, subsequently giving similarly reliable diagnostic information.

Many of the systems included in §2.3 combine CM with diagnostics as a result of the high level of interaction that has been discussed and this seems like an intelligent step towards providing successful CM and diagnosis systems for a large number of WTs.

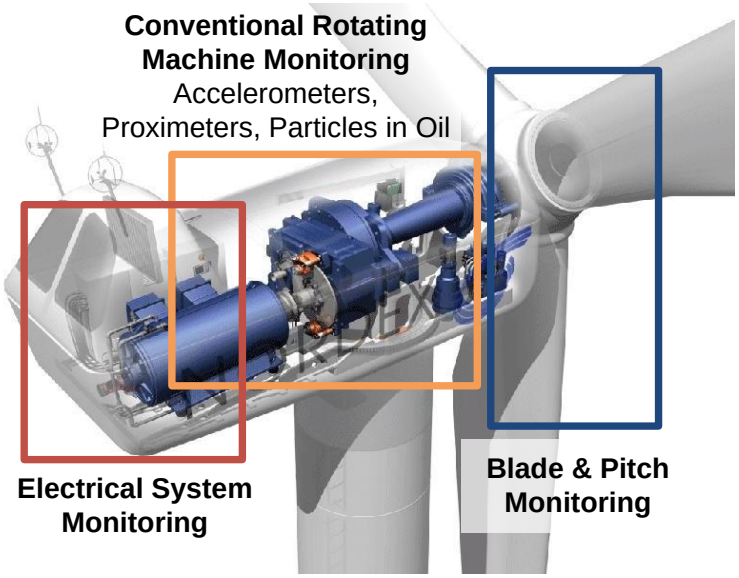

Figure 12: General layout of three areas for condition monitoring and diagnosis within the nacelle

2.3 Commercially Available Monitoring Systems

The table from the Supergen Wind Energy Technologies Consortium survey *Commercially Available Condition Monitoring Systems for Wind Turbines* [25] is provided in Appendix A. The survey lists 20 widely available and popular CMSs that are specifically targeted for WT CM. The information in the table has been collected through interaction with monitoring system and turbine manufacturers, and various product brochures over recent years, and includes information obtained through

personal interaction with sales and technical personnel at the European Wind Energy Conferences from 2008 to 2010. The summary and details of each system are believed to be correct at the time of writing. However, since some information has been acquired through direct discussion with sales and product representatives and not from published brochures and handbooks, it should be noted that the table may not be fully definitive and is as accurate as possible given the available information. The systems are grouped by monitoring technology and then alphabetically by product name.

The first observation to make is that the CMSs listed tend to focus on very similar areas and WT subassemblies. Moving through the turbine these are the:

- Blades;
- Main bearing;
- Gearbox internals;
- Gearbox bearings, and;
- Generator bearings.

However, there are a few systems that have branched out to investigate other signals and technologies. These include the use of techniques to monitor generator windings, converters and pitch control mechanisms.

The products in the survey can be summarised as:

- 14 systems primarily based on drive train vibration analysis (1 – 14)
- 3 systems solely for oil debris monitoring (15 – 17)
- 1 system using vibration analysis for WT blade monitoring (18)
- 2 systems based on fibre optic strain measurement in WT blades (19, 20)

It is clear from this distribution that the industry is currently favouring systems based on methods originating from other, traditional rotating machinery applications. Indeed fourteen of the twenty systems given are based on vibration monitoring of the turbine drive train and are generally using a configuration similar to that in Figure 13 for the Mita-Teknik WP4086 CMS (14).

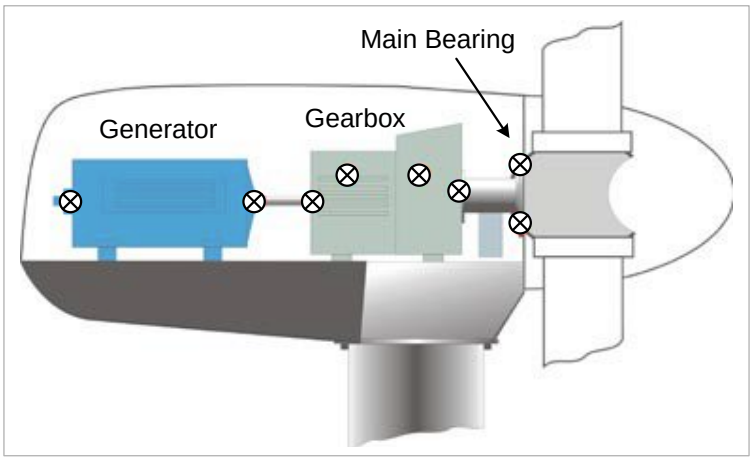

Figure 13: Typical accelerometer positions in a WT nacelle based on [33]

Of the 14 vibration-based systems, all have the capacity to provide diagnostic information once a fault has been detected. In the majority of cases this is done through fast Fourier transform (FFT) analysis of high frequency data, the aim being to identify frequencies or harmonic patterns indicative of a specific fault. In the case of the SKF WindCon 3.0 CMS (11), the Areva OneProd Wind system (7) and several others, high speed data acquisition is triggered by the operational state of the WT. For example, the SKF WindCon 3.0 CMS can be configured to carry out vibration analysis on either a fixed time basis or when a specific load and speed condition is achieved. The aim of selecting certain fixed measurement points is to acquire results that are directly comparable between each measurement point and, importantly, to allow spectra to be calculated under conditions where signals are close to stationary in time across a sample.

When using the traditional FFT it is essential that signals are stationary within the analysis time window in order that a clearly defined spectrum can be calculated without frequency 'smearing'. However, discussion with technical personnel suggests that the Mita-Teknik WP4086 system (14) incorporates advanced signal processing techniques to overcome the effects of small variations in WT speed. These include comb filtering [31], whitening for noise reduction and Kurtogram [32] analysis techniques.

Further to the use of traditional vibration monitoring techniques, three of these systems also state that they allow the inclusion of debris in oil transducers to monitor material breakout in gearbox lubrication oil systems. As a result of this, three oil quality monitoring transducers are included in the survey (15 – 17). While these are

not complete CMSs in themselves, discussion with industrial partners suggests that oil monitoring is gaining greater interest within the wind industry and, as such, is worthy of note in the survey. From the available literature, it appears that one of the most advanced of these oil quality monitoring systems is the MACOM TechAlert 10 (17) system. This system uses an inductive transducer to count both ferrous and non-ferrous particles in the oil circulation system and provide count outputs for the number of particles in various particle size 'bins'. The systems using debris in oil transducers are using either cumulative particle counts or particle count rates alongside vibration monitoring results.

From the survey, there is also a clear interest in the use of operational parameters to assist CM. Several of the thirteen vibration-based monitoring systems allow operational parameters such as load, wind speed, generator speed and temperature to be recorded alongside vibration and other monitoring signals; however the overall capability of some systems is unclear from the available information. The level of interest in operational parameters appears to have stemmed from the fact that the most widely used analysis techniques, for example the FFT, have been developed in constant speed, constant load environments. Given the variable speed, variable load nature of the WT, it has been suggested that traditional methods may encounter difficulties during analysis due to the non-stationary signals involved. However, experienced CM engineers are able to use these techniques to successfully detect faults by comparing spectra at specific speeds and loads. This relies on the monitoring engineer being always aware of the different operational conditions in which the analysis techniques are operating.

It is also apparent from the presence of three blade CMSs in the survey that WT blade monitoring, originally referred to in structural health monitoring, is gaining more industry interest. Two of the systems in the survey (19, 20) are based on blade strain measurement through the use of fibre optic transducers originally intended to provide signals for the blade pitch system. The principle aim of these systems is to detect damage to the blade itself and, in the case of the Moog Insensys system (20), detect the build up of ice or a lightning strike on a blade. The third system, from IGUS (18), uses accelerometers mounted within the blade to detect blade damage, icing and lightning strikes. All three of these systems can be fitted to WT blades retrospectively.

The two fibre optic systems (19, 20) can operate at very low sampling frequencies compared to vibration-based systems as their analysis relies solely on

changes in the time domain signal. Since the IGUS monitoring system (18) is based on vibration analysis its sampling frequency has to be much higher than that of the fibre optic strain measurement systems. The system compares the blade accelerometer FFT with spectra recorded for similar operating conditions to make a diagnosis. As opposed to the other systems discussed, the IGUS system has the power to automatically shut down or restart the WT based on the results of its analysis. This system appears to be particularly popular within the wind industry.

2.4 The Future of Wind Turbine Condition Monitoring

As has been shown by the wide range of CM and diagnosis systems included in §2.3, there is clear industry interest in applying CM to WTs. However, the concept of CM of variable speed, variable load machines like the WT is still very much under development.

2.4.1 How Far Do We Need To Go?

Since there is much less expertise present with regard to these variable speed and load machines, the current trend appears to be that of instrumenting a turbine heavily in order to collect as much data as possible but is this really the best way forward? In the conventional rotating machine industry the number of required transducers has reduced significantly as knowledge about monitoring has increased.

One of the best examples of this reduction in transducers is that of the Rolls Royce military aircraft engines. The RB119 turbofan, used on Tornado combat aircraft since 1980 [34], has a three shaft design with high (HP), intermediate (IP) and low pressure (LP) systems. Rolls Royce is able to monitor these highly popular jet engines through their Engine Health Monitoring (EHM) system. Naturally one would expect a highly detailed range of transducers to be installed on such a safety critical component of an aircraft however personal communication with Rolls Royce has shown that a RB119 engine uses only two accelerometers: one at the front (HP) and one at the rear (LP). The system also measures the shaft speed at the front and rear alongside the IP blade temperature, air speed and altitude of the aircraft. While there are other parameters measured from the aircraft itself, it is these parameters that are used for engine monitoring. The system segregates data by operating conditions such as climb, cruise and land to allow monitoring under different load conditions.

The twin-rotor Chinook helicopter uses a much greater number of accelerometers to monitor its two gearboxes however a similar strategy is carried out whereby data is only recorded during level flight, according to private communication from Qinetiq.

The Rolls Royce example suggests that, given careful planning and research, the number of transducers required to monitor a relatively slow speed WT drive train may not need to be that high. However, while the monitoring of a reduced number of parameters would be preferable, there does not appear to be the required level of knowledge about the drive train available to decide the best places to monitor to achieve clear, reliable results.

2.4.2 Defining a Direction for Development

Based on observations of CM for the safety-critical Rolls Royce RB119 turbofan engine, it would seem that reducing the number of transducers required for CM of WTs should be an achievable goal. However, the success of the Rolls Royce Engine Health Monitoring system is likely to have derived from easily accessible information owned and worked upon within the Company itself. In the wind industry the availability of information could be one of the limiting factors to the development of CMSs.

This data confidentiality appears to stem from the structure of the wind industry in that turbine operators rarely have access to any turbine CM data during the initial WT warranty period. It is also common that Operators cannot retrofit their own preferred monitoring systems to turbines until the turbine is out of the manufacturer's warranty period. Both these issues stem from OEM concerns about their initial warranty being invalidated. This means that valuable data may never be accessible to the operator and, less likely still, to those researching CM.

Despite this, some information can be gained from WT Operators about their preferred methods for CM. Discussion with Operators has suggested that existing systems are able to successfully monitor and diagnose drive train failures, although the best results are currently found amongst those Operators with CM expertise.

Perhaps the most obvious direction for the development of CMSs is not to 'reinvent the wheel' but to take existing systems and incorporate refined monitoring algorithms and techniques into them to increase the clarity of results and simplify or increase confidence in alarm signals generated. This concept is already visible in those

WT CMSs which have developed from other, vibration-based systems. The adaptation of analogue inputs to allow for oil debris particle counters, for example, demonstrates how new analysis methods can be incorporated into existing systems. The same may be true for many other transducers, for example current and voltage probes, which produce signals that are essentially composed of low frequency vibrations.

In addition, the industry is already noting the importance of operational parameters, such as load, speed and wind speed, when monitoring WTs so techniques will begin to adapt further to include these signals within analysis techniques. This should lead to more reliable CM, diagnostics and alarm signals.

Finally, possibly the most important development will be that of automating CM and diagnostic systems to reduce the management load resulting from operating large numbers of WTs. Some systems included in the survey are already able to do this to an extent and one system in particular, the SKF WindCon 3.0 system, will be discussed in Chapter 3. The impact of automated monitoring will be most significant for Operators with many wind farms and large numbers of turbines where manual data interpretation would be time consuming and costly. This point is further enhanced by the need for reliable monitoring offshore where availability is at a premium.

2.5 Justifying Condition Monitoring of Wind Turbines

CM of large rotating plant has been seen as essential for many years. However, there was initially little interest in the area as operators did not see the need for them to monitor their machines, largely because of difficulties in interpretation of data. The first edition of *Condition Monitoring of Electrical Machines* by Tavner and Penman [35] noted that advanced warning of developing faults would be desirable in order to allow maintenance staff “greater freedom to schedule outages” with the aim of reducing downtime and capital losses [35]. But, importantly, the text also highlights the need for justification for CM given the considerable expenditure required of the Operator for implementation.

Tavner and Penman suggest that the monitoring of small electrical machines with outputs below 20kW is unlikely to be beneficial although it is also noted that monitoring even a small machine can be worthwhile where the loss of the machine will impact the performance of a larger system [35]. The text goes on to suggest that the

cost of lost output from a failed high merit turbogenerator could exceed £500k per day. Although the text does not include figures for the cost of monitoring itself, it seems clear that saving one day's outage on a large turbogenerator, say 500MW, could easily cover the capital cost of a CMS.

There is, of course, debate as to whether the monitoring of WTs is justified when we consider the capacity of a WT at 3MW compared to a turbogenerator at 500MW. Despite the obvious importance of this question it does not appear that a publicly available study has been carried out to answer it. This is no doubt the result of data confidentiality within the industry and, as a result, it can be difficult to obtain exact figures. Below is a brief cost justification for WT CM based on discussion with a Supergen Wind industrial partner and, although exact figures could not be included, suitably realistic figures based on experience are used.

Firstly, the example of a fossil or nuclear fired 500MW turbogenerator set was discussed using approximate figures. Assuming that the 500MW set is unavailable for 24 hours, the operator could have lost the cost of 12,000MWh of energy sales. So, if the operator were earning, say, £30/MWh, an unplanned 24 hours outage would cost £360k in lost energy revenue. In this case the operator has used several SKF MasCon CMSs on turbogenerators, on which the SKF WindCon WT CMS is based. This system typically costs around £14k to install, including £7k for transducers and other installation costs. These figures suggest that this CMS could be paid for in as little as 1 hour of saved downtime, provided the CMS can give prior warning of impending failure. In fact, for a 4 unit power station at 500MW per unit, the CMSs for all sets could still be paid for through the prevention of less than 5 hours unplanned downtime. It is quite clear that, even with approximate figures, CM of large plant is entirely justified through the reduction of even a small amount of unplanned downtime.

Secondly, the same calculation for a 3MW WT is applied. The Operator is using the SKF WindCon system with an approximate installation cost of £14k and the cost of energy, including Renewable Obligation Certificates (ROCs) is assumed to be £60/MWh. In this case, despite the increased price for energy, a 24 hour stoppage will only cost the Operator £4.32k per day assuming 100% capacity factor. On this basis, a single CMS would take over 3 days downtime to pay itself back and this would be applied to each turbine with a monitoring system. Therefore, the cost of CM of WTs is not necessarily justified in terms of reduced downtime directly, especially once the actual capacity factors are considered. However, the Operator was able to give an

example of two gearbox faults experienced, one of which resulted in compete gearbox failure while the other was detected in advance through CM and only a bearing replacement was required. The cost of the replacement refurbished gearbox was approximately £170k without consideration of the cost of labour and, importantly, access equipment and downtime, both of which will be large to allow for the replacement gearbox lead time. This is compared to the cost of a planned bearing replacement at approximately £10k with low equipment costs and downtime, which can be kept down to a few hours. The overall saving from the detection of this fault at an early stage is consequently more than £170,000 once other costs are taken into consideration. Through the early detection of this fault, resulting in bearing rather than gearbox replacement, the Operator has paid for monitoring systems at £14k each on up to 12 turbines.

Therefore, we can see that the cost of WT CM may not be justified by downtime prevention alone but is more than justified in terms of the cost of repair should a significant fault on a large subassembly go undetected.

This point was further emphasised by Olivier Gaget of RES in a presentation at the Operation and Maintenance Forum in London, 2010 [36]. Figure 14 shows a comparison of maintenance costs of different WT subassemblies. There are two points to note from this figure. Firstly, for each subassembly the lost production cost is a small percentage of the overall cost. This is clearest for gearbox and generator faults. This follows from the Operator case study point above in that costs resulting from downtime directly do not necessarily justify CM. Secondly, however, Figure 14, also shows very clearly that maintenance costs are very high for certain subassemblies, although no actual cost values are given on the figure. In fact, for gearbox damage, the maintenance cost is nearly twenty times greater than the lost production cost. This is due to the long lead time for replacement gearboxes, their high capital cost and their high installation costs. This further enhances the need for early detection of faults through CM. We see similar results for the generator and yaw systems although in these cases the lost production costs increase to contribute about 20% of the total subassembly cost.

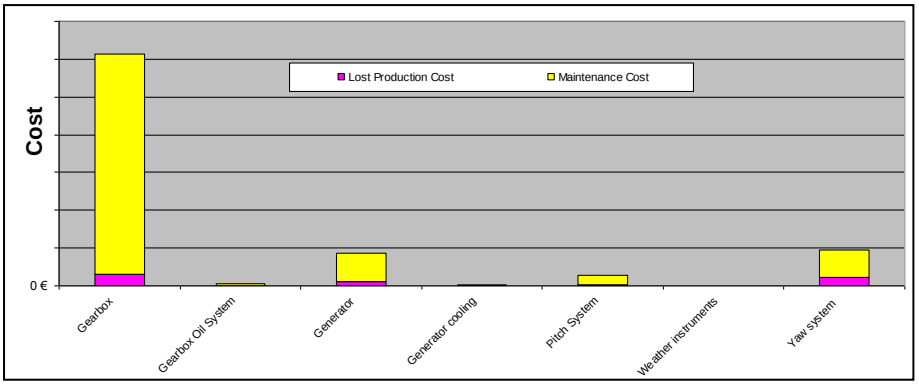

Figure 14: Comparison of unscheduled maintenance costs of certain wind turbine subassemblies [36]

2.6 Conclusions

This Chapter leads to a number of interesting conclusions about CM and its current standing within the wind industry.

It is important to recognise the clear links between the traditionally separate areas of WT monitoring. SCADA systems have a clear and important role in the transmission of operational and health information for WTs although they themselves are not currently designed to provide detailed diagnostic information.

There are a large number of CMSs currently available to operators, manufacturers and developers. The majority of these systems are developments of systems or concepts that have been widely used in other conventional rotating machine applications. In particular, vibration monitoring of drive trains has a large influence on the WT CM market due to the great amount of research that has been carried out and knowledge already gained. However, few of these systems have made the diagnostic link between monitoring signals and turbine operating conditions.

Many of the systems are also based on the idea of installing many transducers on the WT drive train although it has been shown by Rolls Royce that it is possible to successfully monitor a complex machine using few transducers.

It is apparent that WT CM is developing, as can be seen from the survey of monitoring systems where new technologies are encroaching on traditional methods. This suggests that the direction for research of CM should not be to 'build from scratch' but to develop or refine techniques to suit their new working environment. These techniques could then be incorporated into successful existing systems to enhance

their capabilities and above all, increase the accuracy and user confidence in alarm signals.

Finally, the financial case for CM has been explored. Although it is difficult to obtain exact cost figures, the conservative values obtained from discussion with an experienced Operator clearly indicate that WT CM is justified. It is important to note that its justification does not lie in the saving of downtime directly, as was the case for fossil and nuclear-fired units, but in the saving of maintenance costs through prevention of serious failure. Undetected faults in WTs lead to large maintenance costs which are further compounded by downtime. In particular, it should be mentioned that these figures were given for an onshore WT. If CM onshore can be justified through the detection of a single gearbox fault, offshore it will be essential. Onshore the operation and maintenance activities account for around 15% of the energy price rising to double that offshore, around 30%, of the energy cost [37]. A study of UK round one offshore wind farms [38] has, however, shown a lower cost for operation and maintenance varying between 12% and 22% of the cost of energy depending on the wind farm and its operator. However, on average, this is still higher than costs onshore.

Effective CM will be essential to reduce this large, restricting figure.

We can now clearly state that CM of WTs is a worthwhile endeavour and discussion with Operators and monitoring companies has suggested that it is also widely successful. However, much of the success lies in the ability of expert monitoring engineers rather than in the systems directly. Chapter 3 will show case studies of CM based on the experience of a large WT Operator with a wide experience of CM of rotating machines.

2.7 References

[24] Tavner, P. J., Yang, W., *Survey of Commercially Available Wind Turbine Condition Monitoring Systems*, Supergen Wind Energy Technologies Consortium, under revision to April 2009.

[25] Crabtree, C. J., *Survey of Commercially Available Condition Monitoring Systems for Wind Turbines*, available at http://www.supergen-wind.org.uk, last accessed 8th November 2010.

[26] Rademakers, L. W. M. M., Braam, H., Obdam, T. S., *Estimating Costs of Operation and Maintenance for Offshore Wind Farms*, Proceedings of the European Wind Energy Conference, March 2008.

[27] Wiggelinkhuizen, E., Verbruggen, T., et al., *CONMOW: Condition Monitoring for Offshore Wind Farms*, Proceedings of the European Wind Energy Conference, 2007.

[28] Feng, Y., Crabtree, C. J., Long, H., Tavner, P. J., *Use of SCADA and CMS Signals for Failure Detection and Diagnosis of a Wind Turbine Gearbox*, Proceedings of the European Wind Energy Conference, Brussels, Belgium, March 2011.

[29] Zaher, A., McArthur, S.D.J., Infield, D.G., *Online Wind Turbine Fault Detection through Automated SCADA Data Analysis, Wind Energy*, Vol. 12, Iss. 6, pp. 574-593, 2009.

[30] ReliaWind, www.reliawind.eu, last accessed 8th February 2010.

[31] Nehorai, A., Porat, B., *Adaptive Comb Filtering for Harmonic Signal Enhancement*, IEEE Trans. on Acoustics, Speech and Signal Processing, Vol. ASSP-34, Iss. 5, 1986.

[32] Antoni, J., Randall, R. B., *The Spectral Kurtosis: Application to the Vibratory Surveillance and Diagnostics of Rotating Machines*, Mechanical Systems and Signal Processing, Vol. 20, pp. 308-331, 2006.

[33] Isko, V., Mykhaylyshyn, V., Moroz, I., Ivanchenko, O., Rasmussen, P., *Remote Wind Turbine Generator Condition Monitoring with WP4086 System*, Materials Proceedings, European Wind Energy Conference 2010, Warsaw, 2010.

[34] RB199: Power for the Tornado, Rolls Royce PLC, 2009, available at http://www.rolls-royce.com/Images/rb199_tcm92-6699.pdf, last accessed 4th June 2010.

[35] Tavner, P. J., Penman, J., *Condition Monitoring of Electrical Machines*, pp. 6-14, Research Studies Press, 1987.

[36] Gaget, O. (RES), *Increasing Reliability and Minimising Cost through Condition Monitoring*, Optimising Wind Energy Operations and Maintenance Forum, London, May 2010.

[37] van Bussel, G. J. W., Schöntag, C., *Operation and maintenance aspects of large offshore wind farms*, Proceedings European Wind Energy Conference 1997, Dublin, 1997.

[38] Feng, Y., Tavner, P. J., Long, H., *Early Experiences with Round 1 Offshore Wind Farms*, Energy Proc. Institution of Civil Engineers, Vol. 163, Iss. EN4, pp. 167-181, 2010.

3 A Case Study of Wind Farm Condition Monitoring

"Faults and defects every work of man must have"

Samuel Johnson
English critic and writer

In this Chapter an example of CM applied to a specific wind farm is presented to give a view of the current state of the art in WT CM. The Chapter aims to present an overview of how CM could be applied practically, the structure required and examples of faults that have been successfully detected by WT Operations Staff.

3.1 Introduction

During this research there has been a significant degree of industrial interaction with links being built between Universities, WT Owner Operators, Operations Staff and consultants through the Supergen Wind Energy Technologies Consortium.

As a result of this interaction there has been the opportunity to examine how the process of CM is carried out in an industrial environment. In this case the Owner Operator does not monitor the turbines directly but subcontracts to their Operations Staff or Operations Group where a team of experienced CM engineers manages the monitoring strategy.

While data and information confidentiality must be maintained, this Chapter discusses in as much detail as possible points relating to the practical application of CMSs in the field. In particular it describes the system and measurement configuration used by a particular Operations Group alongside their fault detection successes. The results presented were extracted by the author based on discussion with the Operations Group. The difficulties of CM are also discussed as appropriate to the available results and conclusions drawn about the success and future direction of CM in the field.

3.1.1 The Wind Farm

The Owner Operator who provided the information used in this study operates a number of wind farms across the UK and, consequently, a wide range of turbine types and configurations. The WTs featured in this study are rated at 1.3MW and are of conventional two-speed, stall-regulated design. The two-speed squirrel cage induction generator configuration allows the turbine to operate at either 1500rpm or 1000rpm, 4-pole and 6-pole respectively. The shaft speed is controlled through active stall, pitching the blades to maintain an approximately constant shaft speed at the selected generator synchronous speed.

For confidentiality no additional description is given here of the finer details of the turbines under study however they were chosen due to the presence of a number of different faults therefore offering a range of results for presentation.

3.1.2 Selecting a Condition Monitoring System

The turbines themselves have been in operation for over 5 years however CMSs were not commissioned until a later date after the warranty had expired. Before beginning their monitoring campaign, around four years ago, the Operations Group carried out an internal study to establish the CMS best suited to their needs, defining their own requirements, beginning from the decision of whether hand-held or permanent monitoring was the best route forward. It was concluded that permanent monitoring was required given the access issues with large WTs, immediately indicating the Group's understanding of the challenges of remote monitoring of plant and WTs in particular. This decision appears also to have been based on their experience in monitoring pumps and drives in other inaccessible locations.

The study also examined those faults that had previously been experienced on the Owner Operator's WT fleet which formed the basis for the selection of an appropriate monitoring system, with specific analysis requirements in mind. The required analysis methods were primarily based on the Operations Group's experience in fault diagnosis for conventional rotating machines. The range of faults that had been experienced on turbines was considerable, largely as a result of the number of different turbine configurations represented within the fleet. Faults included blade damage due to lightning strikes; blade cracking or imbalance; main bearing damage; and generator faults in bearings or rotor bars.

As a result of the initial survey of fifteen CMSs, the Owner Operator and Operations Group selected two systems for trial and tested them for a period in the field. Both the SKF WindCon and its rival were based on vibration monitoring and following the trial period a number of points led the Owner Operator to select the SKF WindCon system over the other option. One point of particular interest is the number of available channels on the two systems. The SKF has 16 analogue channels compared to the alternative, which had 8. The Operations Group in fact stated that 8 analogue channels was sufficient to monitor most WTs however it was felt that some turbines in the fleet may require a larger number of channels due to their configurations. This careful selection means that the Owner Operator is able to implement the same system across its WT fleet, potentially simplifying the monitoring strategy.

It was also felt that the SKF WindCon system had superior functionality when compared to the alternative. The superiority came chiefly in terms of the alarm signals generated by the two systems, in that the SKF system has individual alarm logs for each channel and each alarm can be set quickly and easily. Additionally, the Operations Group had successful operational experience with the SKF MasCon monitoring system from which WindCon was derived.

Following the period of testing and selection the SKF WindCon CMS was retrofitted to number of wind farms. Overall it was felt that of the two systems trialled, the SKF WindCon system met the requirements of the Operations Group to a greater degree than did the alternative.

3.2 Monitoring Configuration

3.2.1 Transducers and Physical Channels

The SKF WindCon hardware has 16 analogue and 2 digital inputs. For operation and analysis purposes the system requires that a pulsed speed signal be applied to one of the digital inputs as a reference signal for other measurements and as a trigger for Fourier transform analysis. In this example two speed signals are recorded, one from the generator shaft and one from the low speed shaft; 1 pulse/rev and 24 pulses/rev respectively. The operational measurements taken are:

- Generator speed (rpm) (digital)
- Low speed shaft speed (rpm) (digital)

- Load (kW)
- Wind speed (m/s)

The drive trains of WTs fitted with WindCon are instrumented with nine accelerometers in positions that are widely accepted between different WT CMSs as mentioned in §2.3. In detail, they are:

- Main bearing, vertical
- Main bearing, transverse
- Main bearing, axial
- Gearbox low speed shaft, transverse
- Gearbox high speed shaft, vertical
- Gearbox high speed shaft, transverse
- Gearbox high speed shaft, axial
- Generator drive end, transverse
- Generator non-drive end, transverse

The gearboxes are also instrumented with a Macom TechAlert 10 oil debris monitoring system. This transducer, shown in the survey in Appendix A, uses an inductive sensor to detect the presence and size of ferrous and non-ferrous particles, before the oil is filtered. A count output is provided for each type and size of particle to show the level of severity of the amount of debris in the lubrication oil. As a result, a large number of measurements are possible so in this case the SKF WindCon hardware has ten virtual channels connected for oil debris monitoring as shown below. The virtual channels, including cumulative particle count data, are transmitted digitally from the transducer to the WindCon unit via a Modbus interface.

- Ferrous particles, 50-100µm
- Ferrous particles, 100-200µm
- Ferrous particles, 200-400µm
- Ferrous particles, 400-800µm
- Ferrous particles, > 800µm
- Non-ferrous particles, 150-200µm
- Non-ferrous particles, 200-400µm
- Non-ferrous particles, 400-800µm
- Non-ferrous particles, 800-1600µm
- Non-ferrous particles, > 1600µm

Apart from the initial setting of a unit address, the SKF WindCon hardware is configured remotely. This gives the obvious advantage of being able to reconfigure systems without having to return to site, an important benefit for WTs in remote locations. The software used for configuration and analysis of the data is SKF ProCon and allows the user to access different WindCon units remotely as well as any other databases stored by the Operations Group. The operational structure of the SKF WindCon/ProCon system is shown in Figure 15.

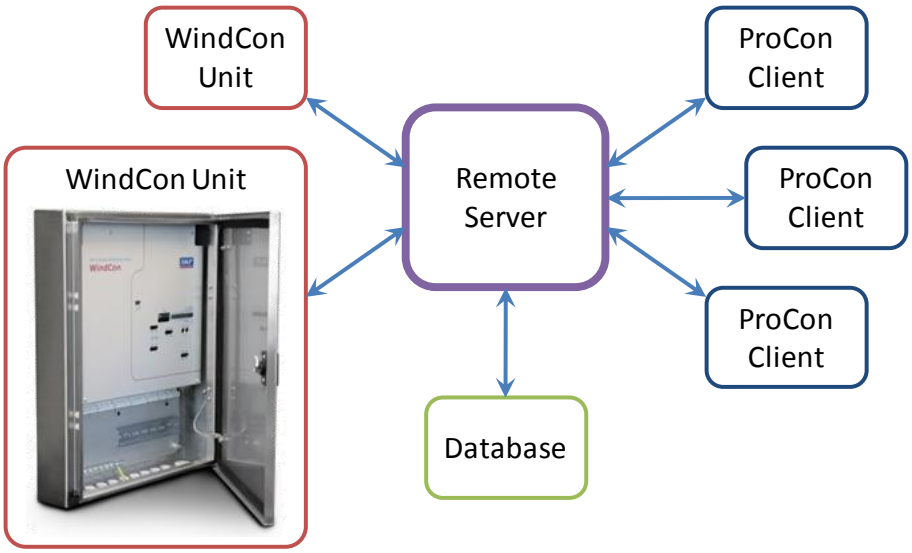

Figure 15: Schematic Diagram of SKF WindCon Monitoring based on [39]

WindCon channels are configured via remote connection through a ProCon client. The user selects the required online unit from the list given in the *'MasCon units'* dialogue (Figure 16), chooses to initiate either a digital or analogue channel and is presented with the relevant dialogue box. As an example, the configuration of an analogue vibration channel is given using the *'Analogue Channel'* dialogue box shown in Figure 17.

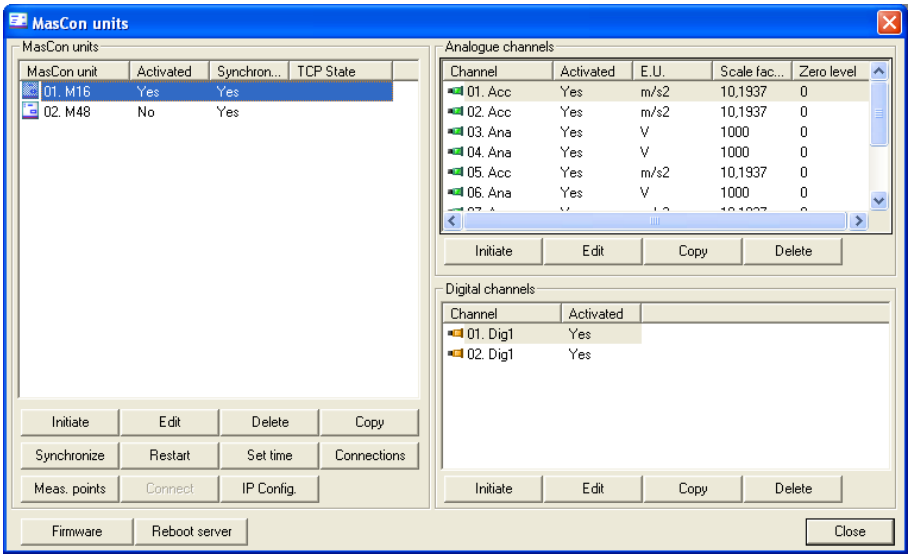

Figure 16: 'MasCon units' configuration dialogue

The *'Analogue channel'* dialogue lists the available channels, that is those which are not already configured for the unit, and the user can then allocate their own channel name for clarity. The type of sensor is selected from a predefined list:

- Acceleration (g)
- Velocity (mm/s)
- Displacement (µm)
- TBU Temperature (°C)
- Other

The engineering units for each type of sensor are predefined as shown except for 'Other' where the user may define their own unit of measurement. Each channel can also provide a 4mA current feed to the transducer if required.

Analogue channels have their own linear calibration, here called 'Sensitivity', which is manually defined. Now the channel configuration is complete but can be edited at any point, with the exception of changing the channel number.

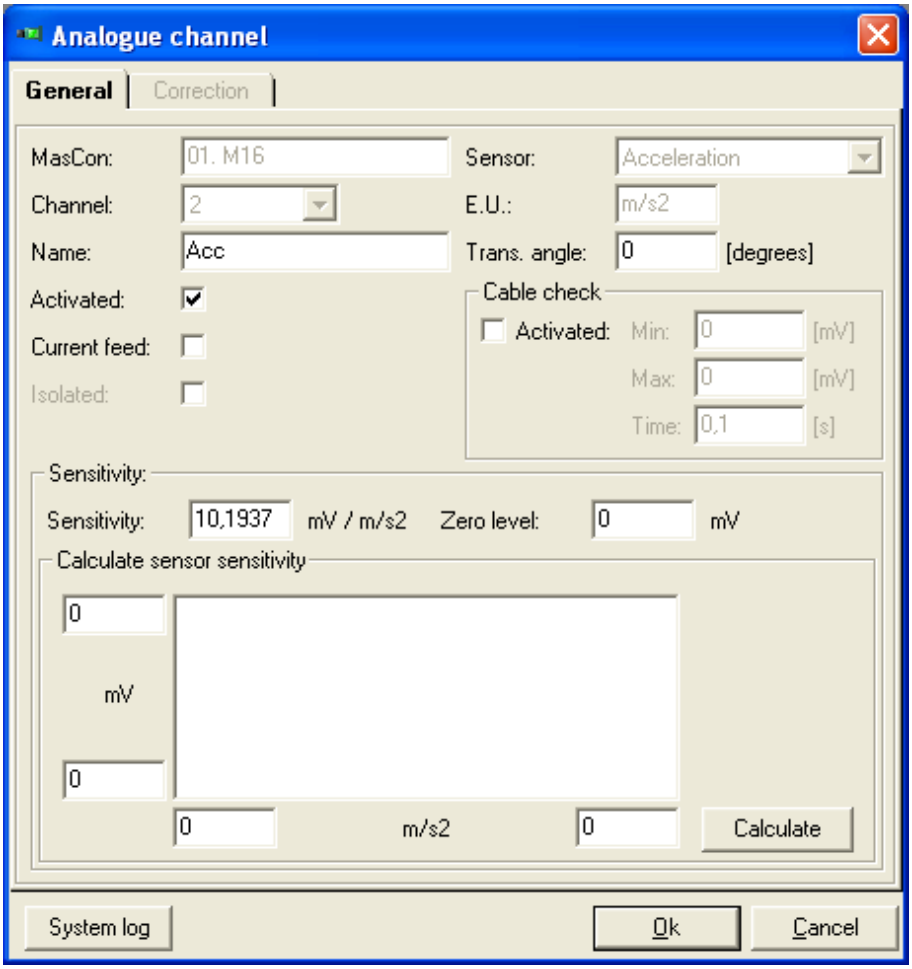

Figure 17: 'Analogue channel' configuration dialogue

A similar but simpler process is carried out for digital channels. Since the digital channels are generally used for speed measurement, all that has to be defined is the channel, name and number of pulses per revolution as shown in the digital channel configuration dialogue box shown in Figure 18.

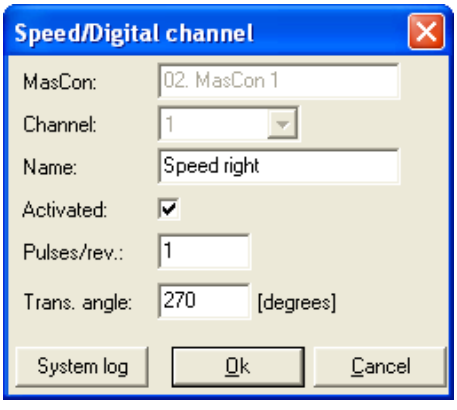

Figure 18: 'Speed/Digital channel' configuration dialogue

As mentioned, a digital speed signal is required by the WindCon system to trigger analysis within ProCon software, as all frequency analysis and diagnosis is reliant on the machine operating condition. For example, when setting up a vibration measurement point in ProCon the user is asked to specify the 'active range' of the measurement point in terms of speed, load and the allowable change in these during the measurement period. By allowing the user to set these limits for operating conditions under which measurements are recorded, the ProCon software aims to produce stationary, directly comparable Fast Fourier Transform (FFT) results to increase the accuracy and reliability of alarms and diagnoses.

Having configured the hardware aspect of the system the user must now specify the measurements they wish to record and analyse.

3.2.2 Measurement Hierarchy

The ProCon measurement hierarchy is shown in Figure 19.

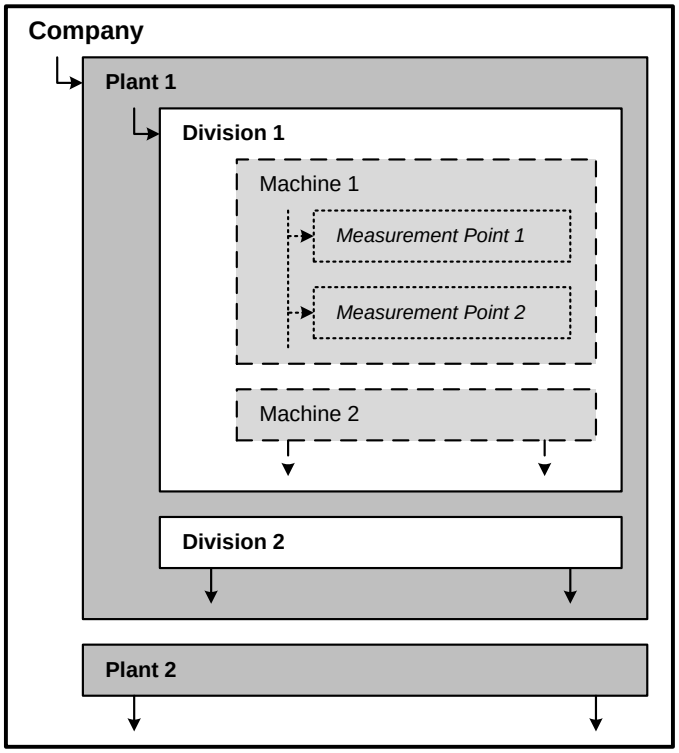

Figure 19: ProCon measurement hierarchy

This structure is particularly suited to operators with large numbers of turbines in different wind farms and also those with a varied portfolio of WT

configuration or generation technologies, since the ProCon software is able to connect to all units on other plant reporting to the same database. In this example case the structure is broken down as given in Table 1. It should be noted that the user can also switch between any other connected databases as required.

Hierarchy Position	Example(s)
Company	Owner Operator / Company name
Plant	Geographic location
Division	Wind turbines / Turbo generators / Coal conveyers
Machine	Turbine 1 / Unit 1
Measurement Point	Gearbox high speed accelerometer / Ferrous oil debris

Table 1: Example hierarchy items

Once the core structure has been established it can be added to or edited at future dates using the configuration tool and without losing previous any measurement points or data.

Before the user progresses to the 'measurement point' level it is worth considering carefully what data and analyses are required to successfully monitor the WT. In this example the number of ProCon (software) measurement points is more than double the number of transducers fitted to the turbine as multiple ProCon measurement points can be requested from each physical or virtual channel on a WindCon unit.

3.2.3 Measurement Configuration

The Operations Group featured in this study has particular experience in monitoring of conventional rotating machinery in the power generation sector and as such had a clear view of what measurements they required for successful WT CM and fault diagnosis.

Initial ‘operational’ measurement points configured were generator speed, turbine speed, load and wind speed. These are configured by selecting either the ‘Speed’ or ‘Process’ measurement point, both of which have similar settings. Firstly the user configures the channels settings for a measurements point. The load measurement settings are given as an example in Figure 20 with the turbine location and number removed for confidentiality.

Here the Operations Staff chose to take a simultaneous measurements for wind speed as this allows direct comparison without concern for timestamp errors between channels. Each measurement point is allocated a specific point number to distinguish it from the same measurement made on a different turbine. Next, the user configures ‘trend’ settings for the measurement point. Figure 21 shows the ‘trend’ settings for the load measurement point. It can be seen that the Operations Group is requesting the maximum value within a 30 second sampling period and that data is to be recorded continuously as opposed to measurement only when turbine operating conditions match a defined ‘active range’. This process is carried out for each speed or process measurement and each can be reconfigured by reopening the dialogue at a later date. Upon leaving the dialogue, the settings are transmitted to the relevant WindCon unit and data acquisition can begin.

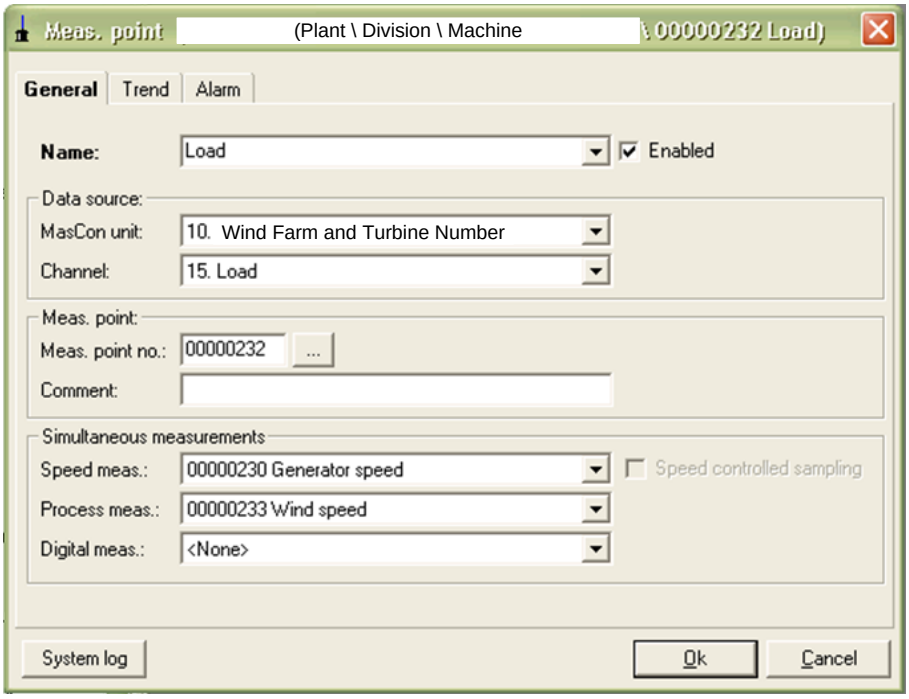

Figure 20: Load measurement settings - 'General' tab

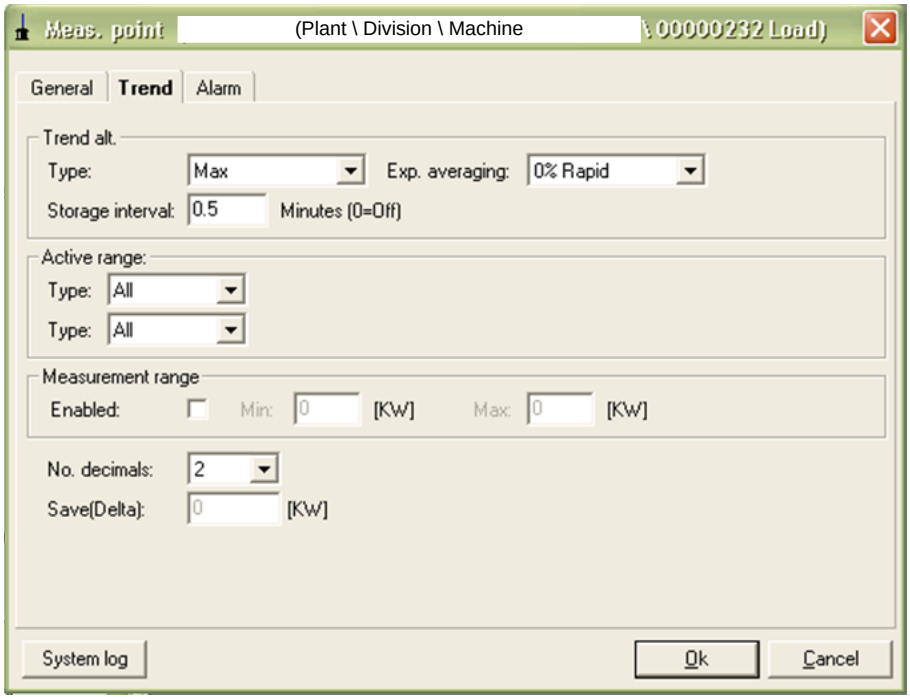

Figure 21: Load measurement settings - 'Trend' tab

Once the speed and load measurement points are defined the Operations Staff can configure vibration measurement points. The general settings are configured in much the same manner, with simultaneous measurements being recorded for generator speed and load and taken continuously rather than in a specific 'active range'.

However, the particular difference when configuring vibration channels is in the spectral analysis settings. An example of vibration spectral analysis settings for the gearbox high speed shaft, transverse, overall vibration measurement point is illustrated in Figure 22.

The Operations Group is able to set the frequency range required as well as the lower frequency limit and recording interval. The measurement time and frequency resolution are calculated by the ProCon software based on the other settings selected by the Operator.

The Operations Group's understanding of CM of variable speed and load machines is visible from the 'active range' settings for the vibration spectra. In this case a spectrum will only be recorded within a speed range of 1490-1550rpm and if the speed varies by no more than 5rpm during the measurement time. If these conditions are not met the spectrum is discarded by the WindCon unit. The selected configuration

means that no spectra are recorded when the generator is running as a 6-pole machine. Furthermore, the turbine load must be within the range 1290-1500kW and vary by no more than 5kW. By setting these tight limits on the conditions under which spectra are sampled the Operations Staff can be confident that they are observing directly comparable, stationary spectra. In addition to this, spectral analysis is carried out using the FFT, a requirement of which is to have a stationary input signal. If the active range is too wide, a non-stationary signal will be presented for analysis causing spectral peaks to become smeared and indistinct, making interpretation difficult.

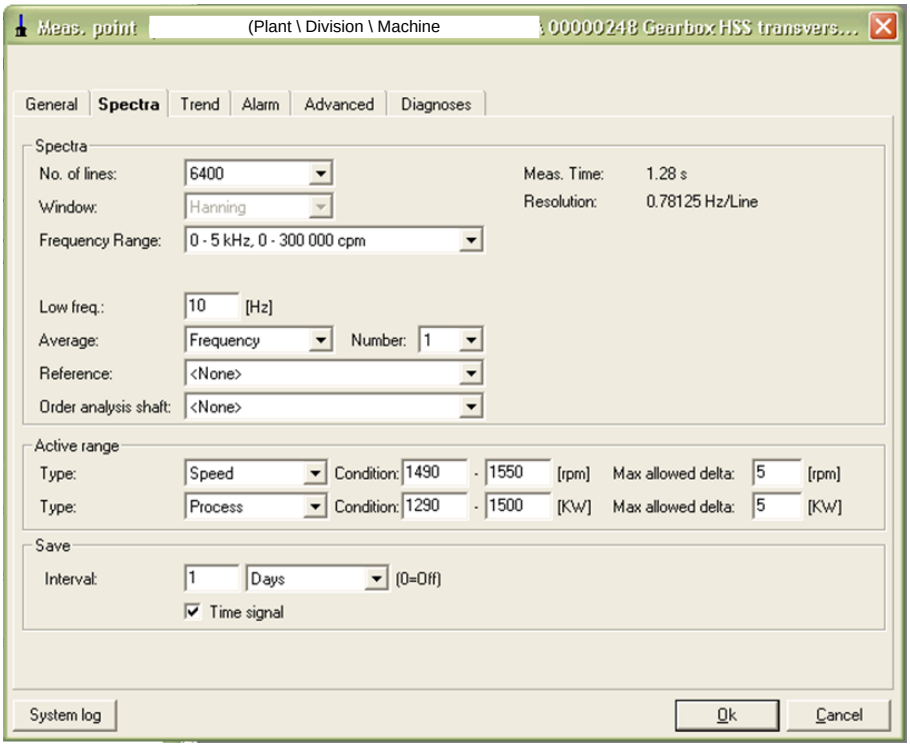

Figure 22: Vibration measurement settings - 'Spectra' tab

During discussions with the Operations Group it became apparent that the use of signal enveloping is of great importance in conventional rotating machine CM. It is of particular interest for the detection of faults with impulsive characteristics. Bearing faults, for example, produce very short impulses in the times domain with a comparatively lengthy interval between impulses [40]. The impulsive feature has very low energy, distributed across a wide frequency range, making detection difficult against the noisy spectrum generated by multiple bearings, gears and shaft speeds. More detailed information on vibration analysis and envelope spectra can be found in [40].

In this case, the Operations Group has an enveloped measurement point for each vibration transducer as well as an overall point. For reference, a typical envelope range used by the Operations Group for gearbox vibration enveloping is 0.5-1kHz. Setting envelope frequency ranges is a task for experienced vibration monitoring engineers and some of the issues associated with it are discussed in [41], where a detailed review of vibration monitoring methods is given.

The envelope measurement points are configured in much the same way as the overall vibration except that an additional setting is required to specify the envelope frequency range. Just as for the trend measurement points, generator speed and load are recorded simultaneously.

Finally, the gearbox lubrication oil debris measurement points are considered. The settings for these are much simpler than those for vibration signals due to the discrete nature of the measurements. Two different measurements are taken for the debris in oil. The first is the cumulative count of both ferrous and non ferrous particles in each particle size 'bin' and the second is the count rate per hour. The count rate gives the rate at which particles are being generated although it does not in itself take account of the loading condition of the turbine. The cumulative particle count records the turbine load simultaneously.

While more measurement point types are possible within the WindCon/ProCon system, they are not described here as they were not used in the following examples.

3.2.4 Diagnosis Configuration

For even the most experienced CM engineer, vibration spectra can be complex and difficult to interpret. A WT gearbox comprising three or more shafts contains several rolling element bearings, each contributing many frequency components to vibration signals. With the addition of meshing frequencies from multiple gear stages, the spectrum soon becomes difficult for both interpretation and diagnosis purposes.

To deal with this, the SKF ProCon software features a machine diagram function. The diagram, an example section being shown in Figure 23, is built up as a block diagram with blocks for shafts, bearings, gears and blades. The components are then specified for each turbine or type of turbine; setting gear tooth number, for example. The software contains a large database of known bearings from major manufacturers so detailed, exact bearing specifications can be attached to each

individual bearing. However, should a bearing not be listed in the library, the Operations Group can insert outer race, inner race, roller and cage dimensions manually.

Once the machine diagram is complete, the ProCon software is able to calculate fault frequencies for an given speed point. This means that for a given spectrum, the frequency signature of each component can be identified by selecting it from a menu of all possible components in the machine diagram and deployed on the FFT spectrum as a cursor. The user is also able to select an unidentified peak in the spectrum and data from the ProCon machine diagram will show whether it is a known frequency of interest, a harmonic or unknown. As a result, the Operations Staff, however inexperienced, have a much improved ability to understand vibration spectra from the complex drive train.

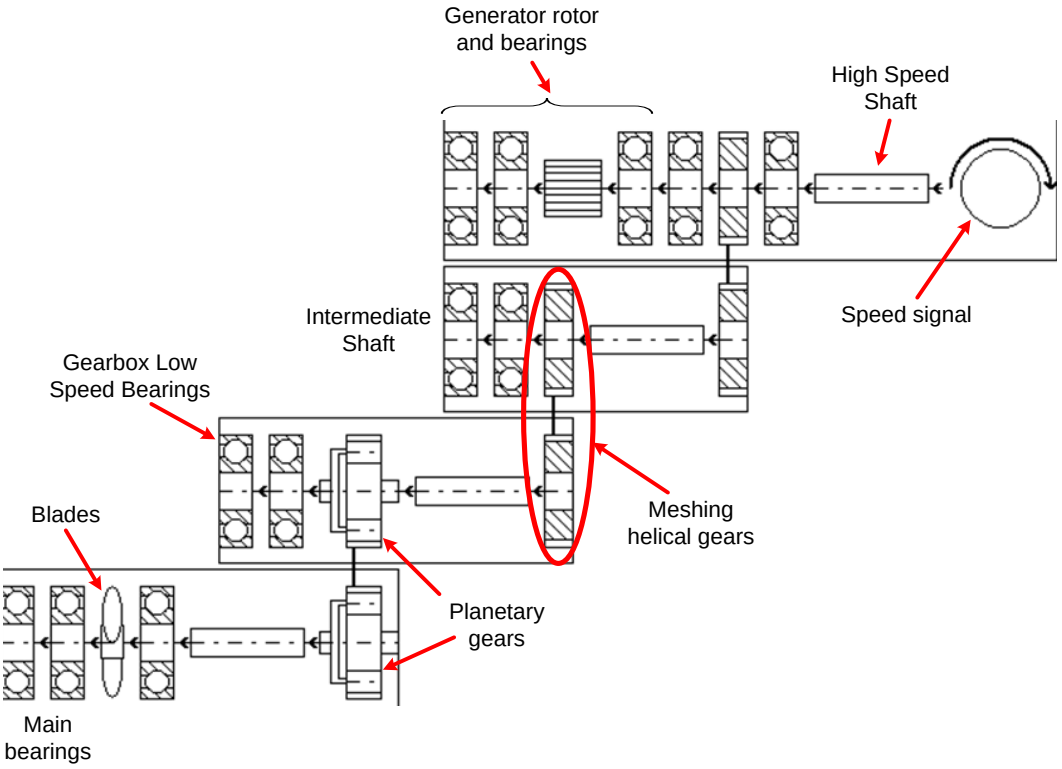

Figure 23: Example section from an SKF ProCon machine diagram including the main features of a wind turbine drive train

Once the machine diagram is complete, the Operations Staff can configure individual alarm settings for each measurement point.

The basic alarm setting for a measurement point consists of two levels: a warning and an alarm for the vibration level within a given frequency range, specified by the Operations Staff. If either level is exceeded, the relevant warning or alarm is triggered. These alarms are based on experience of acceptable vibration and can be easily adjusted to suit each turbine. There are no standardised vibration limits for machines however some Groups may refer to standards such as the German standard VDI 2056 [42] (no longer issued) or the more up to date ISO 10816-1:1995 [43].

The alarms can be used to give an overall picture of the health of a turbine or component but do not necessarily indicate the exact location of a fault, due to their general nature. In order to speed up the diagnostic process, alarms can be set based on the fault frequencies for different components within the drive train.

Figure 24 shows detailed diagnostic settings from ProCon for the gearbox high speed shaft, transverse, overall vibration measurement point.

Each item in the list refers to a component-specific, speed dependent fault frequency as derived from the machine diagram. An individual diagnostic list can be created for each overall or enveloped vibration measurement. When a spectrum is recorded, the amplitude of each chosen frequency is automatically extracted and plotted with respect to time. These frequency-specific graphs, for example Figure 25, can be opened by the Operations Group and the trend with time observed more simply than the alternative of manually inspecting each spectrum. It can be seen from Figure 24 that the Operations Group has set warning and alarm levels for each fault frequency on the diagnostic list. The alarm is activated if its level is exceeded by the amplitude of the fault frequency in question, such as the final data point in Figure 25. By careful selection of fault frequencies and alarm levels the Operator is able to gain effective diagnostic information in a semi-automatic fashion.

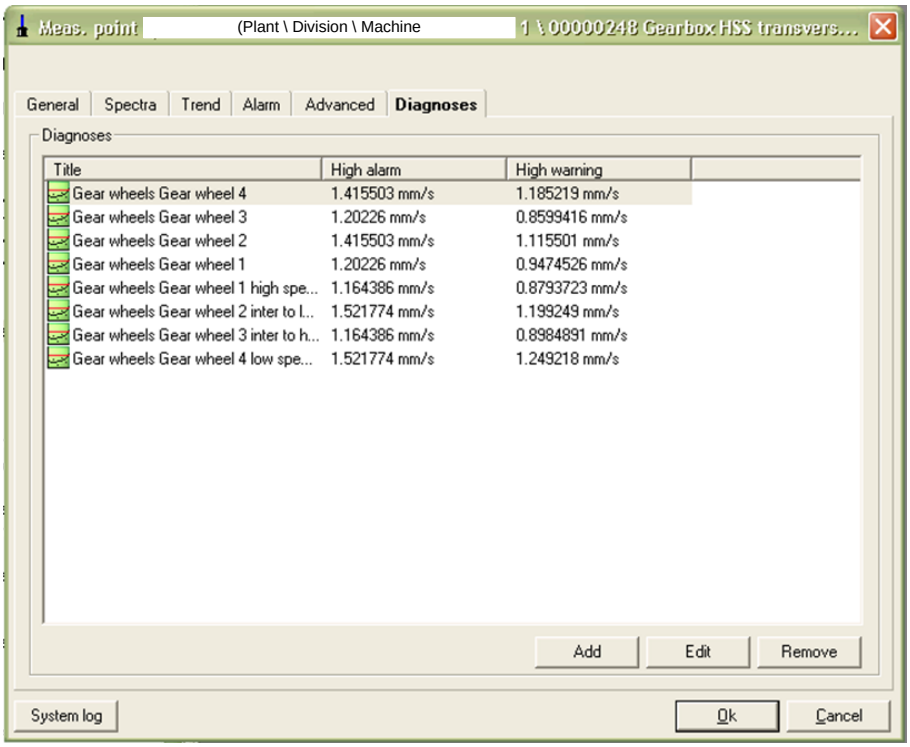

Figure 24: Vibration measurement settings - 'Diagnoses' tab

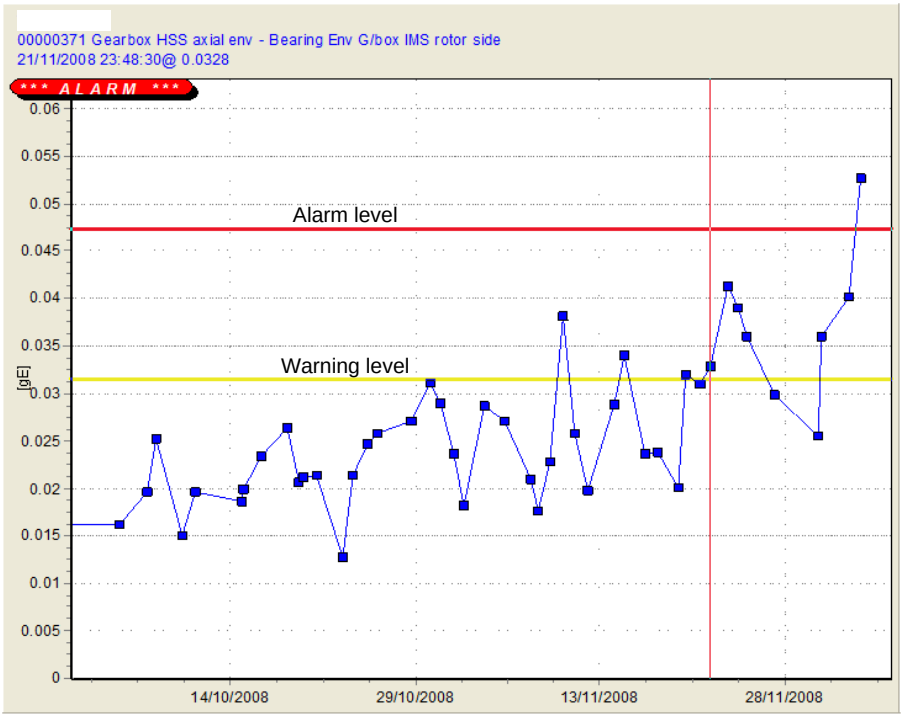

Figure 25: Example diagnostic plot - gearbox intermediate shaft bearing envelope

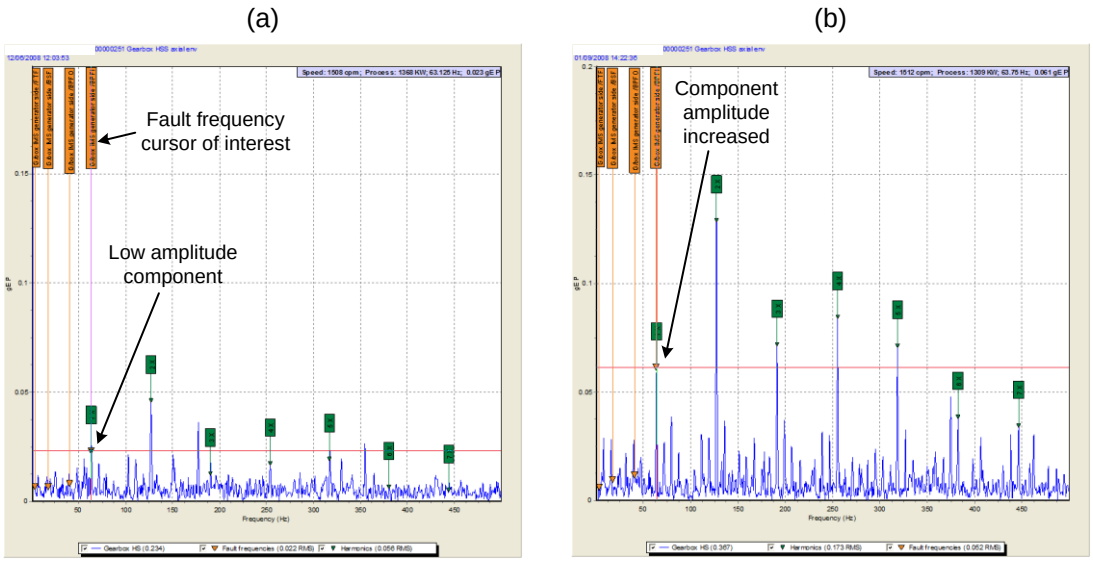

Figure 26: Two spectra contributing to the diagnostic plot, Figure 25. The component extracted to produce the diagnostic plot is labelled (a) early in fault development and (b) as fault severity increased.

Enlarged trend and spectral figures from this Chapter are given in Appendix B.

3.2.5 Data Communication

Communication with the SKF WindCon units is managed through a GPRS modem transmitting back to the Operations Group's central database. Little is known about the communication network however it is understood that there have been few issues with using GPRS communication. A particular point to note is the cost of data transmission. It would be expected that using GPRS transmission would be an expensive means of data communication however the SKF system requires the transmission of remarkably little data. This is a result of the structure of the WindCon system where data acquisition and analysis are carried out in the WindCon unit itself and only the resulting trend and spectral data are transmitted rather than lengthy sections of raw data. These results can be transmitted in packets whereas a raw data stream would require a significant bandwidth, especially where large numbers of signals and turbines are monitored. Therefore, GPRS data transmission has proved cost effective and successful.

3.3 Results

Having discussed the configuration and overall structure of WindCon for WT CM in the field, a selection of CM results are now given from the field. The examples included here are detections made by the Operations Group for gearbox and generator bearing faults on operational WTs. The author extracted and collated these results in discussion with the Operations Group.

3.3.1 Turbine X Gearbox Bearing Damage

During autumn 2008, one WT, here called Turbine X, was shut down for maintenance on the basis of a report from the Operations Group. A number of different indicators of damage were visible in data from the SKF WindCon system installed on Turbine X and a combination of these signals allowed a confident decision to be made with regard to shutting down the turbine.

The first indication of some form of gearbox damage came from an enveloped signal from the axial vibration transducer mounted on the high speed shaft end of the gearbox casing. Its envelope amplitude is plotted with time in Figure 27.

From Figure 27 a clear rise in the amplitude of the vibration envelope can be seen in the period leading up to point 'A'. This trend suggested to the Operations Staff that the gearbox required further investigation. In fact, the Group observed this trend some time before this data set begins however this data was unavailable for this thesis. After point 'A' there was a drop in the vibration envelope level, an explanation of which will be included later.

The upwards vibration trend prompted the Operations Group to examine the gearbox oil debris particle counts recorded by the WindCon system. Figure 28 shows the cumulative count for ferrous particles within the 50μm – 100μm range. In the period to point 'A' the particle generation rate remains fairly constant, the large step down being a reset point for the transducer. However, in the period between points 'A' and 'B' there is an increase in the particle generation rate. This change is also visible in the count of larger particles such as the 400μm – 800μm bin shown in Figure 29, suggesting significant damage causing material breakout.

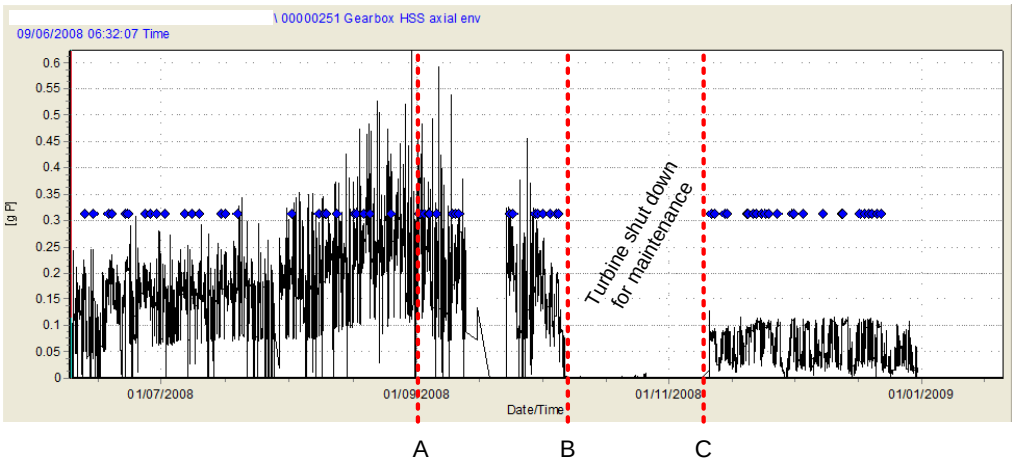

Figure 27: Turbine X gearbox high speed shaft axial vibration envelope

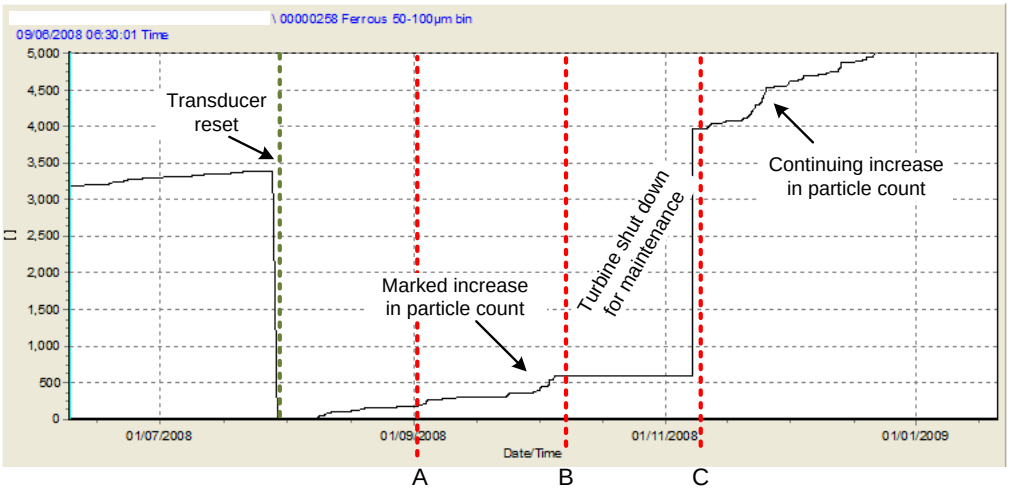

Figure 28: Turbine X ferrous 50-100µm particle count

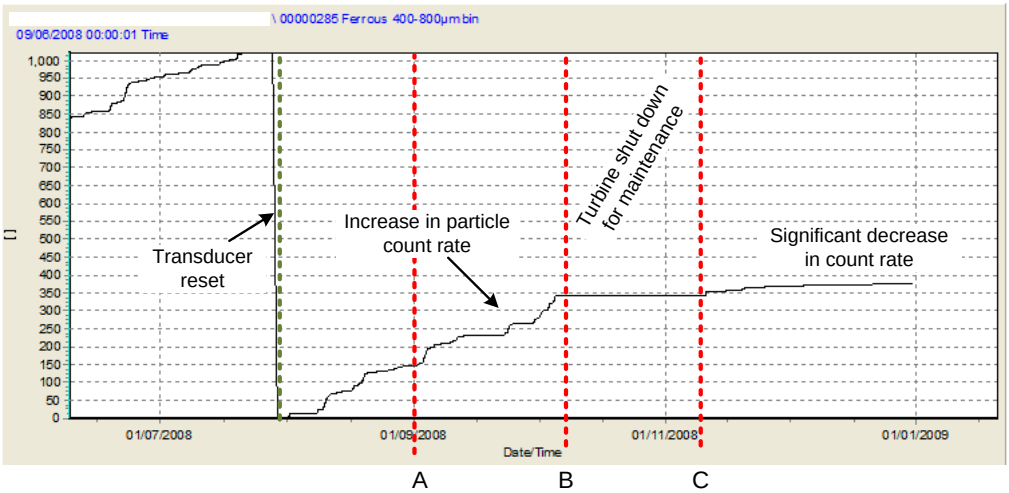

Figure 29: Turbine X ferrous 400-800µm particle count

By comparing the vibration and particle trends the Operations Group concluded that the increase in vibration envelope was a result of ferrous material breaking away from a gearbox component. The Group was also able to make an initial observation on the extent of gearbox damage. As has been observed, the magnitude of the gearbox axial vibration envelope decreased during the period 'A' to 'B', corresponding to an increase in the count rate for both small and large ferrous particles. They concluded that this combination of trends suggested a serious deterioration of the vibration transmission path between the faulty component and the gear case and, therefore, significant deterioration of the component itself.

However, the trend data presented does not in itself provide exact location information for the fault, except that it is within the gearbox of Turbine X. In order to establish the root cause of the trend, the Operations Group examined the enveloped axial vibration spectrum to identify fault-specific frequency components.

At the start of this data set, before point 'A', the enveloped axial vibration spectrum was as shown in Figure 30. The first major harmonic component corresponds to the gearbox, intermediate shaft, generator side, inner race ball passing frequency as calculated by the ProCon software using the machine diagram. The frequency component is clearly present however the Operations Staff would not necessarily be able to confirm a fault based on this spectrum alone. However, Figure 31 shows the same spectrum but recorded at the peak enveloped axial vibration, around point 'A'. The fault frequency is now more pronounced with high magnitude harmonic components indicated in Figure 31(a). To avoid overcrowding the figure, the same spectrum is shown in Figure 31(b) with sideband cursors applied to the third harmonic of the fault frequency for clarity. With the combination of a clear component-related fault frequency, its high magnitude harmonic components and significant sidebands around each harmonic, the Operations Group was able to confirm that Turbine X had damage to the inner race of the gearbox, generator-end, intermediate shaft bearing.

As a result of this detection, Maintenance Management shut down the turbine to replace the damaged bearing and carry out an inspection to confirm the diagnosis. Figure 32 is a photograph taken by the Maintenance Staff of the damaged bearing to show the extent of the damage. As can be seen, the inner race shows signs of asymmetrical loading leading to spalling of material from the race surface.

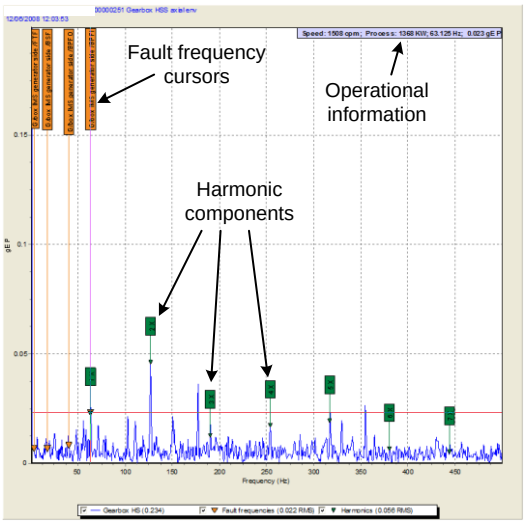

Figure 30: Turbine X enveloped gearbox high speed shaft axial vibration spectrum early in fault development, before point 'A'

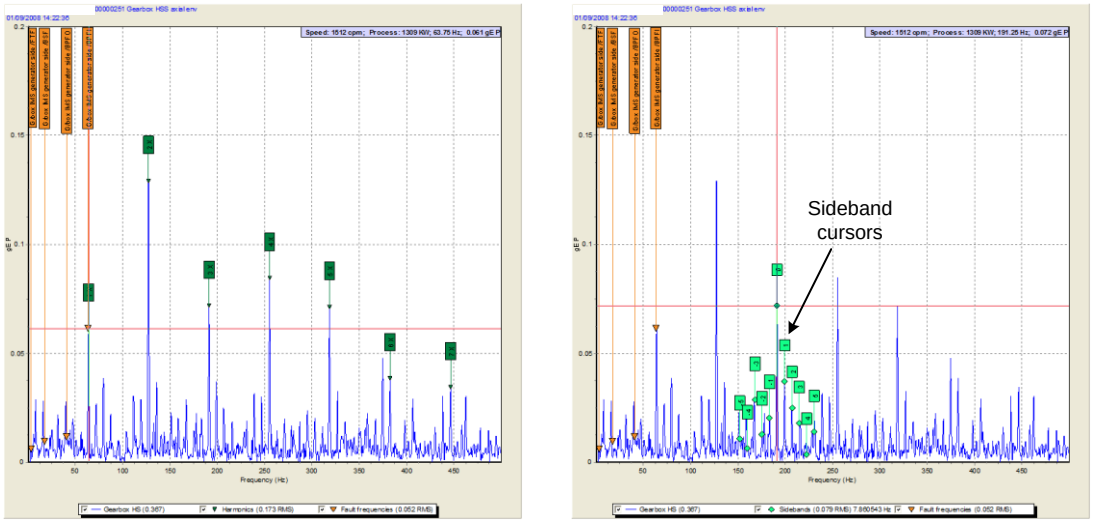

Figure 31: Turbine X enveloped gearbox high speed shaft axial vibration spectrum at peak enveloped vibration level, around point 'A' showing four bearing cursors: (a) labelled to show harmonics; (b) labelled to show sidebands

Figure 32: Turbine X intermediate shaft bearing inner race under inspection following its replacement

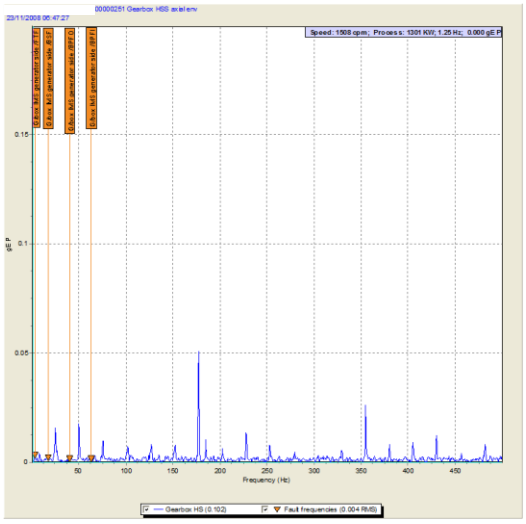

Figure 33: Turbine X enveloped gearbox high speed shaft axial vibration spectrum after bearing replacement

Having replaced the bearing, the enveloped axial vibration dropped significantly, as can be seen from the period after point 'C' in Figure 27. Figure 33 shows a spectrum of the same enveloped vibration signal but following the bearing replacement, using the same scales for clarity. By examining the magnitude of the component-related fault frequencies marked on the figure it is clear that healthy levels of vibration have been restored and the fault is clear. However, another peak is now visible, possibly indicating a fault with a different component, and there is a continuing

increase is small debris production, probably due to the running in of the new bearing, although this is not investigated in this thesis.

3.3.2 Turbine Y Gearbox Bearing Damage

Around the same time as signs of an intermediate bearing fault were found for Turbine X, similar conditions, although less severe, were noticed on a second turbine, Turbine Y, at the same wind farm.

It can be seen from comparing Figure 34 for Turbine Y and Figure 27 for Turbine X that, prior to a communication fault, Turbine Y was showing similar levels in the axial vibration envelope. Once communication to the Turbine Y WindCon unit was restored it was clear that the turbine was following a very similar vibration trend.

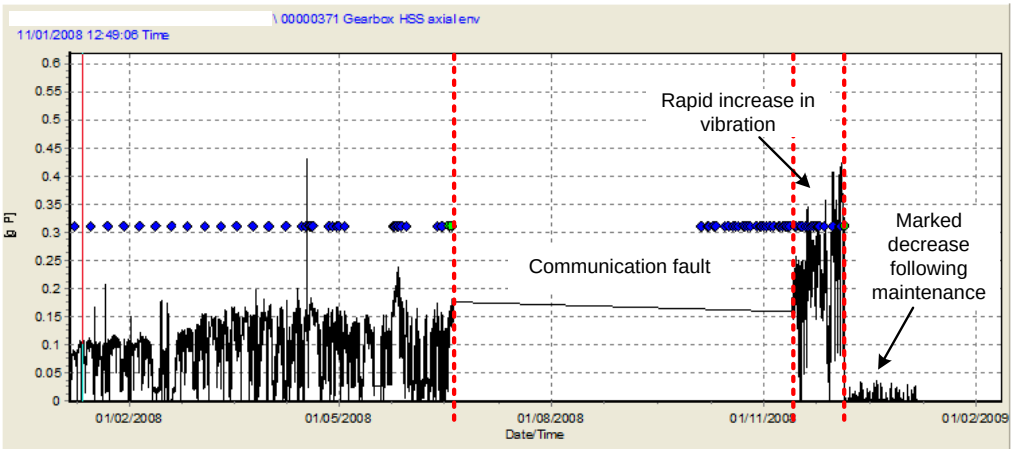

Figure 34: Turbine Y gearbox high speed shaft axial vibration envelope

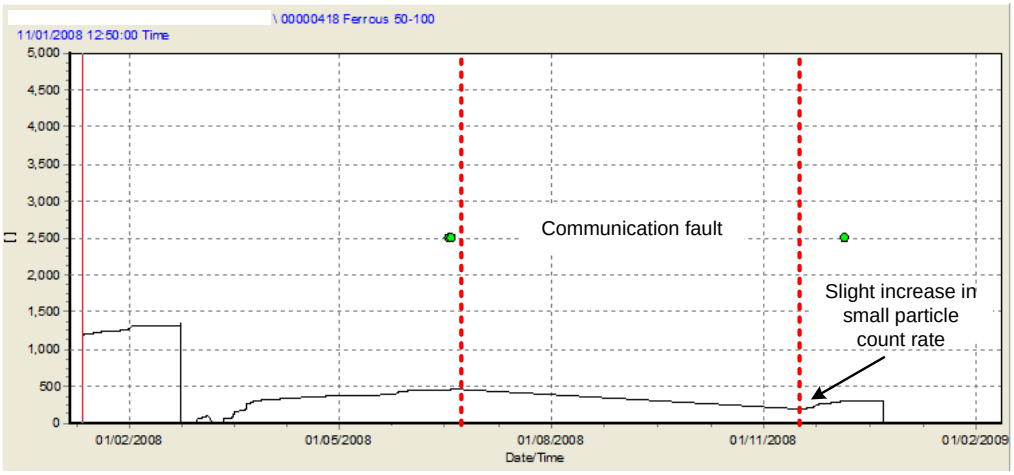

Figure 35: Turbine Y ferrous 50-100µm particle count

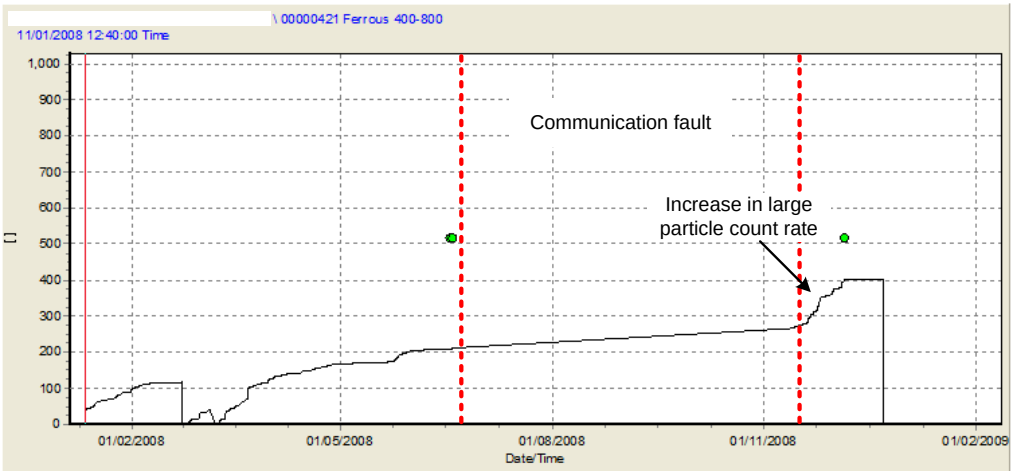

Figure 36: Turbine Y ferrous 400-800µm particle count

In this case the change in ferrous 50µm – 100µm oil debris count rate, Figure 35, was less clear than that for Turbine X however, when the Operations Group examined the counts for larger particles, for example the 400µm – 800µm count shown in Figure 36, it was clear that a large number of particles were being generated.

To confirm the diagnosis the Operations Group examined the enveloped axial vibration spectrum for fault-related harmonics to see how Turbine Y compared with Turbine X. The spectrum early in fault development is shown in Figure 37 and signs of an intermediate bearing inner race defect are already becoming apparent, the first harmonic being similar in magnitude to that early in fault development on Turbine X, Figure 30. Looking at Figure 38 recorded just prior to the bearing being replaced, it is clear that the diagnosis is correct. In particular, it can be seen that the harmonic content of the spectrum is very similar to that for Turbine X, Figure 31, except that the fault frequency and its harmonics are consistently lower in magnitude. As for Turbine X, Figure 38(a) and Figure 38(b) show the same spectrum with harmonics and sidebands respectively to avoid overcrowding the figure. This suggests that the Operations Group had been able to make the diagnosis at an earlier stage in Turbine Y and this can be seen from photographs taken of the two replaced bearings. Figure 39(a) and Figure 39(b) show the Turbine X and Turbine Y bearings respectively showing clearly that Operations Group made the Turbine Y diagnosis at an earlier stage in fault development.

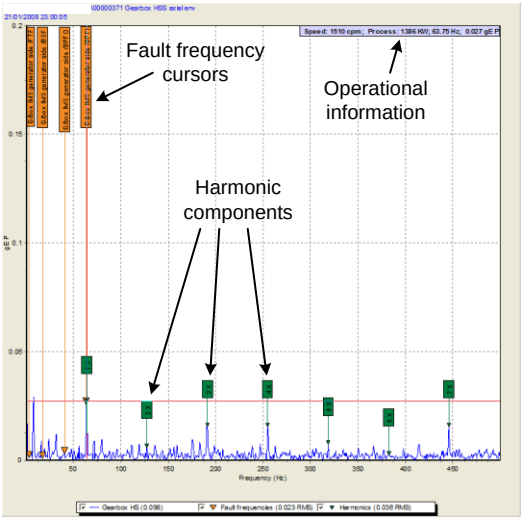

Figure 37: Turbine Y enveloped gearbox high speed shaft axial vibration spectrum early in fault development

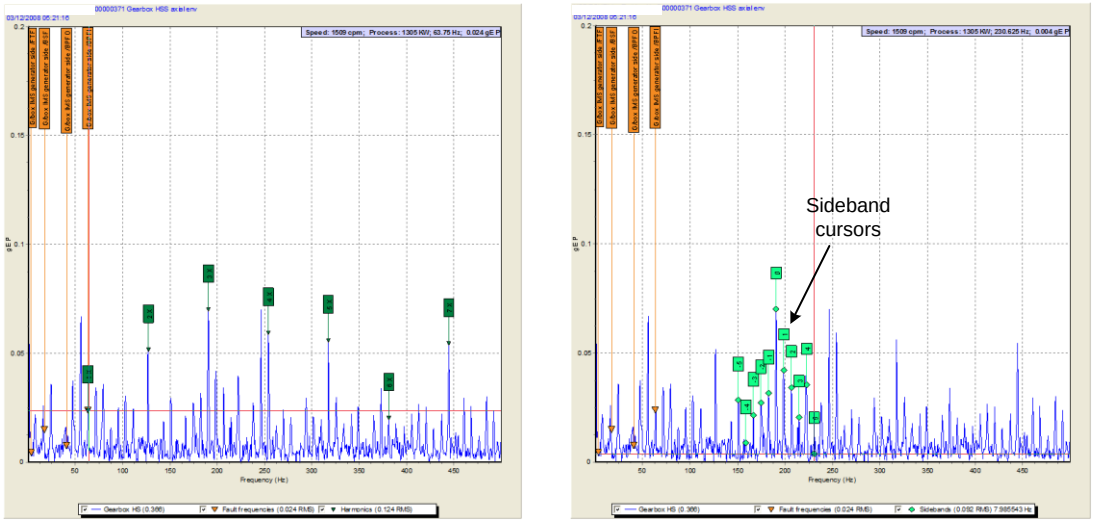

Figure 38: Turbine Y enveloped gearbox high speed shaft axial vibration spectrum at peak enveloped vibration level, around point 'A' showing four bearing cursors: (a) labelled to show harmonics; (b) labelled to show sidebands

Figure 39: Damaged intermediate shaft bearing inner races of (a) Turbine X and (b) Turbine Y

3.3.3 Turbine Z Generator Bearing Damage

Early in the monitoring campaign Operations Staff noticed that the enveloped vibration level of the generator non-drive end bearing of Turbine Z at the same wind farm was significantly higher than that for other turbines of the same type. Figure 40 and Figure 41 show two non-drive end, transverse envelope vibration signals from Turbine Z and Turbine X respectively. The Group decided that although the envelope vibration was much higher on Turbine Z, it was not changing and therefore any bearing fault was not worsening with time. However, the Operations Group decided to examine the signal in more detail to establish the extent of any fault present.

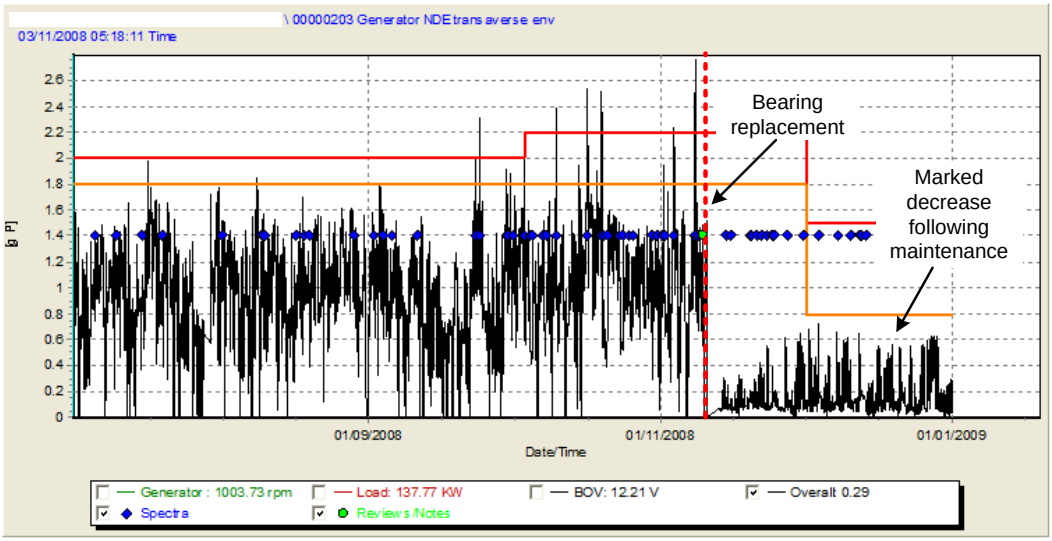

Figure 40: Turbine Z generator non-drive end bearing transverse vibration envelope

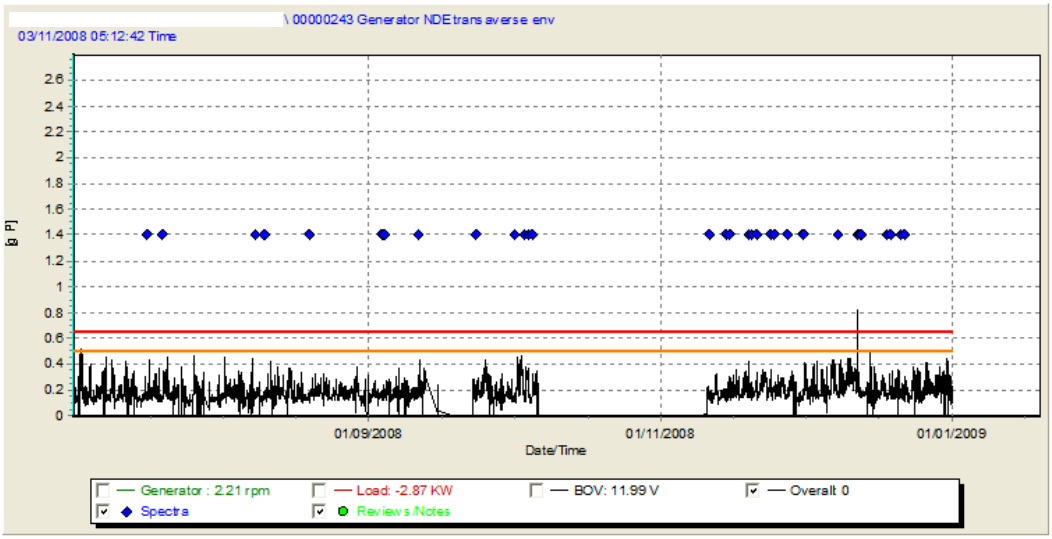

Figure 41: Turbine X generator non-drive end bearing transverse vibration envelope

The Operations Group examined Turbine Z vibration spectra to compare with Turbine X. Figure 42(a) shows the Turbine Z spectrum of enveloped generator non-drive end vibration. By including the cursors for the generator non-drive end bearing it can be seen that bearing inner race ball passing frequency and its harmonics are clearly defined suggesting an inner race defect. However, the outer race component is also visible, as are its harmonics which are shown in Figure 42(b). When compared against a spectrum from the healthy Turbine X, Figure 43, it is clear that a bearing fault is present on Turbine Z as harmonic amplitudes in Figure 42 are much higher than Turbine X, where components were barely visible.

On this basis Maintenance Management took the decision to change both the generator non-drive and drive end bearings on Turbine Z as a precaution against further damage. The result of this is clear in the time and frequency domains, Figure 40 and Figure 44 respectively. The decision to change both bearings was taken as similar characteristics were visible at both ends of the generator and because the two sets of fault frequency cursors align, due to the bearing type and generator speed being the same for both.

Unfortunately no photograph was available to show the extent of the bearing damage.

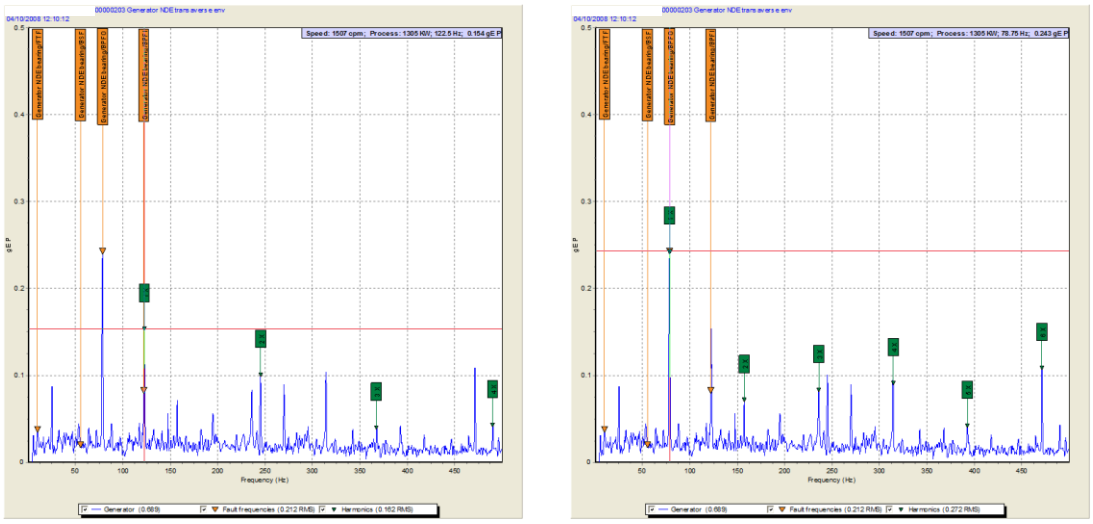

Figure 42: Turbine Z enveloped generator non drive end bearing transverse vibration spectrum at peak enveloped vibration level, showing four bearing cursors: (a) labelled to show harmonics; (b) labelled to show sidebands

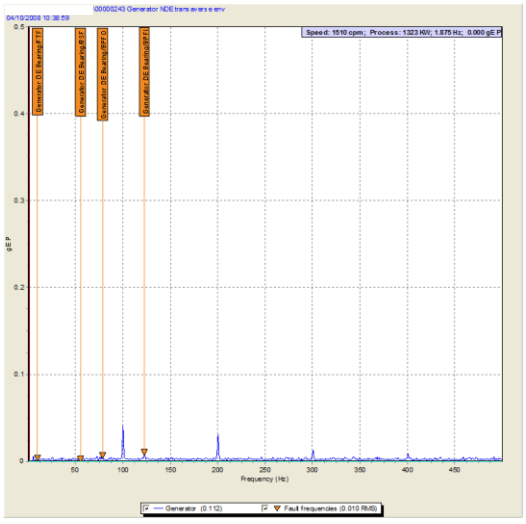

Figure 43: Turbine X enveloped generator non drive end bearing transverse vibration spectrum - healthy machine

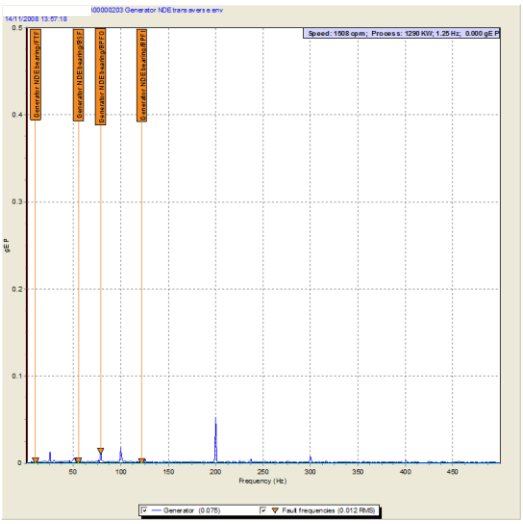

Figure 44: Turbine Z enveloped generator non drive end bearing transverse vibration spectrum following bearing replacement

3.4 Discussion

Having spent time in discussion with the Operations Group and given the example results shown here it is clear that practical CM of WTs is a viable and successful endeavour.

The Operations Group has, to date, had a positive experience in using the SKF WindCon system in the field and this appears to be for several reasons.

Firstly, the usefulness of the ProCon machine diagram. Since a WT is a complex drive train with two or three gearbox stages, slow, intermediate and high speed shafts and many different bearings, the resulting spectra from FFT analysis can be very complex, such as those in Figure 31 or Figure 38. The cursors produced by the machine diagram allow Operations Staff to pick out and identify harmonics within the spectra and relate them quickly and easily to the components which have generated them.

Secondly, the Operations Group's experience from other types of rotating machinery appears to be of great importance in that there is prior understanding of what measurement channels should be configured to allow for successful fault diagnosis.

Furthermore, the Operations Group has a clear understanding of healthy vibration levels and the need for comparison between machines of similar types. This is borne out by the Turbine Z generator bearing fault where the vibration level had not

changed but the observation that the vibration level was higher than for other machines prompted further investigation. While this may seem like a simple point it is unlikely that an inexperienced operator would notice such an indicator when operating a large number of turbines, particularly if alarm levels are configured automatically.

However, this raises an important point, which is that much of this work still has to be carried out manually by experienced monitoring engineers in order to gain confidence in a result. In each of the cases given in this Chapter, the faults were investigated manually, albeit following an alarm signal. However, if this operation is carried out each day on an increasingly large WT population, the resulting man-power costs will be inappropriate to justify WT CM. This point will be further exaggerated when considering large, offshore development where maintenance decisions will need to be made on the basis of very confident diagnoses in order to avoid large access and maintenance costs for unnecessary visits. In this case an increasing degree of automation is vital to reduce false alarms and increase confidence. There is also the issue of variable speed and load included in this point where alarm levels are not related to turbine operating condition. An example of this issue can be seen in Figure 25 where the diagnosis figure was very noisy and confidence may not be given that the signal has crossed an alarm threshold as a result of the presence of a fault or changes in operating condition. In this case, the fault was real however only further investigation was able to confirm it.

In conclusion, it can be said that WT CM has proved successful in the field when applied by an Operations Group of experienced CM engineers given the examples presented here, as faults have been detected and major failures avoided. However, it seems clear that manual analysis still holds an important role for successful detection while alarms cannot be relied upon with any great confidence. Increasing confidence in alarm signals in this noisy variable speed, variable load environment is the key to the future success of WT CM, particularly with the increasing number of turbines in need of monitoring and their installation offshore.

The author has therefore identified this as an area where research must be carried out to develop methods to successfully analyse non-stationary, variable speed and load signals generated by WTs. This is one of the focus points of the work presented in this thesis.

3.5 Time-Domain Analysis using Operational Signals

As has been mentioned, the results of analysis depend upon the careful consideration of operational parameters such as generator speed, wind speed or load. This study of the importance of multi-parameter analysis and consideration of operational parameters was carried out after the event on time domain data from the Operator's SKF WindCon system. A summary of the work is given here and more detailed information can be found in [44].

Since a WT is a variable load machine with loading almost entirely dependent on wind conditions, it is logical that signals such as oil debris particle count are unlikely to be directly related to time. For example, high load conditions over a short period would cause a step increase in the particle count rate at a given point in time while low loading or periods of no generation appear as periods of no particle generation in time. This may make time domain figures difficult to interpret as steps at high load may be read as gearbox faults causing increased particle generation.

An example of this, taken from [44], uses ferrous particle count data from an operational WT gearbox and gearbox enveloped high speed end axial vibration.

When plotted in the time domain, Figure 45, the particle count did not yield much in terms of a change to indicate a fault. However, following the event it is known that a gearbox intermediate shaft bearing fault had occurred, as depicted in Figure 32. When the debris count was plotted against the energy generated by the turbine, changes in the rate of generation of particles, the gradient, were much more visible and the figure shows a steady increase in the rate of particle generation in region 'B' compared to region 'A'.

It is clear that on its own this figure does not give the Operator grounds to carry out an inspection as it is a single signal. The author proposed that comparison between signals may produce a more conclusive result. As such, the gearbox axial enveloped high speed end vibration signals was plotted against energy generated in MWh, Figure 46.

Again, despite the changes occurring in the enveloped vibration signal, the Operator couldn't be certain that a fault was present as the signal was not being compared with another, independent signal.

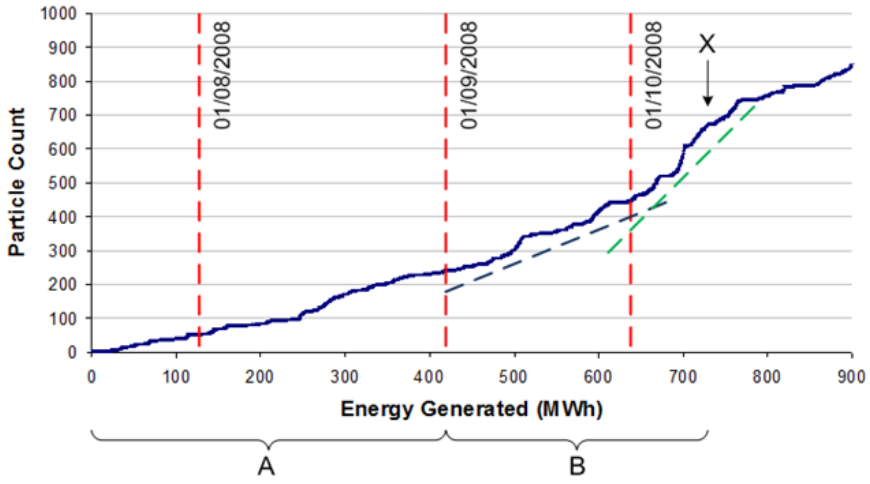

Figure 45: Gearbox oil debris particle count for ferrous 50-100µm particles in the gearbox of an operational wind turbine against energy generated

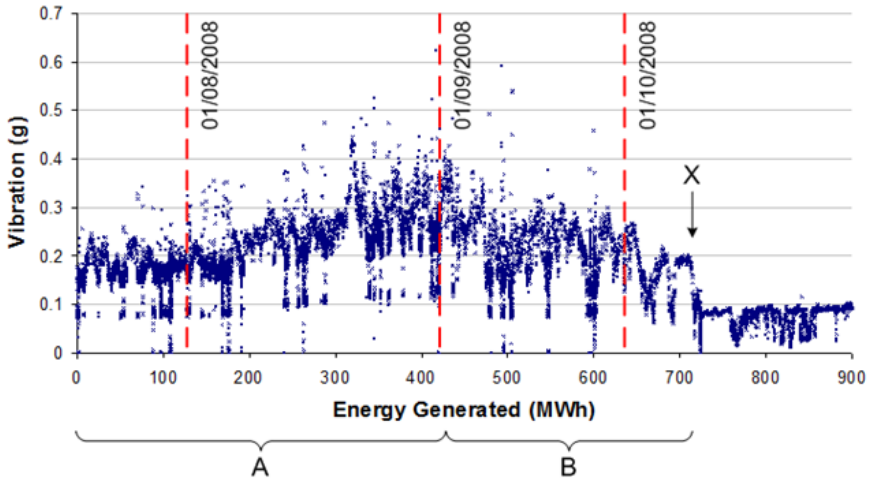

Figure 46: Gearbox high speed end enveloped axial vibration signal for the gearbox of an operational wind turbine against energy generated

If Figure 45 and Figure 46 are compared, it is apparent that the two independent signals are experiencing changes at the same position in the energy scale. During period 'A' there is a steady increase in particle count coupled with an increase in vibration. As the turbine energy passes into region 'B', the particle count rate began to rise, corresponding with a marked change in the vibration as it begins to decrease. The Operator's knowledge of bearings suggested that the reduction in vibration was a result of breakdown of the vibration transmission path due to material breakout, also explaining the increase in particle generation rate.

The gearbox bearing was inspected and replaced at point 'X' in the energy domain and a pronounced drop in vibration is seen in Figure 46. The particle count rate continues to rise for a period after bearing replacement as the new bearing took time to settle and break-in, continuing to generate particles for a short time.

This study, while brief, indicates the useful nature of multi-parameter monitoring of machines in terms of comparison of signals and analysis against operational parameters such as turbine load.

3.6 References

[39] *MasCon16, MasCon16W Manual: On-line system for continuous monitoring*, Version 1.1, Nåiden (SKF), pp1.1, 2003.

[40] McFadden, P. D., Smith, J. D., *Vibration Monitoring of Rolling Element Bearings by the High-Frequency Resonance Technique – A Review*, Tribology International, Vol. 17, Iss. 1, pp. 3-10, 1984.

[41] Feng, Y., *Novel AE Signal Processing Methods for Bearing Monitoring*, University of Leicester, May 2008.

[42] *Beurteilungsmaßstäbe für mechanische Schwingungen von Maschinen. VDI 2056*, Verein Deutscher Ingenieure, Dusseldorf, Germany, 1964.

[43] *Mechanical Vibration – Evaluation of machine vibration by measurements on non-rotating parts – Part 1: General guidelines. ISO 10816-1:1995*, International Organization for Standardization, Geneva, Switzerland, 1995.

[44] Crabtree, C. J., Feng, Y., Tavner, P. J., *Detecting Incipient Gearbox Failure in Wind Turbines: A New Signal Analysis Method for Online Condition Monitoring*, Scientific Proc. European Wind Energy Conference, Warsaw, Poland, 2010.

4 Experimental and Analytical Tools

"The true method of knowledge is experiment."

William Blake
1757 - 1827

In previous Chapters the difficulties involved in CM in the field have been noted. This is not an issue that can be easily resolved as the opportunities for testing large machines of several megawatts capacity are limited due to the scale of the test rig required. The work in this thesis is, as a result, carried out on a small scale test rig at Durham University.

The CM Test Rig at Durham has been developed over several years, initially as a test bed for slow speed rotating machines. It's conversion to a variable speed CM test rig for WTs was initiated by Michael Wilkinson, as part of his EngD research, and is described in [45] where a permanent magnet generator [46][47] was used and, later, an induction machine [45]. As part of the work presented in this thesis, the test rig was substantially modified by the author to reflect the increased volume of knowledge on CM. The test rig in its current form is described briefly in several publications including [48], [49] and [50], however this Chapter will describe in detail the current machines configuration, transducers, data acquisition and control systems including the improvements which have been made. A full specification of the test rig is given in Appendix D.

The Chapter firstly discusses the reasons for and origins of the test rig, going on to briefly describe its original configuration. Secondly, the current test rig configuration is described in detail including the machines and components as well as instrumentation and signal conditioning hardware. As has been previously mentioned, a modern, large WT is a variable speed, variable load machine and so the appropriate driving conditions derived from a detailed WT model are presented. Finally, the data acquisition and control systems are described to give a complete picture of the test rig, its function and its operation.

4.1 Introduction

4.1.1 Justification

There are significant issues associated with experimental research on operational WTs, largely as a result of constraints from OEMs .

As has been briefly mentioned in Chapter 2, WT OEMs are reluctant to allow Owner Operators to fit their own CMSs to turbines during the warranty period. This is primarily because the OEM is responsible for monitoring and maintenance of the turbine during this period and wishes to have a CMS which is developed with and approved by them. There is also a degree of confidentiality with regard to any failures occurring during the warranty period that influences their decision. It is clear from this position on commercial CMSs that the installation of non-commercial, bespoke data acquisition hardware on a turbine within its warranty is not recommended.

Following the warranty period CM responsibilities will fall to the Owner Operator, unless they sub-contract the work to a specialist monitoring body. In this case there are still confidentiality issues associated with data collection and analysis as an Owner Operator is unlikely to want information on failures or downtime to be widely known to their competitors.

However, in the event that an Owner Operator allows the installation of a data acquisition system for research, there is the major issue of accessibility given that many new, large turbines are situated in remote locations. This is likely to be an issue where large volumes of high frequency data are being recorded and cannot easily be transmitted via a remote communications network.

The final major restriction on experimental CM in the field is the certainty of obtaining useful data. If a system is installed on a single turbine it is likely to record large amounts of data during which no faults are present. In fact, there is a great risk that no faults will occur and the system will simply be overrun with data.

The combined result of these issues makes the idea of experimental monitoring in the field a difficult and impractical task, however desirable it might appear. However, a bespoke data acquisition system has been designed and built by a Supergen Wind partner, Strathclyde University, with the aim of acquiring data from an operational WT. The system is installed on a Vestas V47, 660kW turbine at Scottish

Power's Hare Hill wind farm in Scotland. As expected from the discussion above, the turbines are out of their warranty period, having been installed in 2000, and as a consequence are smaller machines than those currently being installed.

The Durham test rig was conceived as a facility for the creation of signals comparable to those encountered on a WT where fault-like conditions could be implemented repeatedly and under controlled conditions. Then, algorithms could be developed using these fault-like conditions in the controllable laboratory environment. Confidence should then be increased when applying these algorithms to field data from operational WTs, reducing uncertainty and risk in applying CM techniques automatically in the field.

4.1.2 Introduction to the Test Rig

Figure 47 shows a schematic diagram of the CM test rig in its current configuration.

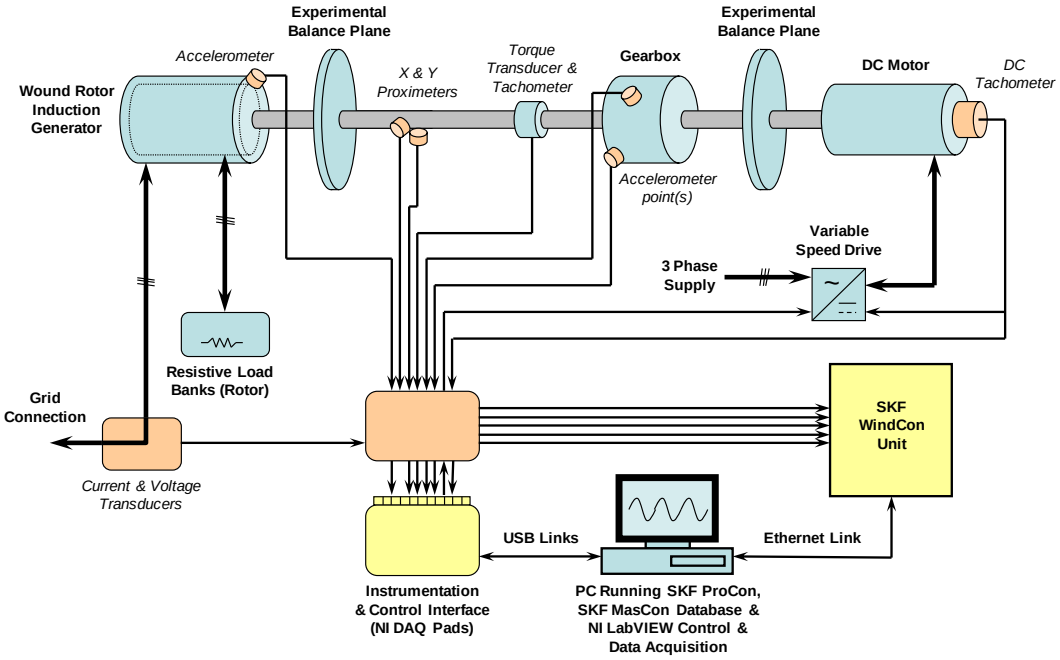

Figure 47: Schematic diagram of the condition monitoring test rig

The initial focus of this research was the design and implementation of a refined test rig for use throughout this thesis and it is this rig that is the focus here. The test rig was also implemented with an SKF WindCon 3.0 CMS for future comparison with industrial data and results. To give an idea of the physical size of the test rig,

Figure 48 shows two photographs of the test rig for comparison with the schematic diagram.

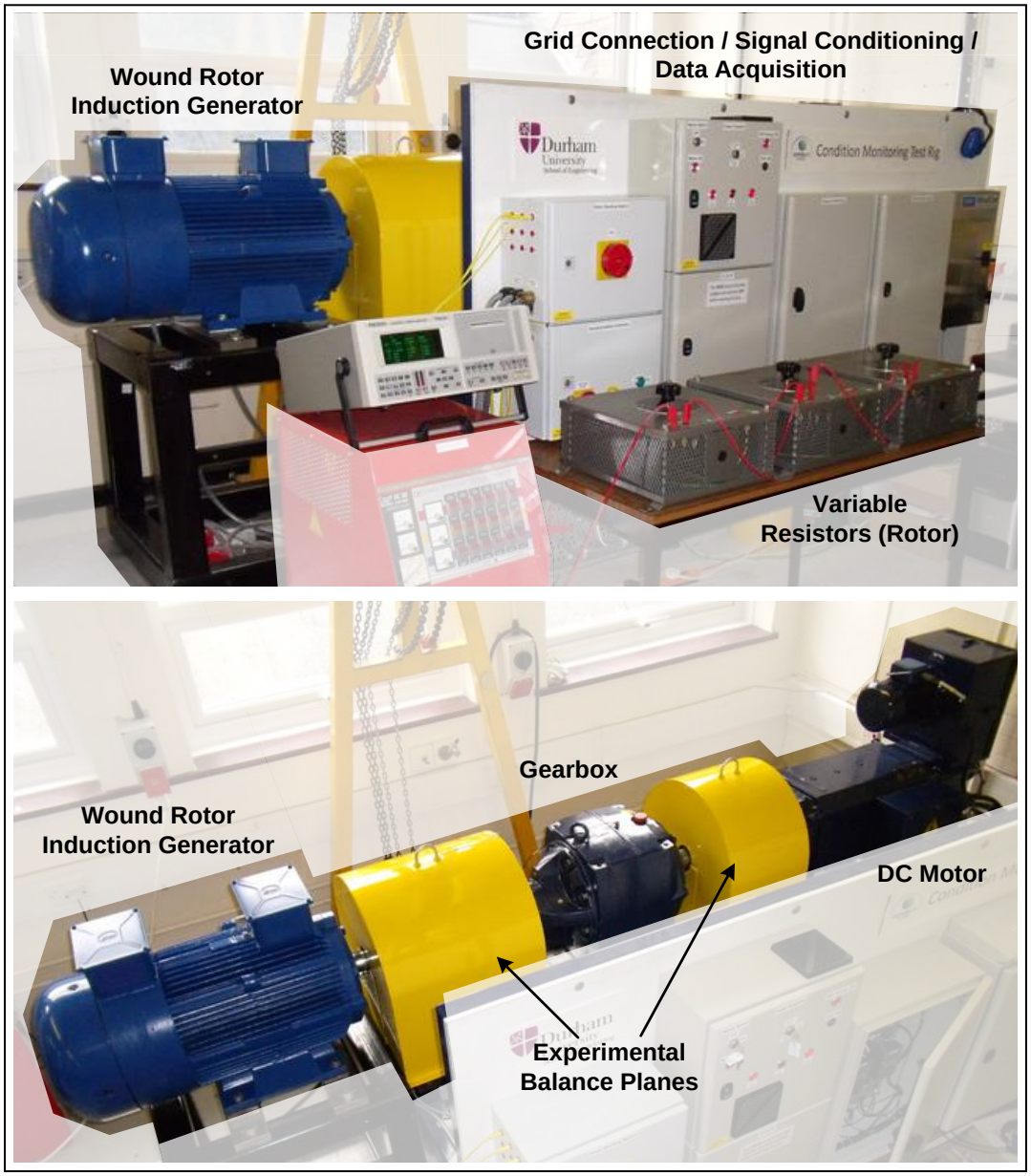

Figure 48: Annotated photograph of the condition monitoring test rig

A summary of the main test rig components is given in §4.2 to §4.4 and specifications of components are given in Appendix D. In summary, the test rig comprises a 4-pole, 30kW wound rotor induction generator driven through a 5:1 gearbox by a 54kW DC motor. The speed of the driving motor is controlled through a variable speed drive, either manually or remotely using a National Instruments LabVIEW environment, allowing the test rig to be driven under either constant or

variable, transient conditions. The wound rotor induction generator can be synchronised with the grid through a contactor circuit.

Signals from transducers positioned along the drive train are transmitted to two National Instruments data acquisition pads (DAQ pads) which are in turn connected by USB connection to the LabVIEW control and data acquisition environment. Certain signals, discussed later, are instrumented with signal conditioning circuitry in order to remove noise artefacts generated from the laboratory environment. All signals can also be connected to the SKF WindCon system.

Fault-like conditions can be induced or removed from the drive train as required enabling several electrical and mechanical fault conditions to be emulated on demand.

While the test rig is not by any means a replica of a WT drive train, it contains similar components and characteristics including low and high speed shafts, a gearbox, grid connection and flexible foundations.

In essence, the test rig is designed to produce signals with characteristics similar to those encountered on operational WTs.

4.2 Mechanical and Electrical Components

The test rig drive train consists of a number of mechanical and electrical components which are described here to give a complete view of the drive train configuration.

4.2.1 Induction Generator

The generator used is a 4-pole, 30kW, wound rotor induction generator (WRIG) by Marelli Motori. The most favoured machine on modern WTs with ratings in excess of 1MW is currently the doubly-fed induction generator (DFIG) [51], which is based on the WRIG. However, it requires complex operation and control systems. In order to gain a good grounding in monitoring it is sensible to begin with a more simple machine layout and so the wound rotor machine is operated with a resistive load bank connected to the rotor circuit rather than as a fully controlled DFIG.

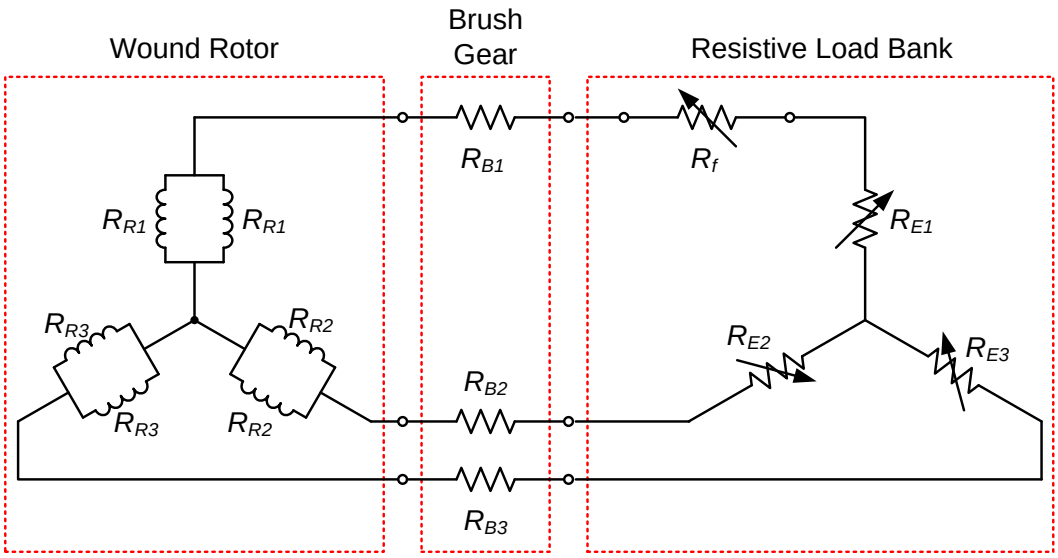

Figure 49: Generator rotor circuit diagram

The rotor circuit of the WRIG is shown in Figure 49. There are two reasons for including rotor external resistors on the rotor circuit rather than shorting the rotor circuit and using the machine as a squirrel cage induction generator.

Firstly, the external resistors allow the balanced phase resistance of the rotor to be increased. The rotor itself has a resistance on 0.06Ω per phase and as a result the possible slip speed variation is very small, given the limitations of the driving motor. A balanced rotor phase resistance of 1.3Ω is used throughout this thesis as this allows a super-synchronous speed variation of 100rpm (1500-1600rpm) before the driving DC motor armature current limit is reached. If was felt that a speed range of 100rpm was sufficient to allow realistic speed variation to challenge and test signal processing techniques. From Figure 49, the balanced rotor phase resistances are given by:

$$R_{1_H} = \frac{R_{R_1}}{2} + R_{B_1} + R_{E_1}$$

$$R_{2_H} = \frac{R_{R_2}}{2} + R_{B_2} + R_{E_2}$$

$$R_{3_H} = \frac{R_{R_3}}{2} + R_{B_3} + R_{E_3}$$

where

$$R_{1_H} = R_{2_H} = R_{3_H}$$

$$R_{R_1} = R_{R_2} = R_{R_3} = 0.12\Omega$$

Secondly, the external resistors allow rotor electrical asymmetry to be introduced or removed as required for fault testing. Rotor electrical fault conditions used in this thesis are discussed in §6.1.1.

4.2.2 Gearbox

The gearbox is a Hansen two-stage, parallel shaft, helical unit with exact ratio 4.9894:1 between input and output shafts, referred to as 5:1 for simplicity. Detailed information can be found in [52] and [53]. As shown in Figure 50, the high speed pinion is mounted on the output shaft of the gearbox, shaft 3. The gearbox construction allows this shaft and pinion to be removed as one assembly without the need to remove the complete gearbox from the test rig. It was therefore chosen for experimentation.

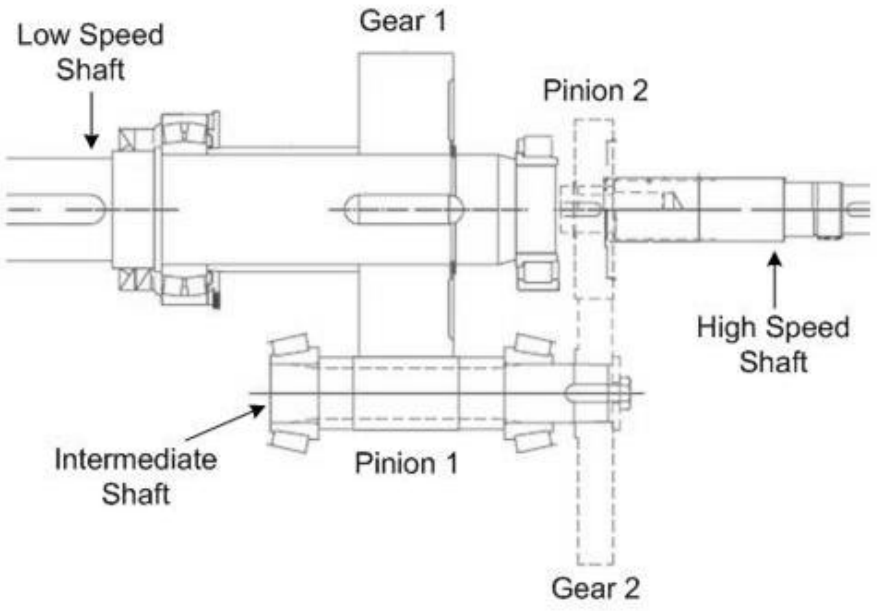

Figure 50: Gearbox components including high speed shaft and pinion on the right

While the investigation in this thesis incorporates faults onto the high speed pinion, it will be referred to as the high speed gear throughout.

To allow the investigation of gear tooth damage, a replica gear was manufactured externally to exactly replace the original Hansen gear. The original gear and high speed assembly and its removal are shown in Figure 51(a) and Figure 51(b)

respectively. Part of the internal gearbox structure is shown in Figure 52. The gear case is particularly rigid, as can be seen from the significant internal webbing in Figure 52. Coupled with the relatively low load that is transferred by the gearbox, it is likely that the case will not vibrate to any great extent, potentially hindering fault detection.

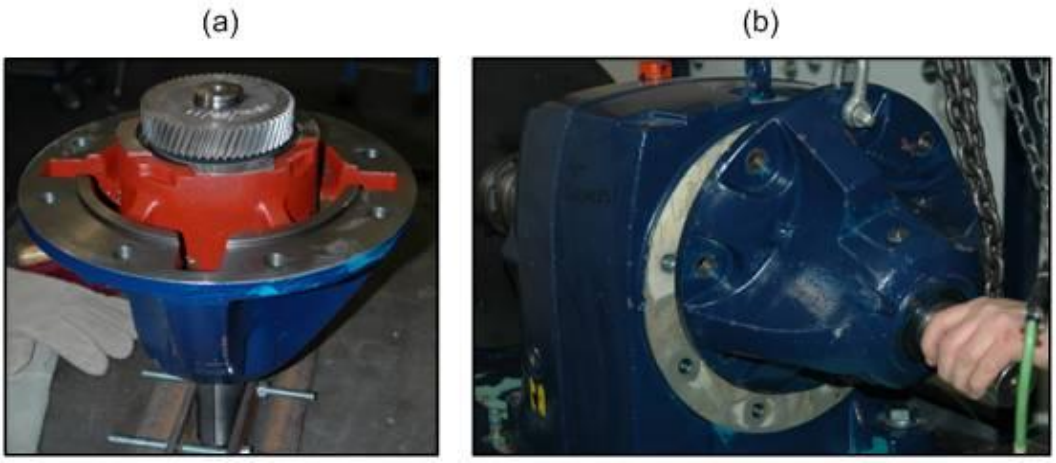

Figure 51: Gearbox showing (a) high speed shaft and pinion assembly with original Hansen gear and (b) its installation

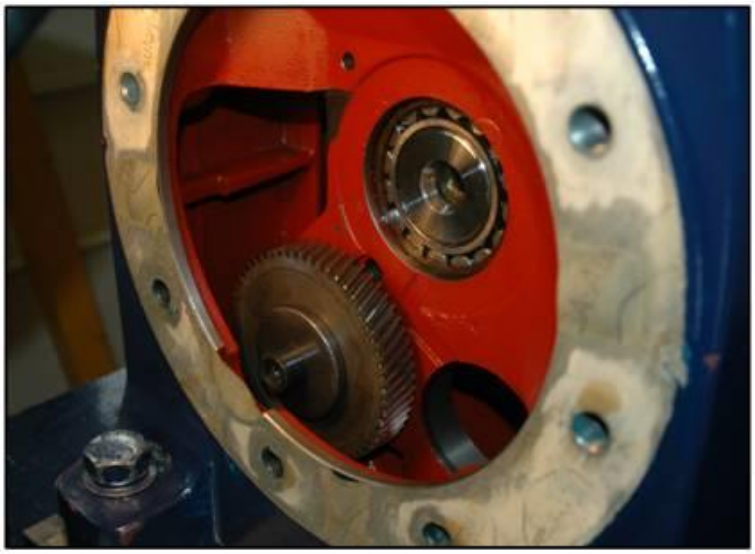

Figure 52: Internal construction of the 5:1 gearbox with high speed shaft and pinion assembly removed showing the substantial, cast structural internal webbing of the gearbox

4.2.3 Torsional Characteristic and Response

During the course of this thesis, several researchers have been involved in the development of a test rig model, under the same supervisor as the author and at the direction of the author.

In 2008 a three-degree of freedom model study [52] was carried out by an MSc student, Hsu Wen-Ko, to model and examine the torsional response of the test rig. The overall test rig configuration has remained unchanged from that used in his report [52].

Constants such as the wound rotor induction generator, DC motor and gearbox lumped inertias could be calculated to a reasonable accuracy from machine drawing data however some parameters, particularly shaft stiffness and damping, were not known or directly measurable. Tests were carried out by the author to allow the model to be compared to the physical response of the test rig to step speed demands. Values for stiffness and damping were calculated by the student [52] based on dynamic responses to different step inputs.

However, it was felt that verification of the model through testing was required and so a simple, repeatable rotational frequency characterisation test was developed by this author.

In order to excite torsional frequencies encountered during normal operation, the DC drive was controlled to run the test rig steadily through high speed shaft speeds of 0-2000rpm, the extremes of normal operation. The ramped speed profile is shown in Figure 53 and the resulting high speed shaft torque spectrum is shown in Figure 54. Several natural frequencies were observed, specifically 0.35Hz, 2.01Hz and 121.1Hz, corresponding closely to results from the test rig model in the report by Hsu Wen Ko [52]. The report [52] concluded from sensitivity analysis that the 2Hz component depends on the generator inertia and high speed shaft stiffness while the 121Hz component is linked to the low speed shaft stiffness and the gearbox inertia. No conclusions were reached as regards the 0.35Hz component as the model was limited by a fixed boundary condition.

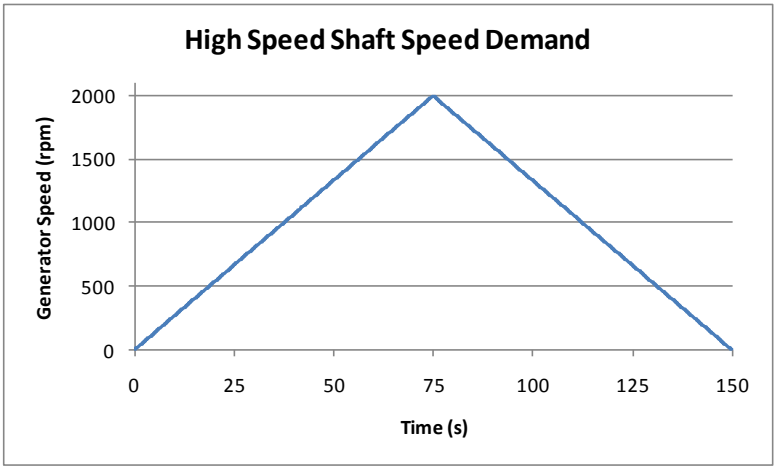

Figure 53: High speed shaft speed demand for torsional characterisation

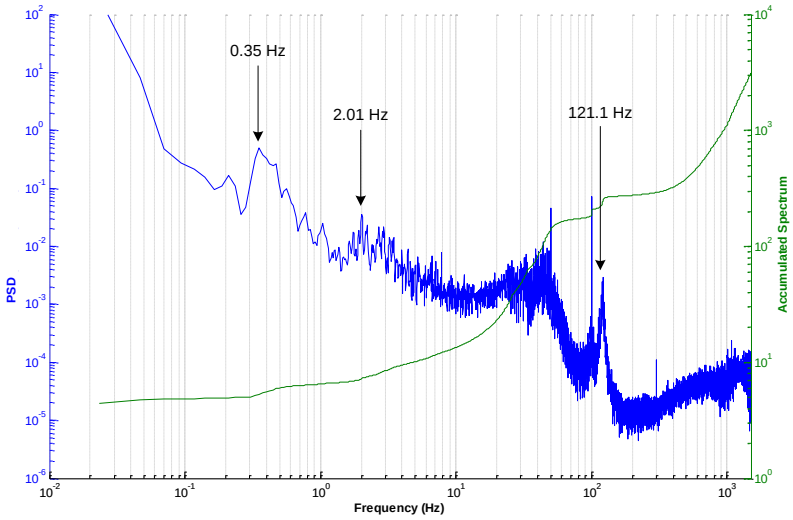

Figure 54: Power spectral density resulting from Figure 53 driving

The test rig model was further developed by undergraduate MEng student Julian Emslie in 2009/2010. Again, tests were carried out by this author to allow a study of the time domain response of the test rig. It was discovered during this study that the time domain response and some parameters in the earlier model were uncertain so further investigation was required. The updated model, described in Emslie's report [53], included the controller of the DC machine due to its significant influence on the time domain response of the test rig. In particular, the model complexity was increased to five-degrees of freedom, including the gearbox tooth compliance and backlash.

Results from the report [53] show that a reasonable time domain response for both torque and speed was achieved. The torsional time domain response is shown in Figure 55, however the torsional frequency domain response was not investigated.

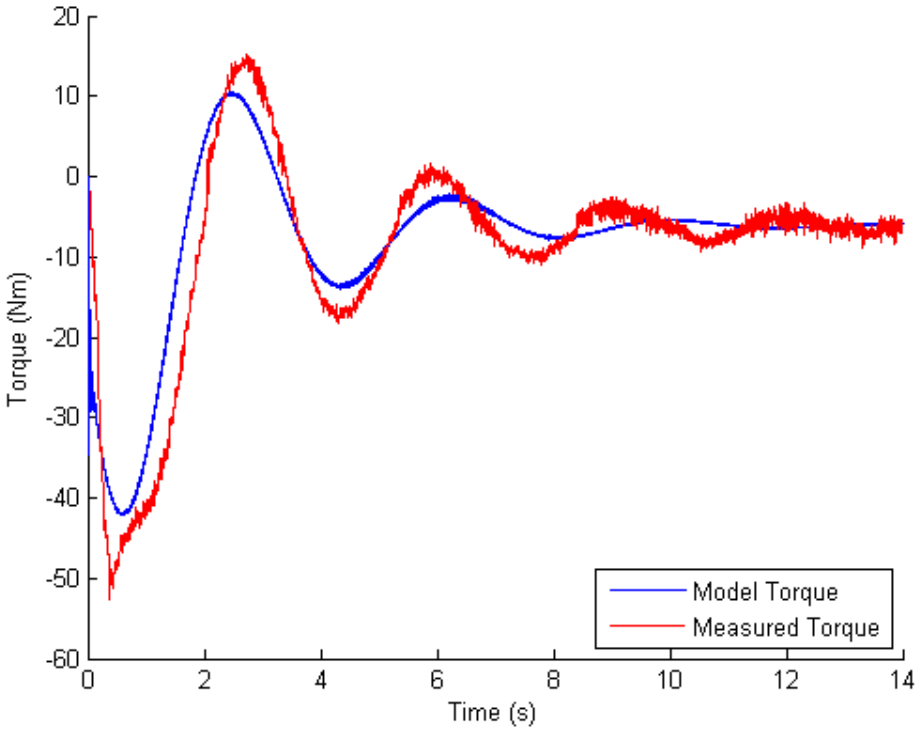

Figure 55: Comparison of model and test rig time domain torque responses [53]

Current MATLAB SIMULINK model development is being carried out by Mahmoud Zaggout, a PhD student in the School of Engineering. This work focuses on detailed modelling of all components in the test rig and, as such, measurement of many parameters was required. At the time of writing the model comprises:

- Electro-mechanical wound rotor induction generator model
- Electro-mechanical DC motor model
- DC motor PI controller/drive with control loop to match rig
- Gearbox model including gear tooth meshing and backlash
- Grid connection
- Time variable speed control and grid synchronisation

With this author's assistance, various tests were carried out to verify the model at each stage of its development. Again, step tests were carried out to examine the time domain response of the model against the physical test rig. Most recently, a test

programme was devised to show both the test rig and model moving through different stages of the same operation cycle. The cycle included a rapid speed increase up to synchronous speed followed by a settling time before the grid synchronisation occurred. Step speed changes were made with the generator connected to the grid before the grid was disconnected and the machine run down. At the time of writing, the model time domain response was that shown in Figure 56, produced by Mahmoud Zaggout [54]. Figure 56(a) and Figure 56(b) show, respectively, the generator speed signals and high speed shaft torque signals.

Several observations can be made from Figure 56. Firstly, the simulated speed signal high very close correlation with the measured signal except at grid synchronisation. This may be as a result of the response time of the transducer or the frequency to voltage conversion.

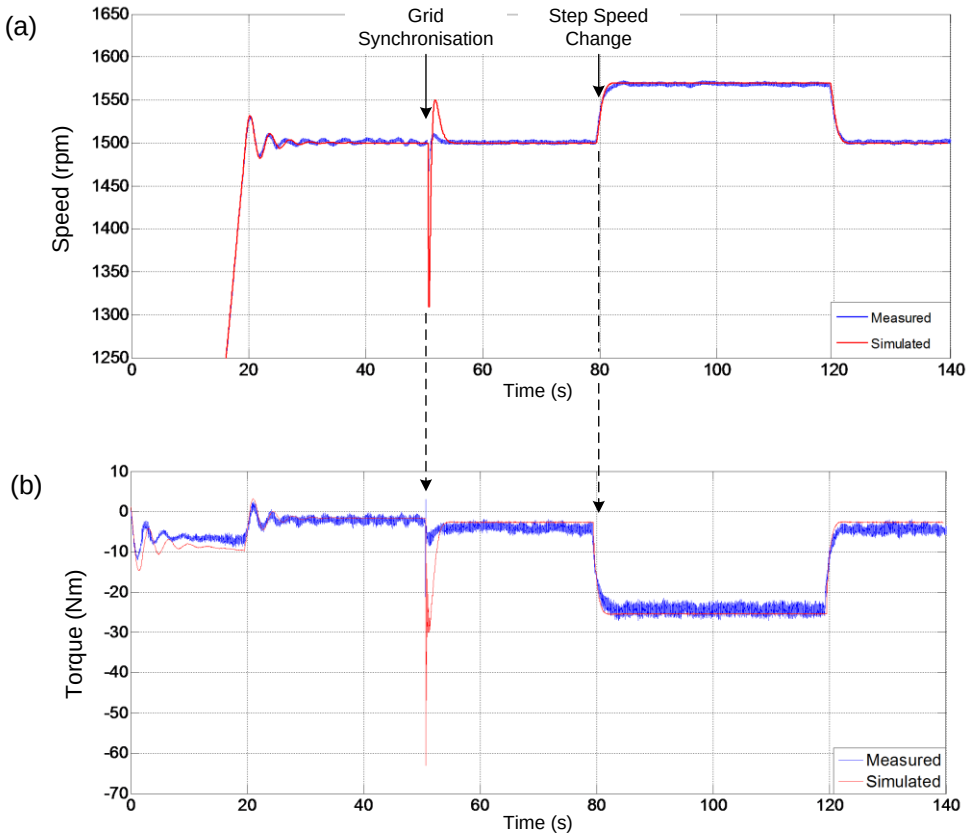

Figure 56: Time domain response of a model of the Durham test rig

Secondly, the torsional response of the signal is also accurate. There is a clear discrepancy during the early part of the test, while the machine is running up to synchronous speed however this may not be too serious due to the small torque

magnitude. Once again, a discrepancy is observed at grid synchronisation. In this case, the error is known to be due to the frequency cut-off of the torque transducer low pass filter. Experimentation with the transducer's settings demonstrated this to be the case however the overall background noise level of the signal was significantly increased causing a loss in other, more useful information.

However, it is clear that the characterisation and parameter measurements made under the author's guidance have allowed the model to accurately emulate test rig time domain behaviour.

Most recently, the model has been tested in the frequency domain to examine its torsional response and compare it with the test rig response. The model was driven with the run up, run down characteristic given in Figure 53. Both the test rig response and model response are shown in Figure 57. It is clear that the model has now achieved good accuracy in both the torsional time and frequency domains with peaks corresponding closely for between the model and physical test rig.

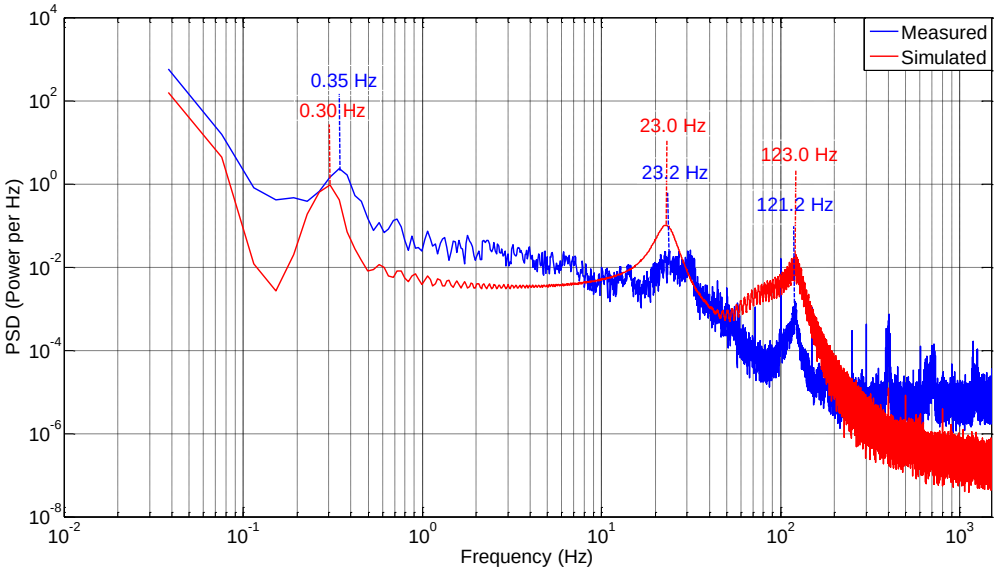

Figure 57: Frequency domain comparison of the torsional responses of the test rig and model driven by run up, run down conditions in Figure 53

While these results are not directly linked to this thesis, it is important that the test rig can be characterised and modelled to ensure that tests are being carried out under comparable mechanical conditions.

4.3 Instrumentation and Control

The original test rig instrumentation, described in [45], was deemed suitable for use in this research however a major project was undertaken as part of this research to refine the instrumentation and control systems and reconfigure the test rig to be more robust but adaptable. This project, coordinated by the author, aimed to isolate instrumentation for different test rig functions to minimise experimental noise and improve the quality of the signals recorded by the data acquisition system. The final system layout of the instrumentation is shown in Figure 58 and is logical given the nature of the machines and requirements of instrumentation. It also resulted in improved safety for the operator as mains voltage and current systems were isolated in separate cabinets to low voltage control and instrumentation systems. In order to reduce electrical noise from the laboratory environment, all instrumentation is isolated from mains voltage electrical signals and power supplies by steel cabinets.

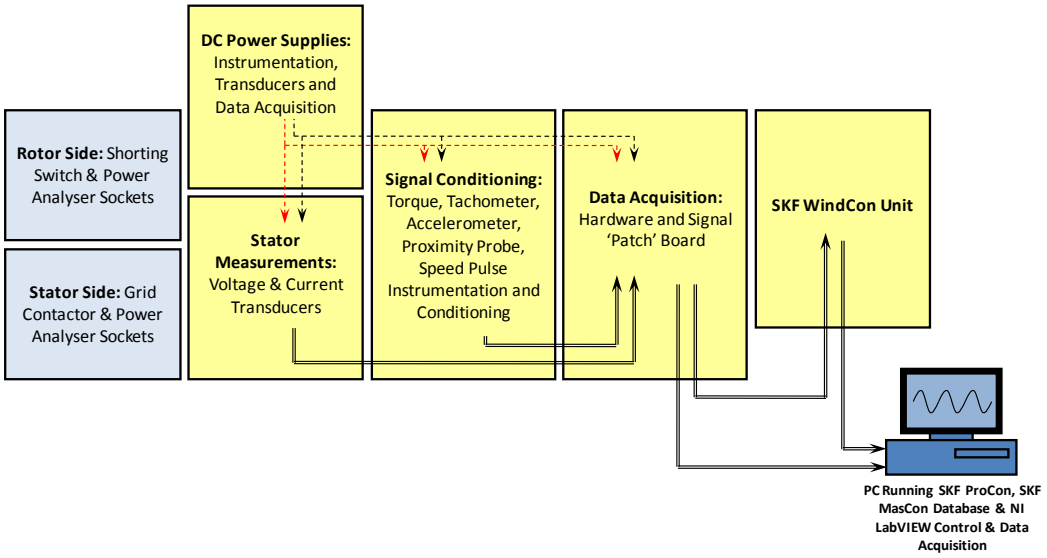

Figure 58: Physical layout of test rig instrumentation as shown in photograph, Figure 48

The transducers, signal conditioning, data acquisition and driving conditions are described in this section, including a brief description of a recently installed SKF WindCon monitoring system.

4.3.1 Transducers and Signal Conditioning

As seen from Figure 47, there is a wide range of transducers and instrumentation applied to the test rig. A number of signals required an amount of signal condition for either data acquisition or noise reduction purposes.

4.3.1.1 High Speed Shaft Tachometer

The high speed shaft is instrumented with a Magtrol TMB 313 torque transducer, capable of outputting a 60 pulse per revolution. Although the LabVIEW control environment could be adapted to perform a digital to analogue conversion for speed, it was felt more appropriate to carry out the conversion in hardware. A frequency to voltage converter was implemented giving linear operation over the required speed range. Additionally, a frequency divider circuit was included to ensure the speed pulse signal was within range for the SKF WindCon digital input.

4.3.1.2 High Speed Shaft Torque

Early examination of the torque signal suggested that there was significant noise being picked up by the torque transducer cabling and data acquisition hardware. Although instrumentation was cased in steel cabinets, a low pass filter to remove high frequency noise was designed. Frequency analysis showed significant noise above 4kHz so this was set as the cut-off frequency. A clear improvement was seen in the quality of the torque signal. The transducer itself has an internal low pass cut-off frequency of 40Hz so the 4kHz filter did not significantly change the overall signal.

4.3.1.3 DC Motor Tachometer

In addition to noise at high frequencies, the signal from the DC tachometer, which is a simple DC generator, included a large amount at low frequencies due to its commutation noise. Since this tachometer is primarily for reference rather than analysis, it was felt appropriate to heavily filter the signal with a 20Hz low pass filter.

4.3.1.4 Accelerometers

Two Bruel and Kjaer accelerometers are available on the test rig and can be placed at various points on either the gearbox or generator. These transducers do not require any additional signal conditioning apart from their standard charge amplifiers.

For the high speed shaft unbalance experiments in Chapter 6, accelerometers are positioned on the generator drive-end bearing end shield and gearbox high speed end gear case. Both accelerometers are mounted vertically, at positions radial to the shaft.

4.3.1.5 Shaft Displacement Transducers (Proximeters)

The high speed shaft is instrumented at the generator end with vertical and horizontal Kaman proximeters measuring the shaft displacement. Once again, these eddy current sensors do not require additional signal conditioning other than their standard charge amplifiers.

The absolute shaft displacement, $d(t)$, is used in this thesis rather than the vertical, $v(t)$, and horizontal, $h(t)$, components of vibration, where the absolute displacement, $d(t)$ is calculated from the orthogonal time vectors $v(t)$ and $h(t)$ as:

$$d(t) = \sqrt{v(t)^2 + h(t)^2}$$

4.3.2 Control and Data Acquisition

The test rig is controlled from a National Instruments LabVIEW environment developed from that described in [45]. The environment allows the operator to run the machine to its synchronous speed before waiting for confirmation of grid connection. Once the operator confirms grid synchronisation the machine is run up to the test starting speed at which point data acquisition begins.

The driving conditions are read from a spreadsheet containing a time and speed vector as defined by the operator. The control environment then transmits a control signal, 0-10V proportional to speed demand, to the Eurotherm variable speed DC drive in real time.

The data acquisition aspect of the control environment runs in parallel with speed control at a defined sampling frequency. A sampling frequency of 5kHz is used throughout this thesis. The DAQ pads sample 500ms of data from each channel at 5kHz before transmitting the packet via USB to the data acquisition environment. Data is saved to a temporary file that is converted to a comma-separated variable at the end of data acquisition.

The environment is configured to record 15 data channels as listed below:

- Timestamp
- DC motor speed (§4.3.1.3)
- High speed shaft speed (§4.3.1.1)
- High speed shaft torque (§4.3.1.2)
- 3 x stator phase voltage waveform
- 3 x stator line current waveform
- Vertical and horizontal shaft proximeter
- 2 x accelerometer
- DC motor armature current

The test rig is operated such that tests are carried out for each healthy or faulted condition for each driving condition. The driving conditions are described in §4.3.4.

4.3.3 SKF WindCon 3.0

A WindCon 3.0 system, the same as that examined in Chapter 3, has recently been installed on the Durham test rig under the direction of the author. While it is not used for analysis purposes in this work, having been installed towards the end of this research, it is worth noting its presence. The system is currently being investigated by another PhD student at Durham.

The system is configured to record:

- Timestamp
- High speed shaft speed (digital)
- High speed shaft torque (§4.3.1.2)
- 1 x stator line current amplitude
- Vertical and horizontal shaft proximeter
- 2 x accelerometer
- DC motor armature current

Just as in the commercial system described in Chapter 2, a machine diagram, Figure 59, has been incorporated to aid analysis and diagnosis in the future. The system records time series data at 10s intervals and records spectra from the vibration signals at regular intervals.

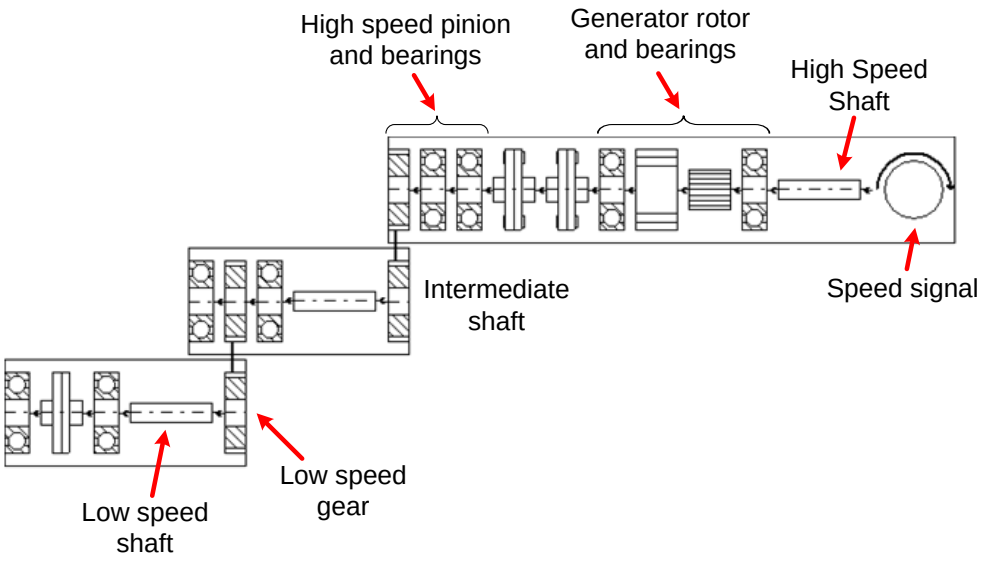

Figure 59: SKF WindCon 3.0 machine diagram of the Durham test rig including main components of interest

4.3.4 Driving Conditions

The test rig can be controlled at either constant or variable speed depending on the user's requirements. While a number of different constant speed and variable speed driving conditions were available, the results in this thesis are limited to two variable speed driving conditions representing known WT driving conditions. The number of different driving conditions was kept to a minimum to reduce the volume of data recorded. The two conditions selected for testing were:

- 7.5m/s mean, 6% turbulence intensity
- 15m/s mean, 20% turbulence intensity

The turbulence intensity, I, is defined in [55] as:

$$I = \frac{\sigma}{\overline{U}}$$

where σ is the standard deviation of variations in wind speed about a mean wind speed, $\overline{U}$. In practice, the mean wind speed is generally taken as the mean speed of a 10 minute period.

The data was produced from a WT model developed by the University of Strathclyde as part of the Supergen Wind Energy Technologies Consortium. A highly detailed 2MW exemplar turbine model was created and wind speed profiles, as listed

above, input to the model. The final driving conditions were scaled to the test rig based on the generator speed data from the model.

These two conditions represent a low mean wind speed, below turbine rated speed, with low turbulence and a high mean wind speed, above turbine rated wind speed, with high turbulence, Figure 60 and Figure 61 respectively. Further to this, the Strathclyde model configuration results in these two conditions being effectively in the turbine's generator control and speed control regions respectively. Each healthy and faulted test is run for 150 seconds using a segment from the 450s driving profile, as indicated in the figures.

Variable speed machine testing has not been widely reported in literature so this work is largely new and independent. The use of more than one variable speed driving condition is also essential to the testing of algorithms developed later in this thesis.

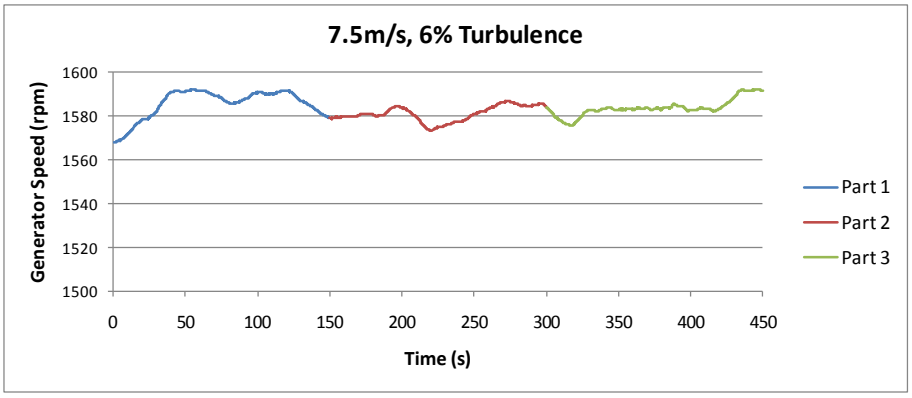

Figure 60: Driving condition based on 7.5m/s, 6% turbulence data

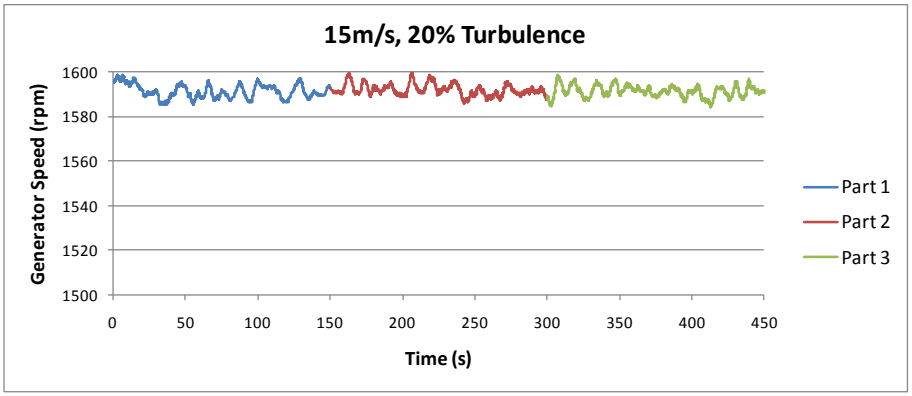

Figure 61: Driving condition based on 15m/s, 20% turbulence data

4.4 Test Rig Faults

The purpose of the test rig was to produce signals of similar noise, variability and frequency content as those encountered on operational WTs. To do this, fault-like conditions can be induced which, while not exact replicas of faults, produce similar responses in the system. Wilkinson [45] called these "fault-like perturbations". Signal processing techniques can subsequently be applied to these noisy, variable signals to investigate and test fault detection algorithms.

4.4.1 Rotor Electrical Asymmetry

A large volume of work has been published over the last 20 to 30 years on the detection of rotor faults in induction motors. Works including [57], [58] and [59] focussed on the characteristics of rotor bar failures in squirrel cage induction motors and the development of motor current signature analysis (MCSA) methods for fault detection in the frequency domain [59]. The focus of work has expanded into the detection of other induction motor faults using MCSA including motor bearing failure [60][61], air-gap eccentricity [61] and static and dynamic eccentricity [62]. It has been suggested that, while stator current monitoring has proved successful, monitoring the instantaneous power signal may be a viable alternative [63]. Instantaneous power was proven to be a suitable signal for WT fault detection in a paper by Caselitz and Giebhardt [64] where rotor unbalance faults were successfully detected on an operational 33kW machine.

There are a number of conflicting arguments as to whether current or power analysis is preferred. One of the major advantages of current monitoring is the ease of access to and wealth of literature available on the detection of various faults, such as listed above. However, it has been suggested that monitoring line or phase current only gives information about the specific phase or line under analysis while total power can offer an equal contribution from all phases. In [65] a brief discussion of the advantages and disadvantages is given. One disadvantage of power monitoring is the increased number of transducers required compared to those required for current monitoring. As a result, care must be taken to minimise measurement errors that will be compounded by the power calculation. However, [65] shows that the total instantaneous power yields a higher spectral content than the current during fault conditions as well as removing the intrusive 50Hz component that dominates the current spectrum. In addition to these measurement-orientated points there will be others that can be

brought out to defend either current or power as the most appropriate measurement. However, it is likely that best method for a given situation will remain the choice of the engineer based on their requirements.

The previous references focus on the detection of known fault frequencies in the current or power signal, as does this thesis. However, in previous work, only steady state machine operation was considered and, as previously mentioned, this is not the case with WT generators.

In this thesis, rotor asymmetry was applied to the test rig induction generator by means of external variable resistors connected into the rotor circuit via the machine slip rings. The original test rig used switched load banks for this however fully variable, 0-4Ω resistors were introduced to allow smaller asymmetry to be introduced in a more controllable fashion.

Rotor electrical asymmetry was introduced when the faulted resistance, R_f, is greater than zero so, assuming the fault to be in phase 1 of the three-phase rotor circuit, the faulted phase resistance is given by:

$$R_{1_f} = R_{R_1} + R_{B_1} + R_{E_1} + R_f$$

Since the rotor is STAR connected, the absolute rotor asymmetry in this case is given by:

$$\delta R = \left| R_{1_f} e^{i\theta_1} + R_{2_H} e^{i\theta_2} + R_{3_H} e^{i\theta_3} \right|$$

where $\theta_1 = 0,\ \ \theta_2 = \frac{2\pi}{3},\ \ \theta_3 = \frac{4\pi}{3}$.

For clarity, the rotor resistance is given as a percentage of the balanced phase resistance so that the rotor asymmetry, ΔR, in percent, is given by:

$$\Delta R = \frac{\delta R}{R_{1_H}} = \frac{\delta R}{R_{2_H}} = \frac{\delta R}{R_{3_H}}$$

where R_{1H}, R_{2H} and R_{3H}, are the balanced phase resistances.

4.4.1.1 Basic Derivation of Fault Frequencies

For an induction generator:

$$f_s = \frac{f_{se}}{p}$$

$$s = \frac{(f_s - f_{rm})}{f_s}$$

The induction generator flux field rotates at the stator electrical frequency, f_{se}. When the rotor rotates at synchronous speed it is effectively stationary with respect to the flux. At other speeds the rotor windings move through the rotating flux field at the slip speed, the difference between the mechanical speed of the rotor and the synchronous speed. The rotor speed relative to the flux, $\hat{f}_{rm}$, is therefore given by:

$$\hat{f}_{rm} = s.f_s$$

This is the speed at which the flux field is cut by the rotor windings.

Since a winding is a complete circuit it must appear at two points on the rotor, 180°/p mechanical degrees apart. Therefore any form of rotor electrical asymmetry has a two pole effect on the flux and the rotational frequency of the fault with respect to the flux is given by:

$$\hat{f}_{frm} = 2s.f_s$$

In the case of an induction machine a rotor winding fault or brush gear unbalance is altering how the flux is cut and will therefore be modulating the amplitude of both the rotor and the stator electrical waveforms. Descriptions of the origins of rotor and stator fault frequencies can be found in [57]. The modulation frequency is therefore the frequency of the fault relative to the field, $\hat{f}_{frm}$, as given above, while the carrier frequency undergoing modulation is the stator supply fundamental frequency, f_{se}. Referred to the rotor side, the stator electrical frequency is the synchronous frequency, f_s.

This gives time domain amplitude modulation equations on the rotor side of:

$$c(t) = \cos(f_s.t)$$

$$m(t) = \sin(2s.f_s.t)$$

where $c(t)$ is the function undergoing modulation and $m(t)$ is the modulation function.

The equation for ordinary amplitude modulation is:

$$y(t) = \big(A + m(t)\big).\, c(t)$$

where $y(t)$ is the general function resulting from amplitude modulation. We will use $r(t)$ to represent the waveform on the rotor side and $s(t)$ to represent the waveform on the stator side which, through substitution gives:

$$r(t) = (A + \sin(2s.\, f_s.\, t)).\cos(f_s.\, t)$$

Using the standard trigonometric identity for sine and cosine multiplication, the resulting rotor-side waveform is:

$$r(t) = A.\cos(f_s.\, t) + \left(\frac{\sin\big((1+2s)f_s.\, t\big) + \sin\big((1-2s)f_s.\, t\big)}{2}\right)$$

Substituting for the synchronous frequency, f_s, we obtain the rotor side faulted waveform in terms of the stator supply fundamental, f_{se}, as:

$$r(t) = A.\cos\left(\frac{f_{se}}{p}.\, t\right) + \left(\frac{\sin\left((1+2s)\frac{f_{se}}{p}.\, t\right) + \sin\left((1-2s)\frac{f_{se}}{p}.\, t\right)}{2}\right)$$

Now converting from the rotor side waveform to the stator side using the pole pair relationship, we get the stator current waveform given by:

$$s(t) = A.\cos(f_{se}.\, t) + \left(\frac{\sin\big((1+2s)f_{se}.\, t\big) + \sin\big((1-2s)f_{se}.\, t\big)}{2}\right)$$

Extracting the frequency components from this equation we see that rotor electrical asymmetry results in stator current harmonic components at f_{se}, the supply fundamental and $(1 \pm 2s)f_{se}$, transforming to $2sf_{se}$ in the total instantaneous power.

However, this derivation only includes the basic harmonic components. As part of this research, a valuable collaborative relationship has been forged within the Supergen Wind Energy Technologies Consortium with the University of Manchester who investigated the other harmonics in the power and current spectra.

4.4.1.2 Collaborative Work on Induction Generator Monitoring

Research at The University of Manchester began by focussing on the construction of a detailed model of an induction generator and its verification against a test rig. The Manchester test rig features a 30kW, 4-pole, WRIG of identical construction to that on the Durham test rig except the generator has been rewound to allow greater access to winding connections on both the rotor and stator so winding faults can be applied. The Manchester test rig has the ability to be run as a DFIG or as a WRIG, as for the Durham test rig, however although it is not configured for variable speed, transient driving. The two test rigs are described and compared in [49] and [50].

The University of Manchester has developed a time-stepped model of the machine including its construction, air gap field and harmonic conductor distributions. It is described in detail in [66], [67] and [68]. The model incorporates a set of analytical expressions which were derived which represent all frequencies in the current and power spectra of both wound rotor and doubly-fed induction machines, given in full in [68]. These expressions not only take into account basic fault frequencies present in the machine but also those that are dependent on air-gap field space harmonics from the machine layout and supply time harmonics in the stator current.

The equations describing the stator current spectral content for the healthy and faulty machines respectively are:

$$f_{ind}^{k} = |6k(1-s) \pm l|f$$

$$f_{ind}^{k} = \left|\frac{k}{p}(1-s) \pm l\right| f$$

where f is the fundamental supply frequency, s is the induction generator fractional slip, k = 0, 1, 2, 3, ... and l = 0, 1, 2, 3, ... Constants k and l relate respectively to air-gap field space harmonics resulting from the layout of the machine and supply time harmonics in the current.

For the total instantaneous power signal, these expressions transform to the two equations below for healthy and faulty machines respectively:

$$f_{ind}^{k} = |j \pm 6k(1-s) \pm l|f$$

$$f_{ind}^{k} = \left|j \pm \frac{k}{p}(1-s) \pm l\right| f$$

where j = 0, 1, 2, 3, ..., k = 0, 1, 2, 3, ... and l = 0, 1, 2, 3, ... The additional constant j relates to supply voltage harmonic order. Additional information on these equations can be found in [69].

Since these equations lead to a large number of harmonic components in the current and power spectra, such that monitoring all components would be impractical in an industrial environment, the author, in collaboration with Dr Sinisa Djurović of The University of Manchester, has established a reduced set of fault-related frequencies to give a clear indication of rotor electrical asymmetry in induction machines. Tests have been carried out by the author on both the Durham and Manchester test rigs to allow a comparison between the machines and the time-stepped model. A summary of the work relevant to this thesis is given here. The work can be followed in detail in a number of published conference papers including [49][50], for which the author was first author. Published papers and those submitted for peer review on this subject are included in Appendix E.

In order to establish a reduced, more practical set of fault-related frequencies, steady state studies were carried out on both the Manchester and Durham test rigs. Two test rigs were used in order that only those fault frequencies consistent between different machines and environments were selected.

For conciseness, only results for the instantaneous power signal are presented here. An example of total instantaneous power data from the healthy Manchester test rig is given in Figure 62 for two operating speeds of the machine. It can be seen that the spectra are rich in harmonic content even for a healthy machine as a result of supply unbalance and inherent electrical unbalances.

- Machine dependent frequencies ‘a’ and ‘b’ were found to be present in both machines and both power and current. These components are a result of machine layout and are present for both healthy and faulty machines.

Rotor electrical asymmetry was then introduced into the machine and spectra rerecorded at the two operating points. These spectra, shown in Figure 63, now show the additional frequency components and were found to be consistent between both the Durham and Manchester test rigs.

- Component frequencies ‘c’ and ‘d’ are $2sf_{se}$ sidebands around zero and 100Hz in power and the fundamental and 3rd harmonic of supply in current.

- Component frequencies ‘e’ and ‘f’ are also $2sf_{se}$ sidebands but now around the machine dependent components ‘a’ and ‘b’.

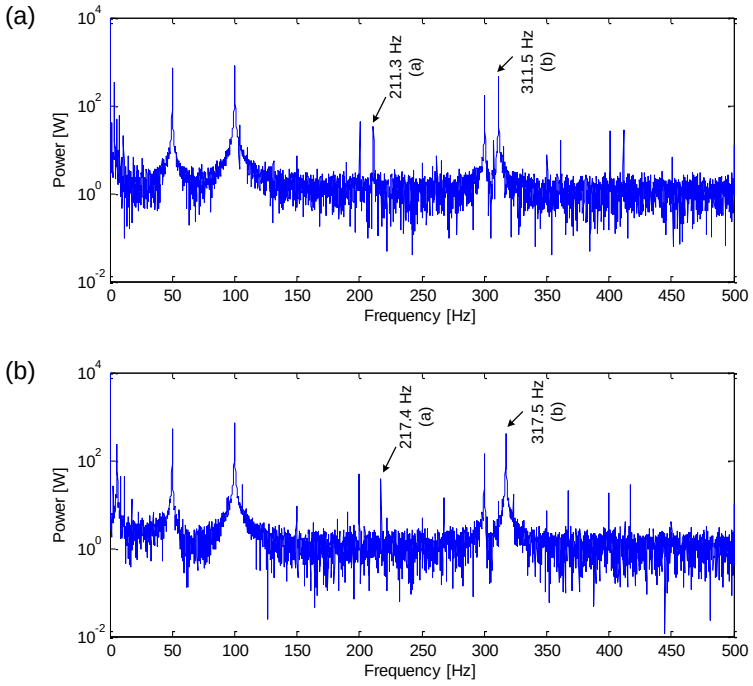

Figure 62: Spectrum of healthy total instantaneous power from the Manchester test rig at (a) 1560rpm and (b) 1590rpm

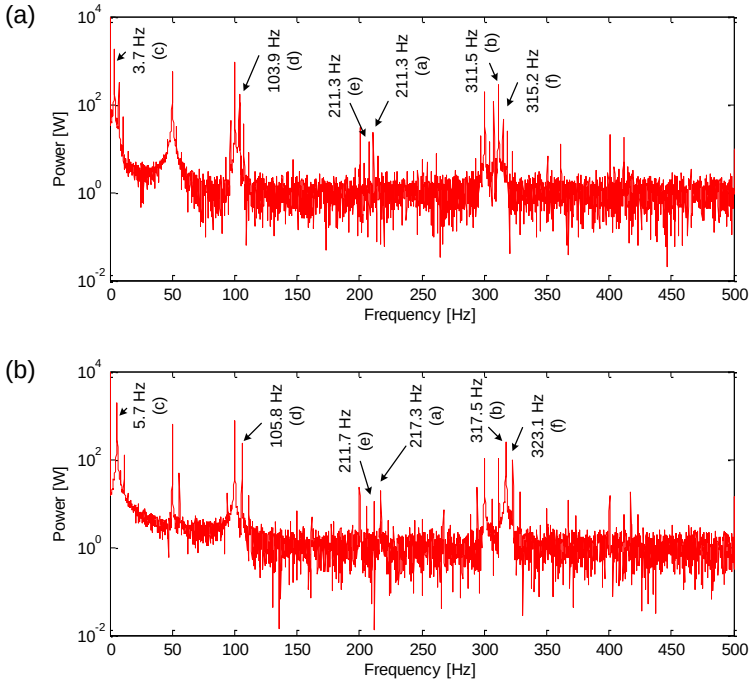

Figure 63: Spectrum of faulty total instantaneous power from the Manchester test rig at (a) 1560rpm and (b) 1590rpm

Steady state results from the Durham test rig were found to be very consistent with those from Manchester. The healthy Durham test rig spectra, shown in Figure 64, appear noisier as a result of the laboratory environment. However, components 'a' and 'b' are visible as expected.

The Durham faulted spectra, Figure 65, also show consistency with Manchester results with the $2sf_{se}$ components clearly visible around zero and 100Hz. The higher frequency components have however been severely attenuated and are not labelled due to their low magnitude. This results from the different test rig environment where the Durham test rig has a larger rotor resistance reducing the magnitude of certain speed ripple-dependent harmonics.

A study of the effect of rotor resistance and machine configuration is forming part of the ongoing collaborative relationship with the University of Manchester.

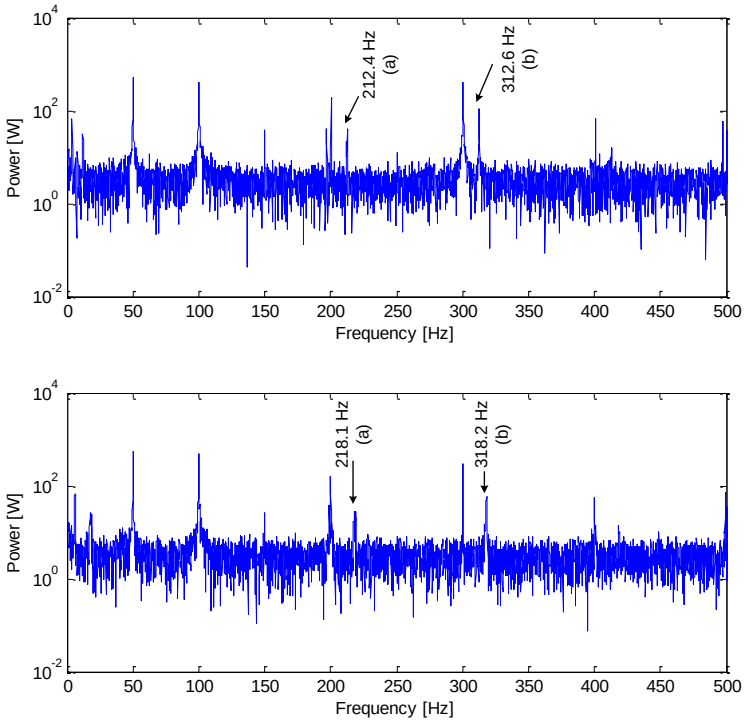

Figure 64: Spectrum of healthy total instantaneous power from the Durham test rig at (a) 1560rpm and (b) 1590rpm

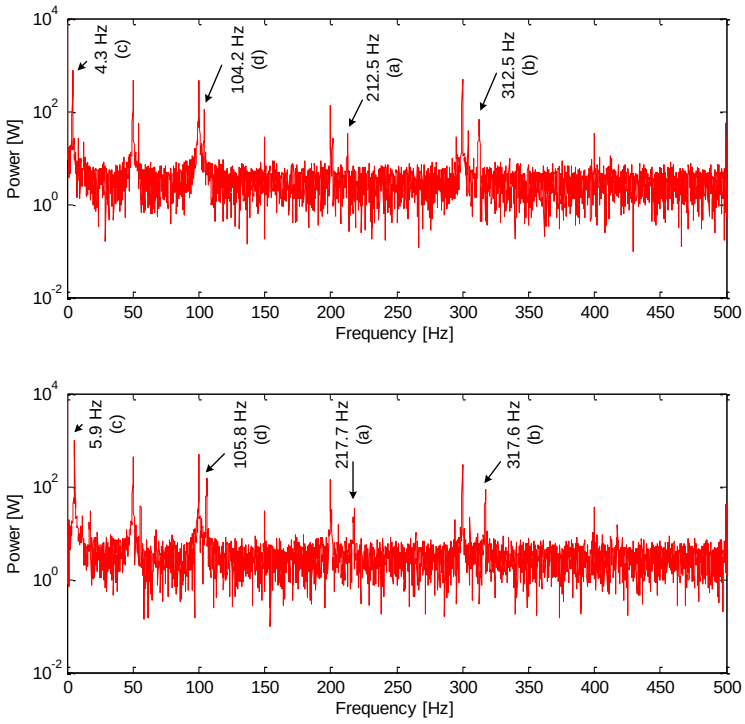

Figure 65: Spectrum of faulty total instantaneous power from the Durham test rig at (a) 1560rpm and (b) 1590rpm

The constants and equations required to calculate these speed dependent, fault-related frequencies are given in Table 2 for total power and Table 3 for current.

Frequency Label	Equation	j	k	l
50Hz Multiples	$f_{ind}^{k} = \lvert j \pm 6k(1-s) \pm l \rvert f$	1, 2, 3, ...	0	1, 2, 3, ...
a, b (Healthy)	$f_{ind}^{k} = \lvert j \mp 6k(1-s) \pm l \rvert f$	1	1	1
a, b (Faulty)	$f_{ind}^{k} = \left\lvert j \mp \frac{k}{p}(1-s) \pm l \right\rvert f$	1	12	1
c, d	$f_{ind}^{k} = \left\lvert j \mp \frac{k}{p}(1-s) \pm l \right\rvert f$	1	4	1
e	$f_{ind}^{k} = \left\lvert j - \frac{k}{p}(1-s) + l \right\rvert f$	1	8	1
f	$f_{ind}^{k} = \left\lvert j - \frac{k}{p}(1-s) + l \right\rvert f$	1	16	1

Table 2: Equations and constants for fault-related harmonic components in stator line current

Frequency Label	Equation	k	l
50Hz Multiples	$f_{ind}^{k} = \|6k(1-s) \pm l\|f$	0	1, 2, 3, ...
a, b (Healthy)	$f_{ind}^{k} = \|6k(1-s) \mp l\|f$	1	1
a, b (Faulty)	$f_{ind}^{k} = \left\|\frac{k}{p}(1-s) \mp l\right\| f$	12	1
c, d	$f_{ind}^{k} = \left\|\frac{k}{p}(1-s) \mp l\right\| f$	4	1
e	$f_{ind}^{k} = \left\|\frac{k}{p}(1-s) + l\right\| f$	8	1
f	$f_{ind}^{k} = \left\|\frac{k}{p}(1-s) - l\right\| f$	16	1

Table 3: Equations and constants for fault-related harmonic components in total instantaneous power

A journal paper has been submitted for peer review following from [50], presented at the IEEE 19th International Conference on Electrical Machines in March 2010.

4.4.2 High Speed Shaft Mass Unbalance

During the course of this research, the Durham test rig has been fitted with experimental balance planes to examine high speed shaft mass unbalance. The high speed shaft plane is pictured in Figure 66 and is normally fully encased within a sheet metal safety cover.

Holes at four different radii are drilled at 60° intervals around the balance plane allowing mass to be applied at various positions as required. The masses themselves are small metal discs are varying diameter which are fitted in pairs with one mass either side of the plane so as to avoid the introduction of axial vibration.

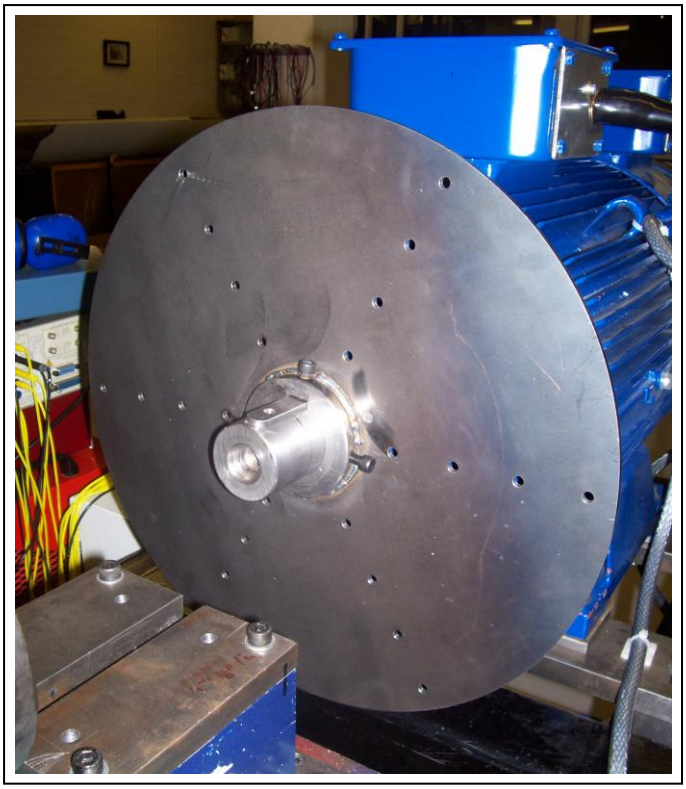

Figure 66: High speed shaft experimental balance plane during installation

The British and International Standard BS ISO 1940-1 [70] defines acceptable limits for machine balance according to a general description for machine size, speed and type. The balance quality grade, G, is given as the product of the residual specific unbalance, e, and the machine rotational speed, ω, so that:

$$e = \frac{m.r}{M}$$

$$G = e.\omega$$

where m is the unbalance mass (kg), r is the radial position of the unbalance mass (mm), M is the rotor mass (kg) and ω is the rotational speed (rad/s).

Guidance on the maximum acceptable balance quality grade, G, for various different machine types is given in Table 4 [70].

Machinery types: General examples	Balance quality grade, G	Magnitude $e_{per}.\omega$ (mm/s)
- Agricultural machinery - Crankshaft drives, inherently balanced, rigidly mounted - Drive shafts (cardan shafts, propeller shafts)	G 16	16
- Aircraft gas turbines - Electric motors, generators (at least 80mm shaft height), maximum rated speeds up to 950rpm - Electric motors, shaft heights smaller than 80mm - Gears - Machinery, general	G 6.3	6.3
- Compressors - Electric motors, generators (at least 80mm shaft height), maximum rated speeds above 950rpm - Gas and steam turbines	G 2.5	2.5

Table 4: Guidance for balance quality grades for rotors in a constant (rigid) state, adapted from [70].

From Table 4 we can see that the 4-pole WRIG on the test rig has a recommended acceptable balance quality grade of G 2.5. However, the standard makes no mention of two speed, geared systems with short, rigid shafts. It is assumed in this thesis that the acceptable balance grade in the case of the Durham test rig is slightly higher than the recommended G 2.5 however no information was found to confirm or refute this. The balance quality grades used in this work are given alongside results for high speed mass unbalance in Chapter 6.

In the case of a large WT, it is expected that the balance quality grades may not be directly applicable due to the nature of the mechanical system where a large ratio, multistage gearbox and very low speed hub will undoubtedly affect the system dynamics.

An alternative method for describing machine unbalance is to use the absolute centrifugal force generated by the unbalance. Figure 67, taken from [64], shows a simplified model of the balanced three blade system with unbalance mass, m_R.

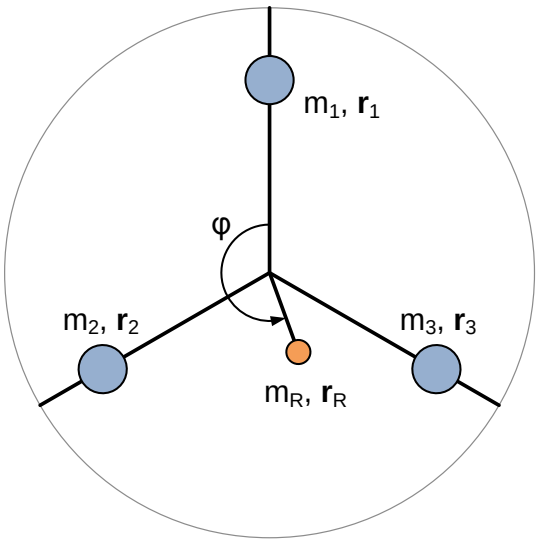

Figure 67: Simplified model of rotor mass unbalance [64]

For a healthy machine it can be assumed that the three blades are of equal mass where the three centres of mass are at the same radius and spaced by 120°. Therefore the resulting centrifugal force is equal to zero:

$$F_{C_1} = F_{C_2} = F_{C_3} = 0$$

$$m_1.r_1.\omega^2 = m_2.r_2.\omega^2 = m_3.r_3.\omega^2 = 0$$

As a result, any unbalance can be represented by an equivalent mass, m_R, and an equivalent radius r_R [64]:

$$F_{C_R} = m_R.r_R.\omega^2$$

A value for the centrifugal force resulting from unbalance will be given alongside the balance quality grade for results in Chapter 6.

4.4.2.1 Basic Derivation of Electrical Fault Frequencies

Following from the derivation for rotor electrical unbalance, §4.4.1.1, a similar amplitude modulation-based derivation is given here for generator rotor mass unbalance.

An unbalanced mass on the rotor shaft will lead to a dynamic eccentricity of the rotor within the air gap. This air gap distortion rotates at the rotational frequency of the rotor leading to an amplitude modulation of the air gap flux and therefore the rotor

and stator current waveforms. The rotational frequency of the fault is equal to the rotational frequency of the stator flux:

$$\hat{f}_{frm} = s.f_s$$

In the case of an induction machine the dynamic eccentricity can be said to be modulating the amplitude of the stator electrical frequency. As for rotor electrical asymmetry, the modulation frequency is therefore the frequency of the fault relative to the field as given above and the signal undergoing modulation is the stator sypply fundamental, f_{se}.

This gives us the amplitude modulation equations on the rotor side:

$$c(t) = \mathrm{A_c}.\cos(f_s.t)$$

$$m(t) = A_m.\sin(s.f_s.t)$$

where c(t) is the function undergoing modulation and m(t) is the modulation function.

Again taking the equation for ordinary amplitude modulation is:

$$y(t) = \big(A + m(t)\big).c(t)$$

where $y(t)$ is the waveform resulting from amplitude modulation. We will use $r(t)$ to represent the waveform on the rotor side and $s(t)$ to represent the waveform on the stator side.

Substituting into and expanding for $y(t)$, we find the rotor-side waveform to be:

$$r(t) = A.A_c.\cos\left(\frac{f_{se}}{p}.t\right) + A_c.A_m\left(\frac{\sin\left((1+s).\frac{f_{se}}{p}.t\right) + \sin\left((1-s).\frac{f_{se}}{p}.t\right)}{2}\right)$$

Multiplying the rotor-side function by the number of pole pairs, p, we find the amplitude modulated stator-side waveform, $s(t)$, to be:

$$s(t) = A.A_c.\cos\left(\frac{f_{se}}{p}.t\right) + A_c.A_m\left(\frac{\sin\big((1+s).f_{se}.t\big) + \sin\big((1-s).f_{se}.t\big)}{2}\right)$$

Extracting the frequency components from this equation we can see that a dynamic eccentricity on the rotor results in harmonic components at f_{se}, the supply fundamental and $(1 \pm s)f_{se}$ in the stator current or $s.f_{se}$ in the total instantaneous power.

4.4.2.2 Fault Frequencies in Mechanical Signals

In the case of high speed shaft mass unbalance, the fault frequency in signals such as accelerometer and shaft vibration signals will simply be the rotational frequency of the machine, f_{rm}, as the mass is directly coupled to the shaft.

4.4.3 High Speed Pinion Tooth Damage

Since the high speed assembly of the gearbox was so readily accessible, it was chosen as the subject for tooth damage investigations. It also has the advantage of being directly coupled to the high speed shaft therefore rotating at the same speed as the generator. A number of operators and monitoring engineers suggested that gear tooth damage was a particular challenge in many situations, from WTs to helicopters. As such, it was appropriate to examine the most accessible pinion in the controlled laboratory environment.

Just as for high speed mass unbalance, a single damaged tooth on a pinion or gear directly coupled to a shaft will have a once per revolution effect on mechanical vibration signals. In this case, the pinion is mounted on the high speed shaft and has the same rotational speed as the generator. The frequency induced in mechanical vibration signals as a result of single tooth damage is therefore f_{rm}, the rotational speed of the high speed shaft.

The major difference between gear tooth damage and the other faults introduced in this chapter is the impulsive nature of the response. Rotor electrical asymmetry and mass unbalance both cause continuous sinusoidal responses in various monitoring signals, whether electrical or mechanical, whereas the effect of tooth damage is a one per revolution pulse when the tooth meshes with its driving gear. This point will be investigated later in §6.2.

4.5 Conclusions

It can be seen from this Chapter that the Durham CM test rig represents a substantial investment in WT CM and has been significantly improved from previous work. The test rig is now capable of operating under a variety of operating conditions with data recorded from a large number of transducers along the drive train under both steady state and transient, variable speed driving conditions.

In this Chapter, three possible test rig fault-like conditions have been introduced:

- Rotor electrical asymmetry;
- High speed shaft mass unbalance, and;
- High speed pinion tooth damage.

The levels of fault used in this work will be introduced alongside their respective results in Chapter 6. However, it is important to note that the primary aim of the test rig is to generate signals of similar harmonic content to those encountered in a real WT. The resulting signals from each fault-like condition contain different harmonic content and are therefore suitable for verifying algorithms under transient, non-stationary conditions.

A summary of collaborative work with the University of Manchester has been discussed which is a significant advance in machine CM and should be noted. Further information can be found in [49][50] and further journal publications are in preparation. The next stage in this work is to examine the detectability of rotor electrical asymmetry, an analysis of which was submitted for peer review in 2010. The author has led the testing work in this area, while the model work was carried out at the University of Manchester.

Having introduced the test rig and its capabilities for variable speed fault testing, Chapter 5 goes on to discuss signal processing techniques and introduce a new algorithm for CM and fault detection in variable speed signals.

4.6 References

[45] Wilkinson, M. R., *Condition Monitoring for Offshore Wind Turbines*, Newcastle University, June 2008.

[46] Wilkinson, M. R., Tavner, P. J., *Condition Monitoring of Wind Turbine Drive Trains*, 17th International Conference on Electrical Machines, Crete, Greece, September 2006.

[47] Wilkinson, M. R., Spinato, F., Tavner, P. J., *Condition Monitoring of Generators & Other Subassemblies in Wind Turbine Drive Trains*, 6th IEEE International Symposium on Diagnostics for Electric Machines, Power Electronics and Drives, Cracow, Poland, 2007

[48] Yang, W., Tavner, P. J., Crabtree, C. J., Wilkinson, M. R., *Cost-Effective Condition Monitoring for Wind Turbines*, IEEE Transactions on Industrial Electronics, Vol. 57, No. 1, January 2010.

[49] Crabtree, C. J., Djurović, S., Tavner, P. J., Smith, A. C., *Condition Monitoring of a Wind Turbine DFIG by Current or Power Analysis*, 5th IET International Conference on Power Electronics, Machines and Drives, Brighton, United Kingdom, April 2010.

[50] Crabtree, C. J., Djurovic, S., Tavner, P. J., Smith, A. C., *Fault Frequency Tracking During Transient Operation of Wind Turbine Generators*, Proc. 19th International Conference on Electrical Machines, Rome, Italy, September 2010.

[51] Amirat, Y., Benbouzid, M. E. H., Bensaker, B., Waumkee, R., *Generators for Wind Energy Conversion Systems: State of the Art and Coming Attractions*, Journal of Electrical Systems, Vol. 3, Issue 1, pp. 26-38, 2007.

[52] Hsu, W., *Measurements on a Wind Turbine Condition Monitoring Test Rig*, MSc Project Report, Durham University, 2008.

[53] Emslie, J., *Mathematical Modelling of the Drive Train of a Wind Turbine Test Rig*, MEng Final Year Project Report, Durham University, 2010.

[54] Zaggout, M, *Condition Monitoring Using the Wind Turbine Generator Control Loop*, First Year PhD Transfer Report, Durham University, 2010.

[55] Burton, T., Sharpe, D., Jenkins, N., Bossanyi, E., *Wind Energy Handbook*, John Wiley, 2008.

[56] Crabtree, C. J., *The Development of Condition Monitoring Techniques for Offshore Wind Turbines Using a Test Rig*, First Year PhD Transfer Report, Durham University, 2008.

[57] Williamson, S. Smith, A. C., *Steady-State Analysis of 3-phase Cage Motors with Rotor-Bar and End-Ring Faults*, Proc. IEE, Part B, Electric Power Applications, Vol. 129, Issue 3, pp. 93-100, 1982.

[58] Bellini, A., Filippetti, F., Franceschini, G., Tassoni, C., Kliman, G. B., *Quantitative Evaluation of Induction Motor Broken Bars by Means of Electrical Signature Analysis*, IEEE Transactions on Industry Applications, Vol. 37, No. 5, pp. 1248-1255, 2001.

[59] Thomson, W. T., Fenger, M., *Current Signature Analysis to Detect Induction Motor Faults*, IEEE Industry Applications Magazine, Vol. 7, pp. 26-34, 2001.

[60] Benbouzid, M. E. H., Beguenane, R., Vieira, M., *Induction Motor Asymmetrical Faults Detection Using Advanced Signal Processing Techniques*, IEEE Transactions on Energy Conversion, Vol. 14, No. 2, pp. 147-152, 1999

[61] Cameron, J. R., Thomson, W. T., Dow, A. B., *Vibration and Current Monitoring for Detecting Airgap Eccentricity in Large Induction Motors*, Proc. IEE, Part B, Electric Power Applications, Vol. 133, pp. 153-163, 1986.

[62] Nandi, S., Bharadwaj, R. M., Toliyat, H. A., *Performance Analysis of a Three-Phase Induction Motor Under Mixed Eccentricity Conditions*, IEEE Transactions on Energy Conversion, Vol. 17, No. 3, pp. 392-399, 2002.

[63] Legowski, S. F., Sadrul Ula, A. H. M., Trzynadlowski, A. M., *Instantaneous Power as a Medium for the Signature Analysis of Induction Motors*, IEEE Transactions on Industry Applications, Vol. 32, No. 4, pp. 904-909, 1996.

[64] Caselitz, P., Giebhardt, J., *Rotor Condition Monitoring for Improved Operational Safety of Offshore Wind Energy Converters*, Transactions of the ASME, Journal of Solar Energy Engineering, Vol. 127, pp. 253-261, 2005.

[65] Djurović, S., Williamson, S., Tavner, P. J., Yang, W., *Condition Monitoring Artefacts for Detecting Winding Faults in Wind Turbine DFIGs*, Scientific Proc. European Wind Energy Conference, Marseille, France, March 2009.

[66] Djurović, S., Williamson, S., *A Coupled Circuit Model for a DFIG Operating Under Unbalanced Conditions*, Proc. 18th International Conference on Electrical Machines, Vilamoura, Portugal, September 2008.

[67] Djurović, S., Williamson, S., Renfrew, A., *Dynamic Model for Doubly-fed Induction Generators with Unbalanced Excitation, both With and Without Faults*, IET Electric Power applications, Vol. 3, Issue 3, pp. 171-177, 2009.

[68] Williamson, S., Djurović, S., *Origins of Stator Current Spectra in DFIGs with Winding Faults and Excitation Asymmetries*, Proc. IEEE IEMDC 2009, Miami, pp. 563-570, 2009.

[69] Djurović, S., Williamson, S., *Influence of Supply Harmonic Voltages on DFIG Stator Current and Power Spectrum*, Proc. 19th International Conference on Electrical Machines, Rome, Italy, September 2010.

[70] *Mechanical Vibration – Balance quality requirements for rotors in a constant (rigid) state – Part 1: Specification and verification of balance tolerances. ISO 1940-1:2003*, International Organization for Standardization, Geneva, Switzerland, 2003.

5 Signal Processing

"Mathematical Analysis is as extensive as nature herself"

Joseph Fourier
1768 – 1830

WT CM has been shown to be a complex task, because of both the rotating machine itself and the nature of the wind, requiring a clear understanding of the effects of variable speed and variable load conditions. It therefore follows that signal processing techniques and algorithms for CM need to be developed with non-stationary and highly variable, stochastic signals in mind.

This Chapter initially discusses two commonly encountered signal processing techniques: the Fourier transform and the wavelet transform. The advantages and disadvantages of these techniques are summarised and conclusions drawn about their suitability for analysis of non-stationary WT signals. The concept of frequency tracking is introduced using a previously published wavelet-based algorithm. This is discussed as it will be useful for comparison later in the thesis. Finally, a new frequency tracking algorithm will be introduced, based on the principles of the Fourier transform, capable of tracking fault-related frequencies in non-stationary monitoring signals.

This new algorithm will be used throughout Chapter 6 and its results will be subsequently compared with the proven and previously published wavelet-based tracking algorithm.

5.1 Common Signal Processing Techniques

In this section, the principles and applications of a number of common signal processing techniques are introduced. The techniques discussed here have been chosen as they lead to a number of useful conclusions for CM WTs.

While there have been many more signal processing techniques developed over recent years, we limit this introduction and discussion to the Fourier transform, its development into the short-time Fourier transform and the wavelet transform. The

discrete Fourier transform is given the most detailed emphasis as this is the basis for the signal processing developments undertaken in this thesis and introduced in §5.2. Should the reader require more information on wavelet transforms, they are directed to the referenced literature.

5.1.1 The Fourier Transform

The Fourier transform has been well documented in engineering and mathematics texts since research was initiated by Joseph Fourier's work on heat transfer in the early 1800s. Coincidentally, for a thesis related to renewable energy, Fourier is also credited with the discovery of the greenhouse effect [71].

The essence of Fourier analysis can be concisely described by the statement that "a periodic function can be broken down into its harmonic components" [72]. This statement is graphically illustrated by Figure 68(a). Here, a periodic square wave is broken down into its Fourier sine components. Each sine component makes a different contribution to the reconstructed square wave and this contribution is indicated by its amplitude in Figure 68(a). The odd sine components up to the 13^{th} harmonic are shown and make a contribution to the reconstructed signal.

Having seen the individual sine components of the square wave function, Figure 68(b) shows the incremental reconstruction of the square wave from the Fourier sine components in Figure 68(a). In each subplot, the next odd harmonic is added to the waveform as indicated. It is apparent that the reconstruction is not perfect. However, an important characteristic of the Fourier transform is visible in that the quality of the reconstruction improves steadily as the number of harmonic components is increased.

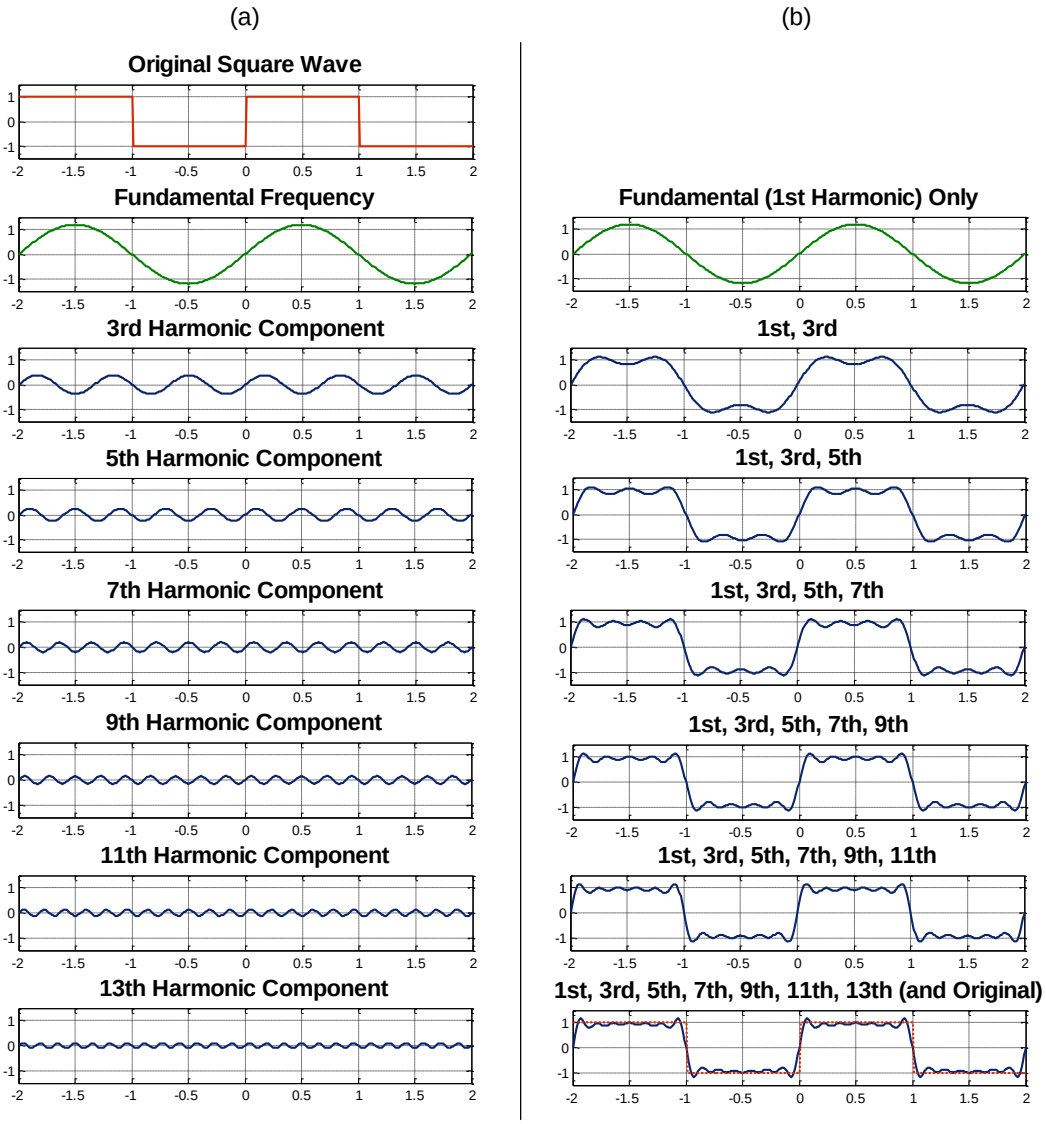

Figure 68: (a) Fourier sine components of a square wave up to the 13th harmonic; (b) Incremental reconstruction of a square wave from sine components given in Figure 68 (a)

For a continuous signal, $s(t)$, the continuous Fourier transform is given by [73]:

$$S(f) = \int_{-\infty}^{\infty} s(t) e^{-j2\pi ft}\, dt$$

From a practical calculation point of view, the signal, $s(t)$, is effectively evaluated against sine and cosine functions of positive and negative frequencies over the entire function length, -∞ to ∞.

This mathematical form is, however, not suitable for use in the large majority of engineering applications. As signals have been sampled in time at a certain sampling

frequency they are therefore no longer strictly continuous in time. In this case, the discrete Fourier transform (DFT) must be used .

For discrete analysis, the continuous signal, $s(t)$, is replaced by a discrete signal, $s(nT)$, a sampled signal of finite length N and sampling period T, giving the transform:

$$S^*(f) = \sum_{n=0}^{N-1} s(nT)e^{-j2\pi fnT}$$

The discrete time domain nature of the signal implies that the signal is now discrete in the frequency domain with a frequency resolution of Δf. The DFT of the discrete signal is therefore given as:

$$S^*(k\Delta f) = \sum_{n=0}^{N-1} s(nT)e^{-j2\pi nk\Delta fT}$$

where $k\Delta f$ defines the frequency components under analysis.

Full mathematical derivations can be found in [72], [74] and [75] however only these equations are required in this thesis.

One of the primary issues surrounding the use of the DFT for WT CM is its reliance on stationary signals. Since the transform is applied across a complete signal, small, time-localised signatures are likely to be insignificant compared to the overall signal content. In a broader sense, this means that, using the DFT, the time location of characteristic frequency components or impulsive responses cannot be examined. This is illustrated by Figure 69 where two linear chirp signals are analysed using the Fourier transform, based on [75]. In the left-hand plot the frequency increases with time, from left to right, while in the right-hand plot the signal is reversed with its frequency decreasing with time. The spectra of these two signals, calculated by a basic FFT implementation of the DFT, are similar despite the significantly different time waveforms. Put simply, the DFT and its FFT implementation take no account of the time localisation of frequency components.

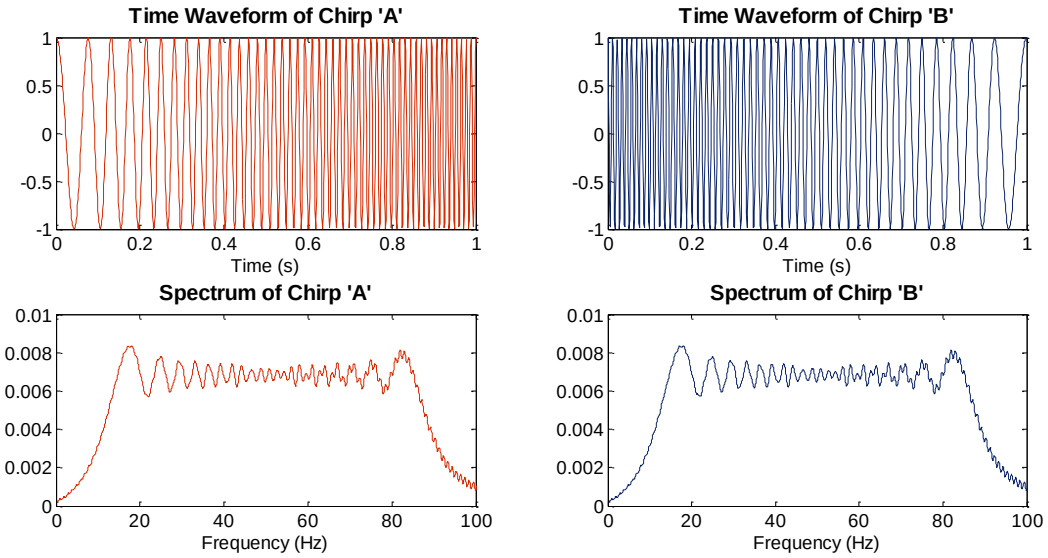

Figure 69: Comparison of chirp spectra, based on [75]

It is apparent in most situations that time information is an essential component in the complete understanding of a signal. In an engineering sense, time-localised frequency analysis can increase diagnosis capability since impulsive, short-time, transient characteristics can be examined.

In an effort to allow time-frequency analysis of signals, the short-time Fourier transform (STFT) was developed as a means of adapting the Fourier transform concept for use on non-stationary, time varying signals.

5.1.2 The Short-Time Fourier Transform

As a result of its availability in analysis software such as MATLAB, the spectrogram implementation of the STFT will be considered. The spectrogram is computed as the squared magnitude of the STFT [75].

As the name suggests, the STFT calculates the spectral content for a short time sample of a particular signal. This process is continued iteratively in the time domain until the entire signal has been processed in these short samples. The spectra from the short time samples are then plotted in time to produce a 3D (time, frequency, amplitude) representation of the signal's spectral content.

To illustrate this, Figure 70(a) shows the FFT of a 60 second signal sampled at 1kHz. The information available from the FFT suggests that three frequency

components are present throughout the entire length of the signal with equal magnitudes. If the STFT spectrogram is examined, Figure 70(b), it can be seen that the frequencies themselves are correct but they are not present throughout the entire signal. The FFT loses all time information contained in the original signal by analysing over the entire signal length. The STFT has the advantage of giving a certain degree of time-frequency information by iteratively analysing short time segments of the signal.

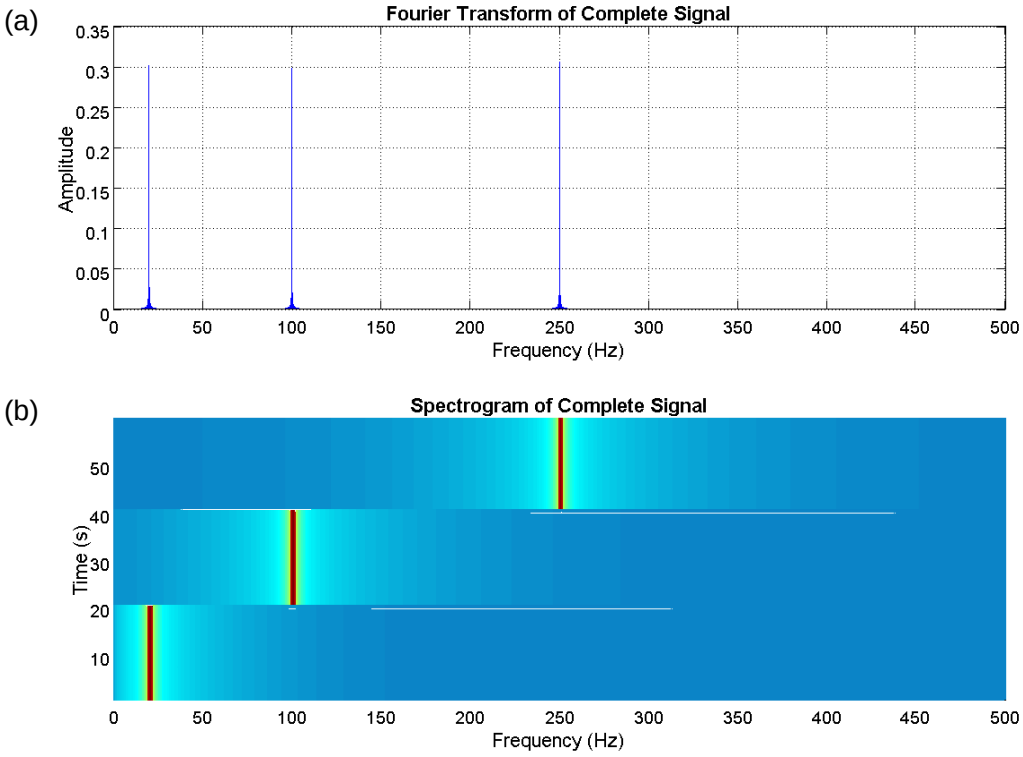

Figure 70: Time varying sinusoidal signal analysed using the (a) FFT and (b) spectrogram

Since the STFT is essentially an iterative DFT process, certain limitations on frequency resolution are applied, in that a longer time window allows for a greater frequency resolution. In the STFT, however, the process cannot consider only the frequency resolution and a certain degree of compromise is required. While a longer time window allows for a high frequency resolution, and therefore an accurate representation of frequency content, it will blur and reduce resolution in the time domain. To improve the time accuracy of analysis, a shorter window is required such that the signal is effectively stationary during analysis. It is largely down to the user to select the most suitable time window or frequency resolution for their individual

application based on knowledge of the signal under analysis and the requirements of analysis.

5.1.3 The Continuous Wavelet Transform

In recent years, the continuous wavelet transform (CWT) has gained popularity in a number of engineering applications including turbulence analysis [77] and damage detection [78] amongst many others. One of its most popular uses is in image compression however its ability to carry out signal decomposition has led to its application to signal analysis. In particular, the CWT has been used as a method for CM and fault detection for certain non-stationary electrical and mechanical signals. The CWT is designed to include both time and frequency information, resulting in similar figures to those from the STFT. However the analysis process is very different.

On a fundamental level, the DFT and STFT both calculate spectral content by comparing a time domain signal with sine and cosine waves of different frequencies. The CWT, however, compares the signal against a particular function called a wavelet, which may assume a variety of standardised shapes. By 'stretching' the wavelet in the time domain, a process known as dilation, the spectral content of the wavelet it altered. The correlation between the signal and analysing wavelet at each stage indicates the wavelet content of the signal.

According to [76], the basic wavelet, known as the mother wavelet, should be oscillatory, have no DC component, be a band-pass filter, decay rapidly towards zero with time and be invertible. An example of this is the Morlet wavelet where the mother wavelet is defined as:

$$\Psi(t) = e^{-j\omega_0 t} e^{-t^2/2}$$

and has the Fourier transform:

$$H(\omega) = \sqrt{2\pi}\, e^{-(\omega-\omega_0)^2/2}$$

This wavelet and its Fourier transform are given in Figure 71(a) and Figure 71(b) respectively.

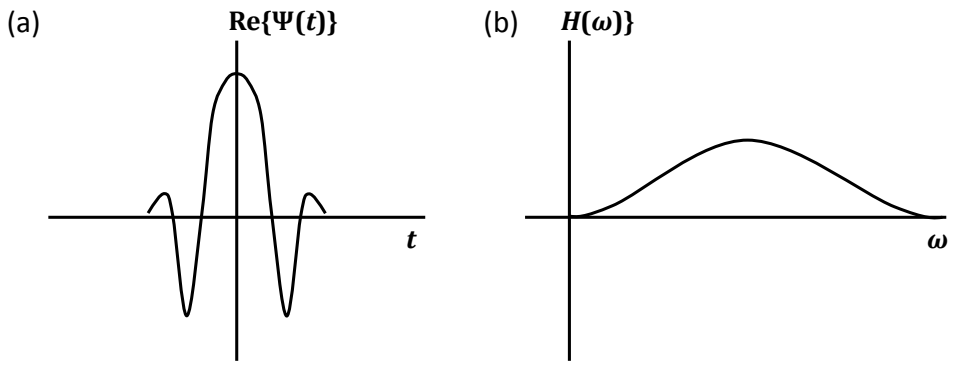

Figure 71: (a) Modified Gaussian or Morlet mother wavelet, Ψ(*t*), and (b) its Fourier transform, *H*(ω), from [76]

The mother wavelet is scaled to give a family of mother and baby wavelets so that each baby wavelet is given by:

$$\frac{1}{\sqrt{c}}\Psi\{(t-\tau)/c\}$$

where c is a variable scaling constant and τ is a constant of translation. The scaling parameter, c, is approximately inversely related to its frequency such that high values of c correspond to low frequencies and vice versa.

If c is increased, the wavelet is dilated in time and therefore contains lower frequencies. Increasing the value of τ moves the wavelet in time along the x-axis such that the CWT is given as:

$$CWT(c,\tau) = \left(\frac{1}{\sqrt{c}}\right)\int s(t)\Psi\{(t-\tau)/c\}dt$$

An example of the use of the CWT for fault detection is given in Figure 72, taken from [79]. Here, the authors were examining short, transient fault-related sidebands in the supply current of a 15kW induction machine. During constant speed operation, the data was analysed using a Fourier method. However, as fault-related components were expected to be prominent during machine start up, this method was unsuitable as the conditions and signals were non-stationary. The wavelet transform was therefore applied to the stator current data recorded during machine start up. Figure 72(a) shows the starting current time waveform. Very little change is observed in the time waveform during faulty behaviour however the result of the wavelet transform, shown in Figure 72(b) shows a clear peak at the sideband frequency indicating not only that a fault is present but also showing its location in time.

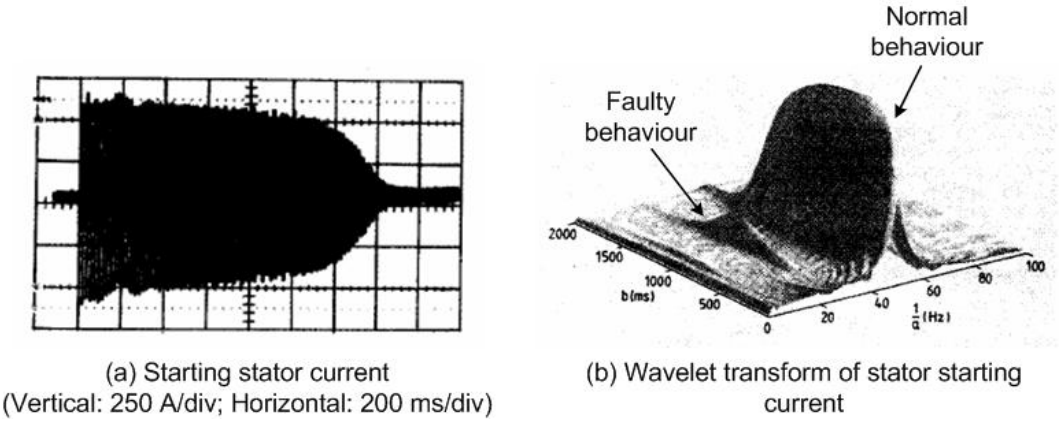

(a) Starting stator current
(Vertical: 250 A/div; Horizontal: 200 ms/div)

(b) Wavelet transform of stator starting current

Figure 72: Detection of fault-related frequencies using a wavelet transform during transient operation of an induction machine, from [79]

5.1.4 Comparison of Techniques

Figure 72 demonstrated that it is possible to detect and observe fault-related frequency components during transient operation of electrical machines. In this case, interest was confined to a short period of variable speed operation with the machine generally operating at constant speed except during run up and run down.

The issue of transient, non-stationary conditions is somewhat exaggerated in the WT as there are few occasions when the turbine is operating at constant speed and load. As a result, transient CM becomes unavoidable. Techniques such as the STFT and CWT are therefore strong candidates when it comes to CM and fault detection in the constantly varying, highly non-stationary signals generated by WT drive trains.

While the selection of the most appropriate technique it likely to be highly subjective, the merits of each technique are discussed here.

One issue to be considered is the ease of understanding the output of each technique. The CWT offers a result in the time-scale domain. While scale is linked to frequency, there is a degree of work involved to understand the result. For example, the fact that the scale parameter is inversely related to frequency easily leads to confusion when presenting results to non-specialist staff. The STFT has an advantage in this respect since it produces result directly in the time-frequency domain. It may also be argued that many of the signals analysed for WT CM are of a sinusoidal nature and, as such, may be more suited to detection by a Fourier method, such as the STFT, rather than a wavelet method, such as the CWT, which is based on impulsive mother functions.

A subjective issue is the clarity of results. Figure 73 shows the STFT spectrogram and CWT of a sinusoidal signal containing three distinct frequency components present at different times in the signal. The STFT result, Figure 73(a), is easier to interpret than the corresponding CWT result Figure 73(b). However, results are strongly dependent on the parameters of the analysis method and so this point should not be taken as a reason for discounting the CWT.

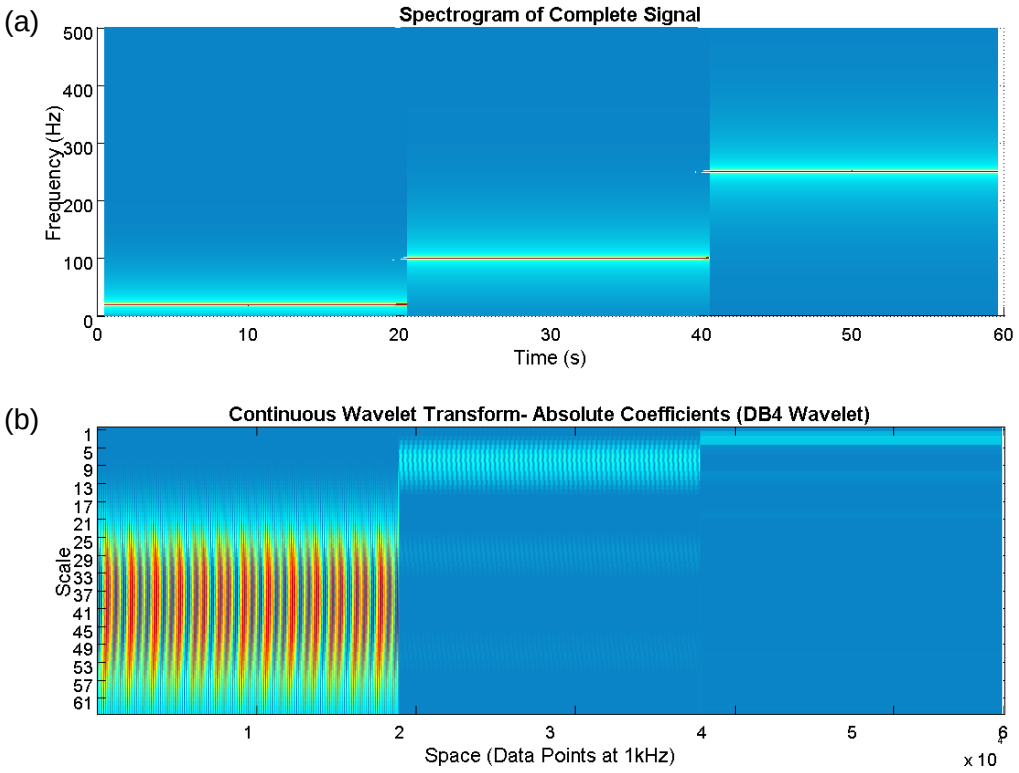

Figure 73: Time varying sinusoidal signal analysed using the (a) STFT and (b) CWT

A key consideration in the selection of a processing method is its computational intensity or the computing time required to produce a suitable result. Despite their clear advantages over the conventional FFT, both the STFT and CWT, when applied over long periods of time and wide frequency or scale ranges, are computationally intensive. A number of repeat calculations were carried out in MATLAB using the STFT and CWT and each time the result showed the CWT taking significantly longer to calculate than the STFT, in turn taking longer than the FFT. The parameters and functions used were those used to calculate Figure 70 and Figure 73 so as to give the values some meaning in terms of the quality of result obtained.

Processing Method	Processing Time	Multiple of FFT Time
FFT (entire data length)	0.13 s	1
STFT	0.46 s	3.5
CWT (DB4 wavelet)	1.77 s	13.6

Table 5: Example processing times for the FFT, STFT and CWT applied to a 10s data record at 5kHz as used to produce Figure 70 and Figure 73

It is could be suggested that the increased processing time required by the CWT is unjustified by the quality of result obtained, Figure 73(a), when compared to the faster STFT, Figure 73(b).

Nevertheless, both methods may be subject to refinement to reduce their processing requirements. One possible methodology for the reduction of processing times is the idea of frequency tracking.

5.1.5 Wavelet-Based Frequency Tracking

Successful CM using frequency analysis on highly non-stationary WT signals depends on techniques which maintain the time-frequency nature of the signals themselves. As such, the STFT and CWT have an important role in CM by frequency analysis. However, there is significant redundancy in the calculations when it comes to useful frequency information, highlighted by the extensive processing times given in Table 5. This must be addressed when considering online CM of large numbers of remote WTs.

The idea of speed-dependent fault-related frequencies has been introduced and discussed in Chapter 4 of this thesis and has been taken as a starting point for the development of a frequency tracking algorithm. The fundamental idea of frequency tracking is to reduce the processing needed, extracting only the frequency information of interest rather than analysing wide frequency bands. One algorithm, discussed in detail in [80], a copy of which is given in Appendix E, was based on the CWT.

The algorithm, CWT_{local}, requires two signals for computation: a machine speed signal and the monitoring signal itself. Just as for the STFT, the algorithm carries out its calculations on small samples of data, progressing iteratively until the entire data set has been analysed. At each step, the fault frequency of interest is recalculated based on the corresponding machine speed signal and the relevant CWT scale constants calculated accordingly. The wavelet coefficients for the particular short sample are calculated using the reduced set of scaling constants before the algorithm moves to the next short sample and repeats the process.

To minimise the effect of speed signal calibration error and therefore ensure a good quality of result, a small range of scaling constants is applied at each step, effectively representing a narrow frequency band. The signal is analysed for each of these scaling constants and then the maximum correlation coefficient is taken. This should result in the detection of a sideband peak alone and reduce the effect of background noise within a signal. The process is illustrated graphically in Figure 74. It should be noted from the figure that the time window length is fixed for every step of the analysis.

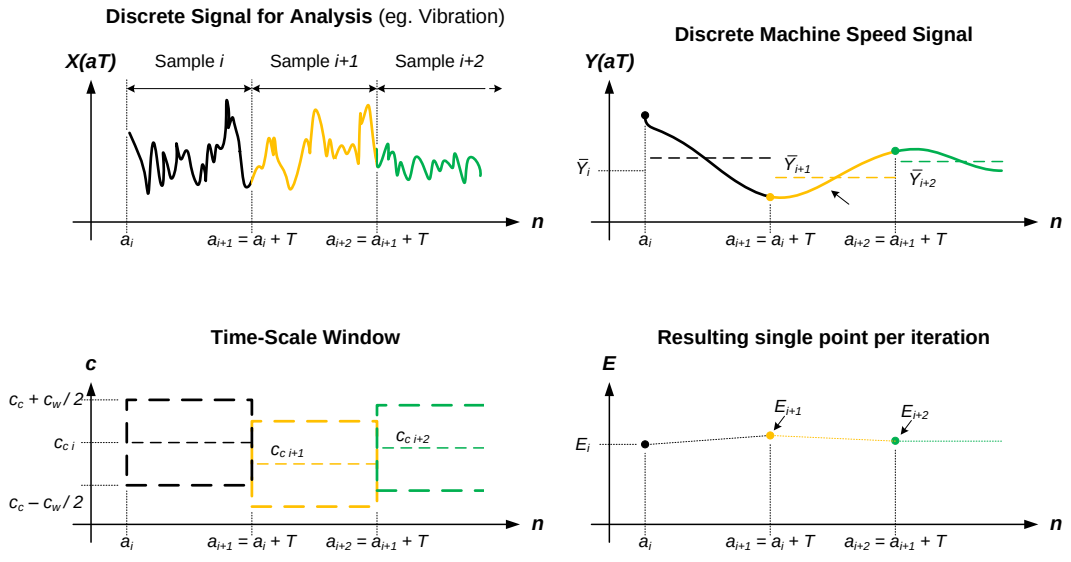

Figure 74: Graphical illustration of the CWT_{local} frequency tracking algorithm proposed by Yang in [80] with fixed time windows

The algorithm shown graphically in Figure 74 and detailed in [80] can be summarised as:

- Extract speed and monitoring signal samples of defined length
- Calculate the mean speed for the sample, $\bar{Y}$
- Calculate frequencies of interest from $\bar{Y}$
- Calculate wavelet scale parameters, *c*, from frequencies of interest
- Calculate wavelet coefficients for each scale parameter
- Extract maximum scale parameter, *E*, representing the signal energy
- Repeat for next sample in time

In [80], the CWT$_{local}$ algorithm is applied to data recorded for rotor electrical asymmetry on a WRIG and mass unbalance on a permanent magnet synchronous generator. In both cases, good results were produced. Figure 75 shows the result presented for frequency tracking of a rotor electrical asymmetry in the power signal. A smaller fault was undetected by the algorithm however it performed well for the larger fault, details of which are available in [80].

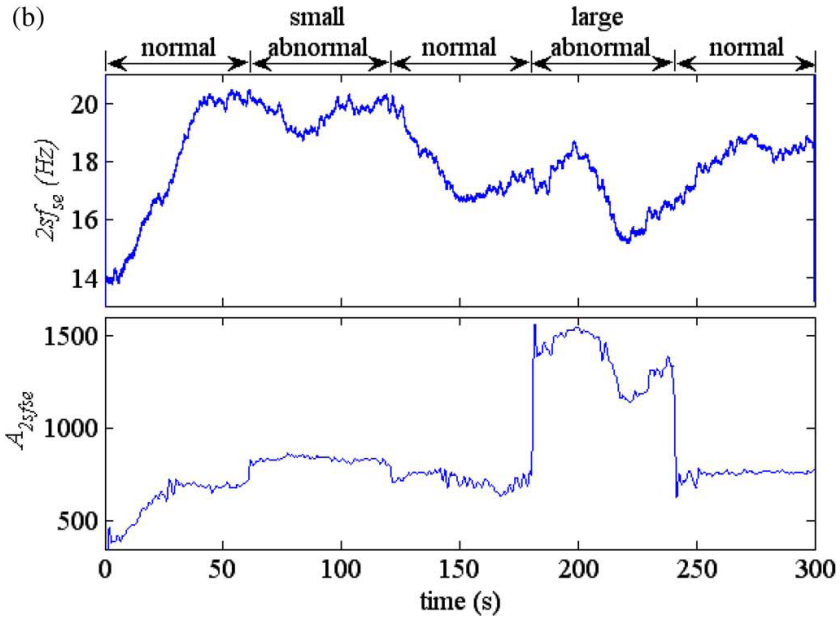

Figure 75: CWT$_{local}$ frequency tracking of the $2sf_{se}$ component of total instantaneous power as shown in [80]

The variability in the result led to the consideration of an adaptable analysis window rather than the fixed time window that was originally used. The author adjusted the algorithm such that the initial speed point is extracted and the time

window length defined by the machine speed in terms of a fixed number of machine rotations rather than a fixed time. The samples are then extracted and analysed as before. The next unanalysed speed point is then taken as the starting point for the next iteration and the process is repeated.

This variable time window implementation of the algorithm is used later in §6.2 when a proposed new frequency tracking algorithm is examined against the published CWT_{local} algorithm.

One particular issue that was still encountered using the CWT_{local} tracking algorithm was that of the length processing times required for analysis. While this was significantly reduced when compared to carrying out a full CWT, the calculation time remained significant if clear results were required. This was further exaggerated when large data sets of high sampling rate data were processed. Processing times will be discussed and compared in §6.2.3.

5.1.6 Summary

Two standard signal processing techniques have been introduced and discussed in terms of their applicability, ease of interpretation of results and complexity in terms of processing requirements. In addition, a method for reducing processing power demand, the CWT_{local} frequency tracking algorithm, has been introduced.

Having examined these methods, including the frequency tracking method, several conclusions were drawn regarding the way forward for analysis.

STFTs and CWTs appear to be inappropriate in their raw forms for WT CM due to the complex result figures they produce. These require a significant amount of interpretation before conclusions can be drawn from them. However, the STFT can arguably be said to give more direct and accessible information given the results seen so far.

The idea of frequency tracking is very attractive when it comes to analysis of many turbine signals. The method reduced processing times and produced figures showing information about a specific fault-related frequency. In terms of the amount of manual interpretation required, this is a significant improvement. The addition of a

variable time window length based on machine parameters should help to refine results further.

Finally, one should return to examine the operational conditions of WT drive trains alongside their fault mechanisms. In addition, one should also consider operational parameters such as machine speed, as introduced in the multi-parameter example in §3.5. When looked at more closely, a large number of WT faults produce sinusoidal responses in monitoring signals and are a function of the rotational speed of the machine.

Given the points discussed above, it seems sensible to point this work in the direction of a Fourier transform-based method with frequency tracking. In §5.2, an algorithm is conceived and developed to incorporate the advantages of the CWT_{local} frequency tracking algorithm and sinusoidal, Fourier-based analysis.

5.2 Fourier Transform-Based Frequency Tracking

The proposed algorithm uses a development of the DFT as a basis for frequency tracking with the signal being broken into short time segments for analysis in a similar fashion to the STFT, CWT and CWT_{local} tracking algorithm.

The analysis of short time samples of data is essential to the successful application of a Fourier transform-based method as signals are assumed to be, and therefore must be, stationary. Under variable speed, variable load conditions, signals can only be said to be stationary over short periods of time. The algorithm adapts the time window to the machine speed by calculating the amount of data required for analysis as a function of machine rotational period such that a fixed number of revolutions are analysed at each stage, assuming the machine speed remains constant over a short number of revolutions. The algorithm is illustrated graphically in Figure 76. Due to its iterative and frequency-localised nature, the final algorithm will be referred to as the iterative localised discrete Fourier transform ($IDFT_{local}$) throughout this thesis. The complete derivation of the $IDFT_{local}$ algorithm is given in §5.2.1 and §5.2.2.

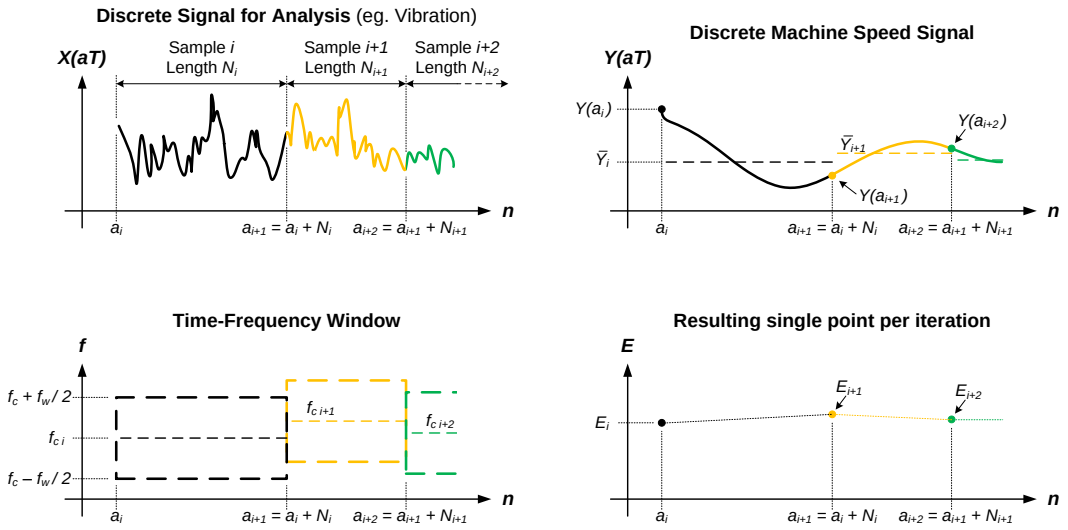

Figure 76: Graphical illustration of the Fourier transform-based frequency tracking algorithm with variable time and frequency windows

The algorithm process shown in Figure 76 can be summarised as:

- Extract the initial speed signal data point
- Calculate the time length of the required number of machine revolutions and extract the relevant amount of data
- Calculate the mean speed for the sample, $\bar{Y}$
- Calculate the frequencies of interest, f
- Calculate discrete constants from frequencies of interest, k
- Calculate amplitudes for each constant k
- Extract maximum amplitude, E
- Repeat the process starting with next unanalysed speed data point

5.2.1 Derivation of a Localised Discrete Fourier Transform

Before the full IDFT_{local} is derived, the calculations necessary for a single iteration, the localised DFT, are introduced.

From §5.1.1 we know that the discrete Fourier transform is given by:

$$S^*(k\Delta f) = \sum_{n=0}^{N-1} s(nT)e^{-j2\pi nk\Delta fT}$$

where the equation is discrete in both time and frequency.

As for the CWT_{local} frequency tracking algorithm in §5.1.5, two signals, continuous in time, are required for analysis. A monitoring signal of interest is given by $x(t)$ and the machine rotational frequency, in Hz, by $y(t)$. The signals are sampled at a frequency f_s, converting them to discrete signals $x(nT)$ and $y(nT)$ where n = 0, 1, 2, ... and $T = 1/f_s$. For analysis, a series of N samples is required where N is a function of a specified number of machine revolutions, r, giving:

$$N = \frac{r.f_s}{y(0)}$$

where $y(0)$ is the initial value of machine rotational frequency.

A central frequency of interest, f_c, is defined as a function of the mean machine rotational frequency, $\bar{y}$, across the series of length N.

$$\bar{y} = \frac{1}{N}\sum_{n=0}^{N-1} y(nT)$$

$$f_c = f(\bar{y})$$

The frequency window width, f_w, is defined so that the window is bounded by:

$$f_{upper} = f_c + \frac{f_w}{2}$$

$$f_{lower} = f_c - \frac{f_w}{2}$$

If the frequency resolution is Δf, the frequencies of interest are given by:

$$k\Delta f \in \left[f_{lower}\,, f_{upper}\right]$$

This implies that for a fixed Δf:

$$k \in [k_{min}\,, k_{max}]$$

$$\begin{cases} k_{min} = \dfrac{f_{lower}}{\Delta f} \\ k_{max} = \dfrac{f_{upper}}{\Delta f} \end{cases}$$

where k is an integer.

In order that sideband fault frequencies are unaffected by their carrier frequency, or other background noise within the frequency window, the maximum amplitude within that window is extracted such that only the fault frequency component amplitude, A, is found.

$$A = \max_{k\in[k_{min},k_{max}]}\left(\sum_{n=0}^{N-1} x(nT)e^{-j2\pi nk\Delta fT}\right)$$

This function allows the analysis of a localised frequency range based on Fourier analysis. However, it is not as yet and iterative procedure and a single analysis is carried out over the entire signal length. In order to analyse non-stationary, variable speed signals, an iterative process much be derived to apply the localised DFT over short time windows along the signal length. This is carried out through use of an iterative localised DFT, abbreviated to IDFT$_{local}$, the derivation of which is presented in §5.2.2.

5.2.2 Realisation of the IDFT$_{local}$

For a non-stationary discrete signal, the localised DFT from §5.2.1 must be applied through a sliding time-sample window such that the signal is stationary within each sample, leading to the complete IDFT$_{local}$ algorithm.

The reference a denotes the data point number whereby the discrete signal for analysis is given by $x(aT)$ with a corresponding machine rotational frequency signal $y(aT)$ representing two finite series of length A with sampling period T.

A moving reference point, a_i, denotes the starting data point of each iteration of the IDFT$_{local}$ so the series length, N_i, is defined by:

$$N_i = \frac{r.f_s}{y(a_i)}$$

where $i = 0, 1, 2, ..., i_{max}$ such that i_{max} is defined so that:

$$a_i + N_i \in [0, A]$$

and for each iteration:

$$a_i = a_{i-1} + N_{i-1}$$

Now the central frequency of interest, f_{ci}, is defined by a function of the mean machine rotational frequency in the particular series.

$$\overline{y_i} = \frac{1}{N_i}\sum_{n=0}^{N_i-1} y\big((a_i + n)T\big)$$

$$f_{c_i} = f(\overline{y_i})$$

The particular frequency window width, f_{wi}, is defined so that the window is bounded by:

$$f_{upper_i} = f_c + \frac{f_{w_i}}{2}$$

$$f_{lower_i} = f_{c_i} - \frac{f_{w_i}}{2}$$

If the frequency resolution is Δf, the frequencies of interest are given by:

$$k\Delta f \in \left[f_{lower_i}, f_{upper_i}\right]$$

Implying that for a fixed Δf:

$$k \in \left[k_{min_i}, k_{max_i}\right]$$

$$\begin{cases} k_{min_i} = \dfrac{f_{lower_i}}{\Delta f} \\ k_{max_i} = \dfrac{f_{upper_i}}{\Delta f} \end{cases}$$

Again, the maximum value within the frequency window is taken so the amplitude of the frequency of interest, A_i, in the frequency window for the particular series i is given by:

$$A_i = \max_{k\in\left[k_{min_i}, k_{max_i}\right]}\left(\sum_{n=0}^{N_i-1} x\big((a_i + n)T\big)e^{-j2\pi nk\Delta fT}\right)$$

From a practical point of view, to observe any changing trend with time, the output IDFT_{local} must include a corresponding time vector since the iterative process may not necessarily carried out on series of equal length, because of changing rotational speed. Therefore the time value, t_i, corresponding to each A_i is given by:

$$t_i = a_i T$$

For MATLAB analysis, the resulting IDFT_{local} of the time-varying signal is given in the matrix form:

$$\text{IDFT}_{local} = \begin{bmatrix} t_0 & f_{c_0} & A_0 \\ t_1 & f_{c_1} & A_1 \\ \vdots & \vdots & \vdots \\ t_{i_{max}} & f_{c_{i_{max}}} & A_{i_{max}} \end{bmatrix}$$

5.3 Conclusions

In this Chapter, the time-frequency nature of the STFT and CWT has been discussed and its relevance to the detection of faults in non-stationary CM signals has been demonstrated and compared. Discussion and investigation has demonstrated that full frequency or scale range analysis is highly computer intensive and therefore unsuitable for automatic WT CM.

The concept of a frequency tracking algorithm was introduced and the previously published CWT_{local} method was used as an example. This method proved successful on data from the Durham test rig however the processing times required were still significant and considered to be impractical for continuous application on large WT populations. The nature of CMSs themselves suggests that the CWT may not be the only option for frequency analysis and the sinusoidal features of monitoring signals suggested that a Fourier-based method could be more applicable, given careful application.

The IDFT_{local} algorithm was proposed as a means of combining frequency tracking and Fourier analysis. The short time samples used in this method allow the IDFT_{local} to be applied to signals that are effectively stationary, avoiding issues associated with the standard FFT. The time window is also adapted to the machine speed in order to ensure comparable frequency amplitudes between samples. This algorithm will be used throughout Chapter 6 when processing data and, in §6.2, will be compared with the CWT_{local} frequency tracking algorithm.

Having established the algorithm, Chapter 6 shows results from the CM test rig, processed using the $IDFT_{local}$.

5.4 References

[71] Cowie, J., *Climate Change: Biological and Human Aspects*, Cambridge University Press, 2007.

[72] Newland, D. E., *Random Vibrations, Spectral and Wavelet Analysis*, Third Edition, Longman Scientific & Technical, p. 33, 1993.

[73] Bellanger, M., *Digital Processing of Signals: Theory and Practice*, 2nd Edition, John Wiley & Sons Ltd, p9. 39-40, 1989.

[74] Kreyszig, E., *Advanced Engineering Mathematics*, 9th Edition, John Wiley & Sons Ltd, 2006.

[75] Qian, S., *Introduction to Time-Frequency and Wavelet Transforms*, Pearson Education Asia Limited and China Machine Press, 2005.

[76] Ifeachor, E. C., Jervis, B. B., *Digital Signal Processing: A Practical Approach*, 2nd Edition, Pearson Education Limited, 2002.

[77] Farge, M., *Wavelet Transforms and their Applications to Turbulence*, Annual Review of Fluid Mechanics, Vol. 24, pp. 395-457, 1992.

[78] Rucka, M., Wilde, K., *Application of Continuous Wavelet Transform in Vibration Based Damage Detection Method for Beams and Plates*, Journal of Sound and Vibrations, Vol. 297, Iss. 3-5, pp. 536-550, 2006.

[79] Yacamini, R., Smith, K. S., Ran, L., *Monitoring Torsional Vibrations of Electro-Mechanical Systems using Stator Currents*, Journal of Vibration and Acoustics, Transactions of the ASME, Vol. 120, Issue 1, pp. 72-79, 1998.

[80] Yang, W., Tavner, P. J., Crabtree, C. J., Wilkinson, M., *Cost Effective Condition Monitoring for Wind Turbines*, IEEE Transactions on Industrial Electronics, Vol. 57, No. 1, pp. 263-271, 2010.

6 Application and Results

"However beautiful the strategy, you should occasionally look at the results."

Winston Churchill
1874 – 1965

A number of different results are shown in this Chapter. Initially, data from the Durham CM test rig was analysed using both the new IDFT$_{local}$ algorithm and the CWT$_{local}$ algorithm. A number of fault-like conditions were investigated to demonstrate the detection of faults with different characteristics and in different signals. The fault conditions were:

- Rotor electrical asymmetry;
- High speed shaft mass unbalance, and;
- Gear tooth damage leading to failure.

In addition to test rig results, the use of electrical power in the time domain as an indicator of torsional drive train characteristics is examined using industrial data from an operational 1.3MW WT. This is believed to be one of the few examples of published field data.

All frequency tracking results in this Chapter are in the same format: subplot (a) shows the tracked frequency of interest; subplot (b) shows the amplitude of the frequency of interest, the raw result obtained from frequency tracking; and subplot (c) shows results filtered by a low pass filter. Each result figure includes its calculation time for later comparison. The absolute calculation time is given in seconds alongside a percentage calculation time, calculated as:

$$\text{Percentage Calculation Time} = \frac{T_A}{T_S} \times 100$$

where T_A is the analysis time and T_S is the time length of the analysed signal, both in seconds.

6.1 Test Rig Faults

Consistency of parameters is maintained throughout this section for each IDFT$_{local}$ analysis and, later, each CWT$_{local}$ analysis. However, the number of rotations in the time window is reduced for gear tooth damage to reduce noise due to small speed variations across the time window. The parameters used are given in Table 6.

Fault-like Condition	Number of Rotations	Frequency Window	Frequency Resolution	Sampling Frequency
Rotor Asymmetry	15	$f_c \pm 0.1$ Hz	0.1 Hz	5 kHz
High Speed Mass Unbalance	15	$f_c \pm 0.1$ Hz	0.1 Hz	5 kHz
Gear Tooth Damage	10	$f_c \pm 0.1$ Hz	0.1 Hz	5 kHz

Table 6: Parameters for IDFT$_{local}$ and CWT$_{local}$ frequency tracking algorithm

6.1.1 Rotor Electrical Asymmetry

As introduced in §4.4.1, rotor electrical asymmetry in the steady state has been examined in a number of previous works. However, fault detection under variable speed driving conditions has not been considered.

Rotor electrical asymmetry in a WRIG may be caused by a number of different fault conditions including inter-turn, winding insulation and brush gear faults. According to a study of WT generator failures [81], brush gear and slip ring damage are the source of 16% of faults in medium scale WTs (1-2MW), second only to bearing faults.

Brush gear damage has the effect of increasing the resistance of one rotor phase compared to the healthy phase resistance as described in §4.2.1. The level of unbalance can be described by:

$$\delta R = \left| R_{1_f} e^{i\theta_1} + R_{2_H} e^{i\theta_2} + R_{3_H} e^{i\theta_3} \right|$$

Where R_{1f} =faulted phase resistance, R_{2H} = R_{3H} = balanced phase resistance, $\theta_1 = 0,\ \theta_2 = \frac{2\pi}{3},\ \theta_3 = \frac{4\pi}{3}$. This can be defined (§4.4.1) as a percentage unbalance using:

$$\Delta R = \frac{\delta R}{R_{1_H}} = \frac{\delta R}{R_{2_H}} = \frac{\delta R}{R_{3_H}}$$

where R_{1H}, R_{2H} and R_{3H} are the balanced phase resistances.

For experimental purposes, two fault levels were implemented on the test rig. The healthy rotor resistance, including winding resistance, was 1.3Ω per phase and additional resistances of 0.3Ω and 0.6Ω were successively added to one phase to give two fault levels. These gave 23% and 46% unbalance respectively. While acceptable levels of unbalanced are undefined, these values were considered reasonable for the emulation of brush gear damage, based on experience. Indeed, for a machine with low rotor resistance, unbalance resulting from brush gear damage may easily exceed 100% of the balanced phase resistance.

Figure 77 and Figure 78 show the generator speed, stator line current and stator total instantaneous power data, hereinafter referred to as 'power', recorded for two wind driving conditions based on 7.5m/s, 6% turbulence and 15m/s, 20% turbulence respectively. Data recorded for balanced operation and the two fault conditions of 23% and 46% unbalance were stitched together to form a continuous signal, with fault-like conditions occurring as indicated. Only one line current signal is presented and analysed here, as is often the case for MCSA, and the power signal was calculated using two-wattmeter method. It can be seen that in the time domain neither the line current nor the power signals give any indication of the presence of a fault. The large amplitude of the power signal is 100Hz noise resulting from unbalance in the stator grid supply voltage to which the generator was connected.

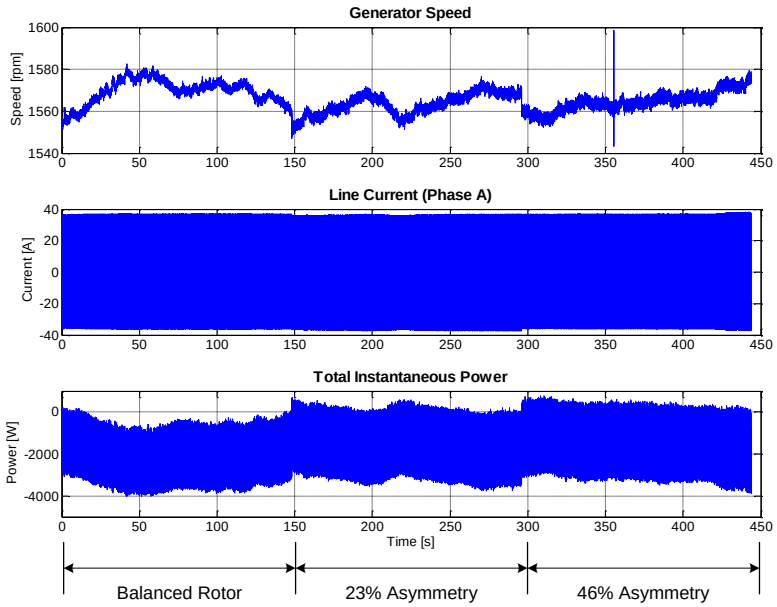

Figure 77: Raw data used in the analysis of electrical signals for the detection of rotor electrical asymmetry Driven by 7.5m/s, 6% turbulence conditions.

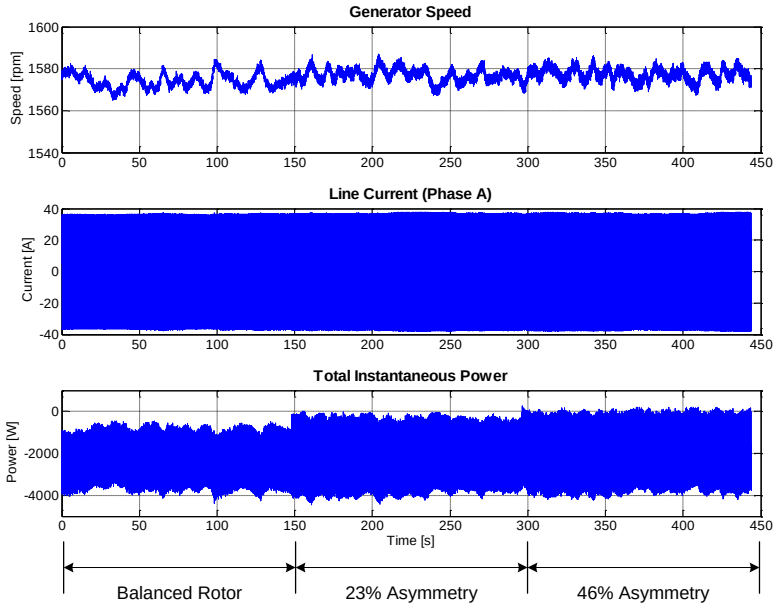

Figure 78: Raw data used in the analysis of electrical signals for the detection of rotor electrical asymmetry Driven by 15m/s, 20% turbulence conditions.

Based on collaborative research described in §4.4.1.2, four fault-related slip-dependent frequencies in line current and four in power were tracked using the $IDFT_{local}$. As a graphical summary, the four frequencies of interest ('c', 'd', 'e' and 'f') are shown in Figure 79 for line current and Figure 80 for power. Components 'a' and 'b' are present under healthy and faulty operation, as previously discussed.

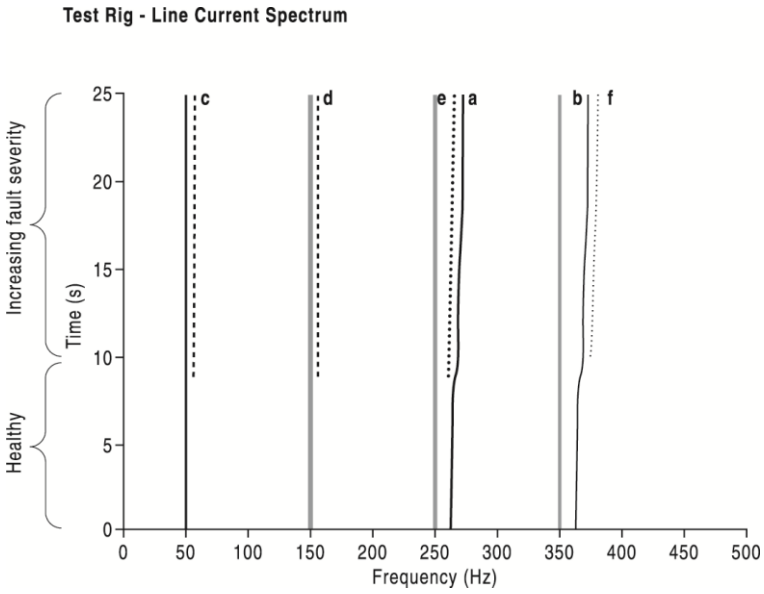

Figure 79: Line current spectrum indicating fault-related harmonic components

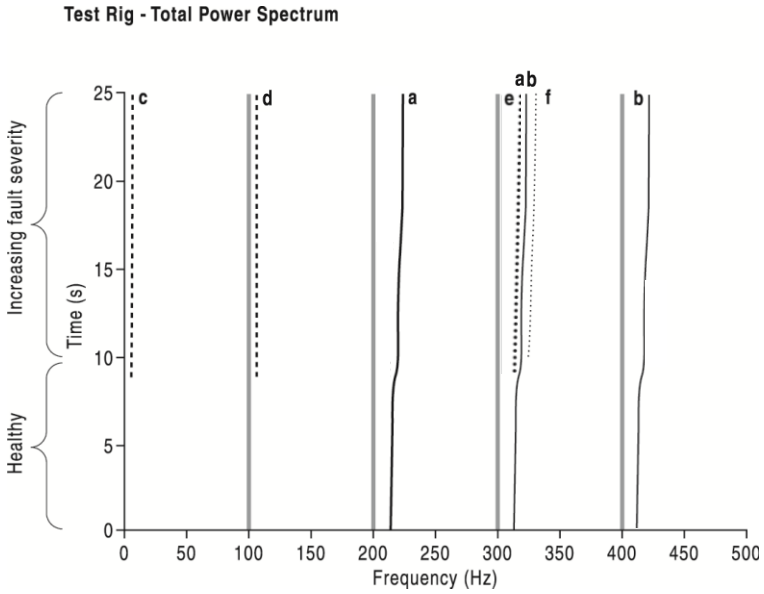

Figure 80: Total instantaneous power spectrum indicating fault-related harmonic components

6.1.1.1 Line Current

Figure 81 shows the results of IDFT$_{local}$ tracking of component 'c', the widely reported (1-2s)f_{se} component in line current. The test rig was driven using the 7.5m/s, 6% turbulence driving condition. The amplitude of the fault-related frequency jumps sharply when the 23% fault is introduced at 150s. A similar jump occurs for the 46% unbalance condition introduced at 300s. There is clearly a degree of noise in the raw

result, subplot (b), however the detection remains clear. It is apparent from subplot (c) that low pass filtering improved the result still further.

Since the algorithm showed a result for the $(1\text{-}2s)f_{se}$ component, processing was extended to the other fault-related harmonic components from §4.4.1.2; components 'd', 'e' and 'f'. The results of analysis of these harmonic components are shown in Figure 82, Figure 83 and Figure 84 respectively.

It can be seen from Figure 82 that the $2sf_{se}$ component 'd' around the third supply harmonic of current gives a detection signal very comparable to that from component 'c' shown in Figure 81. It is even arguable that the detection is improved using analysis of this harmonic component.

The result from component 'e' may also be useful as an indicator of fault severity. In Figure 83 it can be seen that the amplitude of component 'e' does not change significantly until the larger, 46% unbalance is introduced, possibly suggesting it does not appear until higher levels of fault are introduced.

It is interesting to note that component 'f' in current, Figure 84, does not yield a result for this level of unbalance.

In order to illustrate the algorithm's ability to function under different driving conditions, the second variable speed driving condition, 15m/s and 20% turbulence, was applied to the test rig and the same fault-like conditions introduced.

Figure 85 shows the IDFT_{local} result from tracking frequency 'c' in stator current with the higher turbulence, 15m/s, 20% turbulence driving conditions. It can be seen that the result is as clear as that shown in Figure 81 for the less turbulent 7.5m/s, 6% driving condition. Since the results from the second driving condition are comparable to those already presented, they are not included in the main body of the thesis. Instead, an extended set of results from the analysis of stator current for both driving conditions can be found in Appendix C.1.

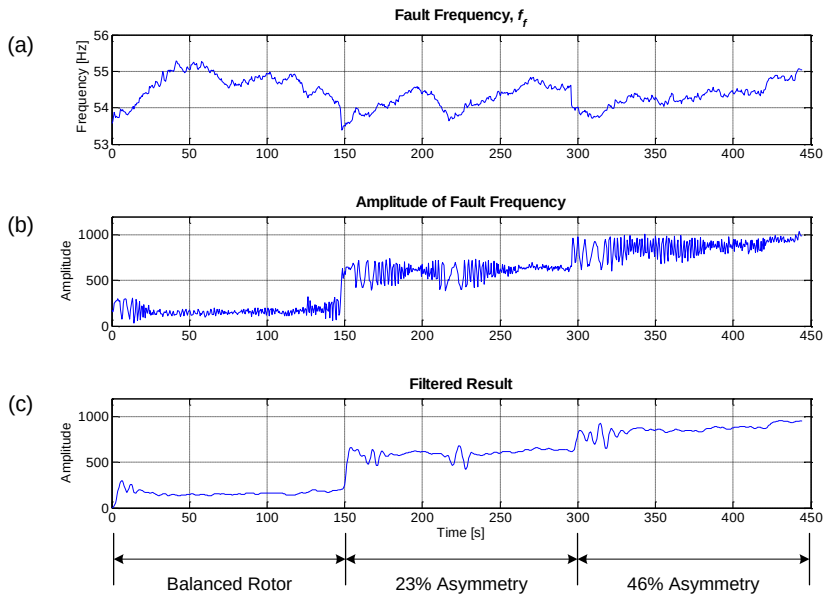

Figure 81: IDFT$_{local}$ analysis of generator line current frequency component 'c' for the detection of rotor electrical asymmetry: (a) Frequency of interest; (b) amplitude of frequency of interest; (c) filtered result. Driven by 7.5m/s, 6% turbulence conditions. Calculation time = 0.98s = 0.22%.

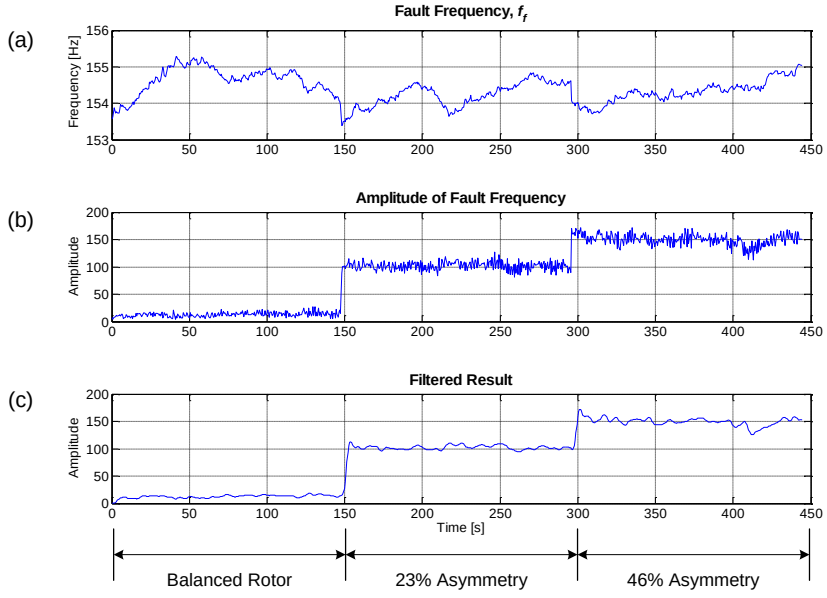

Figure 82: IDFT$_{local}$ analysis of generator line current frequency component 'd' for the detection of rotor electrical asymmetry: (a) Frequency of interest; (b) amplitude of frequency of interest; (c) filtered result. Driven by 7.5m/s, 6% turbulence conditions. Calculation time = 1.05s = 0.24%.

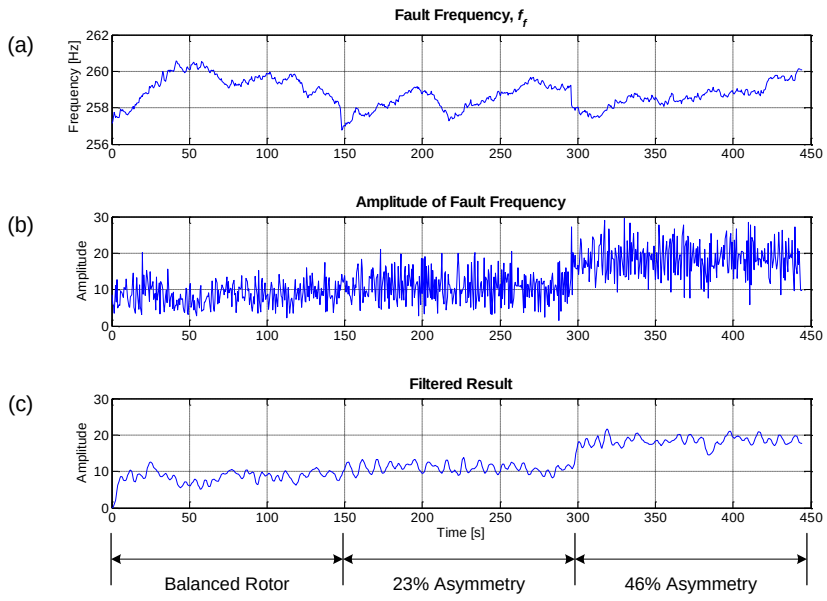

Figure 83: IDFT$_{local}$ analysis of generator line current frequency component 'e' for the detection of rotor electrical asymmetry: (a) Frequency of interest; (b) amplitude of frequency of interest; (c) filtered result. Driven by 7.5m/s, 6% turbulence conditions. Calculation time = 1.09s = 0.25%.

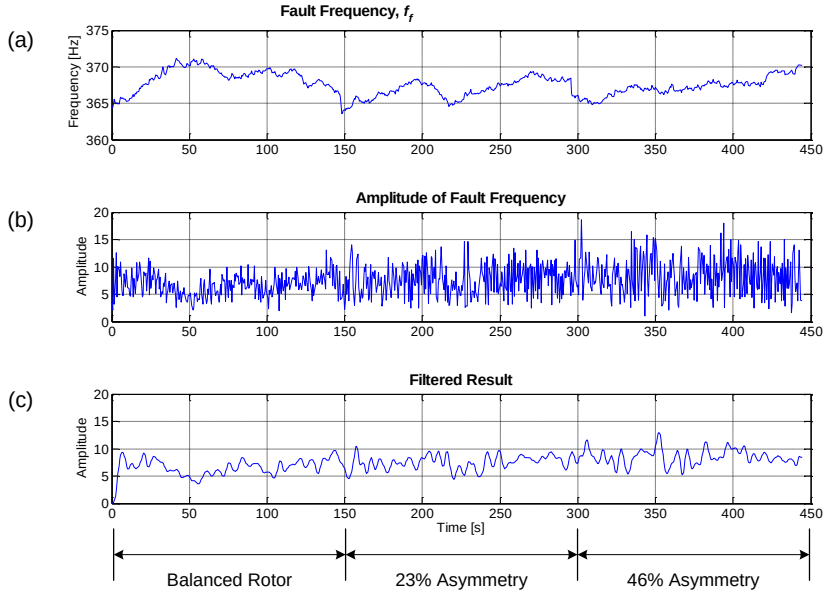

Figure 84: IDFT$_{local}$ analysis of generator line current frequency component 'f' for the detection of rotor electrical asymmetry: (a) Frequency of interest; (b) amplitude of frequency of interest; (c) filtered result. Driven by 7.5m/s, 6% turbulence conditions. Calculation time = 1.11s = 0.25%.

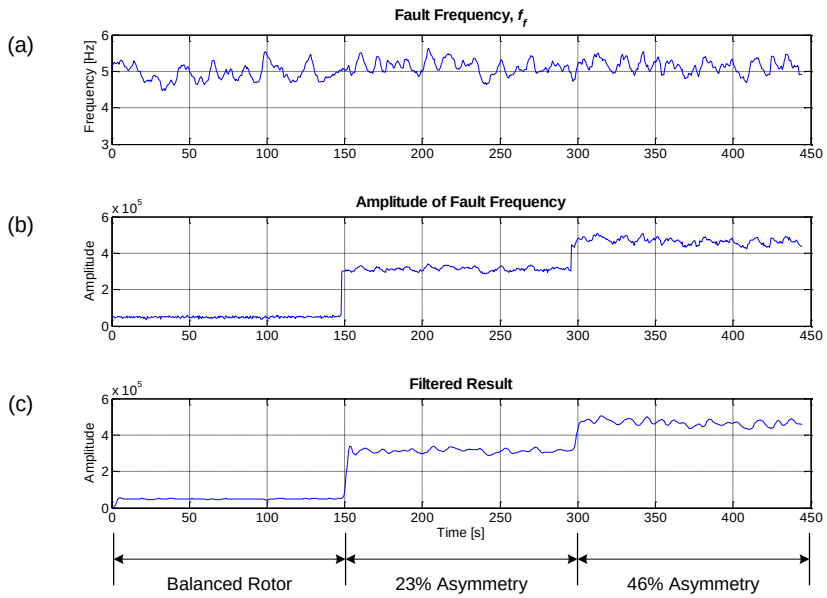

Figure 85: IDFT$_{local}$ analysis of generator line current frequency component 'c' for the detection of rotor electrical asymmetry: (a) Frequency of interest; (b) amplitude of frequency of interest; (c) filtered result. Driven by 15m/s, 20% turbulence conditions. Calculation time = 0.97s = 0.22%.

6.1.1.2 Total Instantaneous Power (Power)

Following successful fault detection in the line current signal, attention is now turned to analysis of the total instantaneous power signal. As before, four results are presented for the 7.5m/s, 6% turbulence driving condition.

Figure 86 shows the result of IDFT$_{local}$ analysis of the $2sf_{se}$ component, 'c', in power. As discussed in §4.4.1.2, this component has the advantage of having shifted from being a sideband around 50Hz in stator current to being a sideband around zero in power. As for current analysis, changes as the fault is introduced and its severity increased are clearly visible although there is a certain amount of variability in the result, possibly a result of the significant changes in the magnitude of the DC power component.

A much clearer detection is given by the $(2\text{-}2s)f_{se}$ component, 'd', shown in Figure 87, where a step change occurs with fault introduction and development. A constant level is then seen for each rotor fault-like condition.

As before, component 'e', Figure 88, shows a certain amount of change but the main increase in its amplitude occurs only when the fault severity is increased to 46%. This, again, suggests that component 'e' may be a useful indicator of fault severity rather than an earlier fault indicator.

Analysis showed a minor change in the amplitude of component 'f', contrary to the equivalent component in current, Figure 84. However the change was not significant. The algorithm was also able to demonstrate correct operation when applied to power data obtained under different driving conditions, just as has previously been indicated for analysis of stator current. The results from the 15m/s, 20% turbulence condition are included in Appendix C.1.2 although are not in the main body of the text.

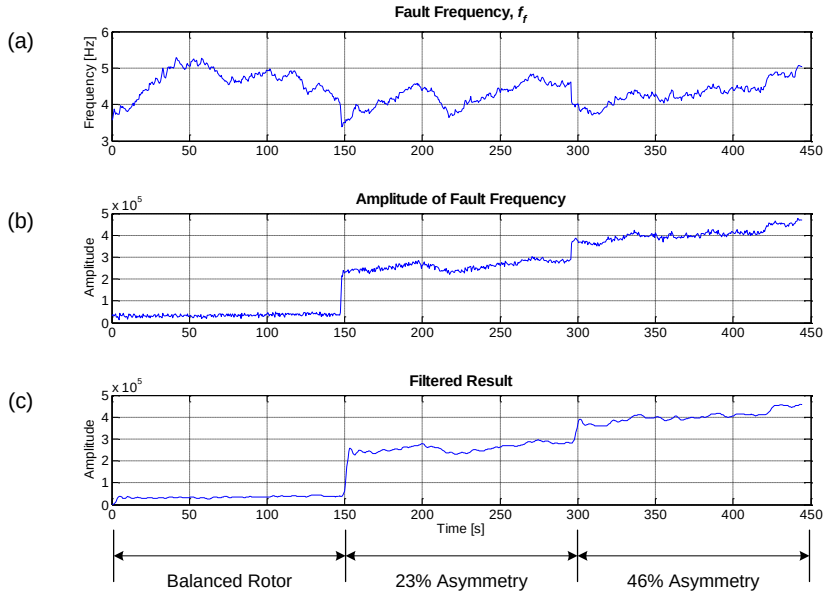

Figure 86: IDFT$_{local}$ analysis of generator total power frequency component 'c' for the detection of rotor electrical asymmetry: (a) Frequency of interest; (b) amplitude of frequency of interest; (c) filtered result. Driven by 7.5m/s, 6% turbulence conditions. Calculation time = 0.91s = 0.20%.

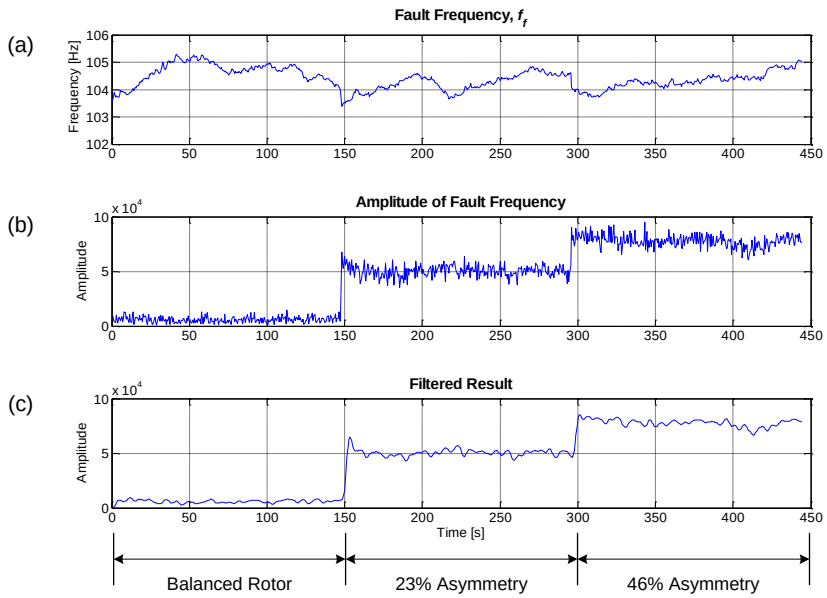

Figure 87: IDFT$_{local}$ analysis of generator total power frequency component 'd' for the detection of rotor electrical asymmetry: (a) Frequency of interest; (b) amplitude of frequency of interest; (c) filtered result. Driven by 7.5m/s, 6% turbulence conditions. Calculation time = 1.02s = 0.23%.

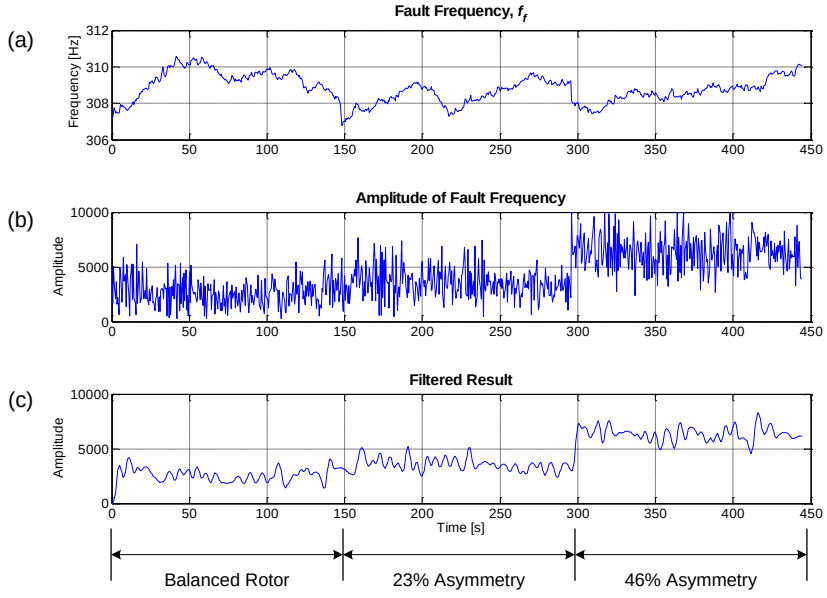

Figure 88: IDFT$_{local}$ analysis of generator total power frequency component 'e' for the detection of rotor electrical asymmetry: (a) Frequency of interest; (b) amplitude of frequency of interest; (c) filtered result. Driven by 7.5m/s, 6% turbulence conditions. Calculation time = 1.09s = 0.25%.

6.1.2 High Speed Shaft Mass Unbalance

As previously stated, individual fault mechanisms and conditions induce their own, different characteristic frequencies in monitoring signals. Monitoring of electrical signals to detect rotor electrical asymmetry has proved successful using the $IDFT_{local}$ however a significant proportion of WT drive train faults stem from mechanical unbalances rather than electrical. Traditional vibration monitoring has been based on the examination of complex spectra recorded from vibration transducers including accelerometers and proximity sensors. Both of these types of transducers are installed on the Durham test rig and so were considered for investigation.

As shown in Chapter 3, real vibration spectra can be complex, noisy and difficult to interpret. The frequency ranges of the spectra have to be kept wide to ensure all relevant harmonics are visible, resulting in unwieldy figures containing a forest of harmonics. In addition, individual spectra have to be examined manually to observe a trend over time. It makes sense, therefore, to analyse these signals using a frequency tracking technique. Here, the $IDFT_{local}$ algorithm is applied to test its capabilities on high noise signals from vibration transducers.

Many mechanical unbalances or faults cause fault frequencies that are a function of rotational speed so the fundamental of this was investigated: high speed shaft mass unbalance. This unbalance causes a once-per-revolution, f_{rm}, component in vibration signals so this frequency will be tracked.

Here, a small mass of 92g was fitted to the high speed shaft experimental balance plane successively at two different radii (80mm and 230mm) to give two different fault levels. Using the International Standard formulae for balance quality given in §4.4.2, these two fault levels correspond to G 13.4 and G 38.5 respectively, at 1600rpm. These levels of unbalance both appear at first glance to be very large however it is important to note that the grades given in §4.4.2 are the limits for healthy machine operation and consequently it should be expected that they will be significantly increased during faulted operation.

Figure 89 shows data recorded for generator speed, high speed shaft displacement, generator vertical (radial) acceleration and gearbox high speed end vertical (radial) vibration under the 7.5m/s, 6% turbulence conditions. Very little change can be observed in the time domain signals when the two levels of fault are introduced. The only apparent change is the increased level of noise on the

displacement measurement during the high fault level. This is thought to be instrumentation noise from the laboratory environment rather than an indication of a fault-like condition. Similar characteristics are observed in raw data recorded using the 15m/s, 20% turbulence driving condition. This data is given in Appendix C.2.2 since these additional results are not in the main body of the thesis.

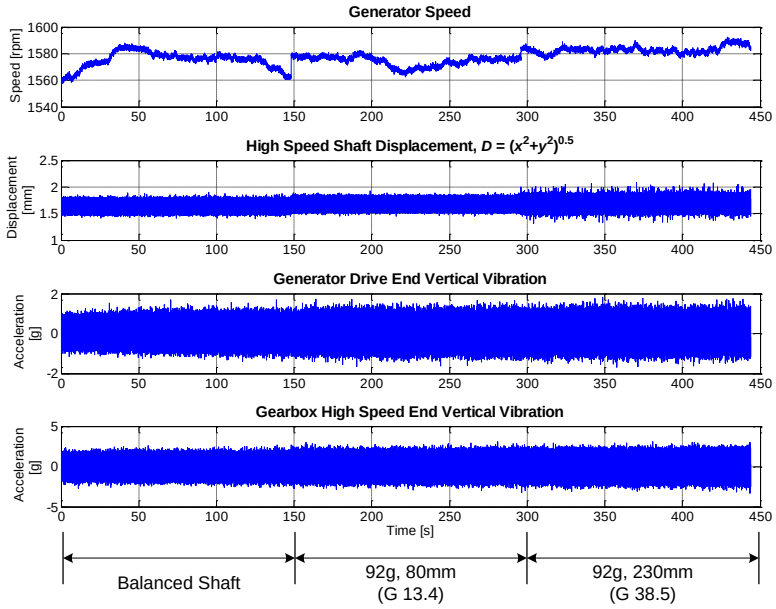

Figure 89: Raw data used in the analysis of mechanical signals for the detection of high speed shaft mass unbalance Driven by 7.5m/s, 6% turbulence conditions.

The once-pre-revolution frequency, f_{rm}, was tracked in each of these vibration signals using the IDFT$_{local}$. The displacement signal was analysed first as the transducers were placed near the high speed shaft mass unbalance plane and a clear result was expected. Figure 90 shows the result obtained from analysis of the displacement signal. The step to the smaller mass unbalance is quite small but is still quite distinct. The larger unbalance has had a much more significant effect, generating a clear step change in the amplitude of the f_{rm} component. Importantly, the result does not appear to have been affected by the noise apparently present in the signal itself.

The amplitude of the f_{rm} component in the generator accelerometer signal is analysed in Figure 91. Again, we see a marked change in vibration between the healthy and two faulty conditions, the magnitude increasing with fault severity. It has already been noted that vibration signals are often noisy and it can be seen that the accelerometer signal has a higher variability in its result than displacement, suggesting acceleration is a noisier signal. Nevertheless, a step change is visible.

This is highlighted by Figure 92 which shows the result of IDFT$_{local}$ analysis of the gearbox accelerometer signal. While there is a change in the amplitude of the fault-related frequency component, it is much less marked than the displacement and generator accelerometer results in terms of noise. It is also noticeable that the amplitude of the fault frequency is much lower. This is thought to be the result of two conditions. Firstly, the vibration transducer is further from the fault, suggesting that accurate vibration monitoring may be heavily dependent on careful positioning of transducers. Secondly, the gearbox casing is very stiff, particularly around its bearings, due to the solid, cast internal structure. Nevertheless, a change is still apparent despite the noise and decreased signal magnitude.

Results recorded using the second driving condition showed very similar trends and are included in Appendix C.2.2 for completeness.

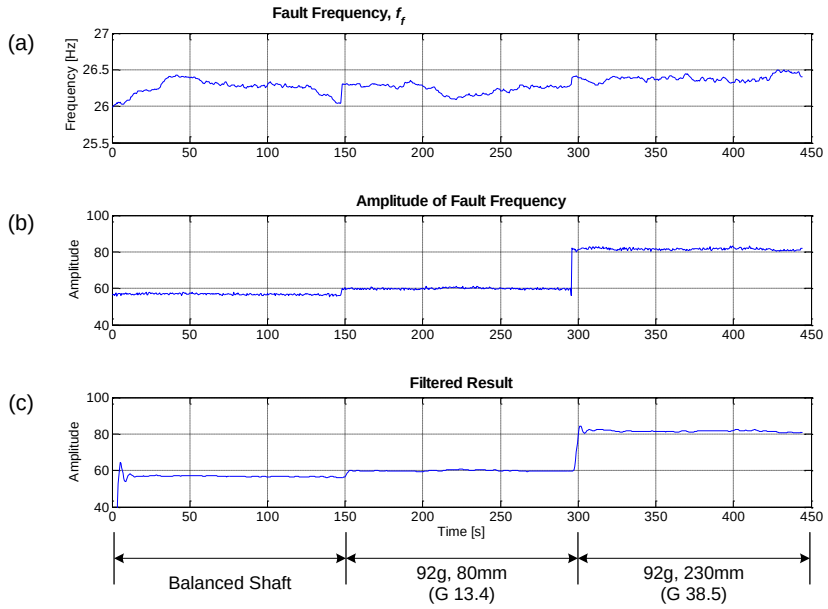

Figure 90: IDFT$_{local}$ analysis of high speed shaft displacement frequency component f_{rm} for the detection of high speed shaft mass unbalance: (a) Frequency of interest; (b) amplitude of frequency of interest; (c) filtered result. Driven by 7.5m/s, 6% turbulence conditions. Calculation time = 0.95s = 0.21%.

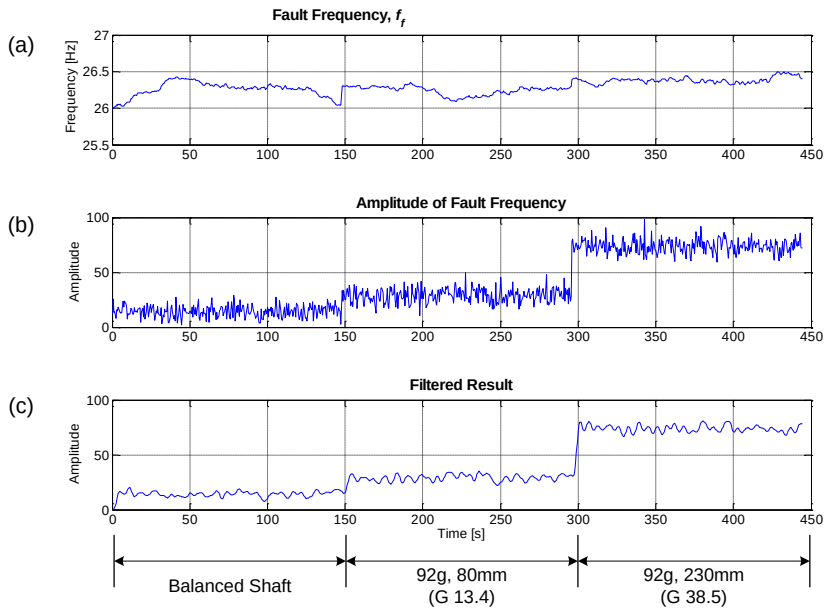

Figure 91: IDFT$_{local}$ analysis of generator vertical vibration frequency component f_{rm} for the detection of high speed shaft mass unbalance: (a) Frequency of interest; (b) amplitude of frequency of interest; (c) filtered result. Driven by 7.5m/s, 6% turbulence conditions. Calculation time = 0.97s = 0.22%.

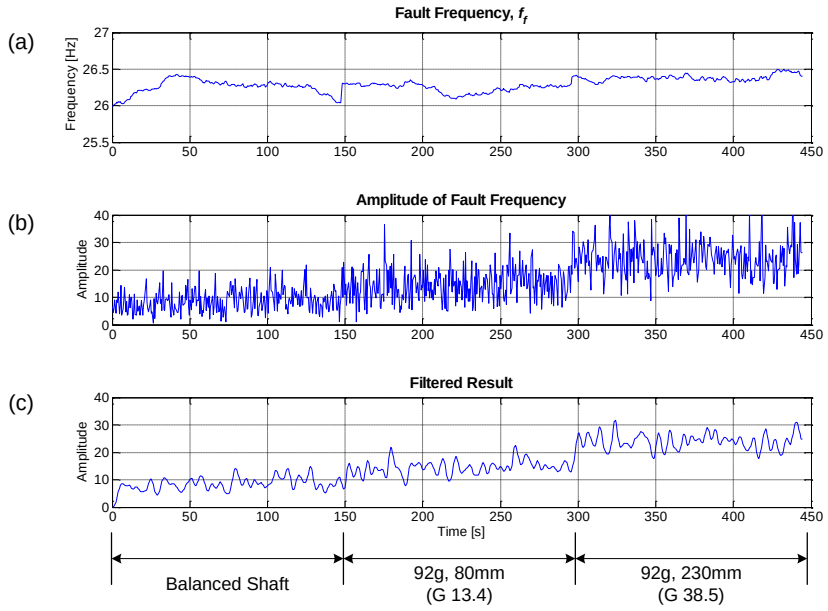

Figure 92: IDFT$_{local}$ analysis of gearbox high speed end vibration frequency component f_{rm} for the detection of high speed shaft mass unbalance: (a) Frequency of interest; (b) amplitude of frequency of interest; (c) filtered result. Driven by 7.5m/s, 6% turbulence conditions. Calculation time = 0.97s = 0.22%.

6.1.3 Gear Tooth Failure

Based on a photos supplied by a WT operator, progressive damage was introduced to the leading contact edge of the gearbox high speed pinion. A typical fault is shown in Figure 93 where a significant portion of a gear tooth has broken away leaving a short amount of the tooth root visible.

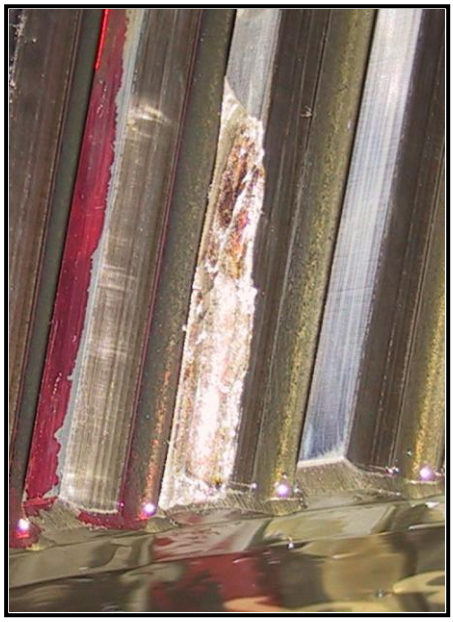

Figure 93: Gear tooth failure from an operational wind turbine, taken from [82]

A damaged tooth will cause mechanical vibrations at its rotational frequency (§4.4.3). As the gear speed is equal to the generator rotational speed, the fault frequency of interest is, again, the rotational frequency f_{rm}. The difficulties of monitoring had already been understood, so both accelerometers were placed on the gearbox: one on the high speed end and one centrally on top of the gear case.

The gearbox high speed assembly was removed between each test and the next fault ground by hand to give eight faults of increasing severity. Figure 94(a), (b) and (c) show the healthy pinion, fault level 3 and fault level 8 respectively. The full set of fault images can be found in Appendix C.3.1. The fault was progressively moved across the tooth face until the while face was missing (fault level 7). The entire tooth was removed except for a small amount of the root in fault level 8.

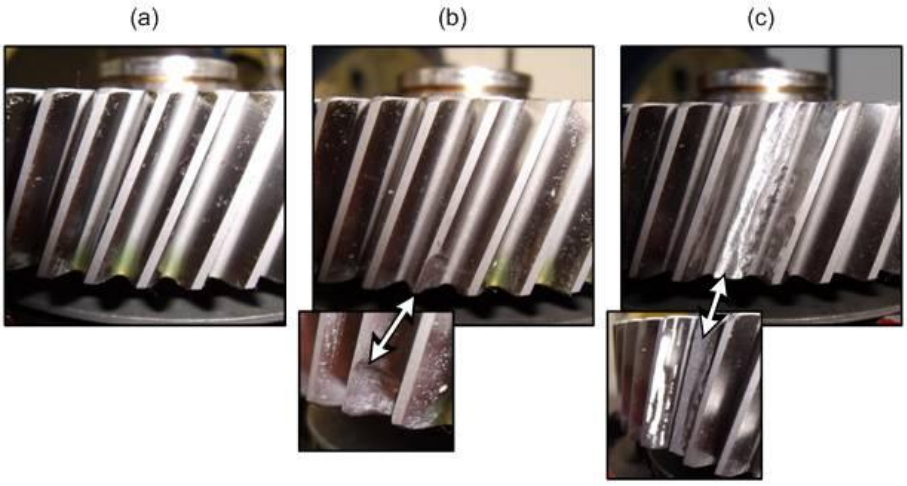

Figure 94: Test rig gearbox high speed pinion damage introduced for fault testing: (a) healthy, (b) fault level 3 and (c) fault level 8

Figure 95 shows raw accelerometer signals recorded for each fault subsequently stitched together in order of severity. The accelerometers were located on the gearbox casing and on the high speed end, as shown in Appendix D, Figure 4. Fault level 4 is missing due to a data file error. It is apparent that there is large variability in the level of vibration signal noise, illustrating one of the issues encountered with vibration monitoring. It is thought much of this variability results from fault incorporation methods. Since the gearbox high speed section was removed at each testing stage, the gearbox vibration characteristic was disrupted by small dimensional errors introduced during successive reassembly. Nevertheless, frequency tracking was still thought to be a worthwhile endeavour.

Figure 96 shows the result of IDFT_{local} analysis of the f_{rm} component in the gearbox high speed end accelerometer signal. As expected from earlier information, the majority of tooth faults yielded no change as a result of either the fault itself or the variation in the overall signal.

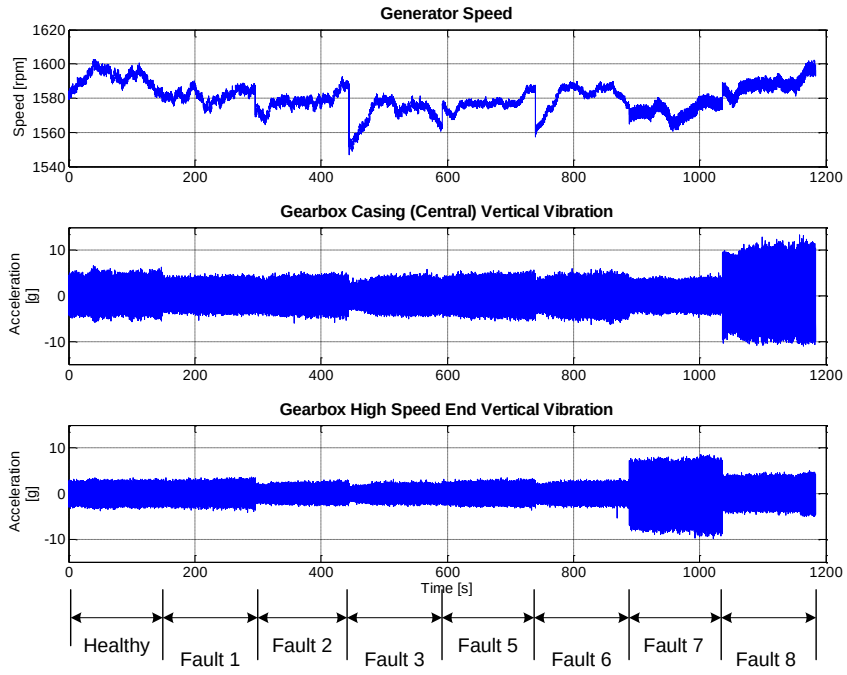

Figure 95: Raw data used in the analysis of mechanical signals for the detection of gear tooth damage (7.5m/s, 6% turbulence)

However, the result shows a step change where fault levels 7 and 8 were incorporated, suggesting detection has occurred. A number of reasons for the lack of detection up to this point are proposed. Firstly, the gears are of helical form meaning that at least two teeth per gear are meshing at any one time and no single tooth carries the full load alone. Secondly, the overall gearbox load is quite low. This may mean that individual tooth faults are not excited to a great extent. Finally, the gearbox construction is very rigid. The gear case has a strong, cast structure with significant internal webbing, shown in §4.2.2, Figure 52. It is thought that vibration resulting from tooth faults is not easily transmitted to the external accelerometers because of this stiff, rigid structure. In an operational WT, the gear case is likely to be much more flexible compared to its loading and the large load being driven through the gearbox will allow greater transmission of healthy and faulty vibrations to the external transducers.

Figure 97 shows the same processing applied to the second accelerometer signal. The accelerometer is mounted on the top of the gear case. The figure does not give a result until the tooth has been fully removed for fault 8. At this point, a change in the amplitude of the f_{rm} component is observed, albeit slight.

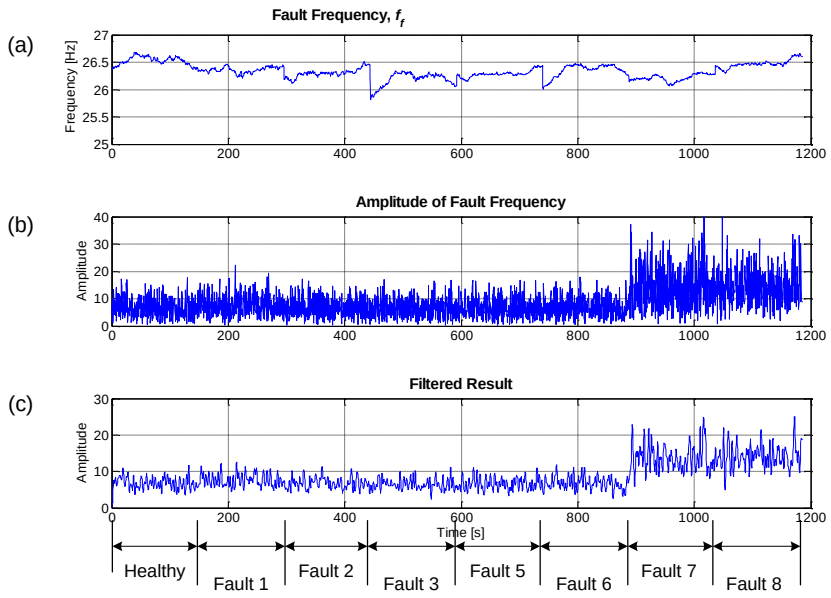

Figure 96: IDFT$_{local}$ analysis of gearbox high speed end vertical vibration frequency component f_{rm} for the detection of gear tooth damage: (a) Frequency of interest; (b) amplitude of frequency of interest; (c) filtered result. Driven by 7.5m/s, 6% turbulence conditions. Calculation time = 3.34s = 0.28%.

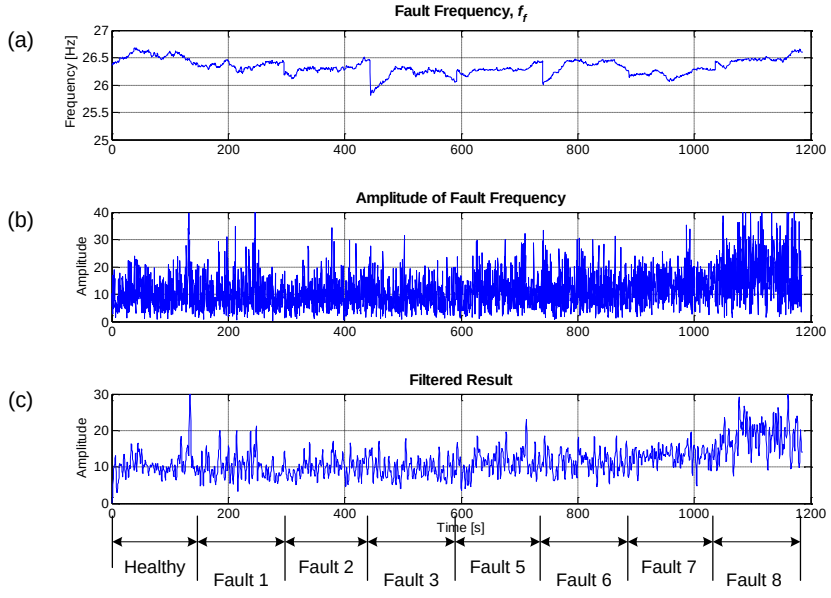

Figure 97: IDFT$_{local}$ analysis of gearbox casing vertical vibration frequency component f_{rm} for the detection of gear tooth damage: (a) Frequency of interest; (b) amplitude of frequency of interest; (c) filtered result. Driven by 7.5m/s, 6% turbulence conditions. Calculation time = 2.63s = 0.22%.

No further data was analysed for gear tooth damage. It is clear that detection of gear tooth damage is difficult, particularly on a small scale where gearbox loading is low and the unit itself rigid and inflexible.

6.2 Comparison of Frequency Tracking Techniques

Throughout this chapter, the newly developed $IDFT_{local}$ algorithm has been used. However, it is only sensible to support this method through comparison against results obtained using an established, published method. In this section, the $IDFT_{local}$ is compared with the CWT_{local} frequency tracking method introduced in §5.1.5.

6.2.1 Electrical Signals

While the $IDFT_{local}$ algorithm was able to give results for both current and power monitoring, the CWT_{local} frequency tracking algorithm was unable to give results for current analysis and very limited results for power. The results obtained are not included here because of their poor quality when analysing data sampled at 5kHz, as has been the case throughout this work. The CWT_{local} method has previously been shown that it is capable of producing results from power signal analysis however its success was dependent on the data sampling rate and the adjustment of parameters. This is an inherent issue for wavelet-based methods as the resolution at low frequencies is poor for high sampling frequencies unless an extremely large range of scale constants is applied, significantly increasing the required processing power.

6.2.2 Mechanical Signals

The CWT_{local} method saw greater success analysing data from accelerometers and displacement transducers. The raw and filtered results for both methods are presented. Subplots show: (a) the tracked frequency; (b) the $IDFT_{local}$ result; (c) the CWT_{local} tracking result. Only data from 7.5m/s, 6% turbulence driving conditions are presented in the interests of clarity and conciseness.

Figure 98, shows unfiltered results from analysis of shaft displacement. While spectral results are generally very subjective, it is apparent that the $IDFT_{local}$ algorithm has dealt more effectively with variable speed operation. Its result, Figure 98(b), is much less variable than the result from the CWT_{local} algorithm, Figure 98(c). As would be expected, the filtered result, Figure 99, only serves to highlight this point.

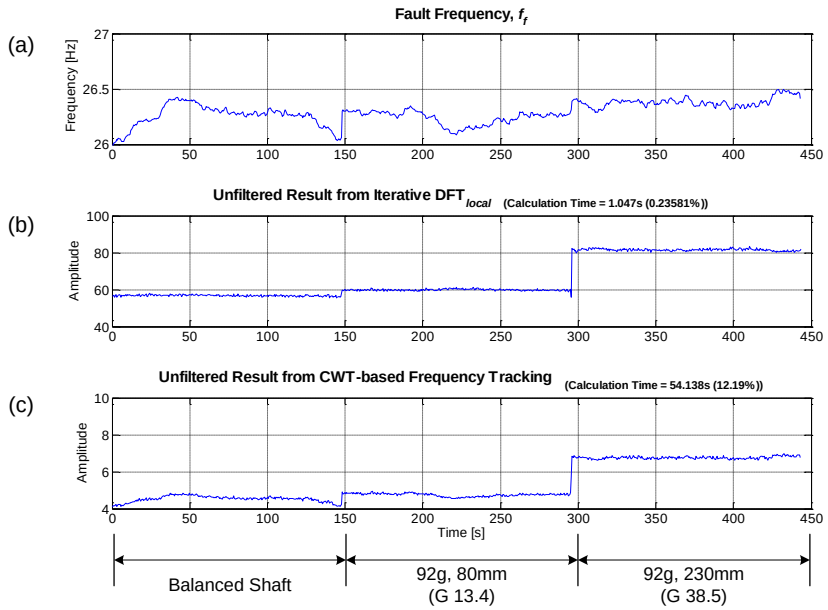

Figure 98: Unfiltered analysis of high speed shaft displacement frequency component f_{rm} for the detection of high speed shaft mass unbalance: (a) Frequency of interest; (b) amplitude of frequency of interest using IDFT$_{local}$; (c) amplitude of frequency of interest using CWT$_{local}$ frequency tracking. Driven by 7.5m/s, 6% turbulence conditions.

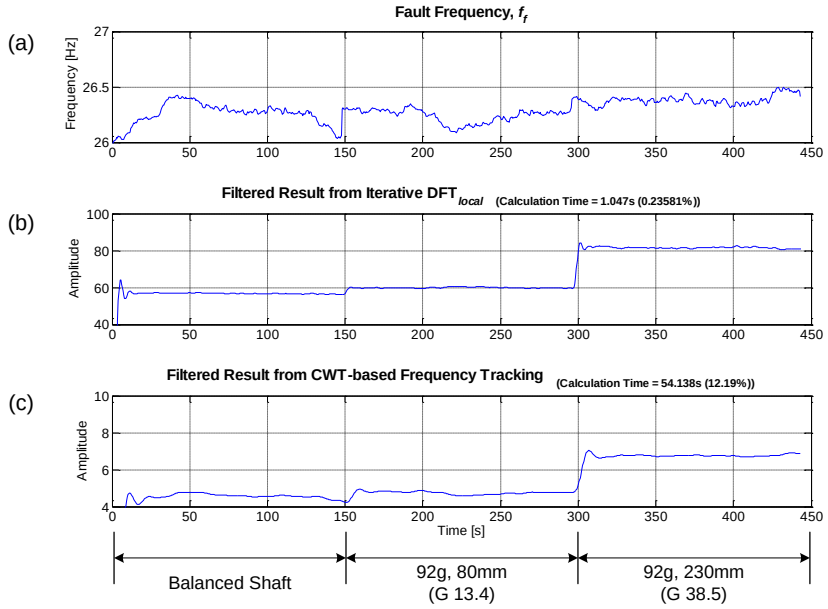

Figure 99: Filtered analysis of high speed shaft displacement frequency component f_{rm} for the detection of high speed shaft mass unbalance: (a) Frequency of interest; (b) amplitude of frequency of interest using IDFT$_{local}$; (c) amplitude of frequency of interest using CWT$_{local}$ frequency tracking. Driven by 7.5m/s, 6% turbulence conditions.

The algorithms were applied in turn to 7.5m/s, 6% turbulence data for gear tooth damage. Under these fault-like conditions, the unfiltered results, Figure 100(b) and Figure 100(c), do not differ greatly however the result from the CWT_{local} algorithm, Figure 100(c), has a significantly reduced level of noise.

Examining the filtered results, Figure 101, it is clear that the CWT_{local} method has been more successful, albeit not greatly, in the detection of gear tooth damage. It should be noted, however, that neither method can be easily said to have the upper hand in this case.

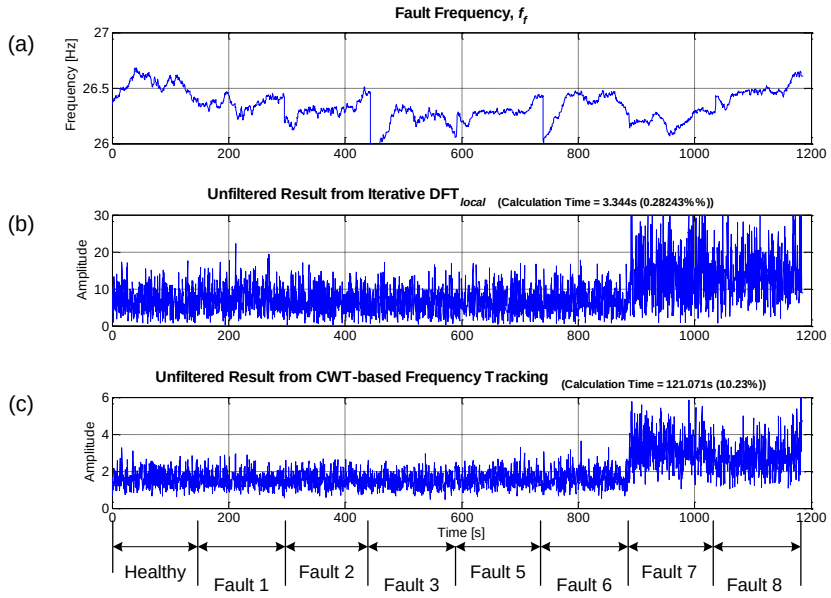

Figure 100: Unfiltered analysis of generator high speed end vibration frequency component f_{rm} for the detection of gear tooth damage: (a) Frequency of interest; (b) amplitude of frequency of interest using $IDFT_{local}$; (c) amplitude of frequency of interest using CWT_{local} frequency tracking. Driven by 7.5m/s, 6% turbulence conditions.

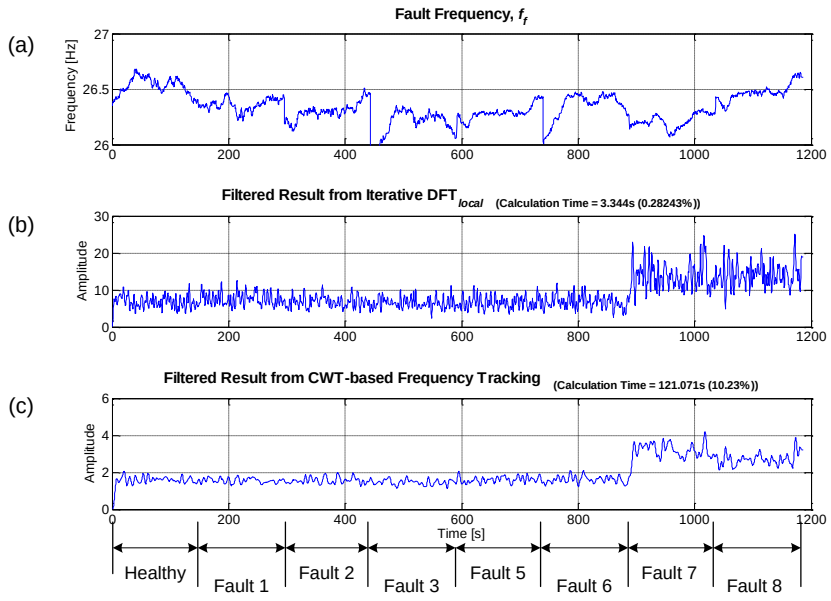

Figure 101: Filtered analysis of generator high speed end vibration frequency component f_{rm} for the detection of gear tooth damage: (a) Frequency of interest; (b) amplitude of frequency of interest using IDFT$_{local}$; (c) amplitude of frequency of interest using CWT$_{local}$ frequency tracking. Driven by 7.5m/s, 6% turbulence conditions.

6.2.3 Summary

It appears from this comparison that each of the two algorithms has its own place in signal analysis.

The IDFT$_{local}$ algorithm proved more successful for analysis of sinusoidal fault indicators, such as those from mass unbalance or rotor electrical asymmetry. A large number of serious fault conditions, such as shaft unbalance, shaft misalignment and blade unbalance among others, will induce a sinusoidal response in monitoring signals.

The CWT$_{local}$ method demonstrated improved results in the detection of more impulsive responses from gear tooth damage. This is a useful characteristic of the CWT$_{local}$ method as certain faults will have an impulsive response in monitoring signals.

Despite the advantage discussed above, one point that must be taken into consideration is that of the processing power required by each method. In all cases, the CWT$_{local}$ algorithm required significantly more processing power than the IDFT$_{local}$. This can be seen from the processing times, representative of the required processing power, that are given in Table 7. The CWT$_{local}$ method was, in both cases, significantly more computer intensive than the IDFT$_{local}$ processed on the same computer.

Fault-like Condition	$IDFT_{local}$		CWT_{local}	
	Processing Time	Percentage Signal Time	Processing Time	Percentage Signal Time
High Speed Mass Unbalance	0.953 s	**0.21 %**	54.232 s	**12.21 %**
Gear Tooth Damage	3.34 s	**0.28 %**	121.07 s	**10.23 %**

Table 7: Processing times for the $IDFT_{local}$ and CWT_{local} frequency tracking algorithms

6.3 Field Torque Analysis using Power Signals

6.3.1 Introduction

Having demonstrated the use of power in fault detection by frequency tracking, an amount of data from an operational WT was examined. A total of 4 weeks of data was made available by a WT operator however no faults occurred during this period and so frequency tracking was not applicable. The data led, however, to an investigation of the power as a medium for turbine monitoring without frequency tracking.

One of the major factors in the damage of WT drive trains is that of torque pulses due to sudden loading and unloading from wind turbulence and, most interestingly, during generator speed changes and synchronisation.

Pulses occurring during grid synchronisation can be over 100% of the turbine's rated torque and frequent and continued pulses are likely to cause significant stress damage over time. The problem is further compounded by negative torque pulses that so often occur alongside positive ones. Again, these can be over 100% of the rated torque however in the opposite direction.

Although torsional effects are important, torque measurement on such a large, low speed, inaccessible machine is practically and logistically difficult, although it is

possible using specialised equipment. The industrial partner referred to in Chapter 3 carried out a measurement campaign over three weeks to record high sampling frequency data from an operational WT. Data from a specially installed low speed shaft torque transducer, and for wind speed, generator speed and power were recorded alongside machine vibration data. The data was recorded at 7.5kHz but was down-sampled offline to 500Hz for this work to reduce computing requirements. The turbine was a 1.3MW, two speed, active stall machine and had been operating for several years. The machine speeds corresponded to 4-pole or 6-pole generator operation. Further details are unavailable for confidentiality reasons.

Due to the difficulties involved in measuring the shaft torques of a WT, it was suggested that torque derived from the electrical power signal may be a viable alternative. The electrical power has a particular advantage in that it is measured by the turbine controller and could be accessed for CM purposes, earlier results in the chapter demonstrating how this could be done.

The low speed shaft torque was measured and will be the mark against which the derived torque is compared.

The derived low speed shaft torque, T_{LSS}, is given by the equation:

$$T_{LSS} = N^2 \left(\frac{P_e}{\omega_{HSS}} \right)$$

where N is the gearbox ratio, P_e is the electrical power of the generator and ω_{HSS} is the high speed shaft speed. The gearbox ratio for this turbine is 78.3:1 and the turbine speed corresponds to either 4-pole or 6-pole operation.

In this short study, speed changes from 6-pole to 4-pole operation, starts from stationary, and turbine stops will be examined to demonstrate the applicability of the power signal as an indicator of mechanical loading. The signals used are shown in Figure 102 where a steady state region, turbine starting phase and speed change from 6-pole to 4-pole operation are visible. A turbine stop is also visible but is not analysed.

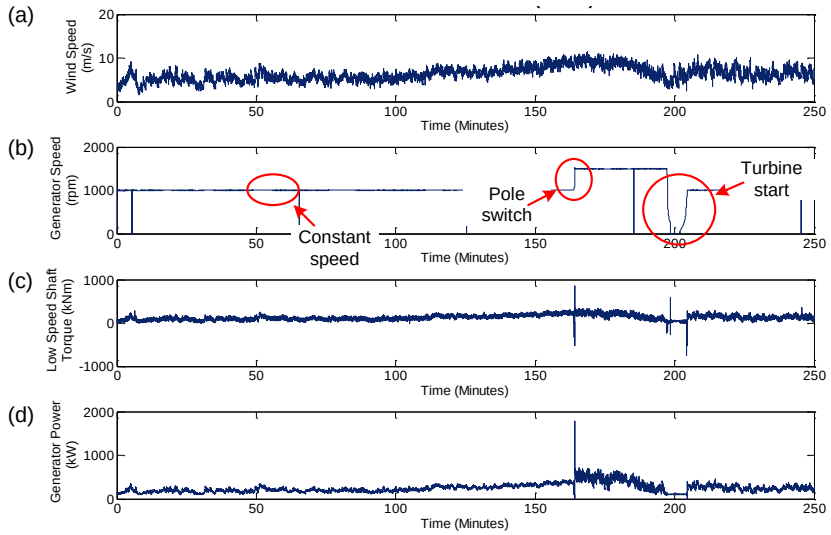

Figure 102: Signals recorded from the operational wind turbine for (a) wind speed, (b) generator speed, (c) low speed shaft torque and (d) generator power

6.3.2 Results

Figure 103 shows the measured torque and the torque derived from the generator power taken while the turbine is operating at 6-pole constant speed with variable load. It appears that the derived torque, Figure 103(b), gives a very close approximation to the measured low speed shaft torque, Figure 103(c).

During the turbine's start-up period, the measured and derived torques, Figure 104(b) and Figure 104(c) respectively, can also be seen to have close correlation in time. It is, however, apparent that negative torque pulses are not present in the derived torque. This is a result of the data acquisition system not allowing negative powers to be recorded. Nevertheless, positive torque oscillations are closely represented by the electrical power both in terms of their time domain positions and magnitudes.

Finally, the speed change transient is analysed. During this period the generator switches from 6-pole to 4-pole operation at low power. The derived torque, Figure 105(c), again closely replicates the measured torque, Figure 105(b) in both time and magnitude. It can also be seen that the torsional oscillations during the speed change, Figure 105 are considerably larger in magnitude and take longer to decay than those for the start-up period, Figure 104.

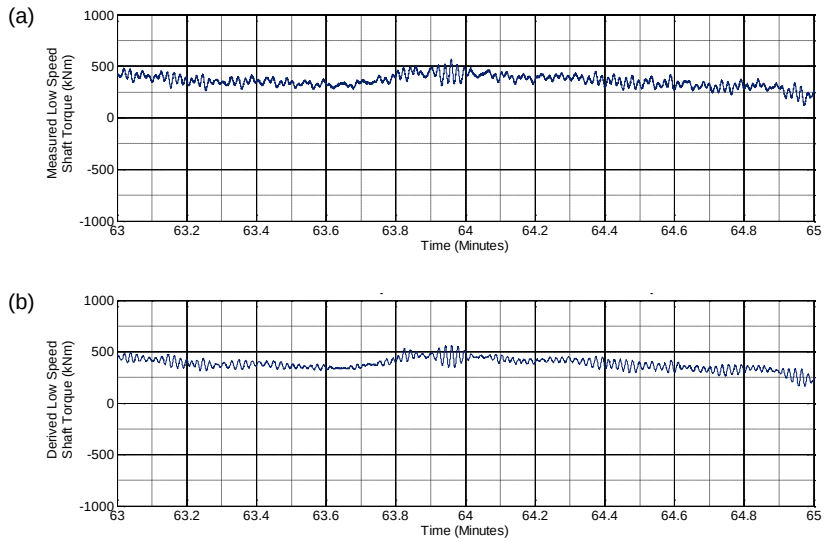

Figure 103: (a) Measured and (b) derived torques during constant speed, variable load operation

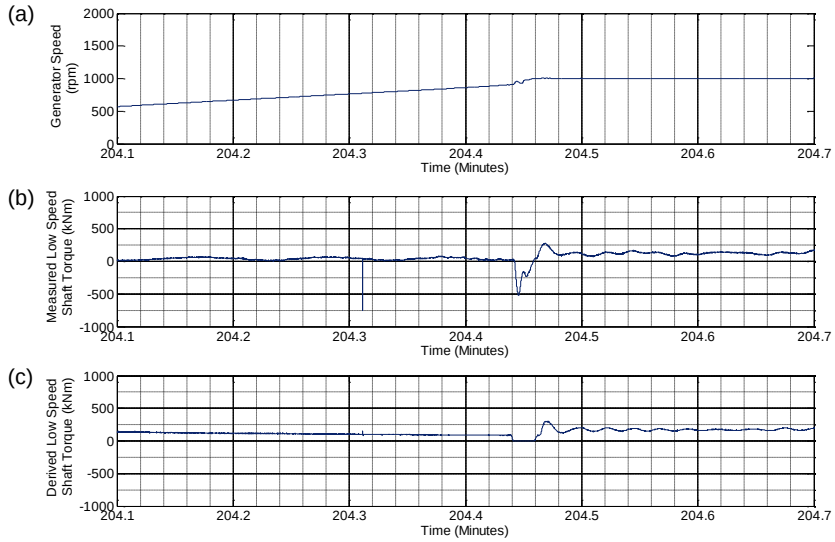

Figure 104: (a) Generator speed, (b) measured torque and (c) derived torque during turbine start from stationary to 6-pole operation

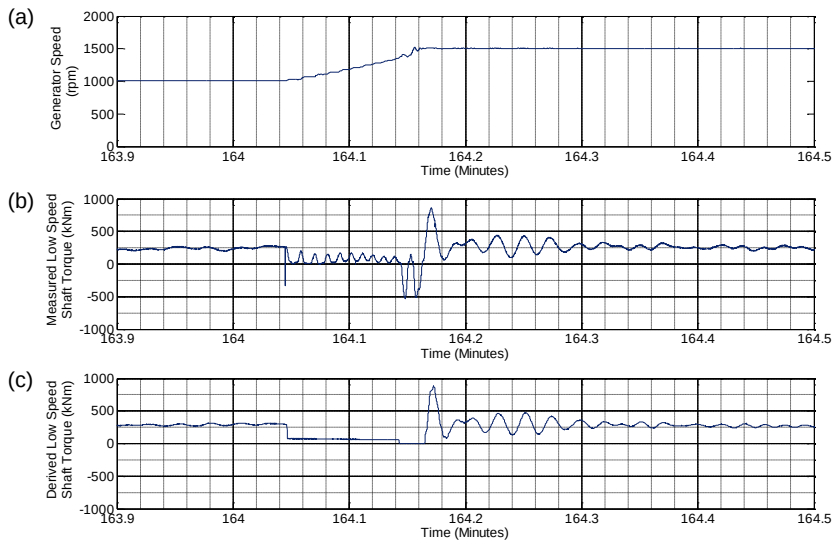

Figure 105: (a) Generator speed, (b) measured torque and (c) derived torque during speed change from 6-pole to 4-pole operation

It is clear from figures 103-105 that the torque derived from the measured generator power could be a reliable indicator of WT low speed shaft torque and could be used as a suitable method for detecting and measuring torque pulsations during transient periods. Given improved measurements where negative powers are recorded, negative torque pulses may also be measured accurately.

6.4 Summary

In this chapter, the IDFT$_{local}$ algorithm has been applied to data from three fault-like conditions on the test rig:

- Rotor electrical asymmetry;
- High speed shaft mass unbalance, and;
- Gear tooth failure.

In each case the relevant fault frequencies of interest, introduced throughout Chapter 4, were analysed by the IDFT$_{local}$ algorithm.

Rotor electrical asymmetry was clearly detected in both the generator stator power and current signals, giving step changes in a number of different harmonic components. The two fault levels were indicated by the step changes in results.

High speed shaft mass unbalance produced a distinct step in mechanical monitoring signals with shaft displacement showing a clear step change for each level of unbalance. Despite the level of noise present in generator and gearbox vibration signals, they too showed a change in the rotational frequency component as fault severity increased.

The algorithm also proved capable of dealing with different variable speed driving conditions. In the cases of rotor electrical asymmetry and high speed shaft mass unbalance, the $IDFT_{local}$ produced consistent results between the two driving conditions.

As expected from discussion with Operators and experienced monitoring engineers, gear tooth failure detection proved difficult using vibration signals from the gear case. However, a broken tooth was detected in two gearbox vibration signals. While the result was not as clear as those from other fault-like conditions, the method still proved capable of detecting failure. A number of reasons for this noisier result are suggested. In particular, the gearbox loading is very low when compared to the rigid, cast gearbox structure suggesting that small vibrations from tooth may not be transmitted strongly. The helical gear configuration also means that the faulted tooth would never be the sole meshing tooth. This would result in heavy damping of any response as loading is always split between at least two teeth.

Having successfully detected fault-like conditions, the $IDFT_{local}$ was compared with the published CWT_{local} algorithm. The $IDFT_{local}$ compared favourably with the CWT_{local} and produced results of better quality for high speed shaft mass unbalance. The CWT_{local} was unable to produce results for electrical unbalance using the raw 5kHz sampling frequency due to the scale resolution of the CWT_{local} discussed in §5.1.5.

It could well be argued that the CWT_{local} was more successful in the detection of gear tooth failure, Figure 101, as a step change was clearer than when the $IDFT_{local}$ was applied. This is expected as gear tooth failure produces a more impulsive response in vibration signals, ideally suited to the nature of the CWT.

However, when processing times were considered, the slight increase in the quality of result became insignificant as the $IDFT_{local}$ required significantly lower processing power, indicated by the reduced calculation times.

Finally, an investigation into the derivation of WT shaft torque from the generator power signal was presented using high sampling frequency data from an operational WT. The derived low speed shaft torque correlated closely with measurements for constant speed, variable load operation as well as for larger transients including turbine starts and generator pole changes.

6.5 References

[81] Alewine, K., Chen, W., "*Wind Turbine Generator Failure Modes Analysis and Occurrence*", Windpower 2010, Dallas, Texas, May 2010.

[82] Skriver, S., *Determining a Strategy for Managing Gearboxes and Spare Parts*, Wind Farm O&M Conference, Glasgow, UK, June 2010.

7 Conclusions

"Finally, in conclusion, let me say just this."

Peter Sellers
1925 – 1980

7.1 Conclusions

In this thesis, the practicalities and challenges of CM in the field have been presented. In particular, a case study of the application of a commercially available CMS has been discussed. The capabilities of the SKF WindCon system are clear and it is apparent that the Operator has achieved success in the field. However, there are limitations and issues for the use of CMSs encountered due to the variable speed, variable load nature of WTs.

In order to investigate and resolve these, an existing CM test rig was developed further. Its instrumentation and ability to introduce fault-like conditions were significantly extended alongside the introduction of realistic wind driving conditions based on a highly detailed WT model from within the Supergen Wind Energy Technologies Consortium.

The fault-like conditions which can now be applied to the test rig include:

- WRIG rotor electrical asymmetry
- High speed shaft mass unbalance
- High speed gear tooth damage and ultimate failure

Several popular and widely applied CMS signal processing methods are discussed including the DFT, STFT and CWT. Their relevance to a WT CMS, advantages and disadvantages are given, including the application of a previously published CWT_{local} frequency tracking algorithm. This algorithm was then taken as the basis for the development of an improved, practical fault frequency tracking algorithm.

Based on this discussion, a DFT-based frequency tracking algorithm, the $IDFT_{local}$, was developed. Its mathematical basis and derivation is given and developed into an iterative process for the analysis of discretely sampled CM signals.

The $IDFT_{local}$ was applied to data recorded form the CM test rig to test its detection capabilities. The results showed that rotor electrical asymmetry and high speed shaft mass unbalance conditions were clearly detectable in electrical and mechanical signals respectively. This also demonstrated the algorithm's applicability to different types of monitoring signal.

High speed gear tooth damage involving serious tooth face deterioration and subsequent failure, were detected. However, difficulties in the detection of this fault-like condition occurred due to the relatively low load conditions being applied in a relatively rigid, stiff gearbox structure.

The $IDFT_{local}$ was compared to the CWT_{local} frequency tracking algorithm in terms of clarity of result and computational intensity, indicated by computing time. The $IDFT_{local}$ algorithm compared favourably against the published CWT_{local} method, giving comparably clear results for rotor electrical asymmetry, high speed mass unbalance and gear tooth damage with very similar processing parameters. Arguably the CWT_{local} algorithm produced a slightly improved result for tooth fault detection. However, in all cases, the computing time of the $IDFT_{local}$ algorithm was much reduced against that for the CWT_{local} algorithm. It did not appear that the CWT_{local} algorithm compared well in terms of computing time and clarity of results, an issue which is highly important in the field.

Finally, a short study of the electrical power signal from an operational WT has shown that WT mechanical torque can be accurately derived from the generator electrical power signal, retaining the same features as the measured torque, in particular indicating large torque pulses during start-up, speed changes and stops.

7.2 Future Areas for Investigation and Development

The CM test rig has undergone significant development over the course of this research however further development based on experience is encouraged. This may be in terms of refined fault capabilities or further signal conditioning.

The WindCon 3.0 system fitted to the test rig could be used to monitor the faults applied here but with the suggested algorithms programmed into the WindCon. This would demonstrate the transferability of these algorithms into a commercial device.

The test rig is currently undergoing an upgrade to full DFIG operation, bringing it yet closer to the most widely installed WT configuration. The aim of this work will be to bring about a fully closed control loop on the test rig opening the possibility of monitoring the drive train through the error signals in the generator controller.

An important aim for future work has to be to gain experience in the analysis of signals from operational WTs. Once the algorithms and method discussed in this thesis have been further tested, their incorporation into the CMS of an operational WT would allow complete testing in the field. However, further progress must be made in terms of practical algorithm implementation and programming. As it stands, the $IDFT_{local}$ algorithm is directly implemented. The FFT has been developed as a refined method of computing the DFT so it would seem apparent that the same could be applied to the $IDFT_{local}$.

Further work could then be done to link the output of a more automatic CMS to Reliability Centred Maintenance packages which schedule maintenance at appropriate times of low energy production, after CMS detection, to defer and avoid failure.

Appendices

A. Survey of Commercially Available Condition Monitoring Systems for Wind Turbines

This appendix contains a copy of the document “Commercially Available Condition Monitoring Systems for Wind Turbines”, available via the Supergen Wind Energy Technologies Consortium. The document is cited in Chapter 2 of this thesis.

Details of copyright are given within the document itself.

Survey of Commercially Available Condition Monitoring Systems for Wind Turbines

Christopher J Crabtree

2nd November 2010
Revision: 05

Confidentiality

Previous Versions

The first survey completed, named *Survey of Commercially Available Wind Turbine Condition Monitoring Systems*, was initially prepared by P. J. Tavner (Durham University School of Engineering and Computing Sciences) as part of the Supergen Wind Energy Technologies Consortium with help and contributions from W. Yang (Durham University, now NaREC, Blyth), C. Booth (University of Strathclyde) and S. Watson (Loughborough University). It was then subject to constant revision up to April 2009 by W. Yang.

The current document is based on this earlier survey and is written by C. J. Crabtree (Durham University School of Engineering and Computing Sciences) as part of the UK EPSRC Supergen Wind Energy Technologies Consortium, EP/D034566/1. It contains information contributed by the C. J. Crabtree, P. J. Tavner, Y. Feng and M. W. G. Whittle, obtained at European Wind Energy Conferences 2009 and 2010.

This document contains 281 (two hundred eighty-one) pages including the cover page.

Abstract

As wind energy assumes greater importance in remote and offshore locations, effective and reliable condition monitoring techniques are required. Failure rate and downtime studies have also highlighted a need for condition monitoring of particular wind turbine drive train components. This survey discusses the reliability of wind turbines and different monitoring configurations currently in use. The document contains a survey of commercially available condition monitoring systems for wind turbines including information on their monitoring technologies based on available literature and discussion with the companies responsible. Observations are made concerning the nature of systems that are currently available and the apparent direction of future monitoring systems.

Contents

1. Introduction

As wind energy assumes greater importance in remote and offshore locations, affective and reliable condition monitoring (CM) techniques are required. Conventional CM methods used in the power generation industry have been adapted by a number of industrial companies and have been applied to wind turbines (WT) commercially.

This survey discusses commercially available condition monitoring systems (CMS) which are currently being applied in the WT industry. Information has been gathered over several years from conferences and websites and includes information available from product brochures, technical documents and discussion with company representatives. The research was carried out as part of Theme X of the Supergen Wind Energy Technologies Consortium [1] whose objective is to devise a comprehensive CMS for practical application on WTs. The report also indentifies some of the advantages and disadvantages of existing commercial CMSs alongside discussion of access, cost, connectivity and commercial issues surrounding the application of WT CMSs.

2. Reliability of Wind Turbines

Quantitative studies of WT reliability have recently been carried out based on publically available data [2][3]. These studies have shown WT gearboxes to be a mature technology with constant of slightly deteriorating reliability with time. This would suggest that WT gearboxes are not an issue however surveys by WMEP and LWK [4] have shown that gearboxes exhibit the highest downtime per failure among onshore sub-assemblies. This is shown graphically in Figure 106 where we clearly see consistently low gearbox failure rate between two surveys with high downtime per failure. Similar results have also been shown for the Egmond aan Zee wind farm [5] where gearbox failure rate is not high but the downtime and resulting costs are. The poor early reliabilities for gearbox and drive train reliability components has lead to an emphasis in WT CMSs on drive train components and therefore on vibration analysis.

The high downtime for gearboxes derives from complex repair procedures. Offshore WT maintenance can be a particular problem as this involves specialist equipment such as support vessels and cranes but has the additional issue of potentially unfavourable weather and wave conditions. The EU funded project ReliaWind is developing a systematic and consistent process to deal with detailed commercial data collected from operational wind farms. This includes the analysis of 10 minute average SCADA data as discussed above, automated fault logs and operation and maintenance reports. The research aims to identify and understand WT gearbox failure mechanisms in greater detail [6]. However, more recent information on WT reliability and downtime, especially when considering offshore operation suggests that the target for WT CMSs should be widened from the drive train towards WT electrical and control systems.

As a result of low early reliability, particularly in large WTs, interest in CMSs has increased. This is being driven forward by the insurer Germanischer Lloyd who published guidelines for the certification of CMSs [7] and certification of WTs both onshore [8] and offshore [9].

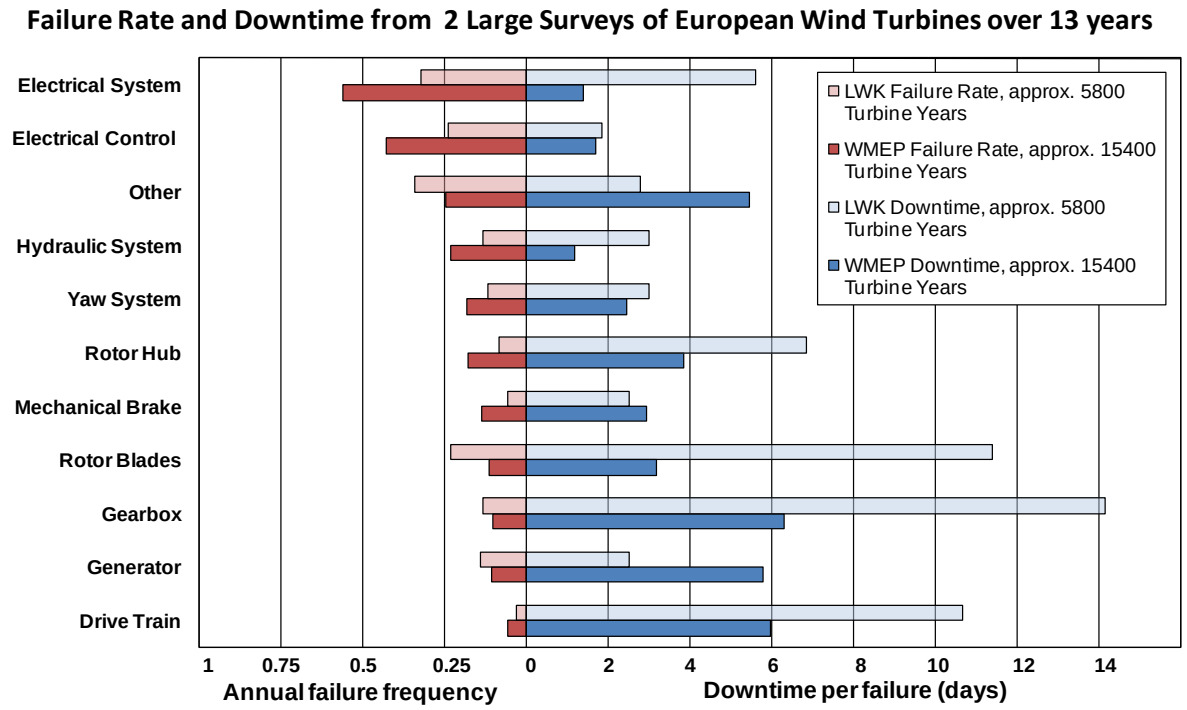

Figure 106: Wind turbine sub-assembly failure rate and downtime per failure for two surveys including over 20000 turbine years of data as published in 0

3. Monitoring of Wind Turbines

WTs are monitored for a variety of reasons. There are a number of different classes into which monitoring systems could be placed and these are shown in Figure 107, showing the general layout and interaction of the various classes.

Firstly, we have Supervisory Control and Data Acquisition (SCADA) systems. Initially these systems provided measurements for a WT's energy production and to confirm that the WT was operational through 5-10 minute averaged values transmitted to a central database. However, SCADA systems can also provide warning of impending malfunctions in the WT drive train. According to Zaher et al. [11] 10 minute averaged signals often monitored in modern SCADA systems include:

- Active power output (and standard deviation over 10 min interval);
- Anemometer-measured win d speed (and standard deviation over 10 min interval);
- Gearbox bearing temperature;

- Gearbox lubrication oil temperature;
- Generator winding temperature;
- Power factor;
- Reactive power;
- Phase currents, and;
- Nacelle temperature (1 hour average).

This SCADA configuration is designed to show the operating condition of a WT but not necessarily give an indication of the health and a WT. However, the much up to date SCADA systems include additional alarm settings based not only on temperature transducers mentioned above but also on vibration transducers. Often we find several transducers fitted to the WT gearbox, generator bearings and the turbine main bearing. The resultant alarms are based on the level of vibration being observed over the 10 minute average period. Research is being carried out into the CM of WTs through SCADA analysis in the EU project ReliaWind [12]. The research consortium consists of a number of University partners alongside industrial consultants and WT manufacturers.

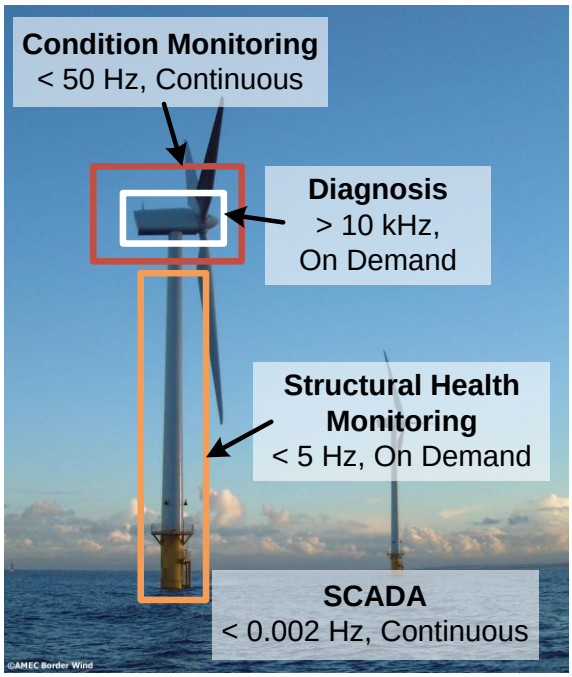

Figure 107: Structural health and condition monitoring of a wind turbine

Secondly, there is the area of structural health monitoring (SHM). These systems aim to determine the integrity of the WT tower and foundations. SHM is generally carried out using low sampling frequencies below 5Hz.

While SCADA and SHM monitoring are key areas for WT monitoring, this survey will concentrate on the remaining two classes of CM and diagnosis systems.

Monitoring of the drive train is often considered to be most effective through the interaction of these two areas. CM itself may be considered as a method for determining whether a WT is operating correctly or whether a fault is present or developing. A WT Operator's main interest is likely to be in obtaining reliable alarms based on CM information which can enable them to take confident action with regard to shutting down for maintenance. The operator need not know the exact nature of the fault but would be alerted to the severity of the issue by the alarm signal. Reliable CM alarms will be essential for any operator with a large number of WTs under its ownership. On this basis, CM signals should not need to be collected on a high frequency basis as this will reduce bandwidth for transmission and space required for storage of data.

Once a fault has been detected through a reliable alarm signal from the CMS, a diagnosis system could be activated either automatically or by a monitoring engineer to determine the exact nature and location of the fault. For diagnosis systems, data recorded at a high sampling frequency is required for analysis however this need only be collected on an intermittent basis. The operational time of the system should be configured to provide enough data for detailed analysis but not to flood the monitoring system or data transmission network with excess information.

Finally, Figure 108 gives an indication of three sections of a WT which may require monitoring based on reliability data such as that in Figure 106 0. While each of the three areas are shown as separate entities it is possible that CM of the areas may well blur the boundaries between them in order to provide clear alarms and, subsequently, diagnostic information.

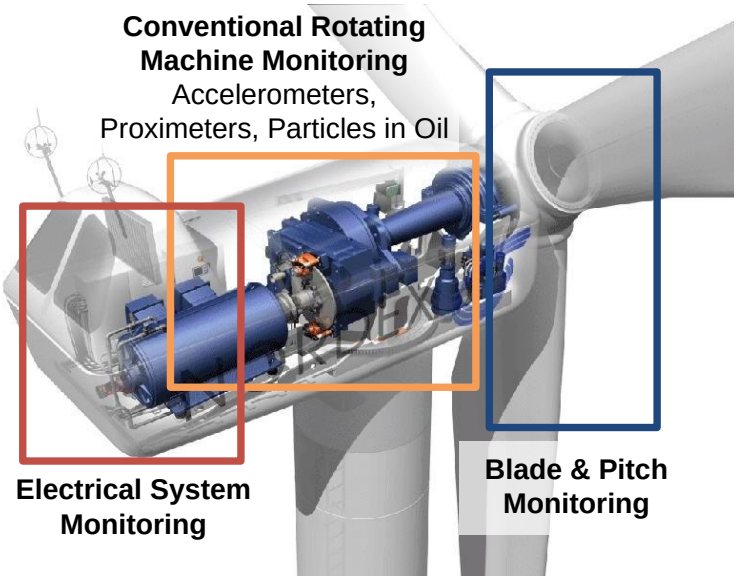

Figure 108: General layout of three areas for condition monitoring and diagnosis within the nacelle

Many of the CMSs included in this survey are a combination of CMSs and diagnostic systems due to the high level of interaction that can exist between the two types of system.

4. Commercially Available Condition Monitoring Systems

Table 8, found on page 174 of this survey, provides a summary of a number of widely available and popular CMSs for WTs. The information in this table has been collected from interaction with CMS manufacturers, WT manufacturers and product brochures over a long period of time and is up to date as of the time of writing. However, since some information has been acquired through discussion with sales and product representatives and not from published brochures, it should be noted that the table may not be fully definitive and is as accurate as possible given the available information. The systems in Table 8 are arranged alphabetically by product name.

The first observation to make from Table 8 is that the CMSs nearly all focus on the same WT subassemblies. Moving through the WT these are:

- Blades
- Main bearing
- Gearbox internals
- Gearbox bearings
- Generator bearings

A quick summery of Table 8 shows that there are:

- 14 systems primarily based on drive train vibration analysis (1 – 14)
- 3 systems solely for oil debris monitoring (15 – 17)
- 1 system using vibration analysis for WT blade monitoring (18).
- 2 systems based on fibre optic strain measurement in WT blades (19, 20)

It is quite clear when reading through the table that the majority of systems are based around monitoring methods originating from other, traditional rotating machinery industries. Indeed 14 of the 20 systems in the table are based on vibration monitoring using accelerometers typically using a configuration similar to that in Figure 109 for the Mita-Teknik WP4086 CMS (14).

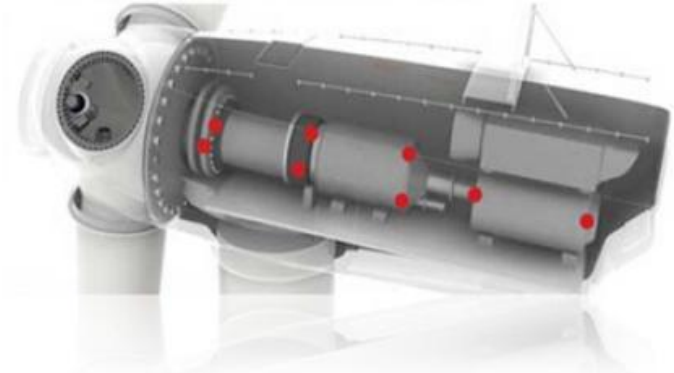

Figure 109: Typical accelerometer positions [13]

Of these 14 CMSs, all have the capability to carry out some form of diagnostic procedure once a fault has been detected. In most cases this is done through fast Fourier transform (FFT) analysis of high frequency data in order to detect fault-specific frequencies. In the case of the SKF WindCon 3.0 (11), the Areva OneProd Wind CMS (7) and several others, high data acquisition is triggered by operational parameters. For example, the SKF WindCon 3.0 CMS can be configured to collect a vibration spectrum on either a time basis or when a specific load and speed condition is achieved. The aim of this is to acquire data that is directly comparable between each point and, importantly, to allow spectra to be recorded in apparently stationary conditions. This is an important point to note when using traditional signal processing methods such as the FFT which require stationary signals in order to obtain a clear result. The Mita-Teknik WP4086 system (14), however, states that it includes advanced signal processing techniques such as comb filtering, whitening and Kurtogram analysis which in combination with re-sampling and order alignment approaches, allow the system to overcome the effects of WT speed variations.

Three of the vibration-based CMSs also state that they are able to monitor the level of debris particles in the WT gearbox lubrication oil system. Further to this, included in the table are three systems which are not in themselves CMSs. These three (15 – 17) are oil quality monitoring systems or transducers rather than full CMSs but are included as discussion with industry has suggested that debris in oil plays a significant role in the damage and failure of gearbox components. Systems using these debris in oil transducers are using either cumulative particle counts or particle count rates.

Several of the 14 vibration-based CMSs also allow for other parameters to be recorded alongside vibration such as load, wind speed, generator speed and temperatures although the capabilities of some systems are unclear given the information available. There is some interest being shown as regards the importance of operational parameters in WT CM. This arises from the fact that many analysis techniques, for example the FFT, have been developed in constant speed, constant load environments. This can lead to difficulties when moving to the variable speed, variable load WT however experienced CM engineers are able to use these techniques and successfully detect faults.

Two CMSs in the table (19, 20) are based on strain measurement using fibre optic transducers. These are aimed at detection of damage to WT blades and, in the case of the Moog Insensys system (20), blade icing, mass unbalance or lightning strikes. Both systems may be fitted to WT blades retrospectively. Compared to vibration monitoring techniques, these systems can be operated at low sampling rates as they are looking to observe changes in for time domain. In addition to (19) and (20) there is the IGUS system (18) using accelerometers to monitor blade damage, icing and lightning strikes. This system compares the blade accelerometer FFT with stored spectra for similar operating conditions and has the power to automatically shut down or restart a WT based on the results. The system appears to be popular within industry.

Table 8: Table of commercially available condition monitoring systems

	Product and Company Information			Product Details (based on available literature and contact with industry including EWEC 2008, 2009, 2010)				
Ref.	**Product**	**Supplier or Manufacturer (Known Users)**	**Country of Origin**	**Description**	**Main Components Monitored**	**Monitoring Technology**	**Analysis Method(s)**	**Data Rate or Sampling Frequency**
1	Ascent	Commtest	New Zealand	System available in 3 complexity levels. Level 3 includes frequency band alarms, machine template creation, statistical alarming.	Main shaft, gearbox, generator	Vibration (Accelerometer)	FFT frequency domain analysis Envelope analysis Time domain analysis	-
2	Brüel & Kjaer Vibro	Brüel & Kjaer (Vestas)	Denmark	Vibration and process data automatically monitored at fixed intervals and remotely sent to the diagnostic server. User-requested time waveforms for frequency and time series analysis Time waveform automatically stored before and after user-defined event allowing advanced vibration post-analysis to identify developing faults.	Main bearing, gearbox, generator, nacelle. Nacelle temperature. Noise in the nacelle	Vibration Temperature sensor Accoustic	Time domain FFT frequency analysis	Variable up to 40kHz. 25.6kHz.
3	CMS	Nordex	Germany	Start-up period acquires vibration 'fingerprint' components. Actual values automatically compared by frequency, envelope and order analysis, with the reference values stored in the system. Some Nordex turbines also use the Moog Insensys fibre optic measurement system.	Main bearing, gearbox, generator	Vibration (Accelerometer)	Time domain based on initial 'fingerprint'	-
4	Condition Based Maintenance System (CBM)	GE (Bently Nevada)	USA	This is built upon the Bently Nevada ADAPT.wind technology and System 1. Basis on System 1 gives monitoring and diagnostics of drive train parameters such as vibration and temperature. Correlate machine information with operational information such as machine speed, electrical load, and wind speed. Alarms are sent via the SCADA network.	Main bearing, gearbox, generator, nacelle Optional bearing and oil temperature	Vibration (Accelerometer)	FFT frequency domain analysis Acceleration enveloping	-
5	Condition Diagnostics System	Winergy	Germany	Up to 6 inputs per module. The system analyses vibration levels, load and oil to give diagnostics, forecasts and recommendations for corrective action. Automatic fault identification is provided. Pitch, controller, yaw and inverter monitoring can also be included.	Main shaft, gearbox, generator	Vibration (Accelerometer) Oil debris particle counter	Time domain FFT frequency domain analysis	96kHz per channel
6	Condition Management Syetam	Moventas	Finland	Compact system measuring temperature, vibration, load, pressure, speed, oil aging and oil particle count. 16 analolgue channels can be extended with adapter. Data acessed remotely via TCP/IP. Mobile interface available.	Gearbox, generator, rotor, turbine controller	Vibration Oil quality/particles Torque Temperature	Time domain (Possible FFT)	-

7	OneProd Wind	Areva (01dB-Metravib)	France	Instrumentation includes operating condition channels to trigger data acquisitions, measurement channels for surveillance and diagnosis, optional additional channels for extended monitoring.	Main bearing, gearbox, generator. Oil debris, structure, shaft displacement, electrical signals	Vibration Oil debris particle counter, electrical transducers.	Time domain FFT frequency analysis	-
8	SMP-8C	Gamesa Eolica	Spain	Continuous on-line vibration measurement of main shaft, gearbox and generator. Comparison of spectra trends. Warnings and alarm transmission connected to Wind Farm Management System.	Main shaft, gearbox, generator	Vibration	FFT frequency domain	-
9	System 1	Bently Nevada (GE)	USA	Monitoring and diagnostics of drive train parameters such as vibration and temperature. Correlate machine information with operational information such as machine speed, electrical load, and wind speed.	Main bearing, gearbox, generator, nacelle Optional bearing and oil temperature	Vibration (Accelerometer)	FFT frequency domain Acceleration enveloping	-
10	TCM (Turbine Condition Monitoring)	Gram & Juhl A/S (Siemens Wind Power A/S)	Denmark	Advanced signal analysis on signals such as vibration, sound, strain and process signals combined with automation rules and algorithms for generating references and alarms.	Blade, main bearing, shaft, gearbox, generator, nacelle, tower	Vibration (Accelerometer)	FFT frequency domain	-
11	WindCon 3.0	SKF (REpower)	Sweden	Lubrication, blade and gearbox oil systems can be remotely monitored through SKF ProCon sofetware. WindCon 3.0 collects, analyses, and compiles operating data that can be configured to suit management, operators or maintenance engineers.	Blade, main bearing, shaft, gearbox, generator, tower, generator electrical	Vibration (Accelerometer, proximity probe) Oil debris particle counter	FFT frequency domain analysis Envelope analysis Time domain analysis	Analogue: DC to 40kHz (Variable, channel dependent) Digital: 0.1 Hz - 20kHz
12	WinTControl	Flender Service GmbH	Germany	Vibration measurements are taken when load and speed triggers are realised. Time and frequency domain analysis are possible.	Main bearing, gearbox, generator.	Vibration (Accelerometer)	FFT frequency domain Time domain analysis	32.5kHz
13	WiPro	FAG Industrial Services GmbH	Germany	Measurement of vibration and other parameters given appropriate sensors. Time and frequency domain analysis carried out during alarm situations. Allows speed-dependent frequency band tracking and speed-variable alarm level.	Main bearing, shaft, gearbox, generator, temperature. (Adaptable inputs)	Vibration (Accelerometer)	FFT frequency domain Time domain analysis	Variable up to 50kHz
14	WP4086	Mita-Teknik	Denmark	Up to 8 accelerometers for real-time frequency and time domain analysis. Alarms set for both time and frequency domains based on predefined thresholds. Operational parameters recorded alongside with vibration signals/spectra and complete integration with SCADA systems.	Main bearing, gearbox, generator	Vibration (Accelerometer)	FFT amplitude spectra FFT envelope spectra Time domain magnitude Comb filtering, whitening, Kurtogram analysis	Variable up to 10kHz
15	HYDACLab	HYDAC Filtertechnik GmbH	Germany	Permanent monitoring system to monitor particles (including air bubbles) in hydraulic and lube oil systems.	Lubrication oil & cooling fluid quality	Oil debris particle counter	N/A	-
16	PCM200	Pall Industrial Manufacturing (Pall Europe Ltd)	USA (UK)	Fluid cleanliness monitor reports test data in real-time so ongoing assessments can be made. Can be permanently installed or portable.	Lubrication oil cleanliness	Oil cleanliness sensor	N/A	-

17	TechAlert 10 TechAlert 20	MACOM	UK	TechAlert 10 is an inductive sensor to count and size ferrous and non-ferrous debris in circulating oil systems. TechAlert 20 is a magnetic sensor to count ferrous particles.	Lubrication oil quality	Inductive or magnetic oil debris particle counter	N/A	-
18	BLADEcontrol	IGUS ITS GmbH	Germany	Accelerometers are bonded directly to the blades and a hub measurement unit transfers data wirelessly to the nacelle. Blades are assesed by comparing spectra with those stored for common conditions. Measurement and analysis data are stored centrally and blade condition displayed using a web browser.	Blades	Accelerometer	FFT frequency domain	≈ 1kHz
19	FS2500	FiberSensing	Portugal	BraggSCOPE measurement unit designed for industrial environments to interrogate up to 4 Fiber Bragg Grating sensors. Acceleration, tilt, displacement, strain, temperature and pressure measurable.	Blades	Fibre optic	Unknown	Up to 2kHz
20	RMS (Rotor Monitoring System)	Moog Insensys Ltd.	UK	Load measuring system for installation in the turbine hub. Can be designed-in during turbine manufacture or retrofitted. Monitors blade icing, imbalance, damage and lightning strikes.	Blades	Fibre optic strain	Time domain strain analysis	< 0.002 Hz (10 minute)

5. The Future of Wind Turbine Condition Monitoring

As can be seen from this survey of current CMSs there is a clear trend towards vibration monitoring of WTs. This is presumably a result of the wealth of knowledge gained from many years work in other fields. It is likely that this trend will continue however it would be reasonable to assume that other CM and diagnostic techniques will be incorporated into existing systems.

Currently these additions are those such as oil debris monitoring and fibre optic strain measurement. However, it is likely that major innovation will occur in terms of developing signal processing techniques. In particular, the industry is already noting the importance of operational parameters such as load and speed and so techniques may begin to adapt further to the WT environment leading to more reliable CMSs, diagnostics and alarm signals.

Automation of CM and diagnostic systems may also be an important development as WT operators acquire a larger number of turbines and manual inspection of data becomes impractical. Further to this, it is therefore essential that methods for reliable, automatic diagnosis are developed with consideration of multiple signals in order to improve detection and increase operator confidence in alarm signals.

However, it should be noted that a major hindrance to the development of CMSs and diagnostic techniques could be data confidentially meaning that few operators are able to divulge or obtain information concerning their own WTs. This is an issue which should be addressed if the art of CM is to progress quickly. Confidentiality has also led to a lack of publicly available cost justification of WT CM, which seems likely to provide overwhelming support for WT CM, particularly in the offshore environment where availability is at a premium.

6. Conclusions

From this survey we can conclude that:

- Current WT reliability is reasonable however in the offshore environment the failure rate will be unacceptable;
- Cost effective and reliable CM is required to enable planned maintenance, reduce unplanned WT downtime and improve capacity factors;
- Successful CMSs must be able to adapt to the non-stationary, variable speed nature of WTs;
- There is a wide variety of commercially available CMSs currently in use on operational WTs;
- Monitoring technology is currently based on techniques from other, conventional rotating machine industries;
- Vibration monitoring is currently favoured in commercially available systems using standard time and frequency domain techniques for analysis;

- These traditional techniques can be applied to detect WT faults but require experienced CM engineers for successful data analysis and diagnosis;
- Some commercially available CMSs are beginning to adapt to the WT environment, and;
- A diverse range of new or developing technologies are moving into the WT CM market.

Finally, it should be noted that there is not currently a consensus in the WT industry as to the correct route forward for CM of WTs. Work in this document and its references suggest that CM of WTs will be important for large onshore WTs, essential for all offshore development and should be considered carefully by the industry as a whole.

7. References

[1] Supergen Wind, *Theme X: Drive train loads and monitoring*, www.supergen-wind.org.uk/research_x0.html, last accessed 8th February 2010.

[2] Tavner, P.J., Xiang, J.P., Spinato, F., *Reliability analysis for wind turbines*, Wind Energy, Vol. 10, Issue 1, 2006.

[3] Spinato, F., Tavner, P.J., van Bussel, G.J.W., Koutoulakos, E., *Reliability of wind turbine subassemblies*, IET Renewable Power Generation, Vol. 3, Issue 4, pp. 1-15, 2009.

[4] Faulstich, S., et al., *Windenergie Report Deutschland 2008*, Institut für Solare Energieversorgungstechnik (Hrsg.), Kassel, 2008.

[5] Various Authors, *Operations Report 2007, Document No. OWEZ_R_000_20081023*, Noordzee Wind, 2008.

[6] Wilkinson, M.R., et al., *Methodology and results of the ReliaWind reliability field study*, Scientific Track Proceedings, European Wind Energy Conference 2010, Warsaw, 2010.

[7] Germanischer Lloyd, *Rules and Guidelines, IV Industrial Services, 4 Guideline for the Certification of Condition Monitoring Systems for Wind Turbines*, Edition 2007.

[8] Germanischer Lloyd, *Guideline for the Certification of Wind Turbines, Edition 2003 with Supplement 2004*, Reprint 2007.

[9] Germanischer Lloyd, *Guideline for the Certification of Offshore Wind Turbines, Edition 2005*, Reprint 2007.

[10] Crabtree, C.J., Feng, Y., Tavner, P.J., *Detecting Incipient Wind Turbine Gearbox Failure: A Signal Analysis Method for Online Condition Monitoring, Scientific Track Proceedings*, European Wind Energy Conference 2010, Warsaw, 2010.

[11] Zaher, A., McArthur, S.D.J., Infield, D.G., *Online Wind Turbine Fault Detection through Automated SCADA Data Analysis*, Wind Energy, Vol. 12, Issue 6, pp. 574-593, 2009.

[12] ReliaWind, www.reliawind.eu, last accessed 8th February 2010.

[13] Isko, V., Mykhaylyshyn, V., Moroz, I., Ivanchenko, O., Rasmussen, P., *Remote Wind Turbine Generator Condition Monitoring with WP4086 System*, Materials Proceedings, European Wind Energy Conference 2010, Warsaw, 2010.

B. Enlarged Figures from Chapter 3

This appendix contains enlarges version of the results figures from Chapter 3 of this thesis. The figures are numbered according to their figure numbers in the main thesis body as an aid to reference.

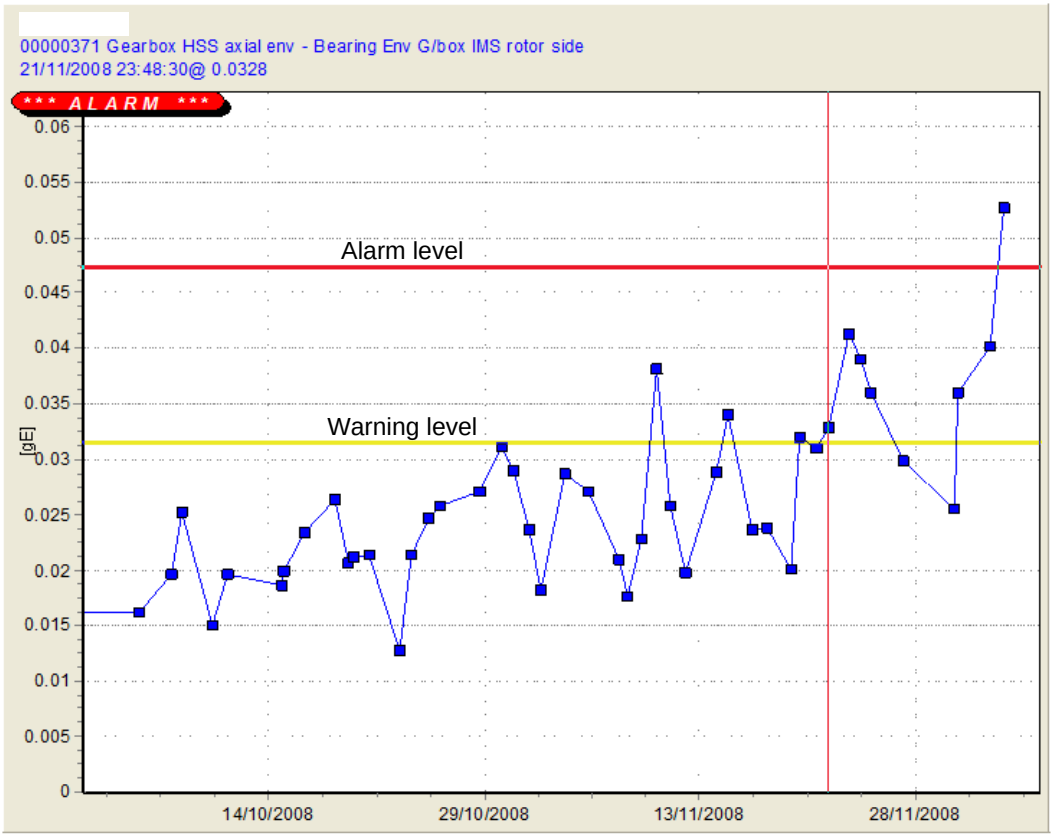

Enlarged Figure 25

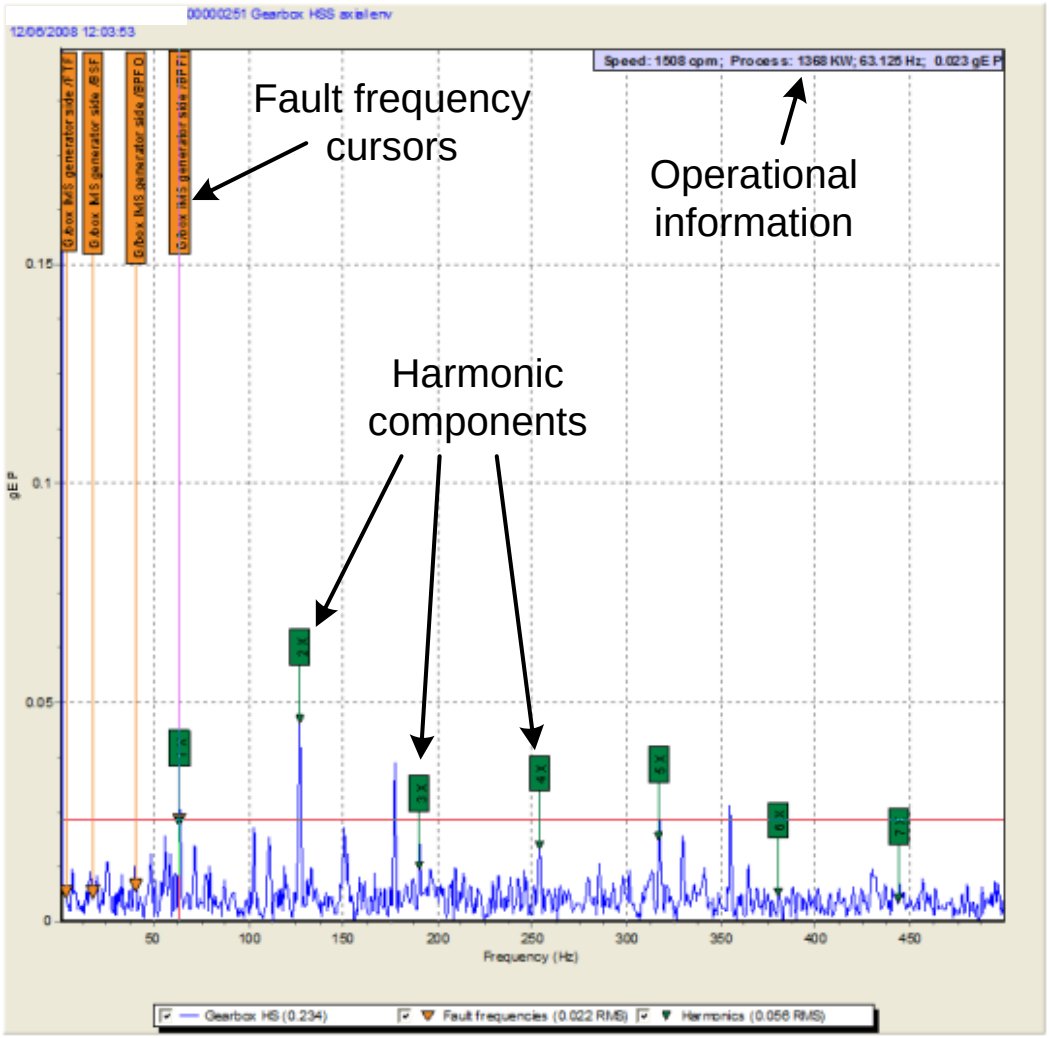

Enlarged Figure 30

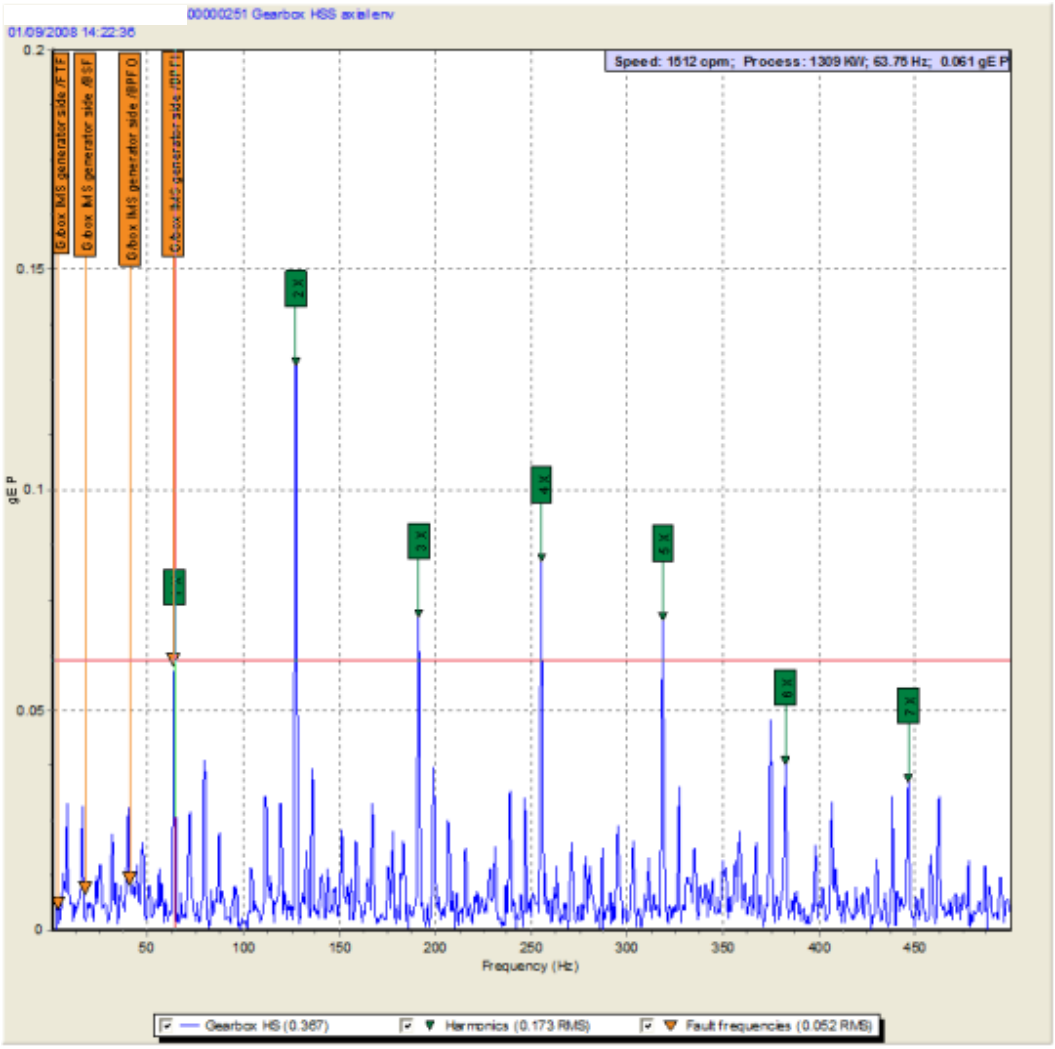

Enlarged Figure 31(a)

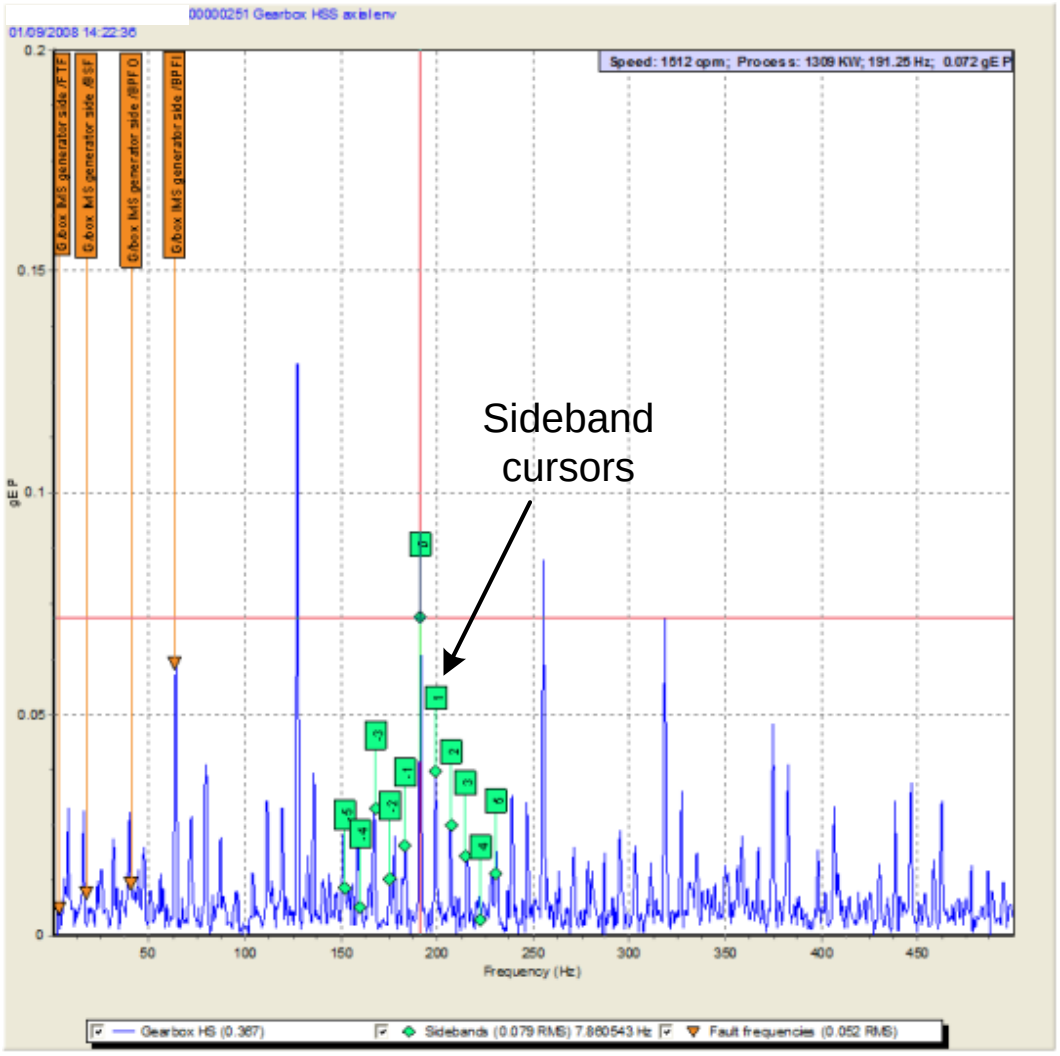

Enlarge Figure 31(b)

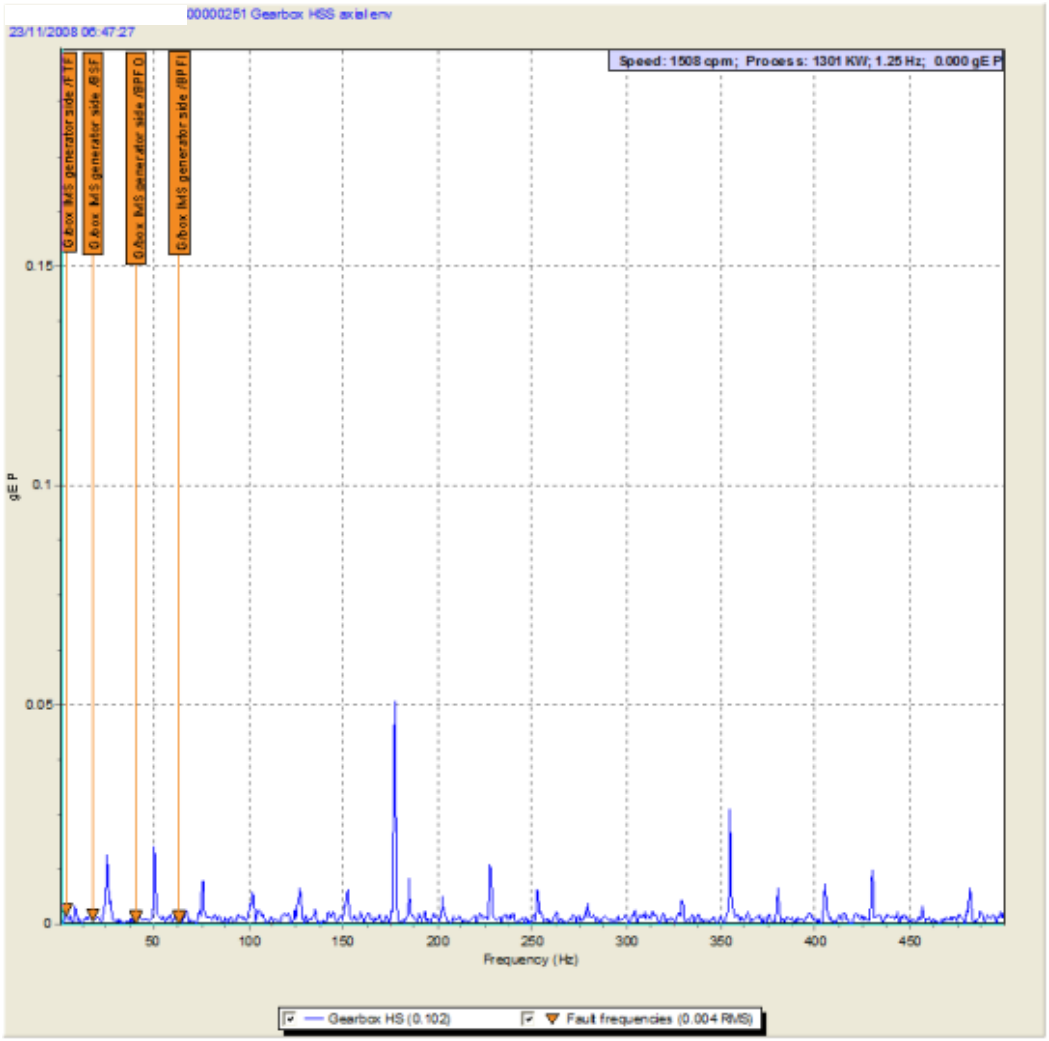

Enlarged Figure 33

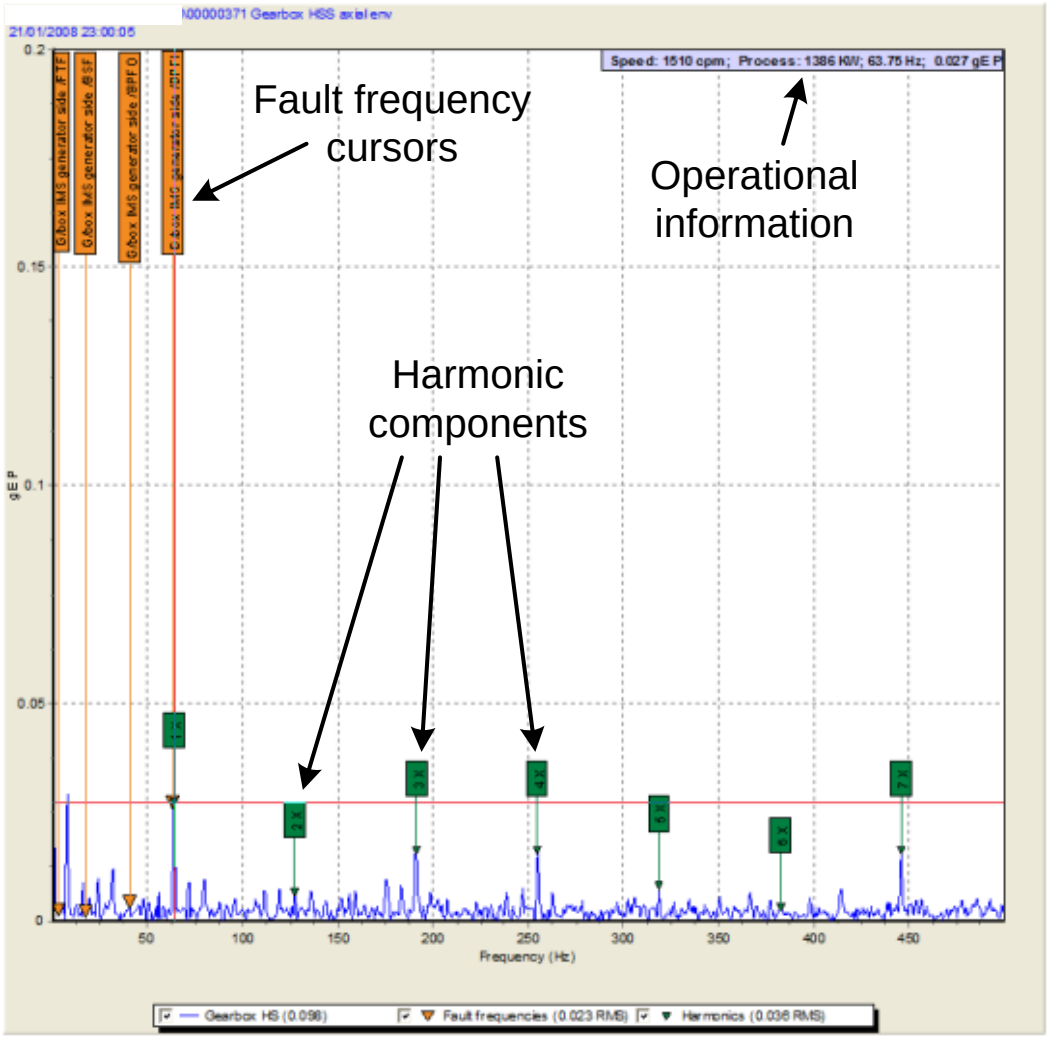

Enlarged Figure 37

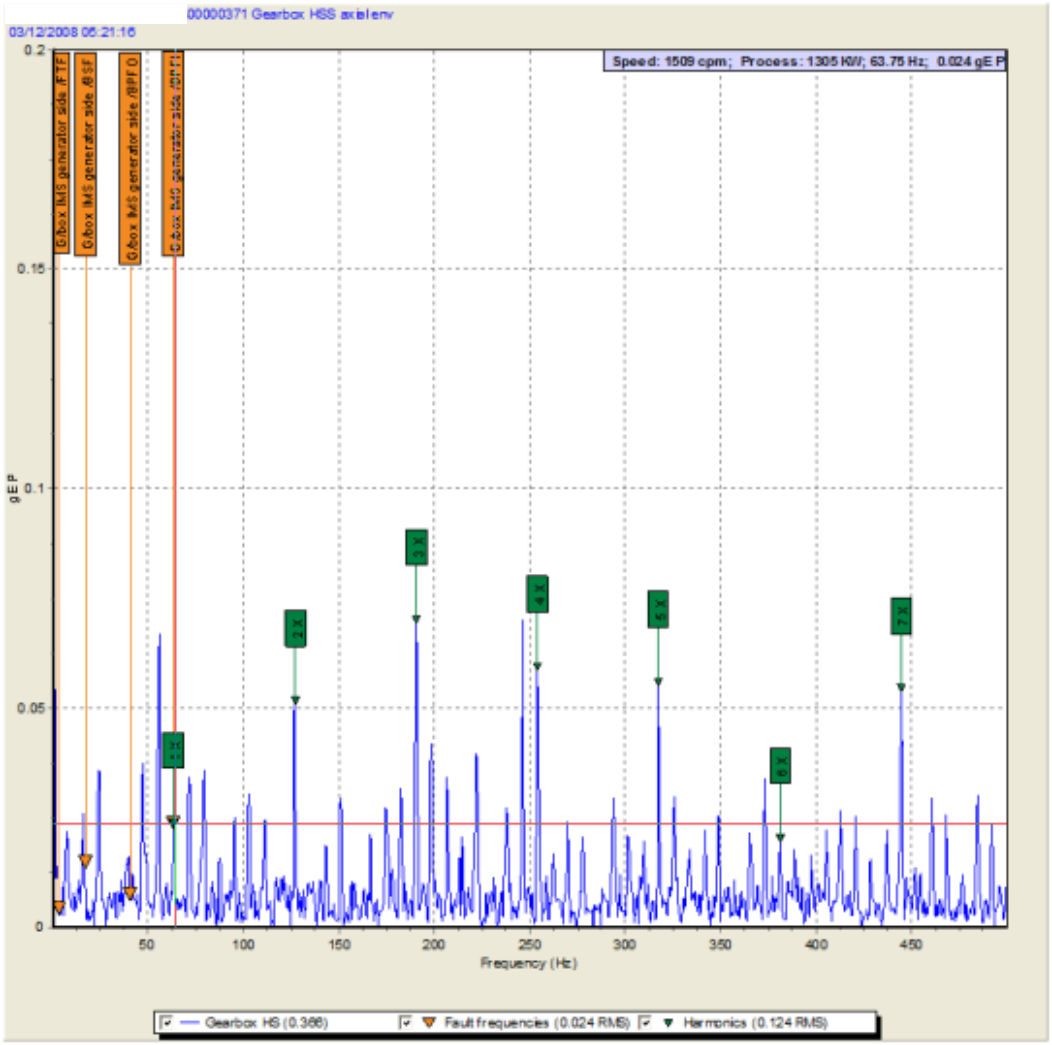

Enlarged Figure 38(a)

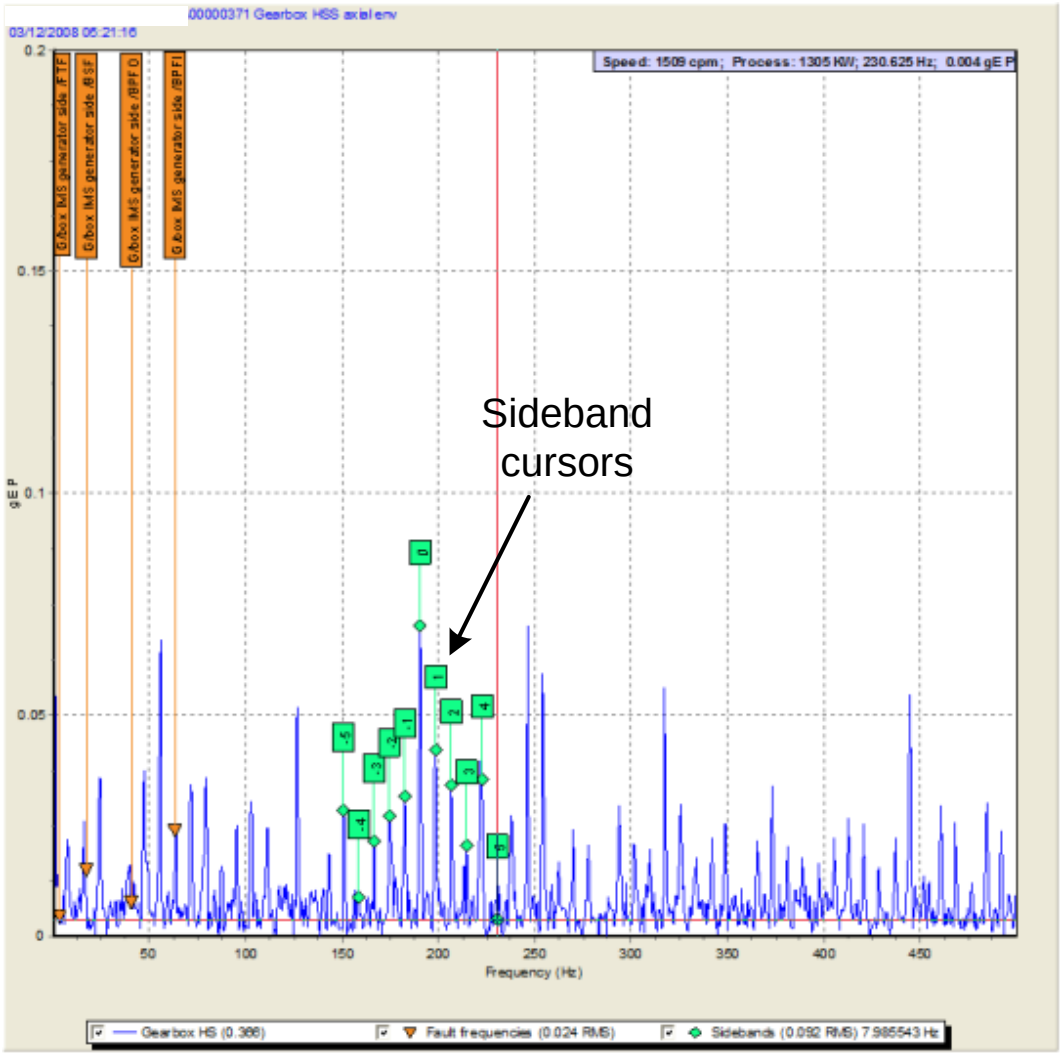

Enlarged Figure 38(b)

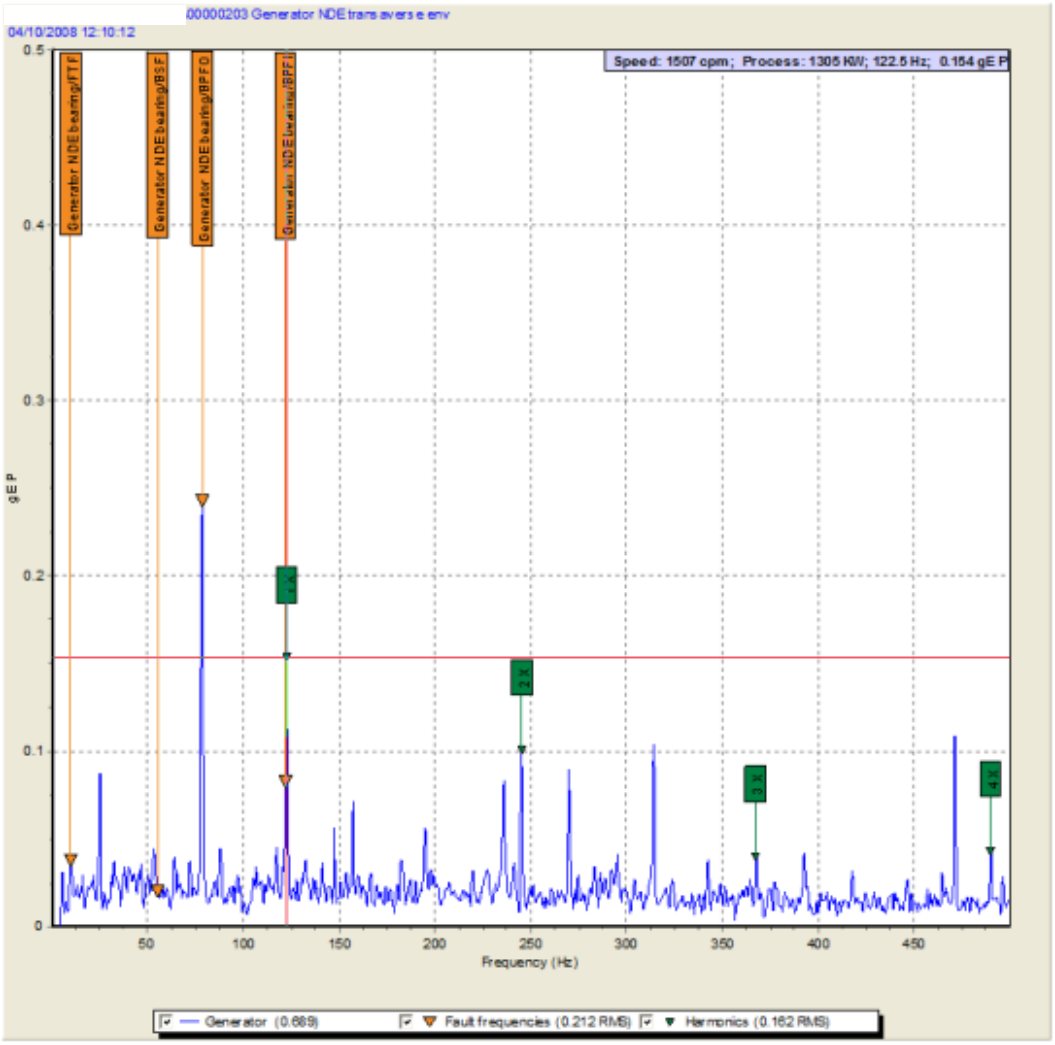

Enlarged Figure 42(a)

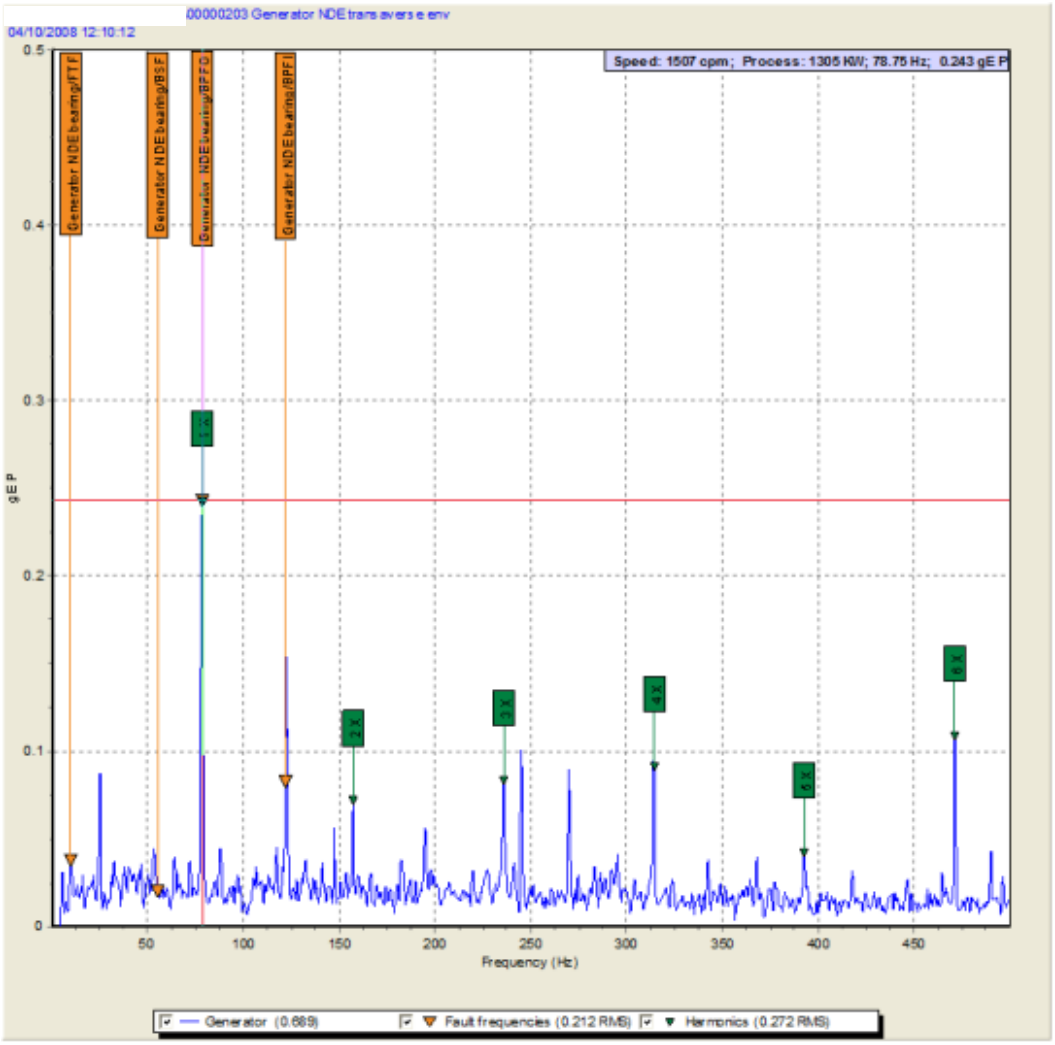

Enlarged Figure 42(b)

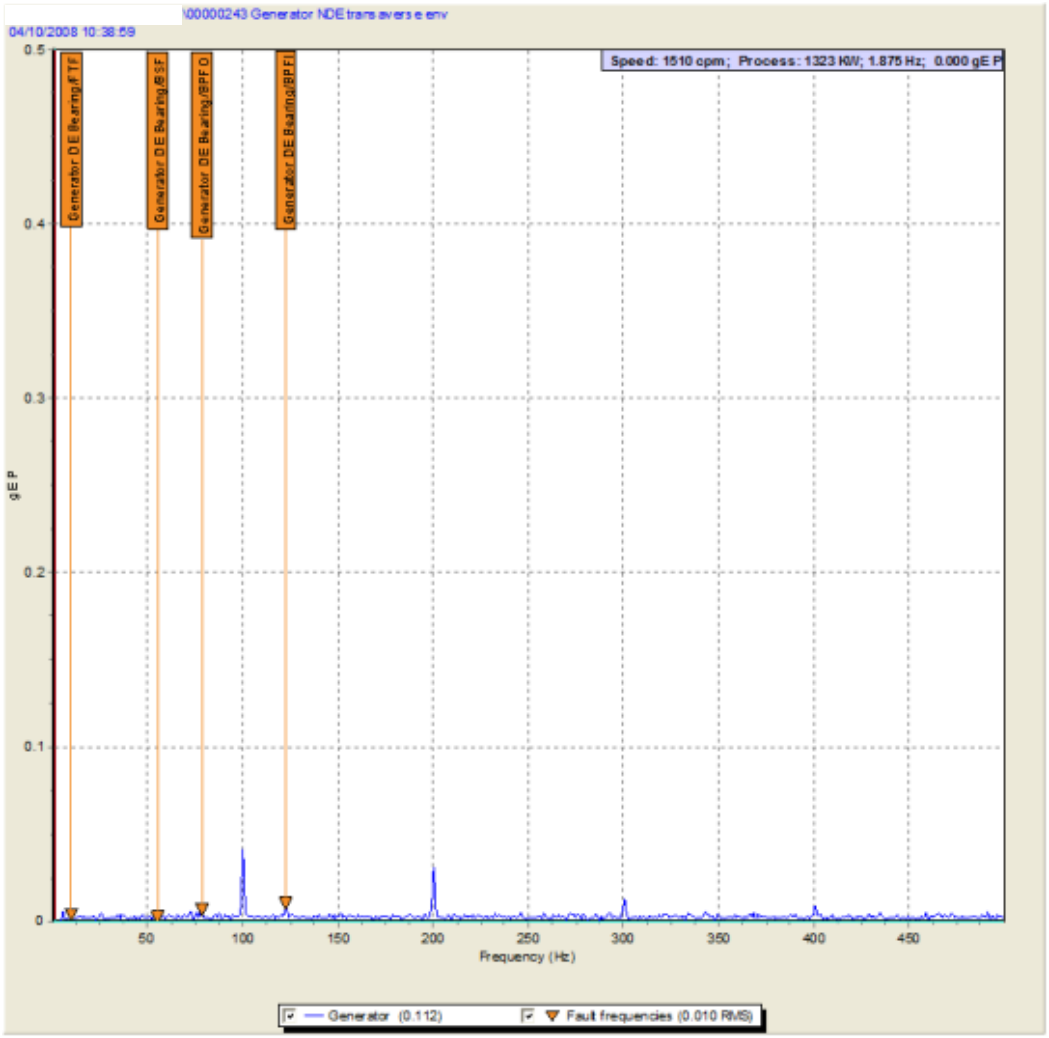

Enlarged Figure 43

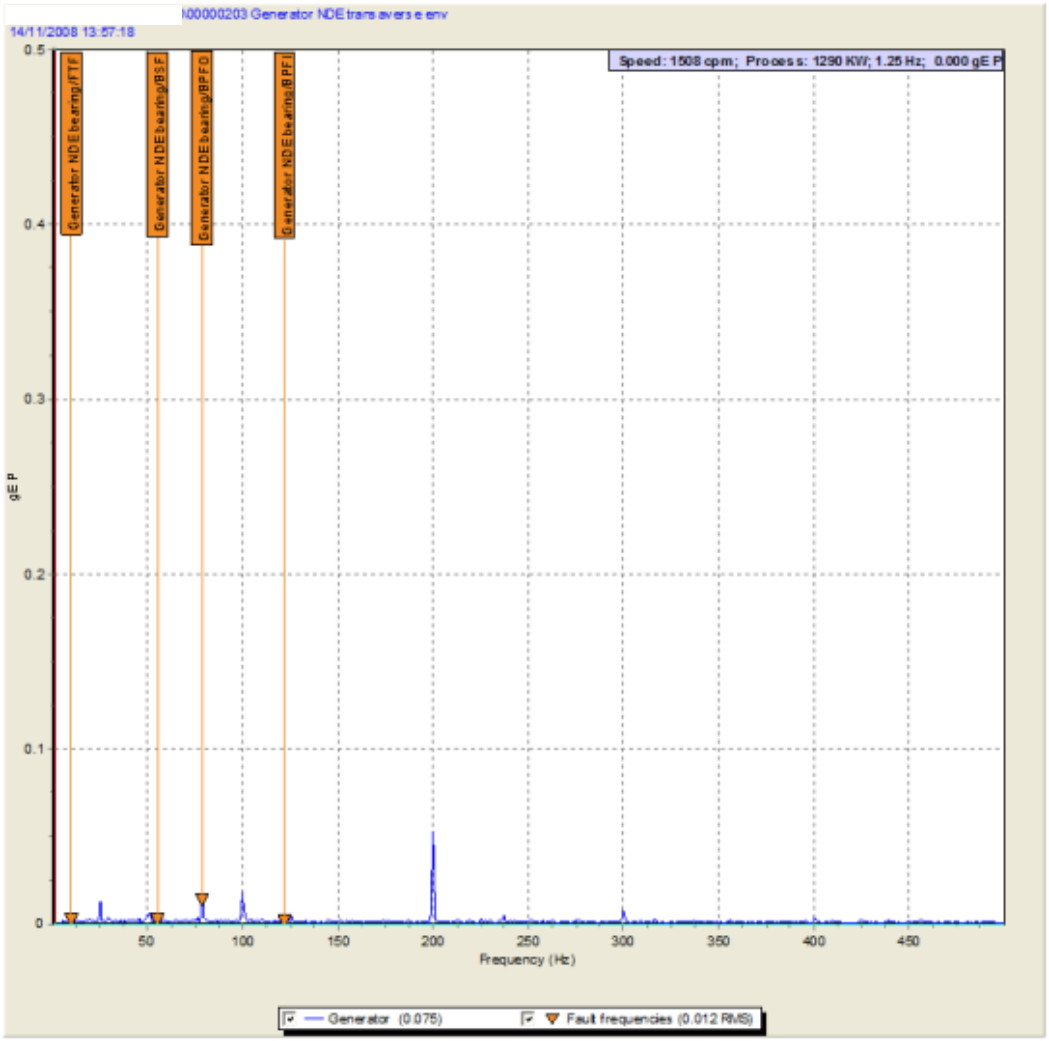

Enlarged Figure 44

C. Extended Results

As stated in Chapter 6, only a reduced selection of results is included in the main body of this thesis. This appendix contains a more complete set of results figures for reference. In particular, results from both variable speed driving conditions are presented.

C.1 Rotor Electrical Asymmetry

This section contains a complete set of figures from §6.1.1.

C.1.1 7.5m/s, 6% Turbulence

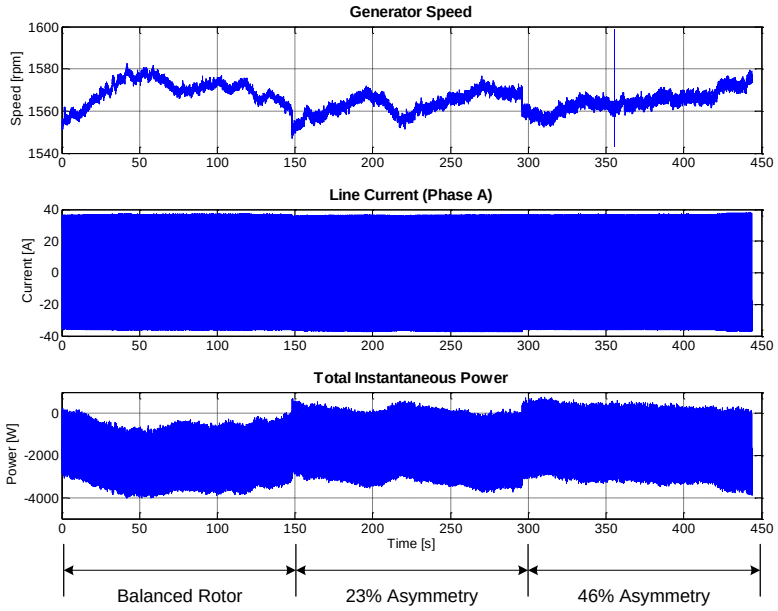

FigureE.1: Raw data used in the analysis of electrical signals for the detection of rotor electrical asymmetry Driven by 7.5m/s, 6% turbulence conditions.

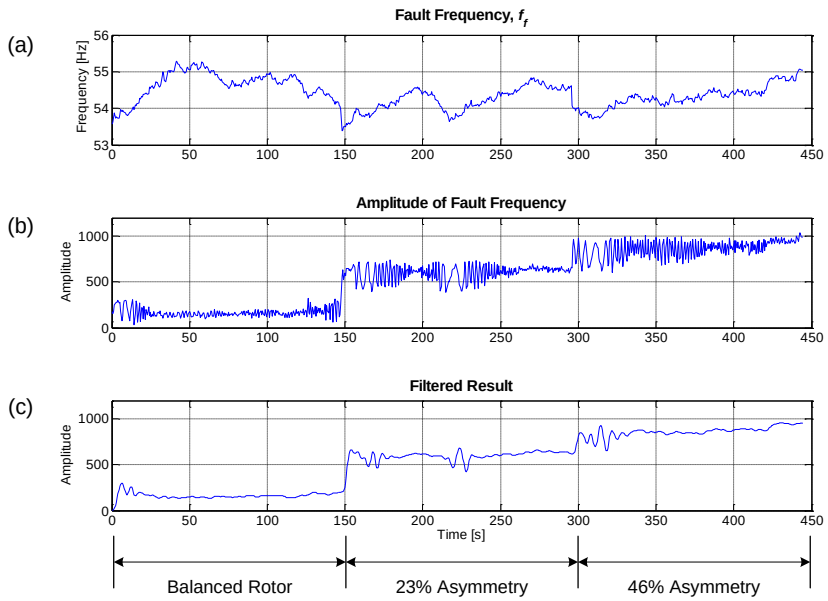

Figure C.2: IDFT$_{local}$ analysis of generator line current frequency component 'd' for the detection of rotor electrical asymmetry: (a) Frequency of interest; (b) amplitude of frequency of interest; (c) filtered result. Driven by 7.5m/s, 6% turbulence conditions. Calculation time = 0.98s = 0.22%.

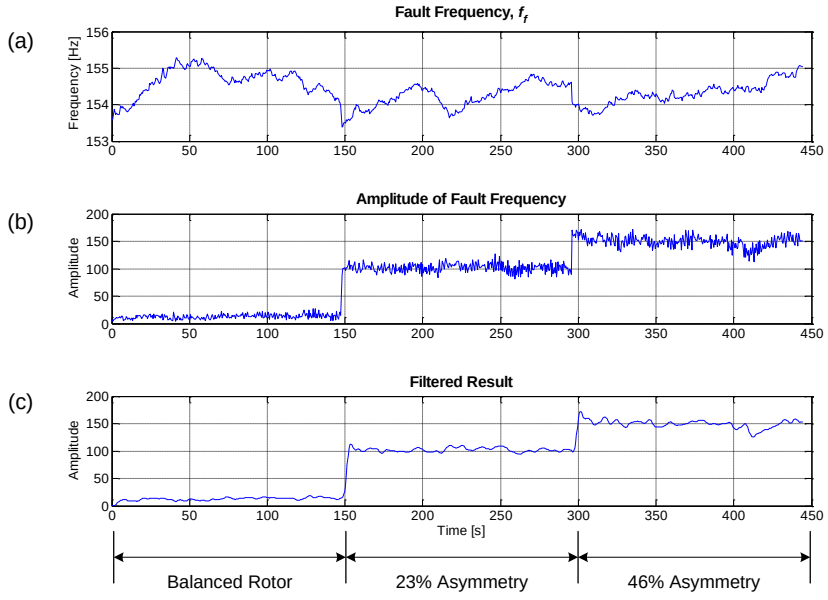

Figure C.3: IDFT$_{local}$ analysis of generator line current frequency component 'c' for the detection of rotor electrical asymmetry: (a) Frequency of interest; (b) amplitude of frequency of interest; (c) filtered result. Driven by 7.5m/s, 6% turbulence conditions. Calculation time = 1.05s = 0.24%.

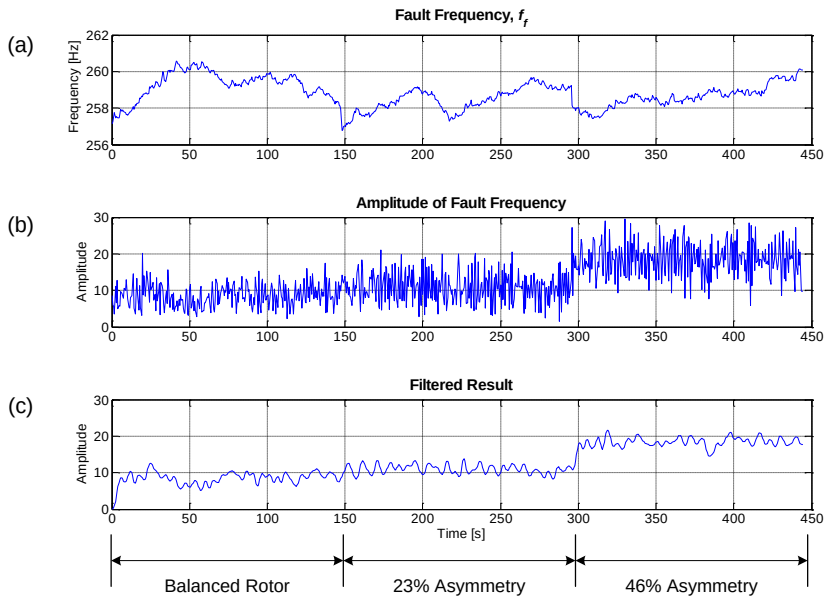

Figure C.4: IDFT$_{local}$ analysis of generator line current frequency component 'e' for the detection of rotor electrical asymmetry: (a) Frequency of interest; (b) amplitude of frequency of interest; (c) filtered result. Driven by 7.5m/s, 6% turbulence conditions. Calculation time = 1.09s = 0.25%.

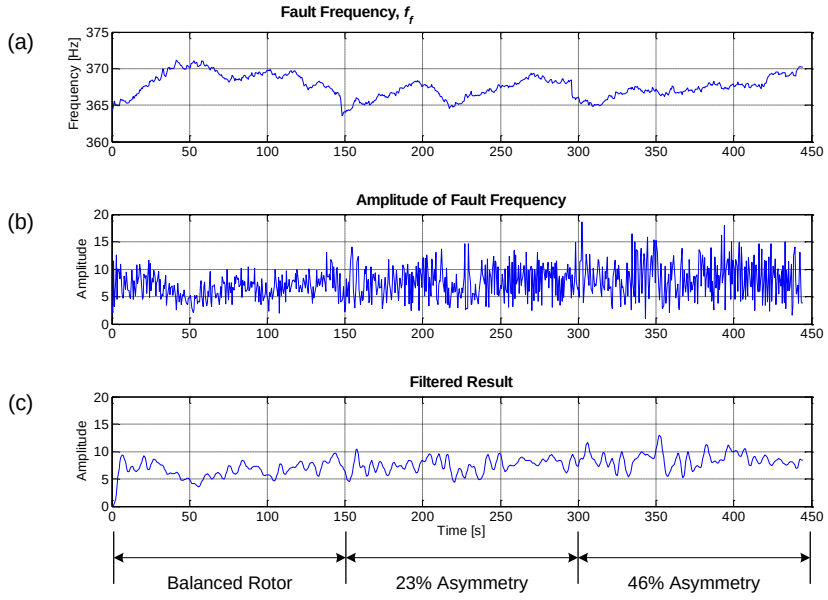

Figure C.5: IDFT$_{local}$ analysis of generator line current frequency component 'f' for the detection of rotor electrical asymmetry: (a) Frequency of interest; (b) amplitude of frequency of interest; (c) filtered result. Driven by 7.5m/s, 6% turbulence conditions. Calculation time = 1.11s = 0.25%.

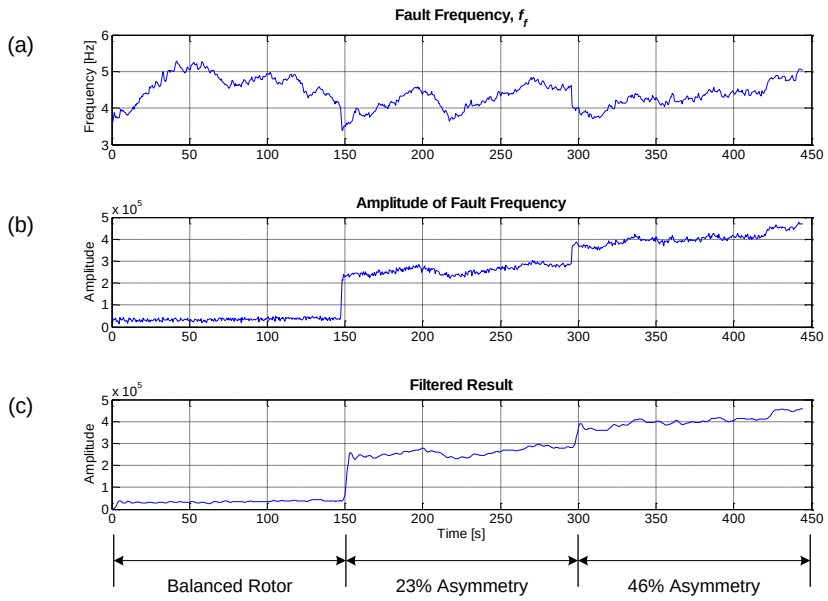

Figure C.6: IDFT$_{local}$ analysis of generator total power frequency component 'c' for the detection of rotor electrical asymmetry: (a) Frequency of interest; (b) amplitude of frequency of interest; (c) filtered result. Driven by 7.5m/s, 6% turbulence conditions. Calculation time = 0.91s = 0.20%.

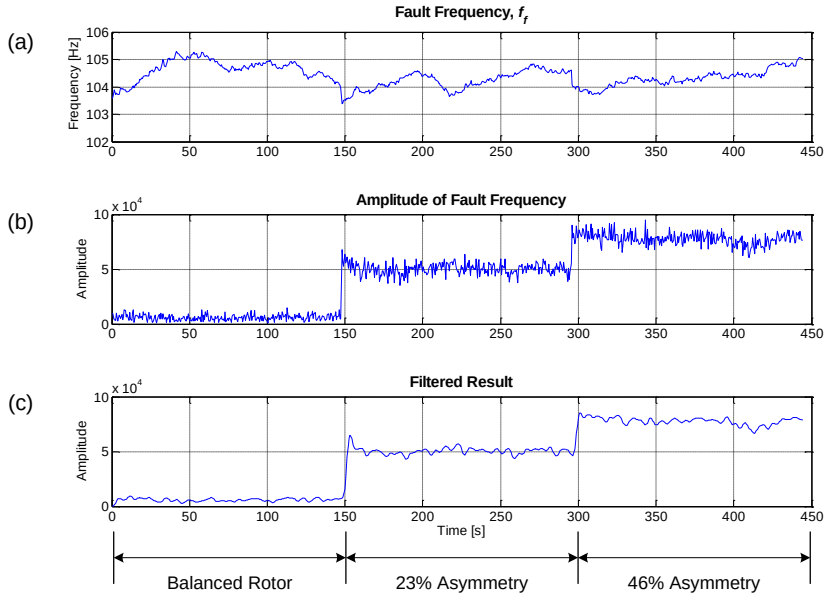

Figure C.7: IDFT$_{local}$ analysis of generator total power frequency component 'd' for the detection of rotor electrical asymmetry: (a) Frequency of interest; (b) amplitude of frequency of interest; (c) filtered result. Driven by 7.5m/s, 6% turbulence conditions. Calculation time = 1.02s = 0.23%.

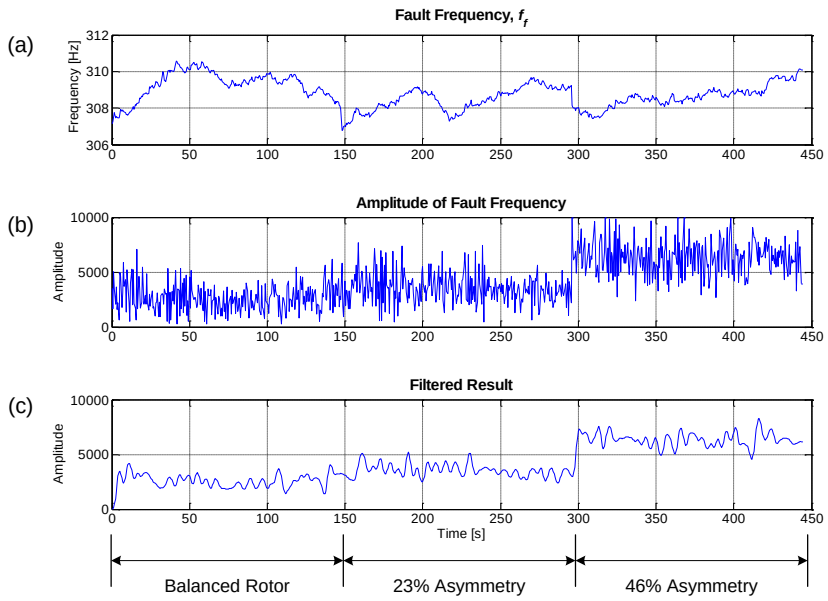

Figure C.8: IDFT$_{local}$ analysis of generator total power frequency component 'e' for the detection of rotor electrical asymmetry: (a) Frequency of interest; (b) amplitude of frequency of interest; (c) filtered result. Driven by 7.5m/s, 6% turbulence conditions. Calculation time = 1.09s = 0.25%.

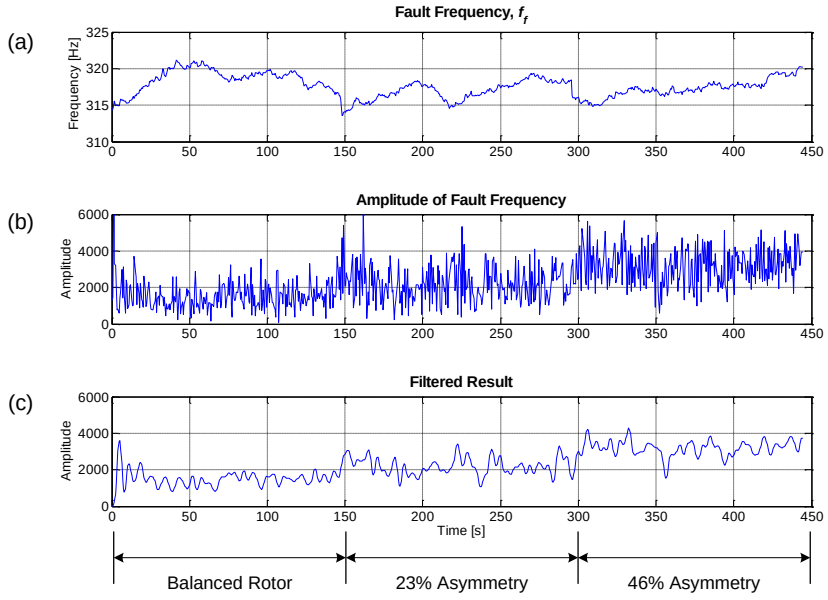

Figure C.9: IDFT$_{local}$ analysis of generator total power frequency component 'f' for the detection of rotor electrical asymmetry: (a) Frequency of interest; (b) amplitude of frequency of interest; (c) filtered result. Driven by 7.5m/s, 6% turbulence conditions. Calculation time = 1.09s = 0.25%.

C.1.2 15m/s, 20% Turbulence

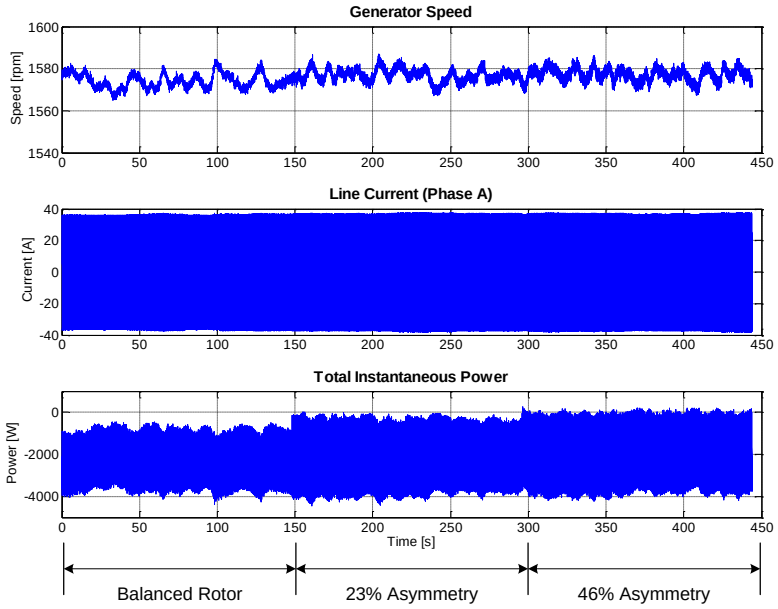

Figure C.10: Raw data used in the analysis of electrical signals for the detection of rotor electrical asymmetry. Driven by 15m/s, 20% turbulence conditions.

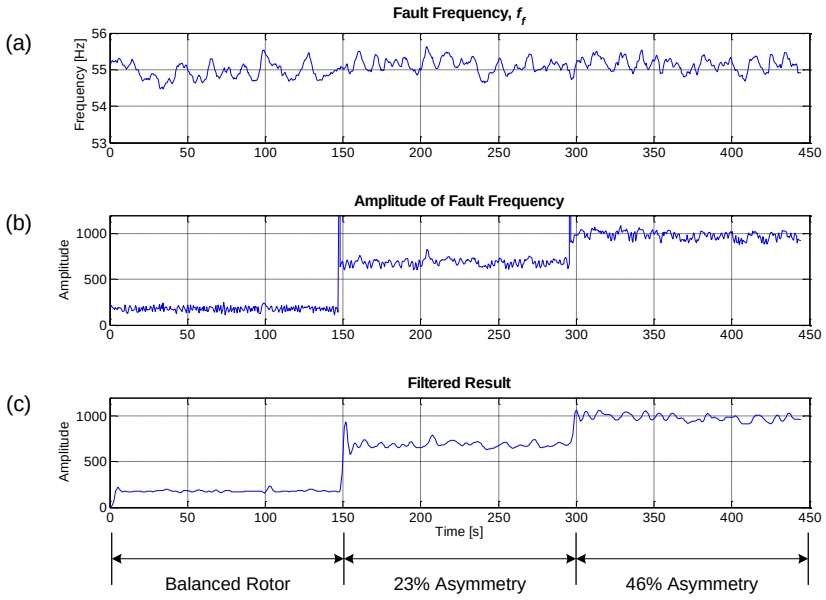

Figure C.11: IDFT$_{local}$ analysis of generator line current frequency component 'c' for the detection of rotor electrical asymmetry: (a) Frequency of interest; (b) amplitude of frequency of interest; (c) filtered result. Driven by 15m/s, 20% turbulence conditions. Calculation time = 0.97s = 0.22%.

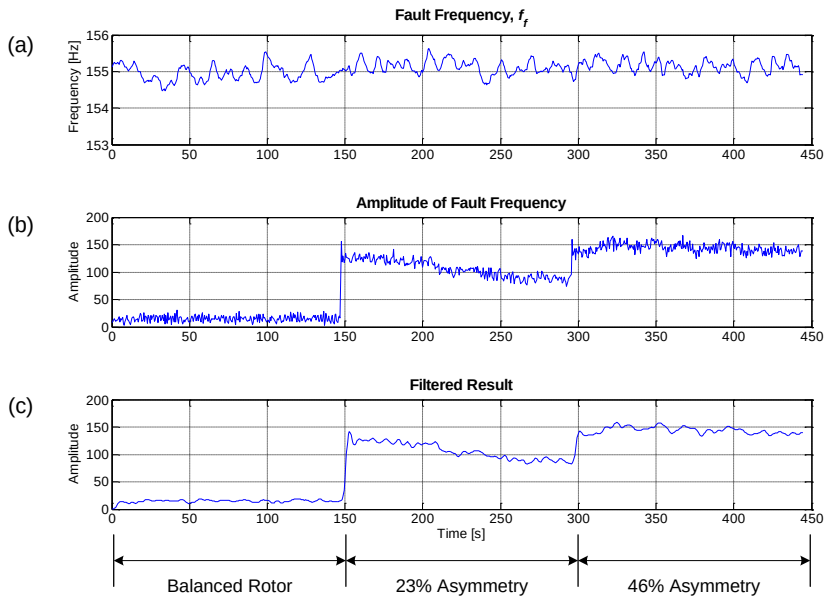

Figure C.12: IDFT$_{local}$ analysis of generator line current frequency component 'd' for the detection of rotor electrical asymmetry: (a) Frequency of interest; (b) amplitude of frequency of interest; (c) filtered result. Driven by 15m/s, 20% turbulence conditions. Calculation time = 1.06s = 0.24%.

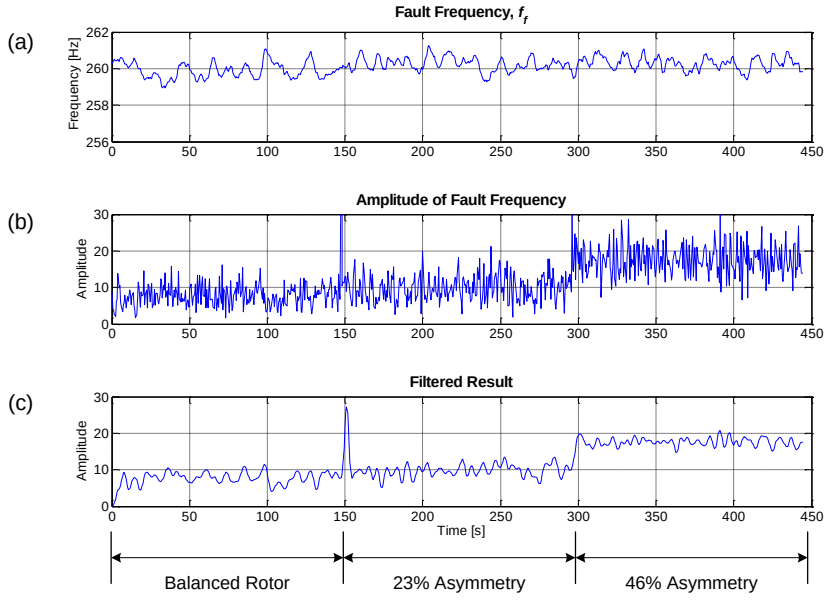

Figure C.13: IDFT$_{local}$ analysis of generator line current frequency component 'e' for the detection of rotor electrical asymmetry: (a) Frequency of interest; (b) amplitude of frequency of interest; (c) filtered result. Driven by 15m/s, 20% turbulence conditions. Calculation time = 1.09s = 0.25%.

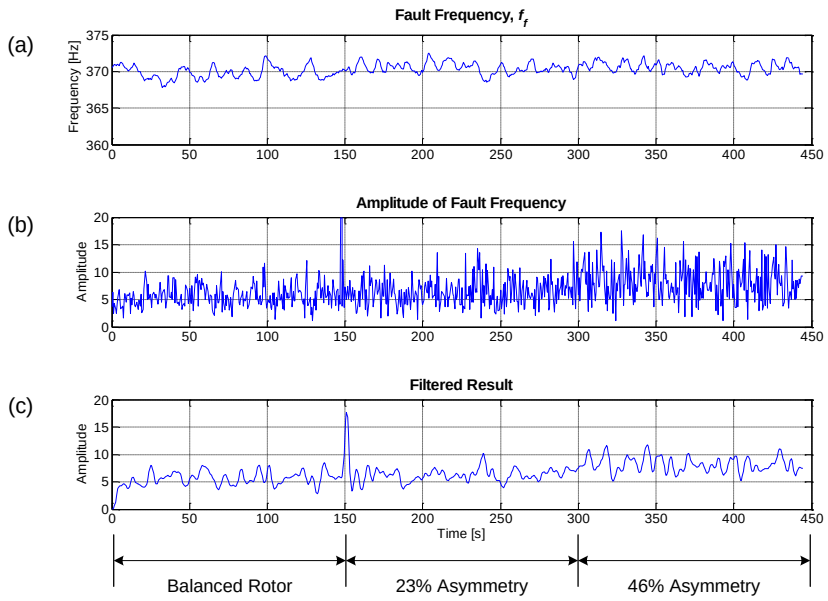

Figure C.14: IDFT$_{local}$ analysis of generator line current frequency component 'f' for the detection of rotor electrical asymmetry: (a) Frequency of interest; (b) amplitude of frequency of interest; (c) filtered result. Driven by 15m/s, 20% turbulence conditions. Calculation time = 1.13s = 0.25%.

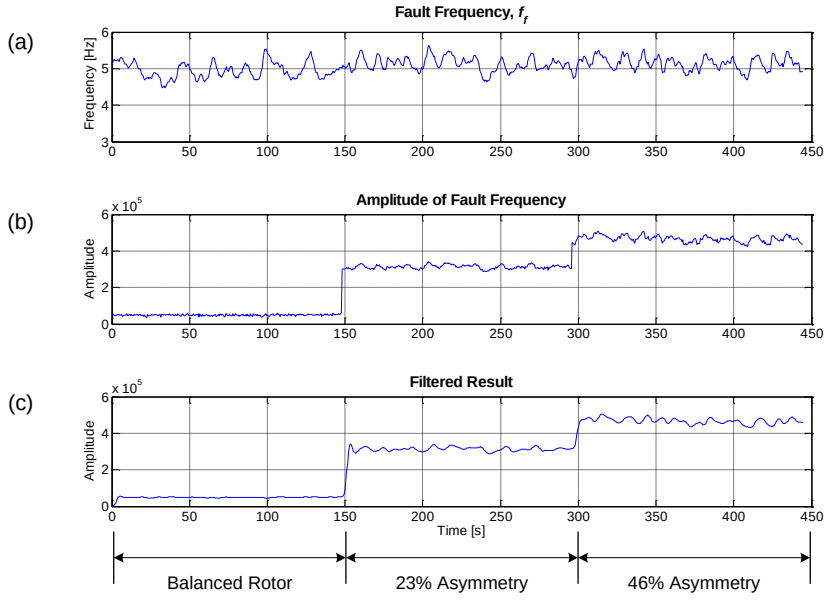

Figure C.15: IDFT$_{local}$ analysis of generator total power frequency component 'c' for the detection of rotor electrical asymmetry: (a) Frequency of interest; (b) amplitude of frequency of interest; (c) filtered result. Driven by 15m/s, 20% turbulence conditions. Calculation time = 0.91s = 0.20%.

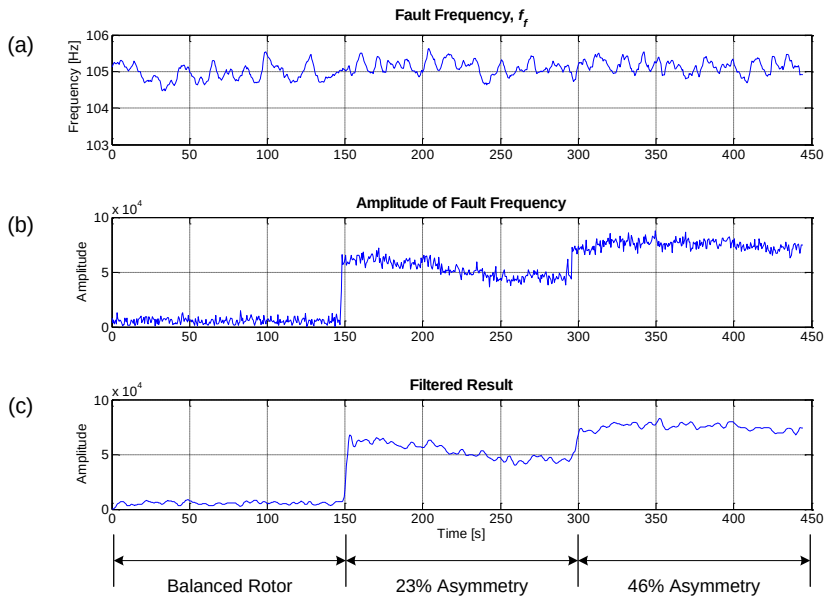

Figure C.16: IDFT$_{local}$ analysis of generator total power frequency component 'd' for the detection of rotor electrical asymmetry: (a) Frequency of interest; (b) amplitude of frequency of interest; (c) filtered result. Driven by 15m/s, 20% turbulence conditions. Calculation time = 1.02s = 0.23%.

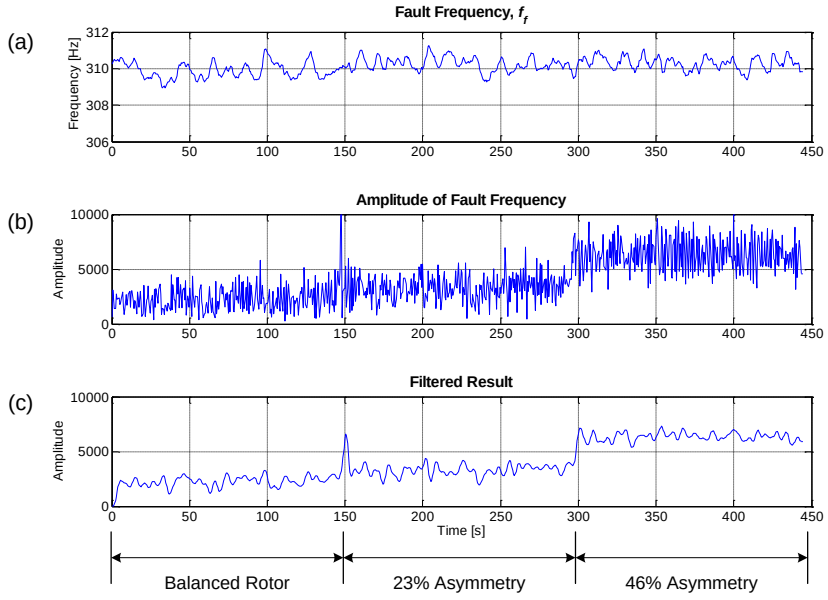

Figure C.17: IDFT$_{local}$ analysis of generator total power frequency component 'e' for the detection of rotor electrical asymmetry: (a) Frequency of interest; (b) amplitude of frequency of interest; (c) filtered result. Driven by 15m/s, 20% turbulence conditions. Calculation time = 1.09s = 0.25%.

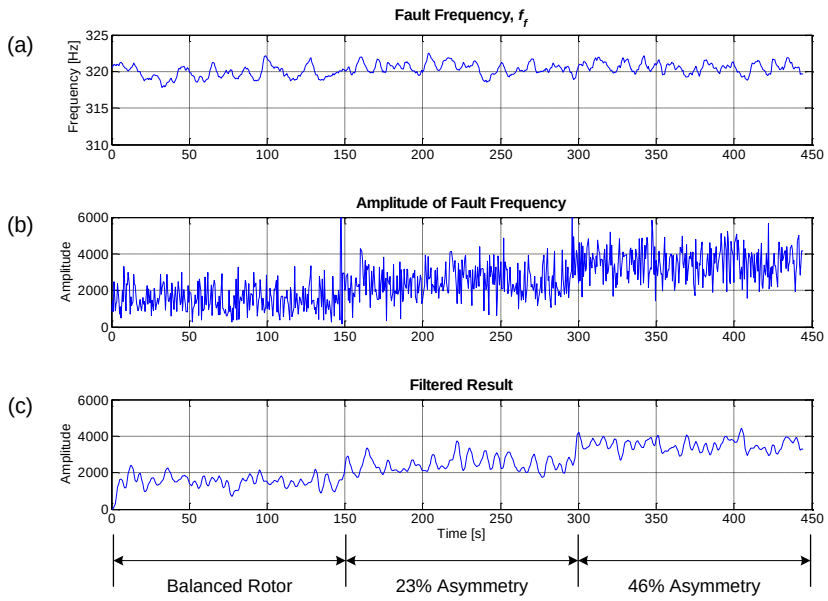

Figure C.18: IDFT$_{local}$ analysis of generator total power frequency component 'f' for the detection of rotor electrical asymmetry: (a) Frequency of interest; (b) amplitude of frequency of interest; (c) filtered result. Driven by 15m/s, 20% turbulence conditions. Calculation time = 1.09s = 0.25%.

C.2 High Speed Shaft Mass Unbalance

This section contains a complete set of figures from §6.1.2.

C.2.1 7.5m/s, 6% Turbulence

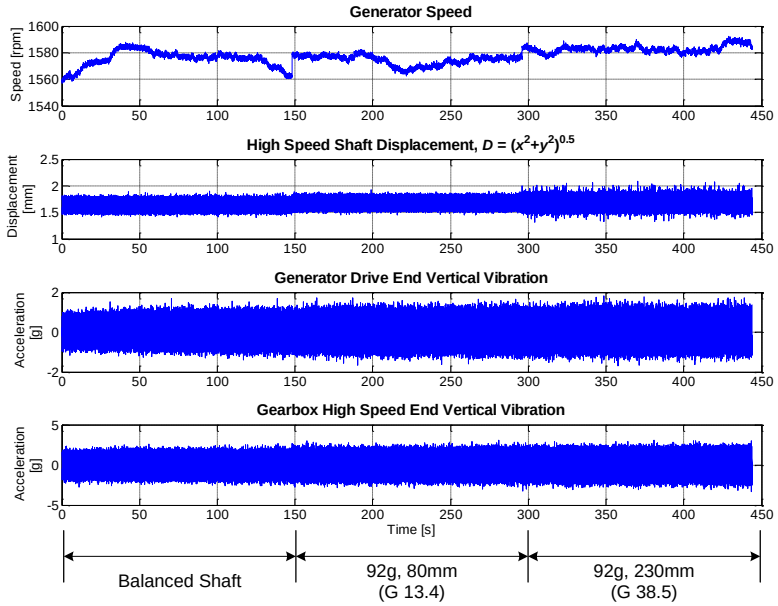

Figure C.19: Raw data used in the analysis of mechanical signals for the detection of high speed shaft mass unbalance Driven by 7.5m/s, 6% turbulence conditions.

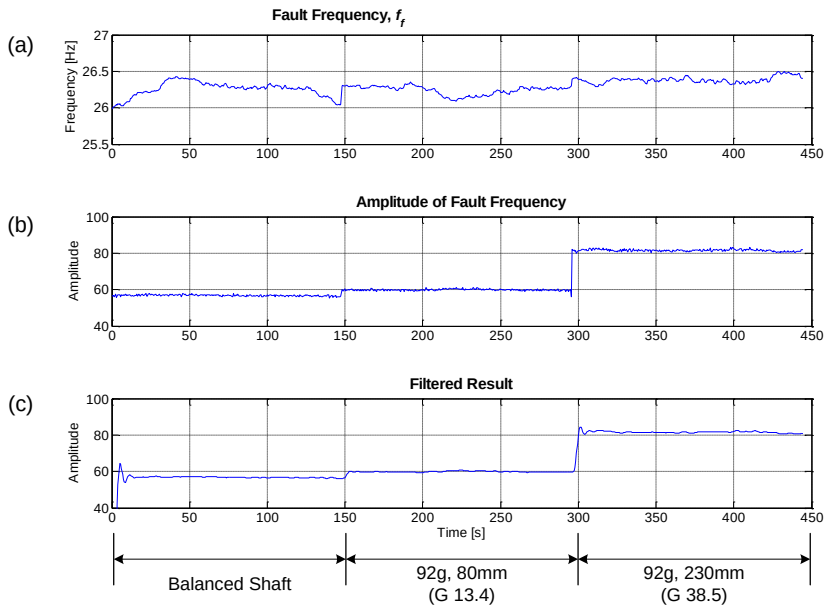

Figure C.20: IDFT$_{local}$ analysis of high speed shaft displacement frequency component f_{rm} for the detection of high speed shaft mass unbalance: (a) Frequency of interest; (b) amplitude of frequency of interest; (c) filtered result. Driven by 7.5m/s, 6% turbulence conditions. Calculation time = 0.95s = 0.21%.

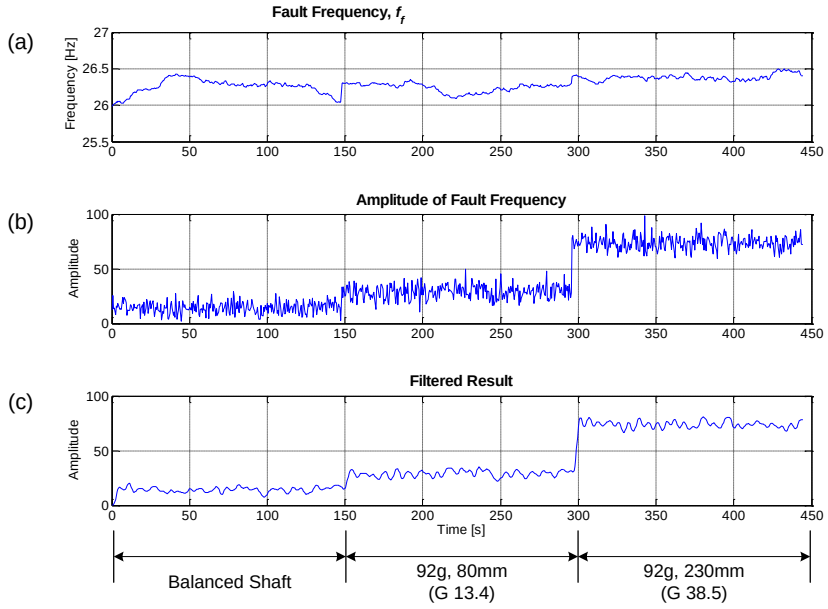

Figure C.21: IDFT$_{local}$ analysis of generator vertical vibration frequency component f_{rm} for the detection of high speed shaft mass unbalance: (a) Frequency of interest; (b) amplitude of frequency of interest; (c) filtered result. Driven by 7.5m/s, 6% turbulence conditions. Calculation time = 0.97s = 0.22%.

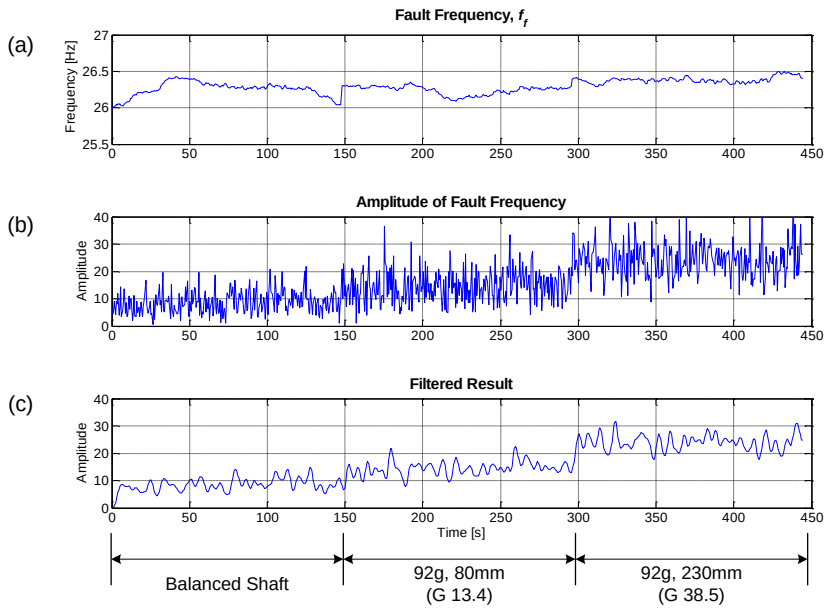

Figure C.22: IDFT$_{local}$ analysis of gearbox high speed end vibration frequency component f_{rm} for the detection of high speed shaft mass unbalance: (a) Frequency of interest; (b) amplitude of frequency of interest; (c) filtered result. Driven by 7.5m/s, 6% turbulence conditions. Calculation time = 0.97s = 0.22%.

C.2.2 15m/s, 20% Turbulence

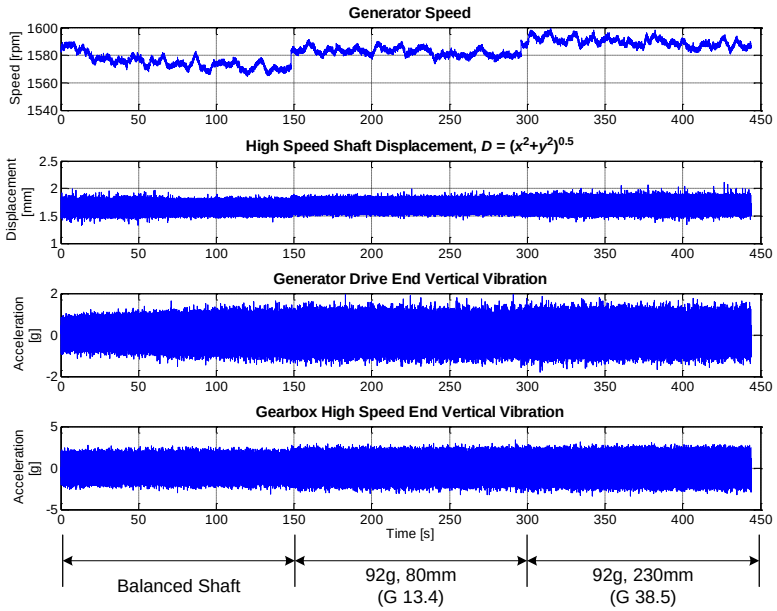

Figure C.23: Raw data used in the analysis of mechanical signals for the detection of high speed shaft mass unbalance. Driven by 15m/s, 20% turbulence conditions.

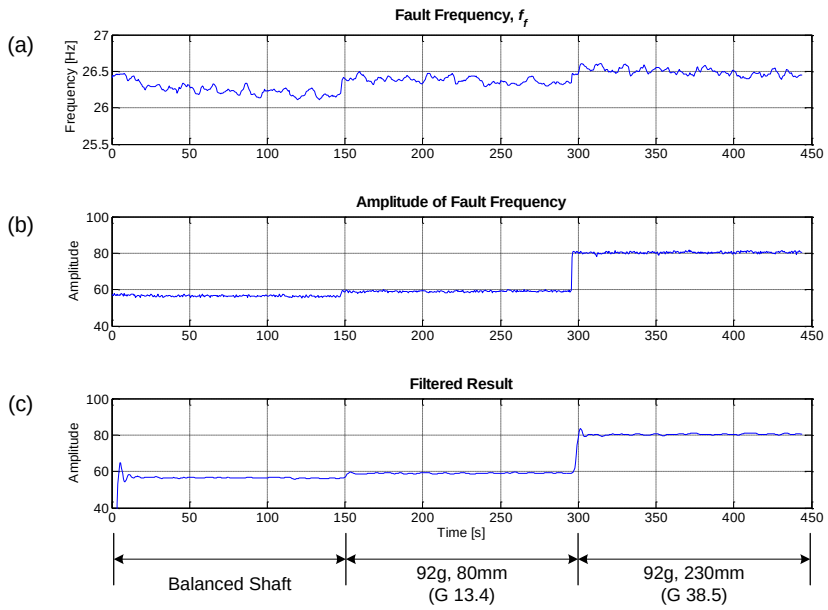

Figure C.24: IDFT$_{local}$ analysis of high speed shaft displacement frequency component f_{rm} for the detection of high speed shaft mass unbalance: (a) Frequency of interest; (b) amplitude of frequency of interest; (c) filtered result. Driven by 15m/s, 20% turbulence conditions. Calculation time = 0.98s = 0.22%.

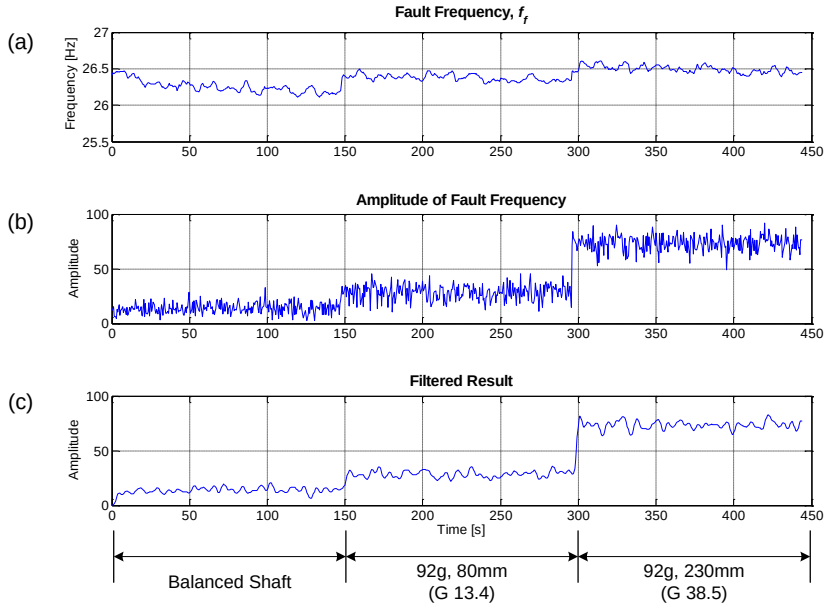

Figure C.25: IDFT$_{local}$ analysis of generator vertical vibration frequency component f_{rm} for the detection of high speed shaft mass unbalance: (a) Frequency of interest; (b) amplitude of frequency of interest; (c) filtered result. Driven by 15m/s, 20% turbulence conditions. Calculation time = 0.95s = 0.21%.

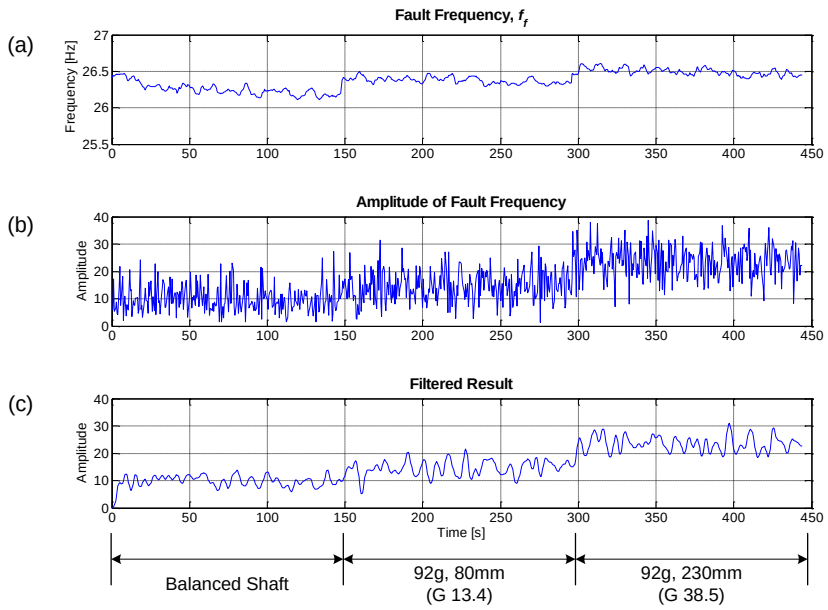

Figure C.26: IDFT$_{local}$ analysis of gearbox high speed end vibration frequency component f_{rm} for the detection of high speed shaft mass unbalance: (a) Frequency of interest; (b) amplitude of frequency of interest; (c) filtered result. Driven by 15m/s, 20% turbulence conditions. Calculation time = 0.99s = 0.22%.

C.3 Gear Tooth Failure

This section contains a complete set of figures from §6.1.3.

C.3.1 Gear Tooth Photographs

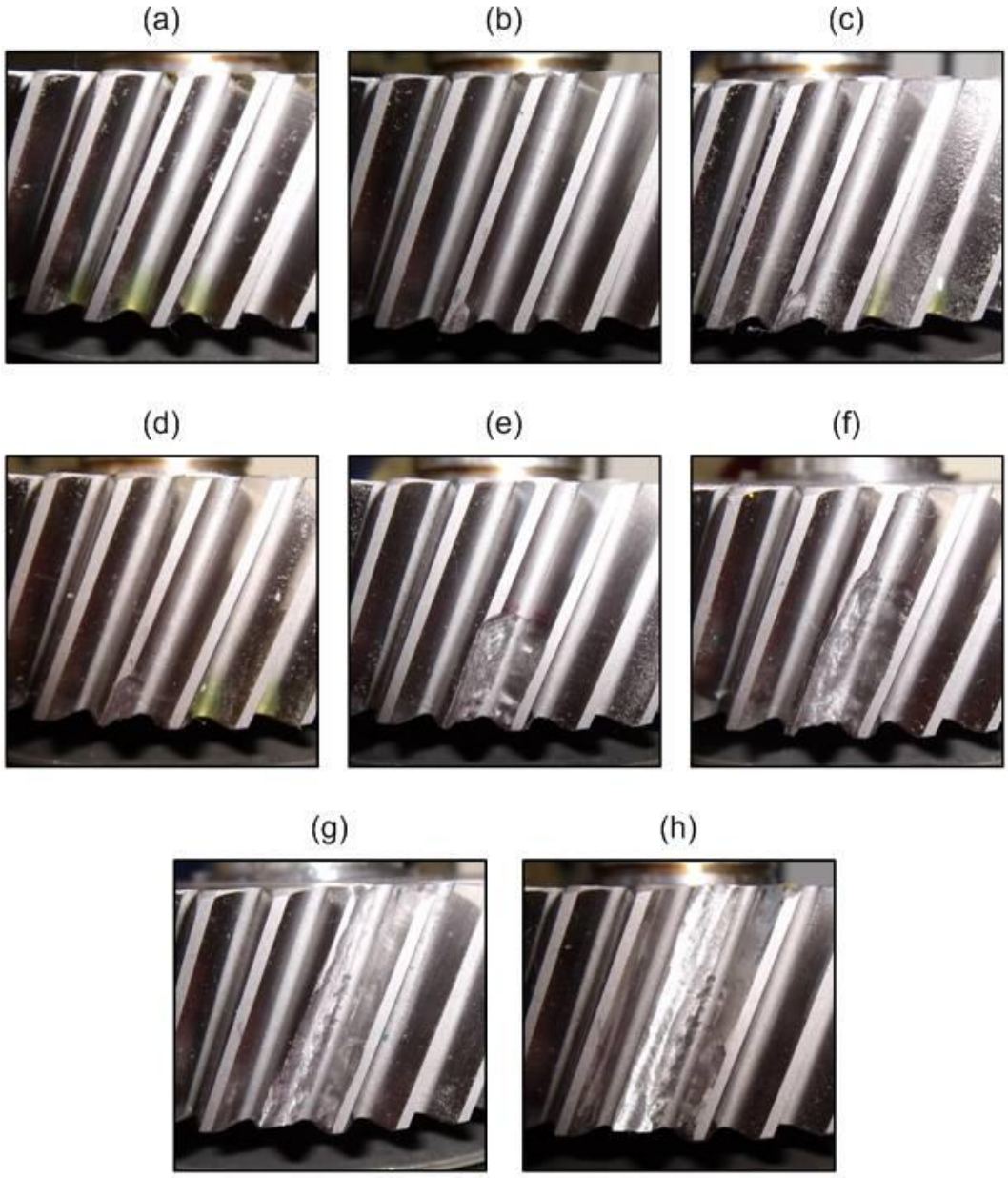

Figure C.27: Gear tooth faults applied to the test rig: (a) healthy tooth; (b) 3mm x 2mm; (c) 5mm x 5mm; (d) 7mm x 5mm; (e) 13mm x 6mm; (f) 18mm x 6mm; (g) 28mm x 6mm; (h) whole tooth.

C.3.2 7.5m/s, 6% Turbulence

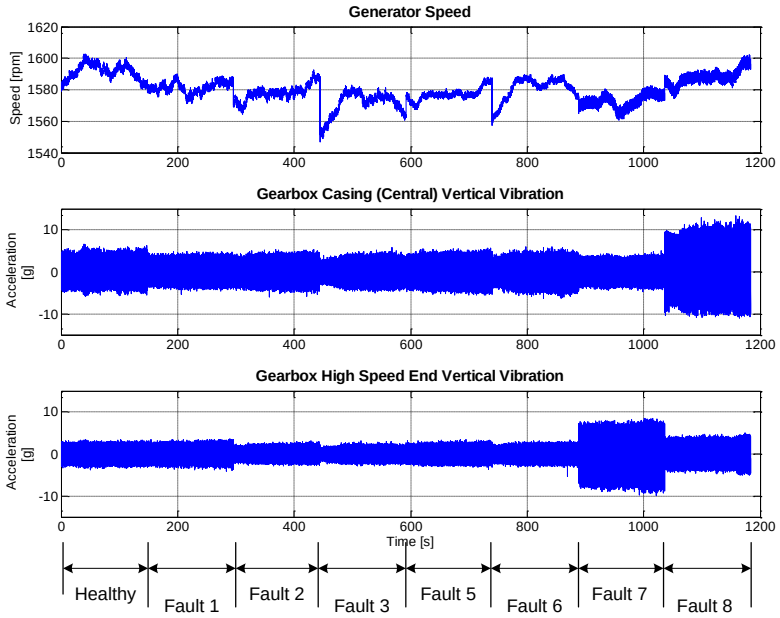

Figure C.28: Raw data used in the analysis of mechanical signals for the detection of gear tooth damage (7.5m/s, 6% turbulence)

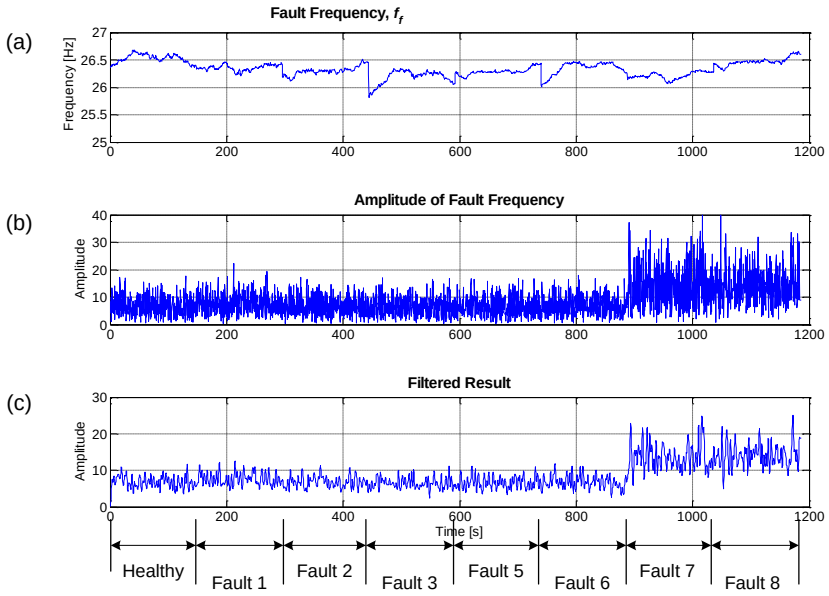

Figure C.29: IDFT$_{local}$ analysis of gearbox casing high speed end vibration frequency component f_{rm} for the detection of gear tooth damage: (a) Frequency of interest; (b) amplitude of frequency of interest; (c) filtered result. Driven by 7.5m/s, 6% turbulence conditions. Calculation time = 3.34s = 0.28%.

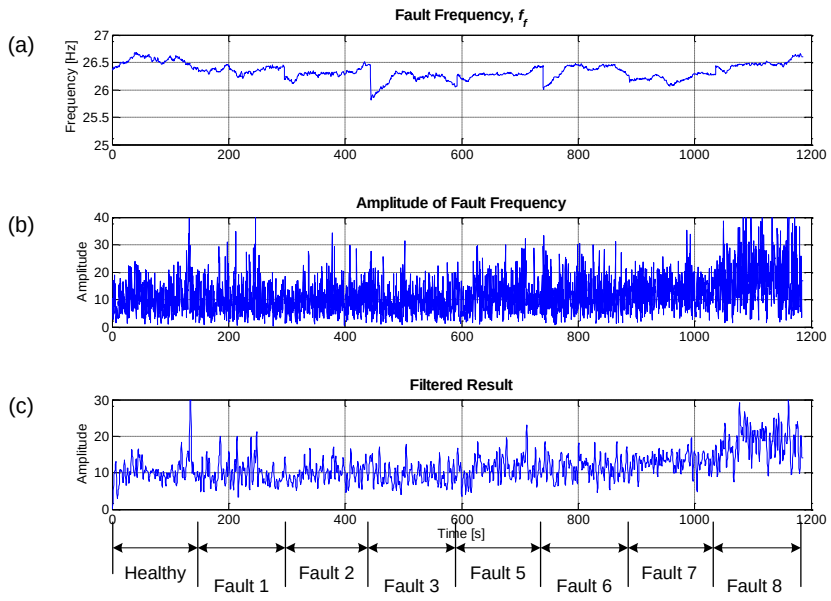

Figure C.30: IDFT$_{local}$ analysis of gearbox vertical vibration frequency component f_{rm} for the detection of gear tooth damage: (a) Frequency of interest; (b) amplitude of frequency of interest; (c) filtered result. Driven by 7.5m/s, 6% turbulence conditions. Calculation time = 2.63s = 0.22%.

C.4 Comparison of Frequency Tracking Techniques

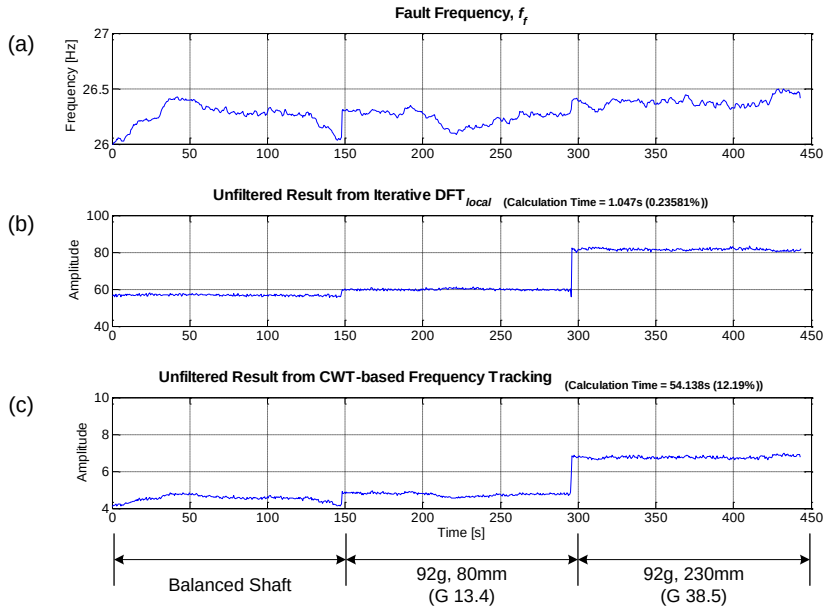

Figure C.31: Unfiltered analysis of high speed shaft displacement frequency component f_{rm} for the detection of high speed shaft mass unbalance: (a) Frequency of interest; (b) amplitude of frequency of interest using IDFT$_{local}$; (c) amplitude of frequency of interest using CWT$_{local}$ frequency tracking. Driven by 7.5m/s, 6% turbulence conditions.

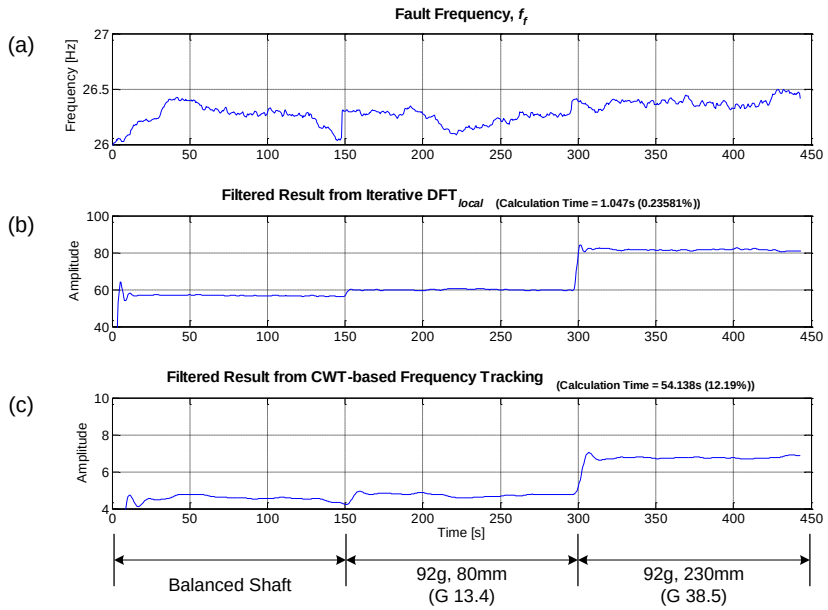

Figure C.32: Filtered analysis of high speed shaft displacement frequency component f_{rm} for the detection of high speed shaft mass unbalance: (a) Frequency of interest; (b) amplitude of frequency of interest using IDFT$_{local}$; (c) amplitude of frequency of interest using CWT$_{local}$ frequency tracking. Driven by 7.5m/s, 6% turbulence conditions.

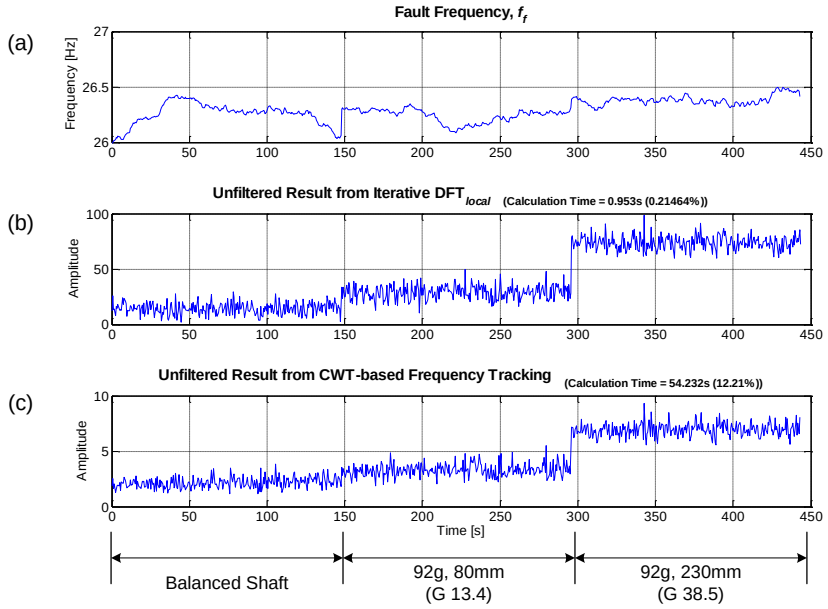

Figure C.33: Unfiltered analysis of generator vertical vibration frequency component f_{rm} for the detection of high speed shaft mass unbalance: (a) Frequency of interest; (b) amplitude of frequency of interest using IDFT$_{local}$; (c) amplitude of frequency of interest using CWT$_{local}$ frequency tracking. Driven by 7.5m/s, 6% turbulence conditions.

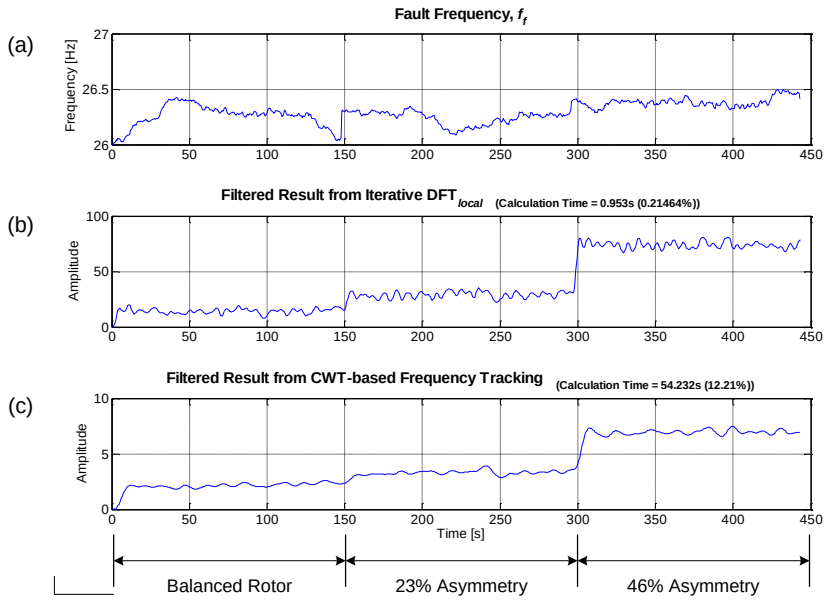

Figure C.34: Filtered analysis of generator vertical vibration frequency component f_{rm} for the detection of high speed shaft mass unbalance: (a) Frequency of interest; (b) amplitude of frequency of interest using IDFT$_{local}$; (c) amplitude of frequency of interest using CWT$_{local}$ frequency tracking. Driven by 7.5m/s, 6% turbulence conditions.

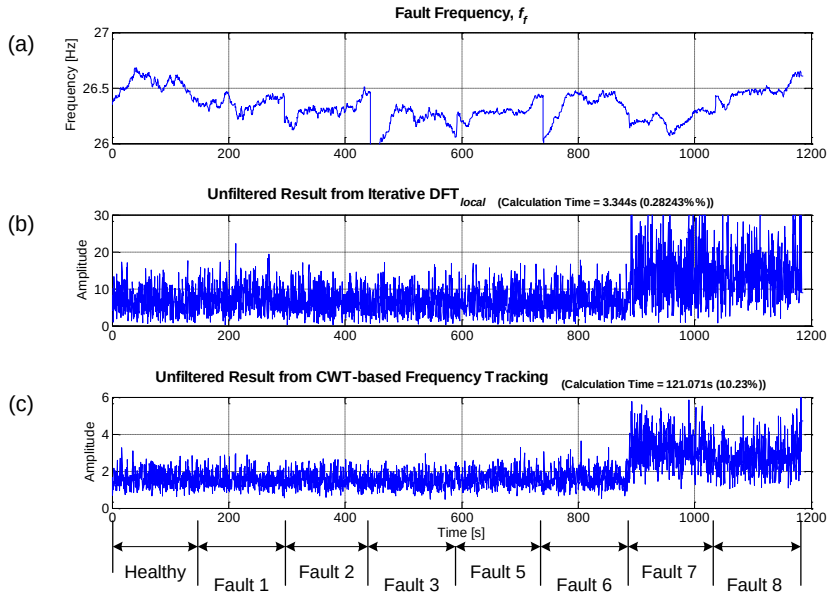

Figure C.35: Unfiltered analysis of generator high speed end vibration frequency component f_{rm} for the detection of gear tooth damage: (a) Frequency of interest; (b) amplitude of frequency of interest using IDFT$_{local}$; (c) amplitude of frequency of interest using CWT$_{local}$ frequency tracking. Driven by 7.5m/s, 6% turbulence conditions.

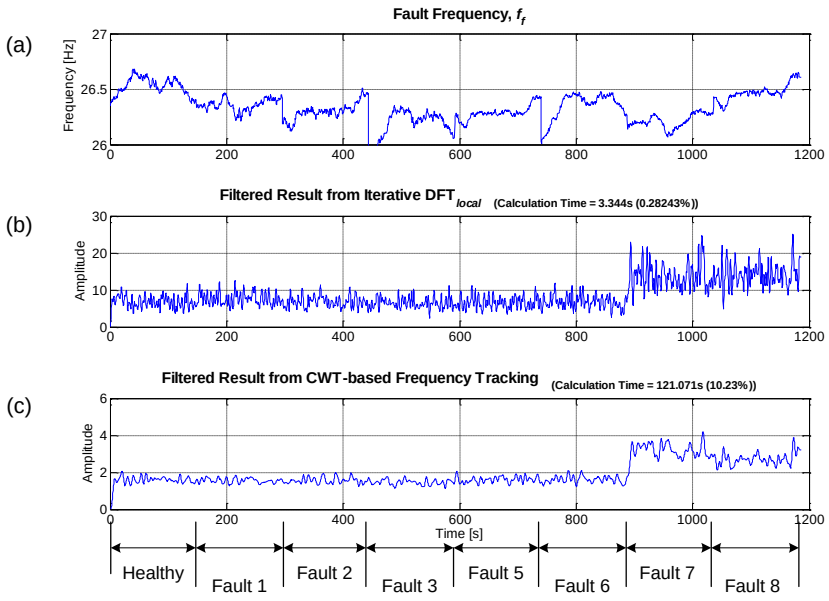

Figure C.36: Filtered analysis of generator high speed end vibration frequency component f_{rm} for the detection of gear tooth damage: (a) Frequency of interest; (b) amplitude of frequency of interest using IDFT$_{local}$; (c) amplitude of frequency of interest using CWT$_{local}$ frequency tracking. Driven by 7.5m/s, 6% turbulence conditions.

D. Test Rig Specification

This test rig specification gives extended information on the configuration and components comprising the Durham condition monitoring test rig.

The document was produced by Dr Tianyu Liu in September 2010 with the assistance of the Author and Prof. Peter Tavner and, with reference to other, previous documents from within the School of Engineering and Computing Sciences, Durham University.

Specification of Durham University Wind Turbine Condition Monitoring Test Rig

Tianyu Liu

Edited: Christopher J Crabtree

2nd November 2010
Revision: 03

Contents

1. Introduction

The Test Rig, Figure 1, was initially constructed using funding from the New & Renewable Energy Centre (NaREC), Blyth, Northumberland. This Test Rig is used to simulate the performance of a wind turbine and permit the analysis of fault signals from the Test Rig.

Figure 1: Photograph of Durham Test Rig

2. Components of Test Rig

2.1. Main Drive Train

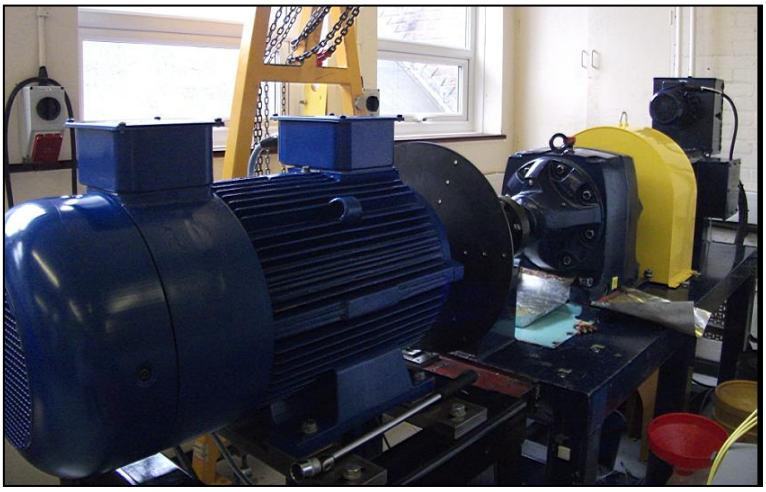

Figure 2: Photograph of main drive train

The components of the Test Rig main drive train, Figure 2, are given in the following sections.

2.1.1. DC Drive Motor

The Test Rig is driven by a 54kW DC motor, Figure 3, powered from a Eurotherm 590+ variable speed drive. The drive is controlled by either the man-machine interface (MMI) or a LabVIEW control environment.

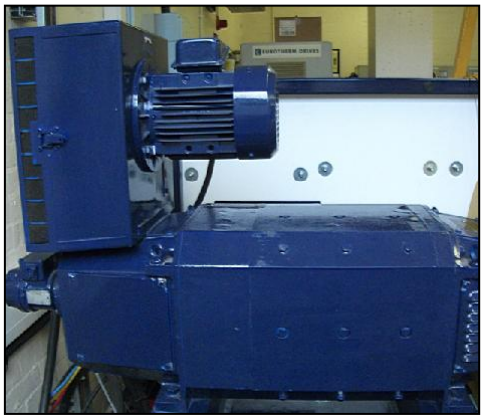

Figure 3: Photograph of the DC motor

2.1.2. Low Speed Shaft:

The low speed shaft links the DC motor to the gearbox

2.1.3. Gearbox

The Test Rig can use either a 4.9894:1 or 11.14:1 gearbox, Figure 4, however the 4.9894:1 gearbox is generally used as it allows for greater speed variation before the DC motor torque limit or armature current limit is reached. The 4.9894:1 gearbox has two helical and two parallel wheel stages: the first stage 36/79, the second 57/78.

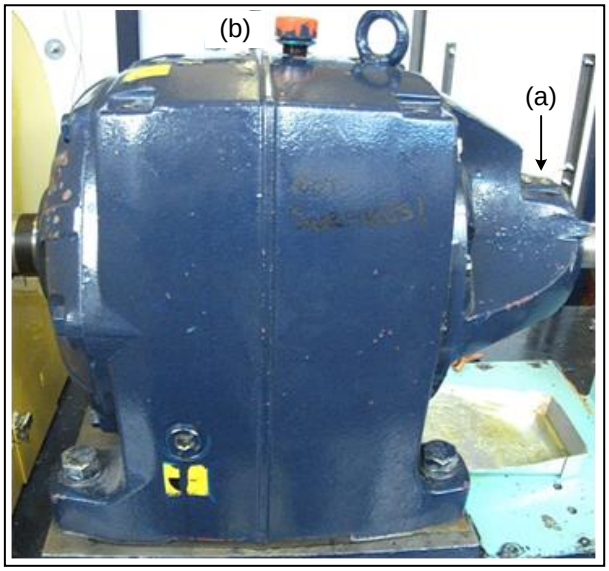

Figure 4: Photograph of the 11.14:1 gearbox showing accelerometer points: (a) high speed end; (b) casing, central.

2.1.4. High Speed Shaft

The high speed shaft links the gearbox to the generator.

2.1.5. Generator

The Generator, Figure 5, is manufactured by Marelli Motori, a company owned by FKI Energy Technology. It is a four pole machine, rated at 30 kW.

Figure 5: Photograph of the generator

2.2. Data Collection and Analysis & Control System

Figure 6: Photograph of the data collection and control system

The components of Data Collection and Analysis and Control System of Test Rig, Figure 6, are:

2.2.1. Torque Transducer

Two Magtrol torque transducers, Figure 7, can be used, with ratings of 200 or 500 Nm. The transducer also outputs 60 pulses per revolution signal, which can be used as a tachometer.

Figure 7: Photograph of the Torque Transducer

2.2.2. Proximeter Sensors

The generator high speed shaft has a machined coupling located between the Torque Transducer and Generator. The accuracy of the final machined surface of the coupling was to 3m. Two proximeters, in the x and y-axes, are fitted adjacent to this coupling, Figure 8.

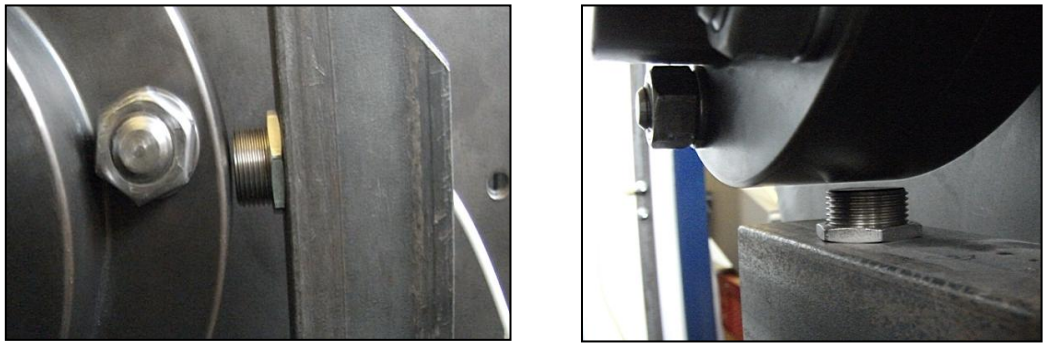

(a) **(b)**

Figure 8: Photograph of the Proximeter sensors: (a) x-axis; (b) y-axis

2.2.3. Mass Balance Plates

In order to apply simulated mass unbalance faults, two experimental balance planes have been fitted to the Test Rig, one on the high speed shaft, towards the generator drive end bearing, and one on the low speed shaft between the gearbox and DC motor. The Balance Plates, Figure 9, are fitted with precision holes in which precision masses can be inserted.

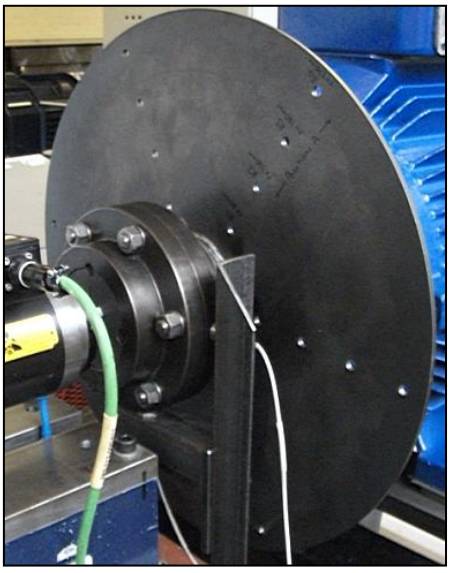

Figure 9: Photograph of the Balance Plate on the High Speed Shaft

2.2.4. Accelerometers

Two accelerometers, such as that in figure 10, are available for monitoring and can be mounted at various screw-fit locations including:

- Gearbox casing
- Gearbox high speed bearing
- Gearbox low speed bearing
- Generator drive end bearing
- Generator non drive end bearing

These can measure generator vibrations and gearbox meshing frequencies and changes to the gearbox condition.

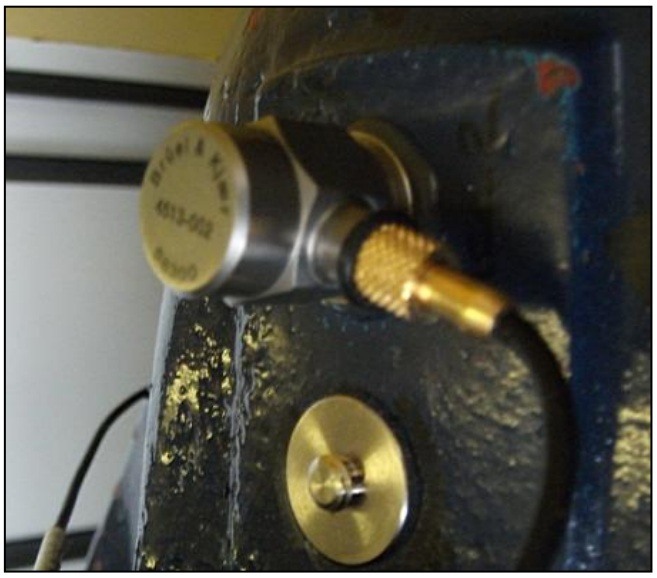

Figure 10: Photograph of an accelerometer on the gearbox high speed end

2.2.5. Voltage & Current Cards

Transducer boards have been installed to measure the three phase Generator terminal voltages and currents and each produce a voltage proportional to those voltages and currents. The bandwidth of these transducer boards is DC-100K Hz. They can be combined in the Data Acquisition System to give the electrical power produced by the Generator.

2.2.6. Data Acquisition and Control Cards (DAQ)

Two National Instruments 6015 DAQ cards were installed for use with a LabVIEW interface, to collect data from the transducers described above. The cards were configurable to sample 16 single-ended or 8 differential channels at a maximum rate of 200 kHz. The cards each contained one analogue to digital (A/D) converter, so the signals were multiplexed, with the maximum sample rate for each channel depending on how many channels were in use, but a lower rate (100kHz) could be set if required.

2.2.7. Control Software

LabVIEW is a computer program designed specifically to facilitate data acquisition and control tasks. It is produced by National Instruments, a company specializing in test and measurement hardware and software. The hardware and software exhibits a good level of interoperability and the low level tasks for interacting with transducer and other device drivers are included. For these reasons, it was decided to use LabVIEW. Programs are constructed in LabVIEW by means of a visual connection diagram, which shows how data flows through the program. The program enabled different wind profiles to be applied to the drive train, while simultaneously acquiring data giving the system state, presented in a graphical format, and saving the data to the PC hard disk, Figure 11.

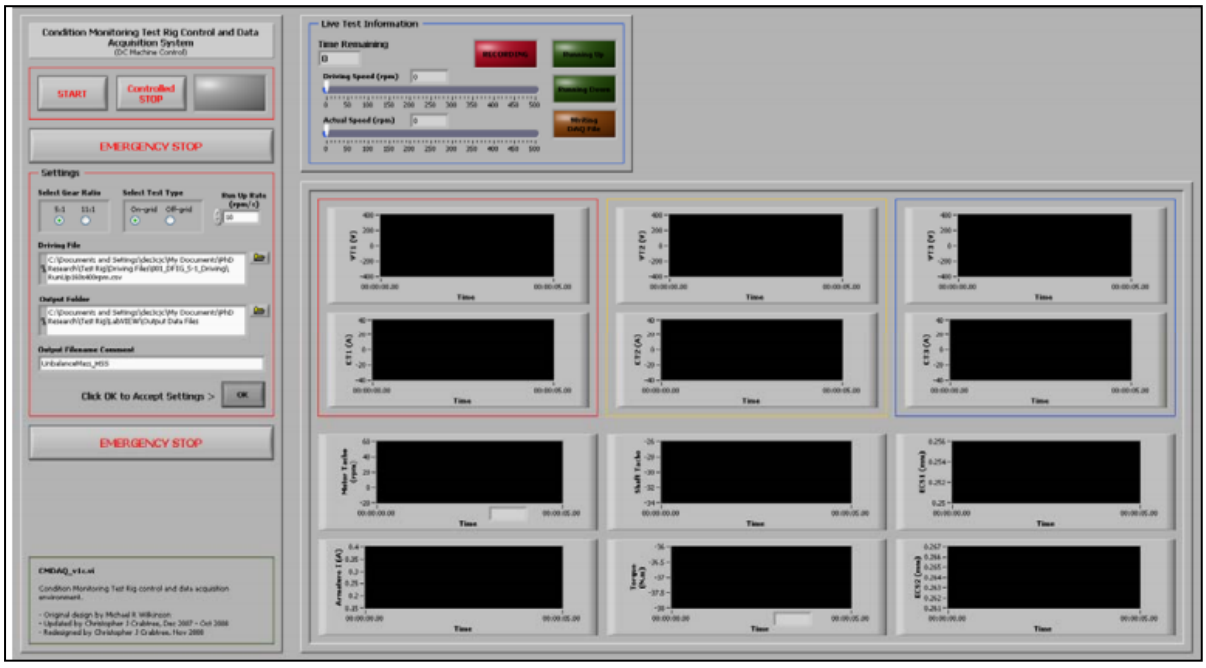

Figure 11: Front Panel of the LabVIEW DAQ Interface

Data is read from the DAQ cards for all the signals described above but is only saved to data files for those shown below:

- Torque;
- High speed shaft speed;
- DC machine speed;
- Generator phase voltage waveform x 3;
- Generator phase current waveform x 3;
- X and Y proximeters - high speed shaft vibration;
- Gearbox or generator accelerometers 1 and 2;
- Generator three-phase power.

The LabVIEW software is organized to start the Test Rig in a controlled way using the following diagram, Figure 12.

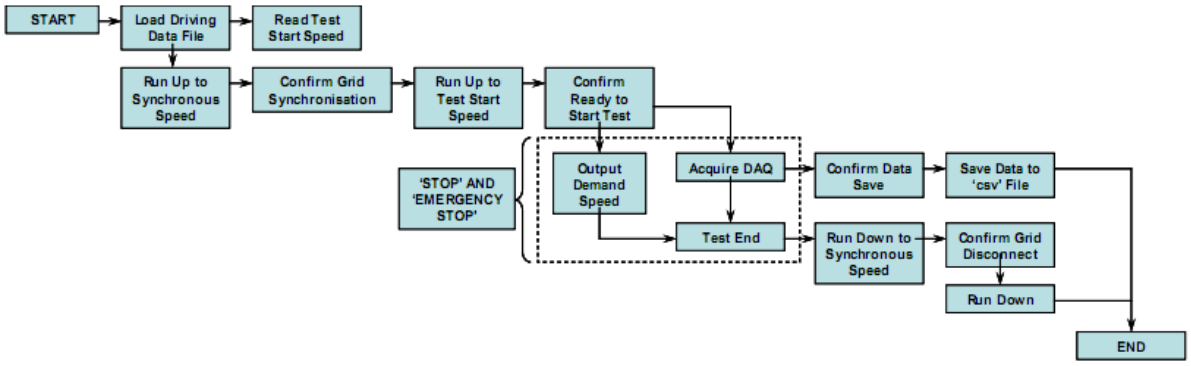

Figure 12: Basic Layout of the LabVIEW Data Acquisition Environment

2.2.8. SKF WindCon System

An SKF WindCon 3.0 condition monitoring system has been installed on the Test Rig as this is the commercial equipment used on full size wind turbines by our industrial partners, a large wind turbine operator.

- WindCon 3.0: S/N 4641-001306 08-04
- ProCon: Version 6.5.3

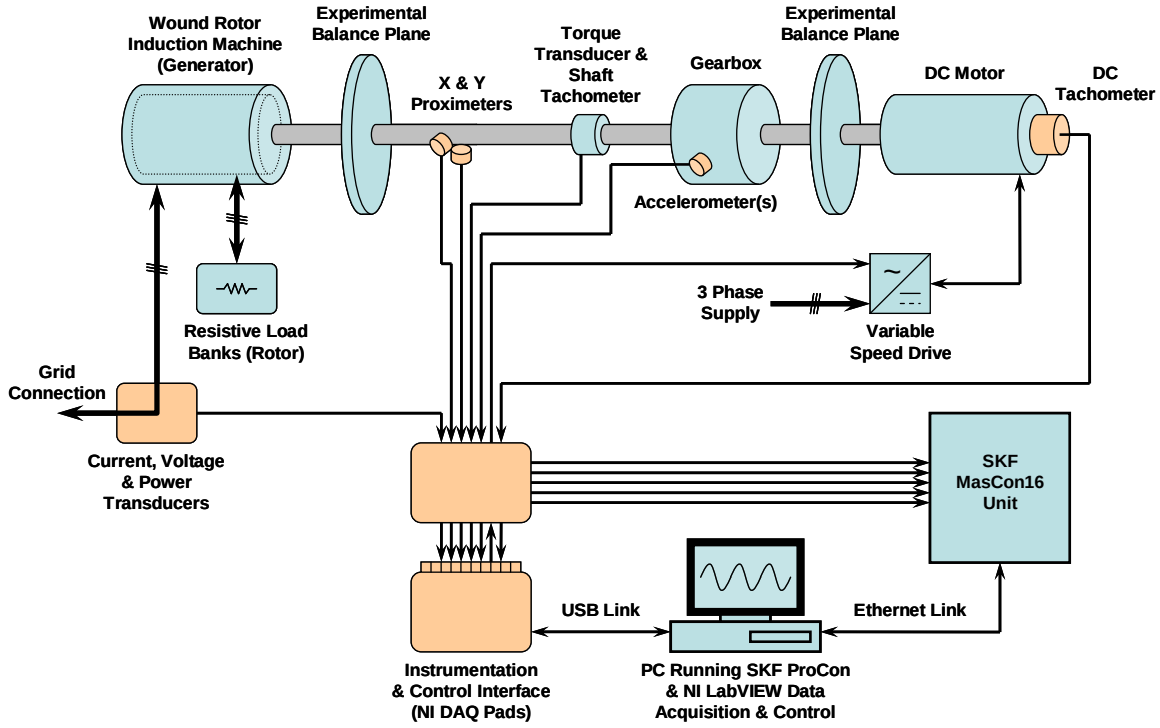

Figure 13: Schematic diagram of the Durham Wind turbine Condition Monitoring Test Rig

Appendix A: Machine, Instrument and Component Data

Parameters of the Test Rig

Table 1: Electrical & Mechanical Parameters of the Test Rig

Component	Parameter	Symbol	Value	Units	How obtained
Whole Test Rig	Damping Ratio		≥ 0 <1	$Ns.m^{-1}$	Test
	Resonant Frequency		0.4	Hz	Test
DC Motor	Inertia	J_{DC}	0.2260	$kg.m^2$	Test
	Inertia with Mass Plate		0.7594	$kg.m^2$	Test
	Damping Ratio		1	$N.s.m^{-1}$	Test
	Resonant Frequency		6.2	Hz	Test
	Max Speed		2120	$rev.min^{-1}$	Nameplate
	Armature Inductance	*La*	0.00904	H	Test
	Armature Resistance	*Ra*	0.4	Ω	Test
	Motor Constant	*Ke*	2.66	$N.m.W^{-0.5}$	Test
	Controller Reset Time	*TI*	2	S	Test
	windage loss coefficient		0.001	$N.m.s^2.rad^{-2}$	Test
	Proportional gain for speed control loop	*Kps*	10		Test
	Integral Gain for speed control loop	*Kis*	60		Test
	Proportional gain for current control loop	*Kpc*	22.28		Test
	Integral Gain for current control loop	*Kic*	4.28		Test
DC Motor & Gearbox	Damping Ratio		>1	$N.s.m^{-1}$	Test

(5:1)	Friction loss coefficient		1.222	N.m.s.rad^{-1}	Test
	Stiction torque		7.159	N.m	Test
	Resonant Frequency		25.0	Hz	Test
Gearbox(5:1)	Total Inertia		0.1068	kg.m^2	Calculated
	Gear1 Inertia		0.0663	kg.m^2	Calculated
	Pinion1 Inertia		0.001	kg.m^2	Calculated
	Gear2 Inertia		0.0384	kg.m^2	Calculated
	Pinion2 Inertia		0.0502	kg.m^2	Calculated
	Stiffness		5,000,000	N.m^{-1}	Test
	Backlash1		0.0625	mm	Test
	Backlash2		0.2825	mm	Test
Gearbox(11:1)	Inertia		0.015	kg.m^2	Test
	Stiffness		5,000,000	N.m^{-1}	Test
Low Speed Shaft	Stiffness		14,000	Nm.rad^{-1}	Test
	Damping		10	Nms.rad^{-1}	Test
High Speed Shaft	Stiffness		50,000	Nm.rad^{-1}	Test
	Damping		10	Nms.rad^{-1}	Test
Generator	Inertia		0.414	kg.m^2	Calculated
	Inertia with Mass Plate		1.0198	kg.m^2	Test
	Windage loss coefficient		0.00006	N.m.s^2.rad^{-2}	Test
	Friction loss coefficient		0.001	N.m.s.rad^{-1}	Test
	Stiction torque		0.298	N.m	Calculated
Generator Stator	Stator resistance	R_s	0.079	Ω	Test
	Stator reactance	X_s	0.252	Ω	Test
	Resistance representing core loss	R_m	131.9	Ω	Test
	Stator magnetizing reactance	X_m	9.39	Ω	Test
Generator Rotor	Rotor resistance	R'_r	0.072	Ω	Test
	Rotor reactance	X'_r	0.408	Ω	Test

DC Motor

Table 2: Specification of DC Motor

Size	Manufacturer	Power(kW)	Rev/min	Voltage (V)	Armature Current (A)	Weight (kg)
160L	Brook Crompton, UK	54	2120	460	131	284

Gearbox

- Manufacturer, Hansen Transmissions, Type：SFN64E
  - With the 5:1 ratio gearbox, 66/13 and 57/78
  - With the 11:1 ratio gearbox, 6/13 and 79/36

Generator

Table 3: Specification of Generator

Size	Manufacturer	Power (kW)	Rev/min	Stator Voltage (V)	Stator Current (A)	Weight (kg)	Frequency (Hz)	Pole
E4F 225 M4 B3	Marelli Motori, Italy	30	1470	400	56	306	50	4

Eddy Current Displacement Transducers:

- Purpose: to measure shaft displacement.
- Description: Kaman 4S1 ECS with KD-2300 signal conditioning electronics units
- Units: 2 - x & y measurement aligned through centre of shaft
- Measuring Range: 4.0 mm
- Typical Offset: 0.51 mm
- Linearity: 0.5 % FS
- Analogue Voltage: 4.0 V

- Sensitivity: 1000 mV / mm
- Conversion Factor: 1 *u*V ≡10^{-6}mm

Torque Transducer

- Purpose: to measure shaft torque.
- Description: Torque Master TM212
- Rated Torque: 200 Nm
- Range: ±10 V ≡±200 % rated torque
- Conversion Factor: 1 V ≡ 4 ×10^{-5} N·m

DC Motor Tachometer

- Purpose: to measure the drive train DC motor end speed.
- Description: Supplied by Eurotherm Drives, fitted with DC motor, provides speed feedback to drive
- Range: Full output at drive full speed, 10 V ≡167rpm
- Conversion Factor: 1 V ≡1.67×10^{-5}

Accelerometer

- Purpose: to measure vibrations on the rig and on the gearbox in particular.
- Description: Endevco (Bruel & Kjaer) 4513-002 Deltatron Accelerometer
- Range: ±10 g
- Conversion Factor: 500 mV ≡1 g

Cables and Connectors

- Purpose: there are three distinct types of cables external to the enclosure: mains power, signal and USB.
- The ability to disconnect the leads is to enable the enclosure to be moved either around the Test Rig or lab.

2.2.9. Requirements

- There should only be one mains power lead to the enclosure. This should be via an standard connector, e,g, IEC 60320 socket (C14) and plug (C13).
- Connection between the DAQ and computer should be via a shielded USB cable. Signal cables should be shielded and connected to the enclosure via a standard connector e.g. DIN sockets and plugs.
- Signal and chassis grounds should be separated i.e. use two wire for each signal. Sensors that require power supply voltages should have this provided in the same cable as the sensor signal. This is to reduce the number of wires around the Test Rig.

Computer

- Purpose: to control the Test Rig and record measurements from rig sensors.

2.2.10. Requirements

- The PC should meet EMC requirements of the electrical machines laboratory. Either a laptop or desktop PC could be selected, provided the first requirement can be met. There may be EMC issues with a laptop computer. A laptop computer would need to have a locking cable for security reasons. It should able to connect to the Engineering Network to enable les to be saved to and retrieved from the Group Directory.
- The mouse input should be optical to ensure it works in the laboratory environment.
- It should run Microsoft Windows XP for stability and le format compatibility.
- It should have LabVIEW installed for control and measurement programs to be run.
- It should be capable of running LabVIEW with multiple input and output signals simultaneously i.e. high processor speed (>2 GHz) and large RAM (1 GB).
- The USB port should be USB2 compatible to increase the data transfer speed. It should have MATLAB installed for signal processing programs to be run.
- A Firewire port may be required if the Firewire DAQ card is selected.

DAQ and Control

2.2.11. Purpose

- DAQ should perform A/D conversion of signals from sensors and D/A conversion of signals

from the computer.

2.2.12. Requirements

- The DAQ and control device should be connected to the computer via a USB. Previous experiments have been conducted with an Eagle Technology USB-30 DAQ device with 16 A/D and 4 D/A channels. This has proven the benefits of a DAQ unit separate from the controlling PC, namely the ability to connect to different PCs that meet the requirements of the different tests.
- Alternatively, a Firewire DAQ card may be selected.
- The number of A/D channels should not be less than 7 to meet existing requirements and should preferably have more channels to enable the connection of additional sensors.
- The number of D/A channels should be not less than 1 to meet existing requirements and should preferably have more channels to enable future expansion of control requirements.
- LabVIEW will be used to control the rig and the DAQ card should be compatible with it.
- MATLAB integration would be desirable.

Power Supplies

- Purpose: sensors and signal conditioning electronics require power supplies with different voltages and current capabilities.

2.2.13. Requirements

- The different load requirements of sensors and signal conditioning electronics must be met.
- The power supply should be from one unit with a cascade of DC-DC converters to provide lower voltages.
- The power supplies should be upgradeable to enable the addition of future, as yet unknown, sensors and equipment.
- DC Voltage (V) Max. Current (mA) Device
- +20 to +32 100 Torque Transducer
- +18 CT
- +15 300 Eddy Current Sensor Conditioning
- +12 30 Accelerometer Conditioning
- +9 to +18 VT
- -15 300 Eddy Current Sensor Conditioning

Appendix B: Operation of the Condition Monitoring Test Rig

This document was produced by Christopher J Crabtree as a complete operating procedure for the Durham condition monitoring test rig.

OPERATION OF THE CONDITION MONITORING TEST RIG

This document gives instructions for the safe operation of the test rig under control from the LabVIEW control environment. The operating procedure for manual control is not described.

Safety

- Be aware of **EMERGENCY STOP LOCATIONS**
- **GUARDS** must be **LOCKED DOWN** during operation
- The **GRID CONTACTOR MUST NOT BE ENGAGED** while the rig is operating below synchronous speed
- Power and instrumentation **CABINETS MUST NOT BE OPENED** while any power supplies are connected
- Rotor resistor and power analyser tap-off **CONNECTIONS MUST NOT BE CHANGED** while power supplies are connected
- **EAR DEFENDERS** are recommended during continuous operation
- This document does not give guidelines on manual operation of the test rig

Test Rig Contacts

In case of any test rig operational or safety issues, please contact:

- **Christopher Crabtree: 41226, E234**
- Prof. Peter Tavner: 42460, E210
- David Jones/Paul Jarvis: Mechanical workshop

Contents

LabVIEW Controlled Operation

A. Initial Setup (LabVIEW Control)

1. **Power on** instrumentation, signal conditioning and data acquisition hardware using key switch marked **"Mains Switch"**
2. Ensure **"Selector Switch"** key switch is turned to **"All Units"**
3. Wait for **"New Data Acquisition Device"** dialogue – **Cancel** without taking action – repeat if a second dialogue appears.
4. Start **"Measurement and Automation"** software
    a. Devices and Interfaces ➔ NI-DAQmx Devices ➔ NI DAQPad-6015: "DAQ1"
    b. Run **"Self-Test"** > "OK"
    c. Run **"Reset Device"** > "OK"
    d. **Repeat steps a, b and c** for NI DAQPad-6015: "DAQ2"

*If either card fails to self test or reset then switch off "**MAINS SWITCH"** with key, restart computer and begin at step 1.*

Otherwise:

5. Start National Instruments **LabVIEW 2009**
6. Open **"CMDAQ_v2b.vi"**
7. Click the **"Run"** button (left-pointing arrow) to run the control environment
8. Ensure **"Select Gear Ratio"** radio button is set to **"5:1"** (default)
9. Ensure **"Select Test Type"** radio button is set to **"Grid Connected"** (default)
10. Ensure **"Run Up Rate"** is defined as **10rpm/s** (default)
11. Select required **"Driving File"** from default directory. Ensure choice is from the ".csv" files:

a. "7m6t_Part1.csv" (default)
b. "7m6t_Part2.csv"
c. "7m6t_Part3.csv"
d. "15m20t_Part1.csv"
e. "15m20t_Part2.csv"
f. "15m20t_Part3.csv"

12. **"Output Folder"** should be left as the **default** value
13. Define **"Output Filename Comment"** as required

The final filename will be in the format date_time_comment.csv and will be 'zipped' with the same filename format, date_time_comment.zip.

14. Click **"OK"** to accept settings – a **"START"** button will appear at the top-left corner. **Do not start yet.**

*After **every couple of tests** or **following unexpected system behaviour** close LabVIEW and repeat **step 3** of the above instructions to ensure correct system operation. In the event that either test is unsuccessful switch off **"MAINS SWITCH"** with key, restart computer and begin at step 1. Be aware that a serious error may require you to restart the computer.*

B. Startup Procedure (LabVIEW Control)

1. **Contact supply** to Eurotherm variable speed drive (above desk)
2. **Power on** Eurotherm drive – wait for display to show:

FORWARD
REF: 0.00 %

3. Press blue illuminated **"EMERGENCY STOP RESET"** button – button will go dark.

If the button remains illuminated, check that all emergency stops are disengaged and repeat step 3.

4. Switch **"MAIN DC DRIVE MOTOR"** to **"OFF"**
5. Press **"L/R"** button on MMI to enable remote control – display will show:

DIGITAL DC DRIVE
DC 4Q 165A

6. Switch **"MAIN DC DRIVE MOTOR"** to **"ON"** – drive may begin to 'buzz' loudly
7. Press **"START"** in LabVIEW environment – machine will run up to synchronous speed
8. Switch **"MAIN DC MOTOR FAN COOLING"** to **"ON"**
9. Dialogue will show **"At synchronous speed. DFIG supply connected?"**
10. Switch on **13A supply** to contactor
11. Switch on **63A supply** (red lever) to contactor
12. Switch **"Grid Supply Isolator"** to **"ON"** on **"Synchronisation Contactor"** cabinet
13. Press **green** button on **"Synchronisation Contactor"** cabinet – grid supply is now connected
14. Click **"Yes"** – machine will run to test starting speed
15. Dialogue will show **"Click OK to start test"** – click **"OK"**

*Test will run until end. It is recommended to leave test to run unless something is seriously wrong. If required, press **"Controlled Stop"** and the following procedure will begin as if the test had completed.*

C. Shutdown procedure (LabVIEW Control)

1. Dialogue shows **"Test session ended. Click OK to return to synchronous speed."** – click **"OK"**
2. Wait for dialogue displaying **"At synchronous speed. DFIG supply disconnected?"**
3. Press **red** button on **"Synchronisation Contactor"** cabinet – generator is disconnected
4. Switch **"Grid Supply Isolator"** to **"OFF"**
5. Switch off **63A supply** (red lever) to contactor
6. Switch off **13A supply** to contactor
7. Click **"Yes"** – machine will run down
8. Dialogue displays **"Output data will be saved as date_time_comment"** – select **"OK"** or **"Cancel"**
    a. If **"OK"** – amber **"Writing DAQ File"** light will show until writing is complete
    b. If **"Cancel"** – dialogue displays **"Data discarded"** – click **"OK"**

*Steps 2 to 8 may appear out of sequence depending which stage is reached first. In this case **read dialogues carefully** to ensure safe disconnection.*

Once the machine has stopped:

9. Switch **"MAIN DC MOTOR DRIVE"** to **"OFF"** – drive contactor will disengage

10. Press **"L/R"** button on MMI – display will show:

    FORWARD

    REF: 0.00 %

11. Switch **"MAIN DC MOTOR DRIVE"** to **"ON"**
12. **Power off** Eurotherm drive
13. **Isolate supply** to Eurotherm variable speed drive (above desk)

Do not exit LabVIEW *until amber* ***"Writing DAQ File"*** *light has gone dark to ensure data is saved. Output data is saved to My Documents ➔ Test Rig ➔ LabVIEW Control ➔ OutputData.*

E. Published and Submitted Papers

The papers in this section are either already published or submitted for peer review at the time of writing and are included in the chronological order given below.

Published Papers

- Watson, S. J., Xiang, J., Yang, W., Tavner, P. J, Crabtree., C. J., *Condition Monitoring of the Power Output of Wind Turbine Generators using Wavelets*, IEEE Trans Energy Conversion, Vol. 25, No. 3, pp. 715-721, 2010.
- Crabtree, C. J., Djurovic, S., Tavner, P. J., Smith, A. C., *Fault Frequency Tracking During Transient Operation of Wind Turbine Generators*, 19th International Conference on Electrical Machines, Rome, September 2010.
- Yang, W., Tavner, P. J., Crabtree, C. J., Wilkinson, M., *Cost Effective Condition Monitoring for Wind Turbines*, IEEE Trans. Industrial Electronics, Vol. 57, No. 1, pp. 263-271, 2010.

Accepted for Peer Review

- Crabtree, C. J., Djurovic, S., Tavner, P. J., Smith, A. C., *Condition Monitoring of a Wind Turbine Induction Generator by Current or Power Analysis*, IEEE Trans. Industry Applications, Awaiting peer review, 2010.

Condition Monitoring of the Power Output of Wind Turbine Generators Using Wavelets

Simon Jonathan Watson, *Member, IEEE*, Beth J. Xiang, *Member, IEEE*, Wenxian Yang, Peter J. Tavner, *Senior Member, IEEE*, and Christopher J. Crabtree

***Abstract*—With an increasing number of wind turbines being erected offshore, there is a need for cost-effective, predictive, and proactive maintenance. A large fraction of wind turbine downtime is due to bearing failures, particularly in the generator and gearbox. One way of assessing impending problems is to install vibration sensors in key positions on these subassemblies. Such equipment can be costly and requires sophisticated software for analysis of the data. An alternative approach, which does not require extra sensors, is investigated in this paper. This involves monitoring the power output of a variable-speed wind turbine generator and processing the data using a wavelet in order to extract the strength of particular frequency components, characteristic of faults. This has been done for doubly fed induction generators (DFIGs), commonly used in modern variable-speed wind turbines. The technique is first validated on a test rig under controlled fault conditions and then is applied to two operational wind turbine DFIGs where generator shaft misalignment was detected. For one of these turbines, the technique detected a problem 3 months before a bearing failure was recorded.**

***Index Terms*—Condition monitoring, electrical generator, signal processing, wind energy, wind turbines.**

I. Introduction

INCREASING land constraints across Europe have led to the development of wind farms offshore with new challenges, particularly with regard to operations and maintenance. Access to turbines for maintenance and repair may be significantly restricted during periods of high wind speed and significant wave height, particularly during the winter. It has been suggested that operations and maintenance costs for offshore wind farms could account for up to 30% of the energy costs [1]. There is a need, therefore, for early warning when problems may be about to occur for a particular wind turbine. Condition monitoring is seen as a way to reduce operations and maintenance costs for wind turbines [2].

The number of wind turbine failures due to the gearbox and generator subassemblies in modern wind turbines has been shown to be significant [3] and the downtime due to such failures is more significant due to procurement times and the need to winch these heavy subassemblies in and out of the nacelle.

It has been suggested that spectral analysis of the power output signal can be used to monitor not only rotor blade unbalance [4] but also gearbox and bearing faults [5]. However, in general to date, more conventional vibration sensor approaches have been favored [6]–[8].

Bearing problems account for between 21% and 95%, respectively, of all failures [9] in electrical machines, and for induction machines of the size and type used in wind turbines this figure is probably >45%. Therefore, early detection of such problems would significantly reduce wind turbine downtime if maintenance could then be planned in advance. Vibration monitoring has been applied to conventional power generation with generators running at a fixed frequency and current monitoring has been deployed, primarily motor current signature analysis (MCSA), for inferring problems due to broken rotor bars and air gap eccentricity, e.g., [10]–[12]. Instantaneous power has also been used to monitor such faults [13], including in the case of a wind turbine generator [14]. Indeed, the monitoring of power, as opposed to current, may yield more information with regard to induction machine faults [15] because of its ability to deal with all three phases under both balanced or unbalanced conditions. More recently, work has extended to monitoring instantaneous power to detect bearing damage [16].

The use of wavelets in the analysis of electrical machine current waveforms has been established for fault diagnosis of rotor eccentricity in a brushless dc machine [17] and in the detection of broken rotor bars in an induction machine [18]. These examples have employed steady-state monitoring. The monitoring by wavelets of transient current signals during machine start-up can also yield useful information with respect to broken rotor bars [19]–[23]. Although there has been much work looking at the application of wavelets and Fourier transforms to the detection of broken rotor bars, this type of failure represents a negligible fraction of generator faults in wind turbines. More recently, the use of wavelets for detecting shaft misalignment and bearing problems using the power signal has been demonstrated for the condition monitoring of variable speed wind turbines [24]. The use of wavelets has an advantage over Fourier analysis when analyzing nonstationary signals, such as are seen in variable speed electrical machines.

Manuscript received February 13, 2009; revised July 2, 2009, October 31, 2009, and December 1, 2009. This work was supported in part by the Condition Monitoring for Offshore Wind (CONMOW) project of European Commission under Contract ENK5-CT-2002-00659. The work of B. J. Xiang and W. Yang was supported by the Engineering and Physical Sciences Research Council (EPSRC) Supergen Wind Energy Technologies Consortium (Durham and Loughborough Universities are partners in the consortium) under Grant EP/D034566/1. Paper no. TEC-00065-2009.

S. J. Watson and B. J. Xiang are with the Department of Electronic and Electrical Engineering, Centre for Renewable Energy Systems Technology, Loughborough University, Loughborough, LE11 3TU, U.K. (e-mail: s.j.watson@lboro.ac.uk; j.xiang@lboro.ac.uk).

W. Yang, P. J. Tavner, and C. J. Crabtree are with the School of Engineering, Durham University, Durham, DH1 3HP, U.K. (e-mail: wenxiang.yang@durham.ac.uk; peter.tavner@durham.ac.uk; c.j.crabtree@durham.ac.uk).

Color versions of one or more of the figures in this paper are available online at http://ieeexplore.ieee.org.

Digital Object Identifier 10.1109/TEC.2010.2040083

In this paper, we present the analysis of the power output of a DFIG by the use of wavelets to detect rotor eccentricity. The theory behind the wavelet analysis is presented and the principle of analyzing particular frequency components characteristic of mechanical and electrical faults is established. The method is then applied to a laboratory test rig under known fault conditions, first in fixed and then in variable-speed operation. Finally, the method is applied to two operational, variable-speed, pitch-regulated wind turbines with DFIGs (1.5 and 2.5 MW, respectively), where rotor eccentricity was detected and, in the case of one of these turbines, well in advance of an eventual bearing failure.

II. Mathematical Analysis of Induction Machine Power Output

A. Characteristic Signatures in Power Output

For an induction machine where static and dynamic eccentricity may be present, fault characteristics at a frequency of $f_1 \pm mf_r$ in the stator current [13] will appear where f_1 is the supply frequency, f_r is the machine rotational frequency and m is a positive integer. This component manifests itself in the instantaneous single-phase power as in (1)

$$p(t) = \frac{\sqrt{3}}{2} \times \left\{ \begin{array}{l} U_{m1} I_{m1} [\cos(2\omega_1 t - \varphi) + \cos\varphi] \\ + \sum_{m=1}^{\infty} \left\{ \begin{array}{l} U_{m1} I_{\mathrm{ecpm}} \left[\begin{array}{c} \cos\left((2\omega_1 - m\omega_r)t - \varphi_{\mathrm{ecpm}}\right) \\ + \cos\left(m\omega_r t + \varphi_{\mathrm{ecpm}}\right) \end{array} \right] \\ + U_{m1} I_{\mathrm{ecnm}} \left[\begin{array}{c} \cos\left((2\omega_1 + m\omega_r)t - \varphi_{\mathrm{ecnm}}\right) \\ + \cos\left(m\omega_r t - \varphi_{\mathrm{ecnm}}\right) \end{array} \right] \end{array} \right\} \end{array} \right\} \tag{1}$$

where

U_{m1}	maximum value of the supply line-to-line voltage;
I_{m1}	maximum value of the fundamental supply current;
I_{ecpm}	maximum value of the fault characteristic component in the stator current at a frequency of $f_1 + mf_r$;
I_{ecnm}	maximum value of the fault characteristic component in the stator current at a frequency of $f_1 - mf_r$;
φ_{ecpm}	initial value of the phase angle for fault characteristic component at a frequency of $f_1 + mf_r$;
φ_{ecnm}	initial value of the phase angle for fault characteristic component at a frequency of $f_1 - mf_r$;
$\omega_1 = 2\pi f_1$	stator supply angular frequency;
$\omega_r = 2\pi f_r$	rotor angular velocity;
φ	initial phase angle of the fundamental supply current.

This gives rise to a number of components in the instantaneous power, namely a dc component, a component at a frequency of $2f_1$, components at frequencies of $2f_1 \mp mf_r$, and additional components at frequencies of mf_r. In [13], it was also shown that for a similar analysis where broken rotor bars were present, additional components at $2ksf_1$ should be seen in the instantaneous power, where s is the slip defined as

$$s = \frac{f_1 - pf_r}{f_1} \tag{2}$$

where p is the number of pole pairs. It is easy to show that in the case of eccentricity, when $m = 2p$, then a characteristic component at a frequency of $2sf_1$ in the instantaneous power should be seen. Indeed, the experimental results in [13] confirm this, where the Fourier transform of the instantaneous power from a three-phase squirrel-cage induction motor was analyzed. The $2sf_1$ component appears in the case where the machine had an induced eccentricity, and this component increased in magnitude when the motor had increasing numbers of broken rotor bars.

These "additional components" (mf_r and $2ksf_1$) may not be the only frequency components characteristic of eccentricity and broken rotor bars. Indeed, Tavner [9] reports that frequency components of $2ksf_1/p$ and $2k(1-s)f_1/p$ will be observed when a broken rotor bar occurs. These components arise from the interaction of the electromagnetic air gap torque and the mechanical torque reaction, dependent upon the drive inertia. They are seen in the power signal as there is coupling between the shear stress field supporting the torque reaction and the air gap magnetic field.

There are similarities between the effects of rotor electrical imbalance and an eccentric rotor which mean that a rotor imbalance, whether due to electrical effects or an eccentric air gap, is likely to give rise to additional components which are indicative of both these faults, albeit their magnitudes may differ. This means that the $2ksf_1/p$ and $2k(1-s)f_1/p$ components may also appear in the case of an eccentric rotor. To date, the authors are not aware of a full mathematical analysis of these current and power frequency components and further work will be required to establish this for both rotor winding asymmetry and eccentric rotors in induction machines.

Analysis of the $2ksf_1$ and $2ksf_1/p$ frequency components of the instantaneous power has the advantage that these are generally of low frequency. For a wind turbine, sampling of sensors that may be used for the detection of modes of oscillation of the turbine structure are required to be in this same low frequency range.

B. Analysis of the Power using Wavelets

MCSA and instantaneous power analysis of electrical machines has been done using Fourier transforms, e.g., [13], [15], [16]. This yields satisfactory results when the machine is running at fixed speed but is more problematic to apply in variable-speed situations. The majority of large modern wind turbines operate under variable-speed conditions.

Short-term Fourier transforms (STFTs) may be used, however, they have the drawback of giving a fixed time and frequency resolution at all frequencies and there will always be a tradeoff between frequency and time resolution. Wavelet transforms have the feature that they give better frequency resolution

(but worse time resolution) at low frequencies and better time resolution (but worse frequency resolution) at high frequencies. This is in general desirable for most practical signals where higher frequency components tend to be short-lived whereas lower frequency components tend to be longer in duration. As described earlier, the use of wavelets has been investigated for the detection of eccentricity and broken rotor bars in dc and induction machines by the analysis of machine currents. In this paper, we adopt the use of wavelets for the analysis of the machine instantaneous three-phase power to deal with these issues of variable speed. There are other potential tools for time- and frequency-domain analysis of the power signal, however, the purpose of this paper is not to provide an in depth analysis of these techniques, rather to illustrate the practical application of a signal-processing technique that is able to cope with a nonstationary signal for the purposes of detecting a fault on a wind turbine generator shaft.

The continuous wavelet transform (CWT) of a time series $x(t)$, in this paper, and the instantaneous three-phase power $p(t)$, is given by

$$W_{a,b}(t) = \int_{-\infty}^{\infty} x(t)\psi^*_{a,b}(t)dt. \tag{3}$$

This is a function of the so-called daughter wavelets defined as transformations of the mother wavelet

$$\psi_{a,b}(t) = \frac{1}{\sqrt{a}}\psi\left(\frac{t-b}{a}\right) \tag{4}$$

where t is time, a is the scale applied to the mother wavelet, and b is the translation applied to the mother wavelet.

The CWT, thus, gives information with regard to the correlation between the mother wavelet and the signal, which is being analyzed in both time domain (related to b) and frequency domain (related to a), respectively. The mother wavelet used, in this paper, is based on the Morlet wavelet as defined in the MathWorks MATLAB software Wavelet Toolbox, namely

$$\psi(t) = e^{-\frac{t^2}{2}}\sin(\sigma t) \tag{5}$$

where the default value of $\sigma = 5$ was used that represents a reasonable balance between frequency and temporal resolution.

The Morlet wavelet is essentially a sinusoidal oscillation, which is localized using a Gaussian function. It is, therefore, well suited to the analysis of a signal where a periodic shock event is to be detected, such as is the case with a shaft misalignment and a worn bearing. The discussion described in Section II has indicated that perturbations such as rotor eccentricity resulting from shaft misalignment will modulate the power signal and the frequency of this modulation will vary in the case of a variable-speed wind turbine. The objective of using the Morlet wavelet transform was to localize a given variable frequency component ($2ksf_1$ and $2ksf_1/p$) in time and determine its magnitude. This was then used as an indicator of the severity of shaft misalignment, which could be the precursor to eventual bearing failure.

The aforementioned CWT was applied to the power output from generators in both a test rig and a variable-speed wind turbine, sampled at 3 kHz and 32 Hz, respectively. The test rig was sampled at a higher frequency simply to capture higher frequency components in other signals not considered in this paper. The results of these analyses are described in the following section.

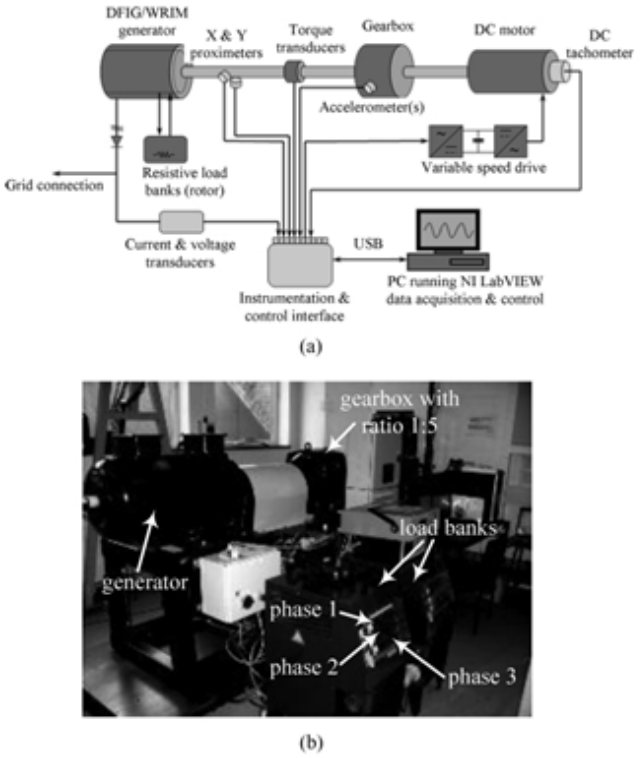

Fig. 1. Wind turbine condition monitoring test rig. (a) Schematic presentation of the test rig. (b) Photograph of the test rig.

III. Results of Generator Power Analysis

A. Test Rig

A test rig was used to simulate a fault as might be seen in a variable-speed wind turbine with a DFIG. The test rig consisted of a 50-kW dc variable-speed drive connected via a 5:1 gearbox to a four-pole DFIG connected as a wound rotor induction generator as shown in Fig. 1.

The test rig was controlled using LabVIEW software to drive the dc motor and collect data from the drive train, including generator torque, rotor speed, current, and voltage. The motor could be driven at a variable speed to realistically simulate the changing aerodynamic torque on a wind turbine rotor. A number of faults could be applied to the wound rotor induction generator, including circuit imbalance by adjusting the balance of the rotor resistors in the resistance bank, to emulate the effect of a faulty or eccentric rotor. The test rig is described in more detail in [13].

The rotor circuit imbalance was applied under both fixed and variable-speed operating conditions. The test rig was run for a period of 100 s and the rotor circuit imbalance applied and removed alternately in 20 s bursts. In this way, the rig was made to operate during the experiments under alternately "healthy" and "faulty" conditions. Data were sampled at 3 kHz. A CWT, as described above, was applied to the time series of the

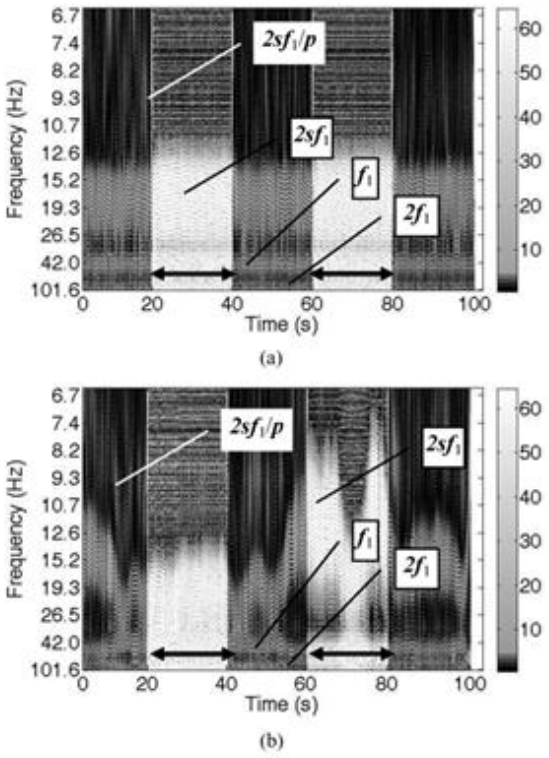

Fig. 2. CWT of test rig power signal for circuit imbalance during (a) fixed speed and (b) variable-speed conditions. The double-headed arrows show the condition when the circuit imbalance was applied ("faulty" state) otherwise the machine was in the healthy state.

three-phase power output, calculated from the three-phase current and voltage measurements.

The test rig experiments were performed with alternating periods of "healthy" and "faulty" conditions, to allow a relative comparison between frequency components in the power signal under these two operating conditions. Fig. 2(a) shows the result of this CWT for the test rig run at a fixed speed with the circuit imbalance applied periodically. The scale parameter a has been converted to a frequency in Hertz on the vertical axis and the time in seconds is shown on the horizontal axis. Because of the characteristics of the wavelet transform, the bandwidth increases with increasing frequency (decreasing a). There are three relatively prominent bands that can be seen: the most prominent corresponding to $2sf_1$, and two further bands at f_1 and $2f_1$. The magnitude of these three bands clearly shows an abrupt increase when the circuit imbalance was applied (faulty condition). There is some evidence of a band at $2sf_1/p$ though its magnitude is significantly less than the other three bands.

Fig. 2(b) shows a similar CWT for the case where the test rig was run at a variable speed to simulate the case of a variable-speed wind turbine under changing wind speed conditions when operating between cut-in and rated wind speed. Once again, the three frequency bands corresponding to $2sf_1$, f_1 and $2f_1$ can be seen. The band at $2sf_1/p$ is more visible than for the fixed speed case. As expected the f_1 and $2f_1$ bands are horizontal lines, whereas the $2sf_1$ band varies in frequency as the slip of the generator varies in response to changes in rotor speed.

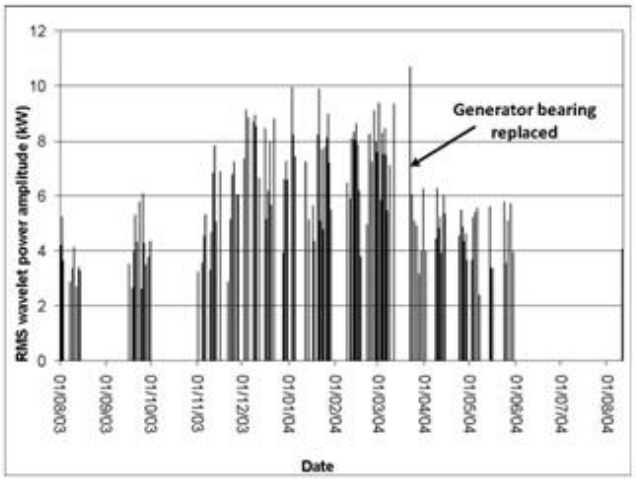

Fig. 3. Daily root mean squared value of the CWT of the 1.5-MW wind turbine power corresponding to a frequency of $2sf_1/p$.

Also, the magnitudes of all three bands show an abrupt increase in the faulty condition when the circuit imbalance is applied. The increase in magnitude of the $2sf_1/p$ band is less obvious. These frequencies were all much less than the 3 kHz collection frequency of the test rig.

It should be noted here that the magnitude of the faults applied represent extreme conditions. In reality, the level of fault seen in an operational wind turbine will be lower. The point of monitoring such as the $2sf_1$ component using a wavelet is that its magnitude shows an increase under fault conditions and that it can be tracked easily in time even though its frequency may be constantly changing.

B. Operational Wind Turbines

A 1.5-MW variable-speed pitch-regulated wind turbine with a DFIG was instrumented to provide moderate frequency (32 Hz) data for a number of operational parameters including rotational speed and three-phase power output. Additional sensors were installed on the turbine to provide high-frequency vibration data on the gearbox and generator. Ten-minute data from the standard supervisory control and data acquisition (SCADA) system were also collected. Data were recorded over a period of two years and a CWT applied to the three phase power data. In order to reduce power signal noise, the power data were filtered so that only values less than 40 kW were used in the CWT transform. This meant that this was applied only when the turbine was operating just above its cut-in wind speed. From the CWT transformed values, the rms values of the power data corresponding to frequencies of $2sf_1$ and $2sf_1/p$ were calculated for each day, where available. Clearly, the turbine may not necessarily have been operating in the low power range above cut-in on every day. The $2sf_1$ component was quite small in magnitude and showed little change in magnitude throughout the 2-year period, however, the $2sf_1/p$ component was clearly visible and did show changes in magnitude during the period. The results of this analysis for the $2sf_1/p$ frequency component are shown in Fig. 3. It can be seen from this figure that the daily rms

value showed an increase in November 2003. In January 2004, a generator misalignment was noted by the operator and an attempt was made to correct this by other means. This attempt was not successful and in March 2004, the generator bearing failed. When the bearing was replaced, the wavelet rms values of the $2sf_1/p$ frequency component from the three phase power output were reduced in magnitude, as shown in Fig. 3.

Monitoring of the $2sf_1/p$ frequency by use of a CWT, therefore, detected the generator shaft misalignment at least 3 months before the bearing failure occurred.

A similar analysis was undertaken for a 2.5-MW-variable-speed pitch-regulated wind turbine with a DFIG. In this case, 30-Hz data were collected over the period of 1 year. In addition, vibration data from the gearbox and generator were collected. Fig. 4(a) shows the daily rms CWT power amplitude corresponding to $2sf_1/p$. In this case, the $2sf_1$ component could not be monitored as it was outside the sampling frequency. For comparison, Fig. 4(b) shows the band-filtered radial vibration velocity values over the same period in the frequency range 10–30 Hz from a vibration sensor placed on the generator casing near the drive-end bearing. This turbine was one of a group of five and increased generator drive-end bearing vibration had been reported on this turbine as compared with the other turbines. This was first picked up in December 2005. Around this time, the CWT power amplitude shows an increase. During the period from 20th March to 24th April 2006, this vibration level increased still further, as seen in Fig. 4(b). The CWT power amplitude values also increased during this period, as seen in Fig. 4(a). The increased vibration was found from inspection to be due to shaft misalignment. Corrective maintenance was undertaken at the beginning of May 2006, and initially some small reduction in the vibration level and CWT power amplitude was noted, but these levels started to increase again. At the beginning of July 2006, an attempt was made to realign the generator shaft once again. However, high vibration levels were still present. It was not until around September 2006 that the levels started to decrease slightly due either to the settling of the generator or to wear of the bearing. The CWT power amplitude values also decreased slightly over this period. It should be noted that bearing failure had not occurred over this period, so it is unlikely that such large increases in the CWT power amplitude would be seen, compared with the 1.5-MW wind turbine. Although, the *reduction* in the CWT and vibration signal levels would not in themselves indicate possibly bearing problems, the time history of the levels in conjunction with the maintenance log would give the necessary information assuming a complete failure modes and effects analysis (FMEA) had been carried out.

Although the result of analyzing the power signal using the CWT is not as clear cut in the case of the 2.5 MW wind turbine, in terms of detecting shaft misalignment, there is nonetheless sufficient change in the CWT power amplitude over the monitoring period, consistent with independent vibration monitoring, to conclude that DFIG rotor eccentricity due to misalignment has been detected by analysis of the $2sf_1/p$ frequency component. The technique is certainly worthy of further investigation on a larger number of similar wind turbines incorporating DFIG machines. The technique could also be applied to fixed-speed wind turbine with induction generators but CWT would then not be essential.

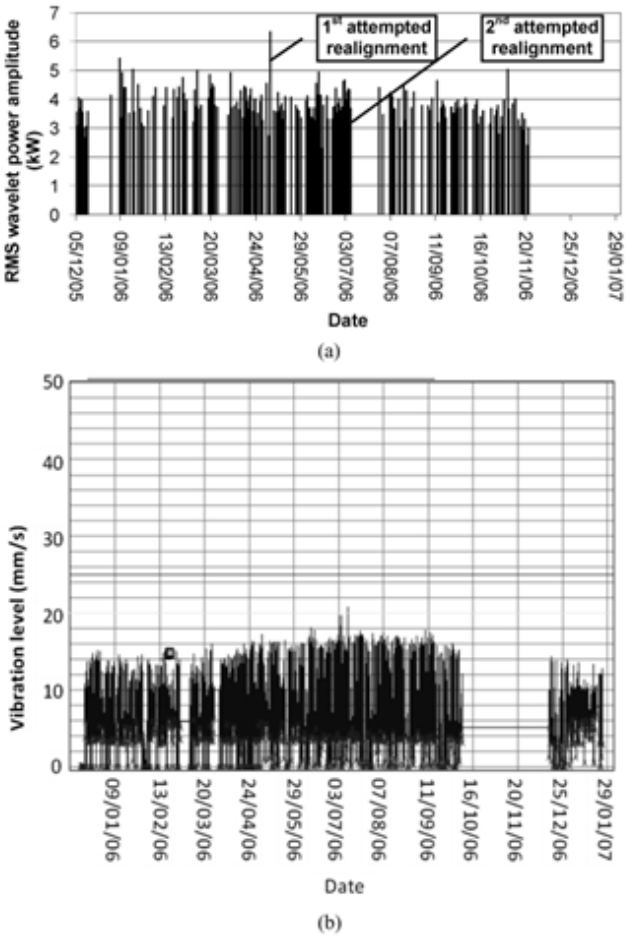

Fig. 4. (a) Daily root mean squared value of the CWT of the 2.5-MW wind turbine power output corresponding to a frequency of $2sf_1/p$. (b) Vibration level in the frequency range 10–30 Hz measured on the casing close to the generator drive-end bearing of the wind turbine over the same period.

IV. Conclusion

The move to offshore wind farms has highlighted the requirement for predictive and pro-active maintenance. One way to do this is through intelligent condition monitoring. Bearing failures in gearboxes and generators can result in lengthy and costly downtime. One way to monitor the health of such subassemblies is through relatively costly vibration monitoring. A lower cost approach, which may yield sufficient information for bearing health, is to monitor the wind turbine power output, already available from the turbine control system.

Traditional SCADA systems record data at 10-min intervals. Additional logging at a modest frequency of ~30 Hz could be used in the future to measure mechanical modes of vibration in a turbine using accelerometers and strain gauges to allow advanced control in order to reduce fatigue loads.

It has been shown, in this paper, that by monitoring the power at these modest frequencies and by applying a CWT to the

resulting data, the magnitude of the component at twice slip frequency divided by pole pairs ($2sf_1/p$) may be tracked as an indicator of rotor eccentricity in a DFIG. Rotor eccentricity is often the result of increased bearing wear and an indication of potential failure. It is possible that other potential faults may give rise to an increase in the $2sf_1/p$ component and this warrants further mathematical and experimental investigation. Nevertheless, it has been shown that rotor eccentricity may be detected using this component.

The advantage of using a wavelet is that it can be used to track the $2sf_1/p$ frequency component under varying rotor frequency (slip), which is more problematic when using the more traditional frequency Fourier transform. Another advantage of monitoring the $2sf_1/p$ component is that it is generally at a low frequency.

Although the application of the CWT can be computationally expensive, it is only the $2sf_1/p$ component that needs to be tracked in time and if this were done this would substantially reduce the required computational resources.

This technique described in this paper could be applied to any variable-speed wind turbine using an induction generator and would require only modest additional instrumentation over and above the standard SCADA system.

Further work will be required to establish a full mathematical analysis of the relationship between frequency components in the current and power signal for both rotor winding asymmetry and eccentric rotors in induction machines. Future work is also required to apply this method to other operational wind turbines, which may be suffering from incipient generator bearing faults, and to use the detection of a faulty condition to potentially predict failure some time in advance. The analysis presented in this paper has shown in a subjective way that shaft misalignment has been detected, but further work is required to turn this technique into a predictive tool where detection of potential bearing failure is automated. This will require the analysis of a number of machines to establish thresholds for healthy and faulty machines. Once sufficient data have been collected for a particular type of machine, it would be possible to set appropriate alarm levels, which would be automatically triggered. These levels would alert operators to the possibility of bearing failure and the requirement for proactive maintenance. Work is also necessary to assess whether this technique could be used to detect gearbox-bearing problems.

REFERENCES

[1] G. J. W. Van Bussel and C. Schöntag, "Operation and maintenance aspects of large offshore windfarms," in *Proc. Eur. Wind Energy Conf.*, Dublin, Ireland, Oct. 6–9, 1997, pp. 272–275.

[2] L. W. M. M. Rademakers, T. W. Verbruggen, and H. Braam, "Condition monitoring for lowering maintenance costs of offshore wind turbines," in *Proc. ISMA 2004: Int. Conf. Noise Vibration Eng.*, 2005, vol. 1–8, pp. 3943–3952.

[3] P. J. Tavner, J. Xiang, and F. Spinato, "Reliability analysis for wind turbines," *Wind Energy*, vol. 10, pp. 1–18, 2007.

[4] W. Q. Jeffries, J. A. Chambers, and D. G. Infield, "Experience with bicoherence of electrical power for condition monitoring of wind turbine blades," *Inst. Electr. Eng. Proc.-Vis. Image Signal Process.*, vol. 145, pp. 141–148, 1998.

[5] P. J. Caselitz, J. Giebhardt, and R. Kewitsch, "On-line fault detection and prediction in wind energy converters," in *Proc. Eur. Wind Energy Conf.*, Thessaloniki, Greece, Oct. 10–14, 1994, pp. 623–627.

[6] P. J. Caselitz, J. Giebhardt, T. Krüger, and M. Mevenkamp, "Development of a fault detection system for wind energy converters," in *Proc. Eur. Union Wind Energy Conf.*, Göteburg, Sweden, May 20–24, 1996, pp. 1004–1007.

[7] P. J. Caselitz, J. Giebhardt, and M. Mevenkamp, "Application of condition monitoring systems in wind energy converters," in *Proc. Eur. Wind Energy Conf.*, Dublin, Ireland, Oct. 6–9, 1997, pp. 579–582.

[8] P. J. Caselitz, J. Giebhard, and R. Kewitsch, "Advanced condition monitoring system for wind energy converters," in *Proc. Eur. Wind Energy Conf.*, Nice, France, Mar. 1–5, 1999, pp. 63–66.

[9] P. J. Tavner, "Review of condition monitoring of rotating electrical machines," *IET Electr. Power Appl.*, vol. 2, pp. 215–247, 2008.

[10] M. E. H. Benbouzid, M. Vieira, and C. Theys, "Induction motors' faults detection and localization using stator current advanced signal processing techniques," *IEEE Trans. Power Electron.*, vol. 14, no. 1, pp. 14–22, Jan. 1999.

[11] R. R. Schoen, T. G. Habetler, F. Kamran, and R. G. Bartheld, "Motor bearing damage detection using stator current monitoring," *IEEE Trans. Ind. Appl.*, vol. 31, no. 6, pp. 1274–1279, Nov./Dec. 1995.

[12] G. G. Acosta, C. Verucchi, and E. R. Gelso, "A current monitoring system for diagnosing electrical failures in induction motors," *Mech. Syst. Signal Process.*, vol. 20, pp. 953–965, 2006.

[13] Z. X. Liu, X. G. Yin, Z. Zhang, D. S. Chen, and W. Chen, "Online rotor mixed fault diagnosis way based on spectrum analysis of instantaneous power in squirrel cage induction motors," *IEEE Trans. Energy Convers.*, vol. 19, no. 3, pp. 485–490, Sep. 2004.

[14] W. Yang, P. J. Tavner, and M. R. Wilkinson, "Condition monitoring and fault diagnosis of a wind turbine synchronous generator drive train," *IET Renewable Power Gen.*, vol. 3, pp. 1–11, 2009.

[15] S. F. Legowski, A. H. M. S. Ula, and A. M. Trzynadlowski, "Instantaneous power as a medium for the signature analysis of induction motors," *IEEE Trans. Ind. Appl.*, vol. 32, no. 4, pp. 904–909, Jul./Aug. 1996.

[16] M. Bloedt, P. Granjon, B. Raison, and G. Rostaing, "Models for bearing damage detection in induction motors using stator current monitoring," *IEEE Trans. Ind. Electron.*, vol. 55, no. 4, pp. 1813–1822, Apr. 2008.

[17] S. Rajagopalan, J. M. Aller, J. A. Restrepo, T. G. Habetler, and R. G. Harley, "Analytic-wavelet-ridge-based detection of dynamic eccentricity in brushless direct current (BLDC) motors functioning under dynamic operating conditions," *IEEE Trans. Ind. Electron.*, vol. 54, no. 3, pp. 1410–1419, Jun. 2007.

[18] H. Douglas, P. Pillay, and A. K. Ziarani, "Broken rotor bar detection in induction machines with transient operating speeds," *IEEE Trans. Energy Convers.*, vol. 20, no. 1, pp. 135–141, Mar. 2005.

[19] J. A. Antonino-Daviu, M. Riera-Guasp, J. R. Folch, and M. P. M. Palomares, "Validation of a new method for the diagnosis of rotor bar failures via wavelet transform in industrial induction machines," *IEEE Trans. Ind. Appl.*, vol. 42, no. 4, pp. 990–996, Jul./Aug. 2006.

[20] M. Riera-Guasp, J. A. Antonino-Daviu, J. Roger-Folch, and M. P. M. Palomares, "The use of the wavelet approximation signal as a tool for the diagnosis of rotor bar failures," *IEEE Trans. Ind. Appl.*, vol. 44, no. 3, pp. 716–726, May/Jun. 2008.

[21] M. Riera-Guasp, J. A. Antonino-Daviu, M. Pineda-Sanchez, R. Puche-Panadero, and J. Perez-Cruz, "A general approach for the transient detection of slip-dependent fault components based on the discrete wavelet transform," *IEEE Trans. Ind. Electron.*, vol. 55, no. 12, pp. 4167–4180, Dec. 2008.

[22] Z. Zhang, Z. Ren, and W. Huang, "A novel detection method of motor broken rotor bars based on wavelet ridge," *IEEE Trans. Energy Convers.*, vol. 18, no. 3, pp. 417–423, Sep. 2003.

[23] F. Briz, M. W. Degner, P. Garcia, and D. Bragado, "Broken rotor bar detection in line-fed induction machines using complex wavelet analysis of startup transients," *IEEE Trans. Ind. Appl.*, vol. 44, no. 3, pp. 760–768, May/Jun. 2008.

[24] E. Wiggelinkhuizen, T. Verbruggen, H. Braam, L. Rademakers, J. P. Xiang, and S. Watson, "Assessment of condition monitoring techniques for offshore wind farms," *J. Solar Energy Eng.-Trans. ASME*, vol. 130, pp. 1004-1–1004-9, 2008.

Simon Jonathan Watson (M'05) received the B.Sc. degree in physics from Imperial College, London, U.K., in 1987, and the Ph.D. degree from Edinburgh University, Edinburgh, U.K., in 1990.

He was engaged in renewable energy research at the Rutherford Appleton Laboratory, Oxfordshire, U.K., until 1999. He then joined Good Energy, Wiltshire, U.K., which provides green electricity to domestic and small commercial customers. Since 2001, he has been a Senior Lecturer in the Department of Electronic and Electrical Engineering, Centre for Renewable Energy Systems Technology, Loughborough University, Loughborough, U.K.

Peter J. Tavner (SM'08) received the M.A. degree from the University of Cambridge, Cambridge, U.K., in 1969, and the Ph.D. degree from the University of Southampton, Southampton, U.K., in 1978.

He is currently a Professor of new and renewable energy and Head of the School of Engineering, Durham University, Durham, U.K. He has held senior research and technical positions in industry, including the Group Technical Director of FKI Energy Technology, Loughborough, U.K., an international business manufacturing company of wind turbines, electrical machines, and drives. His research interests include the reliability and availability of new and renewable energy devices.

Dr. Tavner is a recipient of the Institution Premium Award of the IET.

Beth J. Xiang (M'01) received the B.Sc. degree in industrial automation from Hunan University, Changsha, China, in 1982, the M.Sc. degree in automatic control and the Ph.D. in geophysics from the Central South University, Changsha, in 1996 and 2000, respectively.

Since 2005, she has been a Researcher in the Department of Electronic and Electrical Engineering, Centre for Renewable Energy Systems Technology, Loughborough University, Loughborough, U.K., where she has been engaged in reliability analysis, condition monitoring, signal processing, and data analysis. She has also been a Researcher in the field of renewable energy in the United Kingdom, since 2001.

Christopher J. Crabtree received the Master's degree in engineering from Durham University, Durham, U.K., in 2007. He is currently working toward the Ph.D. degree in condition monitoring of offshore wind turbines from the School of Engineering, Durham University, Durham.

He has been engaged as an Electrical Engineer in the research of new and renewable energy. His current research interests include the development of condition monitoring techniques using industrial data and a test rig.

Wenxian Yang received the Ph.D. degree in mechanical engineering from Xi'an Jiaotong University, Xi'an, China, in 1999.

From 2001 to 2009, he was a Research Associate in the Hong Kong City, Nottingham Trent, Cranfield, and Durham Universities. He is currently at the School of Engineering, Durham University, Durham, U.K. His research interests include signal processing, machine condition monitoring and fault diagnosis, artificial intelligence, and nondestructive testing techniques. Since 2007, he has been engaged in research on the condition monitoring of large on/offshore wind turbines.

Fault Frequency Tracking During Transient Operation of Wind Turbine Generators

C. J. Crabtree, S. Djurović, P. J. Tavner, A. C. Smith

Abstract -- **As remote and offshore wind turbines increase their contribution to renewable energy generation, effective and reliable condition monitoring techniques will be required to reduce failure downtime. This paper examines the possibilities for analysing electrical signals from the stator of wound rotor induction generators, commonly used in wind turbines. Previous work derived analytical expressions for the frequency content of line current and total instantaneous power for healthy and faulty wound rotor induction generators under steady state conditions. This paper builds upon those results to examine fault detection under transient, variable speed conditions, such as encountered in a wind turbine. Through comparison between a time-stepped analytical model and a physical test rig it is concluded that the tracking of speed dependent fault frequencies is possible and could be an effective and reliable way to monitor the health of a wind turbine wound rotor induction generator.**

Index Terms-- **condition monitoring, current spectrum, induction generator, power spectrum, wind turbine**

I. Introduction

As wind turbines (WT) increase in capacity and move to less accessible, offshore environments condition monitoring of WTs and their electrical generators will become essential to reduce downtime and improve capacity factors. The Doubly Fed Induction Generator (DFIG) is one of the favoured conversion devices for WTs with ratings in excess of 1MW [1]. An undetected generator fault may have a catastrophic effect on the WT drive train and so prompt detection of incipient faults is essential to enable timely maintenance and ensure correct system operation. Therefore, the development of reliable and effective methods for condition monitoring is gaining greater importance as generator defects have been shown to be a major contributor to WT downtime.

This paper builds on the work described in [3] to further investigate the effect of unbalanced rotor windings on the generator stator current and total instantaneous power signals under transient, variable speed conditions such as encountered in a WT. Previous work [2][7] has shown that faults in cage rotor induction machines can be detected by current or power frequency domain analysis and [6] has demonstrated power signal analysis for fault detection on an operational WT. Prior work [3] uses a set of analytical expressions to obtain the frequency content of the stator line current and total instantaneous power signals of two different wound rotor induction generator (WRIG) test rigs. These results enabled a consistent group of constants to be defined which were applicable between machines. The analysis described here is based on data from a time-stepped model of a WRIG at the University of Manchester and experimental data from a WRIG test rig at Durham University.

This paper first introduces analytical expressions and constants for stator harmonic content as further defined in [3] supported by an example of two test rigs in steady state operation. Data from the time-stepped model is analysed to demonstrate the application of the analytical expressions through modelling under transient conditions before experimental results from the Durham test rig are shown. Finally, results from the time-stepped model under highly variable speed conditions are shown to further demonstrate the consistency between different operating conditions.

II. Analytical and Experimental Tools

A. Analytical Expressions

Analytical expressions for the frequency content of WRIG stator line current and total instantaneous power signal are provided by previous work at the University of Manchester [4][5][8]. Here we consider the effect of rotor winding or brush gear unbalance so a reduced set of equations is presented. Expressions for other machine electrical faults are given in [8]. Equations (1) and (2) give all possible frequencies in the healthy and faulty WRIG current signals respectively.

$$f_{ind}^{k} = \left|6k(1-s) \pm l\right| f \qquad (1)$$

$$f_{ind}^{k} = \left|\frac{k}{p}(1-s) \pm l\right| f \qquad (2)$$

where f is the fundamental supply frequency, s is the WRIG slip, k = 0,1,2,... and l = 1,2,3,... Constants k and l relate respectively to air-gap field space harmonics resulting from the layout of the machines and supply time harmonics in the current.

For the total instantaneous power signal these expressions transform to equations (3) and (4) for healthy and faulty machines, respectively.

$$f_{ind}^{k} = \left|j \pm 6k(1-s) \pm l\right| f \qquad (3)$$

$$f_{ind}^{k} = \left|j \pm \frac{k}{p}(1-s) \pm l\right| f \qquad (4)$$

where j = 1,2,3,..., k = 0,1,2,... and l = 1,2,3,... The additional constant j relates to supply time harmonics in the voltage.

Using two different test rigs, [3] has shown that not all of these harmonic components will be identifiable for all

This work is funded as part of the UK EPSRC Supergen Wind Energy Technologies programme, EP/D034566/1.

C. J. Crabtree and P. J. Tavner are with the New and Renewable Energy Group, School of Engineering and Computing Sciences, Durham University, UK (e-mail: c.j.crabtree@durham.ac.uk / peter.tavner@durham.ac.uk).

S. Djurović and A. C. Smith are with the School of Electrical and Electronic Engineering, University of Manchester, UK (e-mail: sinisa.durovic@manchester.ac.uk / sandy.smith@manchester.ac.uk).

machines as they will be attenuated or highlighted by various machine design artefacts or operating conditions. This can be seen from Figure 1 which shows the faulted current spectra for the two test rigs in the steady state.

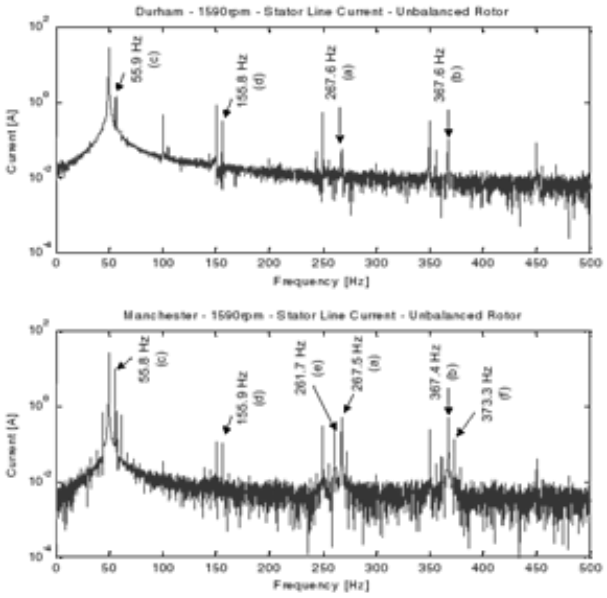

Fig. 1. Line current spectra for two faulty test rigs operating at 1590rpm [3]

A set of constants consistent between machines was proposed and is shown by Table 1 and Table 2 for current and power respectively. Frequencies (a) and (b) are present for both healthy and faulted operation while (c), (d), (e) and (f) arise as a result of machine rotor unbalance. For steady state operation it was found that frequencies (c) and (d) were the most prominent fault frequencies for the Durham test rig [3] although (e) and (f) were visible. It is apparent that the amplitudes of the latter frequencies are significantly influenced by the level of rotor resistance, which was higher in the Durham test rig. These were therefore attenuated when compared to the Manchester data.

TABLE I
CONSTANTS FOR HEALTHY AND FAULTY WRIG LINE CURRENT SPECTRA

Frequency Label	Equation	k	l
50Hz Multiples	$f_{ind}^{k} = \lvert 6k(1-s) \pm l \rvert f$	0	1,2,3,..
a, b (Healthy)	$f_{ind}^{k} = \lvert 6k(1-s) \mp l \rvert f$	1	1
a, b (Faulty)	$f_{ind}^{k} = \left\lvert \frac{k}{p}(1-s) \mp l \right\rvert f$	12	1
c, d	$f_{ind}^{k} = \left\lvert \frac{k}{p}(1-s) \mp l \right\rvert f$	4	1
e	$f_{ind}^{k} = \left\lvert \frac{k}{p}(1-s) + l \right\rvert f$	8	1
f	$f_{ind}^{k} = \left\lvert \frac{k}{p}(1-s) - l \right\rvert f$	16	1

Having obtained a set of constants which are applicable to two machines in different operating environments, tests were carried out on a time stepped model and experimental test rig as briefly described below.

TABLE II
CONSTANTS FOR HEALTHY AND FAULTY WRIG TOTAL POWER SPECTRA

Frequency Label	Equation	j	k	l
50Hz Multiples	$f_{ind}^{k} = \lvert j \pm 6k(1-s) \pm l \rvert f$	1,2, ...	0	1,2 ...
a, b (Healthy)	$f_{ind}^{k} = \lvert j \mp 6k(1-s) \pm l \rvert f$	1	1	1
a, b (Faulty)	$f_{ind}^{k} = \left\lvert j \mp \frac{k}{p}(1-s) \pm l \right\rvert f$	1	12	1
c, d	$f_{ind}^{k} = \left\lvert j \mp \frac{k}{p}(1-s) \pm l \right\rvert f$	1	4	1
e	$f_{ind}^{k} = \left\lvert j - \frac{k}{p}(1-s) + l \right\rvert f$	1	8	1
f	$f_{ind}^{k} = \left\lvert j - \frac{k}{p}(1-s) + l \right\rvert f$	1	16	1

B. Time-stepped Model

The analytical model used in this work is based on harmonic conductor distributions and a coupled circuit modelling approach [5]. The model mathematical system comprises of standard induction machine equations that are solved in a time-stepping iterative procedure. The model also facilitates the analysis of various healthy and faulty winding configurations through the incorporation of the investigated winding configuration's connection matrix in the machine voltage and flux linkage equations. In addition, higher order air-gap field space harmonics are included in the calculations when evaluating the machine parameters thus making this model competent for frequency domain analysis of machine electrical quantities. The validity of the model was verified in both time and frequency domains by comparison with experimental data. More details can be found in [4], [5] and [8].

The speed profile applied in the WRIG model was based on data from a detailed WT model created in the Supergen Wind Consortium, a similar example being shown in [9]. Wind data is fed into the WT model and the relevant generator speeds and torques generated. For the purpose of this work the generated speed profile is used as a look-up table in WRIG model calculations, thus enabling the simulation of realistic transient operation. The data is scaled to the operating range for the Durham WRIG, 1500 rev/min to 1600 rev/min. The authors do not feel that this scaling detracts from the validity of the driving data as the variable nature of the WT is represented and the slip-dependant asymmetry specific harmonic components in the current and power spectrum are valid.

The model's rotor winding phase resistance was defined as 0.07Ω for the 'healthy' machine. For the faulted condition the rotor resistance was increased to 0.27Ω. This value is considered reasonable for a WRIG with a faulty winding or, particularly, brush gear damage. In the simulation the stator supply is modelled as unbalanced and the stator windings are balanced.

C. *Experimental Test Rig*

The Durham test rig comprises a 4-pole, 30kW WRIG driven through a 5:1 two stage, helical gearbox by a 54kW DC motor. Two phase voltages and line currents were sampled by a National Instruments LabVIEW control environment and the two wattmeter method was used to calculate the total instantaneous power. The LabVIEW environment also allows the test rig to be driven using shaft speed data derived in the same fashion as for the model described above, allowing realistic variable speed operation. The test rig and driving conditions have been previously discussed in [3] and [9]. An accurate speed signal was also recorded for reference. In order to allow for variable speed driving using the 54kW DC motor a small amount of additional resistance was added in the WRIG rotor circuit allowing a WRIG speed variation of 100rev/min (7% slip) above synchronous.

The 'healthy' phase resistance of the WRIG was 1.3Ω per phase with an additional resistance of 1.3Ω added in one phase to emulate a brush gear or winding fault. Again, this change in resistance is not unreasonable for a machine with brush gear damage.

III. Results

A. *Time-stepped Model Results*

Having previously verified the analytical expressions in the steady state, the model was run at variable speed as described.

The figures used in this paper are traced from the short time Fourier transforms of the calculated and measured data with the dominant frequencies highlighted for clarity. Figure 2 shows the calculated line current spectrum for the time-stepped model under transient conditions. The rotor was balanced for the period 0-10 seconds and a step fault was present in the period 10-25 seconds. As expected, several speed dependent harmonic components are visible in the result. Frequencies (a) and (b) are present throughout the result as these result from physical design artefacts such as machine winding layout. When the rotor unbalance is introduced after 10 seconds we see an increase in the number of visible frequencies. As predicted in Table 1 the fault frequencies of interest are (c), (d), (e) and (f). The component around the 50Hz supply frequency (c) is the highest in magnitude. Other components (e) and (f) appear around the speed-dependent frequencies always present within the current spectrum. In this case, the component around 150 Hz, (d), is not visible. This results from the model only taking into account of the fundamental supply frequency. It is not therefore predicting the effects of interaction of higher order supply harmonics that are expected to exist at multiples of 50 Hz.

Similar effects are observed in the spectrum of total instantaneous power, Figure 3. In this case the current frequencies are present in the total power signal but shifted by the fundamental supply frequency. The addition of the (a) component around 200 Hz and (b) component around 400Hz arises from the combination of reverse rotating 50Hz components resulting from the modelled stator supply unbalance. These can be calculated from the expressions given in Table 2. The interaction with forward rotating components results in a frequency component labelled (a/b) which combines the two components (a) and (b). The same patterns are recognizable for fault frequencies (c), (e) and (f). For total power the most prominent fault frequency, (c), is shifted by 50Hz to become a low frequency component.

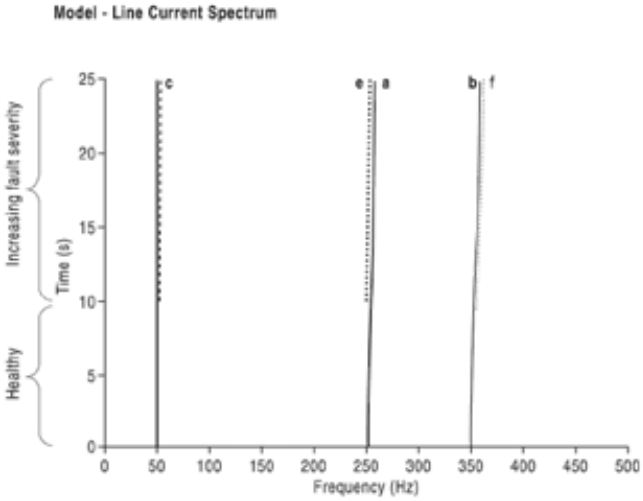

Fig. 2. Traced line current spectrum of the time-stepped model

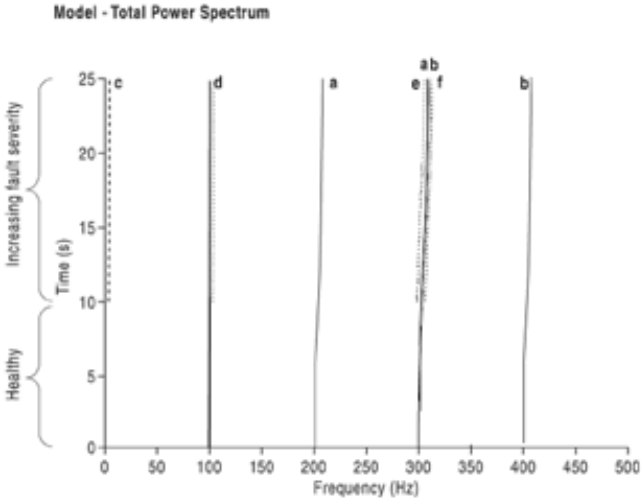

Fig. 3: Traced total power spectrum of the time-stepped model

B. *Experimental Test Rig Results*

The line current spectrum from the Durham test rig is shown in Figure 4. We find much higher spectral content in the test rig signal than for the model as the test rig is subject to grid unbalance and therefore higher frequency supply time harmonics are present. As a result, we expect fault frequencies around supply harmonics to increase in magnitude and clarity. As for the model, we expect to be able to observe the speed dependent nature of fault frequencies.

Fault frequency (c), around the 50Hz supply frequency, remains the most visible for the line current spectrum however there is now a component around 150Hz borne out by the presence of supply harmonics.

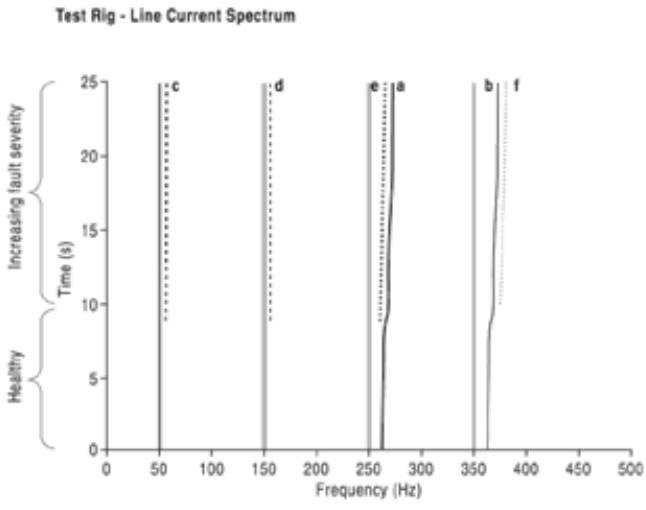

Fig. 4. Traced line current spectrum of the test rig

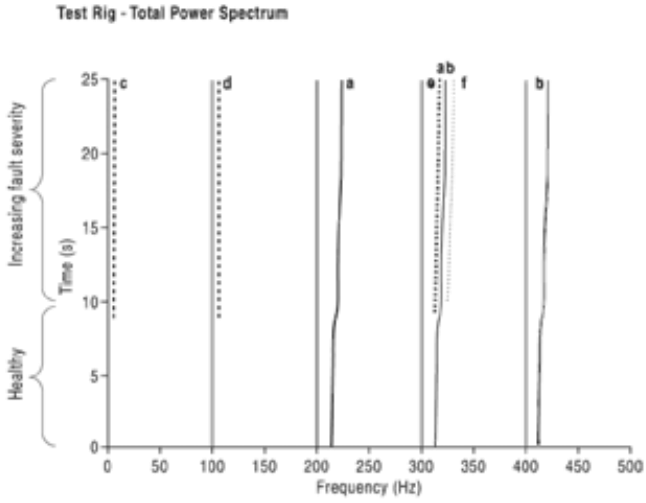

Fig. 5. Traced total power spectrum of the test rig

The test rig total power result is similarly consistent with that of the model. Again, fault frequencies are shifted by 50Hz and demonstrate the same speed dependent characteristics. The effect of the forward rotating fundamental component is also visible in the close set of harmonics (a/b), (e) and (f). Compared with the model result, Figure 3, we see that (d) is higher in magnitude for the test rig power signal. This frequency is not present in the model current spectrum, Figure 2, but is in the test rig spectrum as a result of higher order supply harmonics. When shifted into the test rig power spectrum, (d) becomes more prominent than for the model, where it is of low magnitude.

C. *Highly Variable Driving Model Results*

In order to further demonstrate consistency between results, the time-stepped model was run under more highly variable speed conditions with the same level of fault introduced. The results of this are shown in Figure 6 for line current and Figure 7 for total instantaneous power.

The line current spectrum for the model with high speed variability is, as expected, consistent with that shown in Figure 2. As before, components at higher order supply harmonics are not visible as only the fundamental supply harmonic is modelled. Again, there are certain clear fault frequency components, (c), (e) and (f), which could be tracked to give an indication of the generator condition.

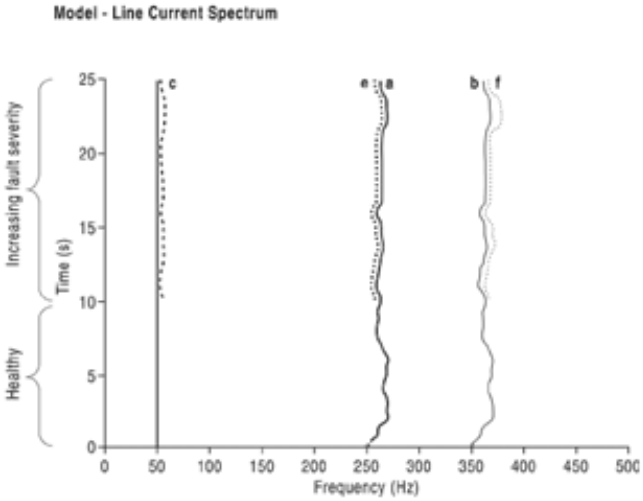

Fig. 6. Traced line current spectrum of the time-stepped model

There is also clear consistency for the total power spectrum shown in Figure 7. In this case we see the expected 50Hz shift of frequencies including a low frequency $2sf$ component. As for current, these fault related frequencies could be tracked for use in condition monitoring of wind turbine generators.

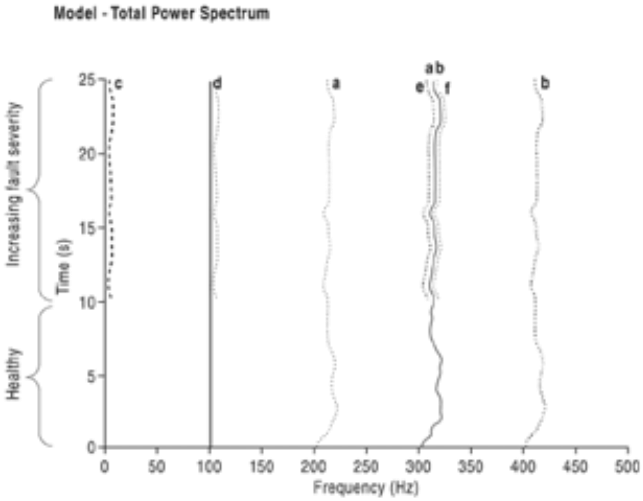

Fig. 7. Traced total power spectrum of the time-stepped model

IV. Conclusions

From the work described in this paper we can conclude that:

- The time-stepped model, demonstrated to be valid in steady state operation, has now been shown to be valid in transient, variable speed operation;
- Fault frequency results obtained from the WRIG test rig are shown to be consistent with the analytical expressions developed from the WRIG time-step model;
- Constants defined in [3] for the steady state are demonstrated to be valid for a WRIG operating

under transient, variable speed conditions;

- These expressions and constants remain consistent for a model operating under more highly variable speed conditions, such as would be encountered by a wind turbine in higher, turbulent wind speeds.
- Rotor electrical unbalance faults can be detected in the frequency domain during variable speed operation, representative of that experienced on a wind turbine, and;
- Speed dependent fault frequencies could be used as a reliable method for condition monitoring a wind turbine WRIG.

Further work will include deeper investigation of electrical fault frequencies for different faults and their detection in a test rig environment. In particular, practical analysis of faulted signals using frequency tracking algorithms will be investigated based on the results of this paper.

The rotor asymmetry used in this paper considers low levels of unbalance representative of typical brush gear damage; however the authors have found no direct figures for asymmetry in previously published works. Since there is a high degree of confidence in results to date, a study is being carried out to establish the minimum detectable rotor asymmetry. This will be presented in a future publication and where possible compared to industrially observed levels of rotor electrical unbalance due to brush gear faults.

V. Acknowledgment

This work is funded as part of the UK EPSRC Supergen Wind Energy Technologies programme, EP/D034566/1.

VI. References

Periodicals:

[1] Y. Amirat, M. E. H. Benbouzid, B. Bensaker, R. Wamkee, "Generators for Wind Energy Conversion Systems: State of the Art and Coming Attractions", *Journal of Electrical Systems*, Vol. 3-1, pp. 26-38, (2007).

[2] M. E. H. Benbouzid, "A Review of Induction Motor Signature Analysis as a Medium for Faults Detection", *IEEE Transactions on Industrial Electronics*, Vol. 47, No. 5, (2000).

[3] C. J. Crabtree, S. Djurovic, P. J. Tavner, A. C. Smith, "Condition Monitoring of a Wind Turbine DFIG by Current or Power Analysis", *Proc. of 2010 IET PEMD*, Brighton, UK (2010).

[4] S. Djurović, S. Williamson, "A coupled circuit model for a DFIG operating under unbalanced conditions", *Proc.of 2008 IEEE Int. Conf. on Electrical Machines, ICEM*, pp. 1-6, (2008).

[5] S. Djurović, S. Williamson, A. Renfrew, "Dynamic Model for Doubly-fed Induction Generators with Unbalanced Excitation, both With and Without Faults", *IET Electric Power Applications*, Vol. 3, Iss. 3, pp. 171-177, (2009).

[6] W. Q. Jeffries, J. A. Chambers, D. G. Infield, "Experience with Bicoherence of Electrical Power for Condition Monitoring of Wind Turbine Blades", *IEE Proc. Vision, Image and Signal Processing*, Vol. 145, No. 3, pp. 141-148, (1998).

[7] S. F. Legowski, A. H. M. Sadrul Ula, A. M. Trzynadlowski, "Instantaneous Power as a Medium for the Signature Analysis of Induction Motors", *IEEE Transactions on Industrial Applications*, Vol. 32, No. 4, (1996).

[8] S. Williamson, S. Djurovic, "Origins of Stator Current Spectra in DFIGs with Winding Faults and Excitation Asymmetries", *Proc. of IEEE IEMDC 2009 Miami*, pp.563-570, (2009).

[9] W. Yang, P. J. Tavner, C. J. Crabtree, M. Wilkinson, "Cost-Effective Condition Monitoring for Wind Turbines", *IEEE Transactions on Industrial Electronics*, Vol. 57, No. 1, pp. 263-271 (2010).

VII. Biographies

Christopher J. Crabtree received an M.Eng. in engineering from Durham University, UK, in 2007, having studied new and renewable energy as an electrical engineer. He is currently working towards a Ph.D. degree in condition monitoring of offshore wind turbines. His research interests include the development of condition monitoring techniques for wind turbines using industrially sourced data and a machine test rig.

Peter J. Tavner received an M.A. from Cambridge University and a Ph.D. from Southampton University. He has held research and technical positions in industry, including being a Group Technical Director with FKI Energy Technology, Loughborough, U.K. He is currently Professor of New & Renewable Energy and Head of the School of Engineering and Computing Sciences, Durham University.

Sinisa Djurovic (M'09) recieved his Dipl. Ing. degree in Electrical Engineering from University of Montenegro in 2002 and his Ph.D. degree from The University of Manchester in 2007. He is currently a Research Associate with the School of Electrical and Electronic Engineering at The Univesity of Manchester. His current research interests are in the area of modelling, fault analysis and condition monitoring of induction machines and the application of electrical machines in renewable generation systems.

Sandy Smith (M'89-SM'02) received B.Sc. (Eng) and Ph.D. degrees from Aberdeen University, U.K. Academic appointments at Imperial College (1983-1990) and Cambridge University (1990-1997). Joined Invensys Brook Crompton in 1997 and UMIST (now University of Manchester) in 2000. Currently Professor of Electrical Machines and Director of the Roll-Royce University Technology Centre on Electrical Systems for Extreme Environments. Research interests lie in the area of design and modelling of motors, generators and drives.

Cost-Effective Condition Monitoring for Wind Turbines

Wenxian Yang, Peter J. Tavner, *Senior Member, IEEE*, Christopher J. Crabtree, and Michael Wilkinson

***Abstract*—Cost-effective wind turbine (WT) condition monitoring assumes more importance as turbine sizes increase and they are placed in more remote locations, for example, offshore. Conventional condition monitoring techniques, such as vibration, lubrication oil, and generator current signal analysis, require the deployment of a variety of sensors and computationally intensive analysis techniques. This paper describes a WT condition monitoring technique that uses the generator output power and rotational speed to derive a fault detection signal. The detection algorithm uses a continuous-wavelet-transform-based adaptive filter to track the energy in the prescribed time-varying fault-related frequency bands in the power signal. The central frequency of the filter is controlled by the generator speed, and the filter bandwidth is adapted to the speed fluctuation. Using this technique, fault features can be extracted, with low calculation times, from direct- or indirect-drive fixed- or variable-speed WTs. The proposed technique has been validated experimentally on a WT drive train test rig. A synchronous or induction generator was successively installed on the test rig, and both mechanical and electrical fault-like perturbations were successfully detected when applied to the test rig.**

***Index Terms*—Adaptive signal processing, condition monitoring, fault diagnosis, induction generators, signal processing, synchronous generators, time–frequency analysis, wavelet transforms, wind power generation.**

NOMENCLATURE

A	Estimated energy of the frequency component of interest.
$a_{\min}, a_{\max}$	Minimum and maximum wavelet scales considered by the adaptive bandpass filter.
a	Wavelet scale.
b	Wavelet time-shift parameter.
ε	Voltage or current transducer error.
e	Specific unbalance.
f_{rm}	Rotational frequency of the generator rotor.
f_{se}	Electrical supply frequency.
G	Balance quality grade.
I_i	Line currents.
m	Unbalanced mass.
M_{eq}	Equivalent mass of the test rig rotor.
ω	Angular frequency of interest.
ω_c	Mean frequency of the prescribed frequency component during the time interval T.
ω_{fg}	Fluctuation of the generator rotational frequency.
ω_f	Fluctuation of the frequency of interest.
$\omega_{\text{upper}}, \omega_{\text{lower}}$	Upper and lower cutoff frequencies of the adaptive filter.
ω_0	Central angular frequency of the mother wavelet.
ω_{rm}	Angular rotational frequency of the generator rotor.
P	Three-phase total power output from the generator.
r	Effective radius of the equivalent unbalanced mass.
R_{AB}, R_{BC}, R_{CA}	Combined line-to-line resistances.
R_{AS}, R_{BS}, R_{CS}	Brush gear and slip ring resistances.
R_{AV}, R_{BV}, R_{CV}	Load bank resistances.
R_A, R_B, R_C	Generator rotor winding resistances.
δR	Electrical resistance imbalance.
s	Induction machine slip.
ψ	Mother wavelet function.
T	Sliding window averaging time interval.
t_0	Starting time moment of the sliding window.
U_e	Electrical asymmetry on the generator rotor.
U_m	Mechanical unbalance on the generator rotor.
V_i	Phase voltages.
x	Real-time signal.
η	Constant between ω_{fg} and ω_f.

Manuscript received December 5, 2008; revised September 3, 2009. First published September 22, 2009; current version published December 11, 2009. This work was supported by the U.K. Engineering and Physical Sciences Research Council Supergen Wind Program EP/D034566/1.

W. Yang is with the New and Renewable Energy Centre, NE24 3AG Blyth, U.K.

P. J. Tavner is with the School of Engineering and Computing Sciences, Durham University, DH1 3LE Durham, U.K. (e-mail: Peter.Tavner@durham.ac.uk).

C. J. Crabtree is with Durham University, DH1 3LE Durham, U.K.

M. Wilkinson is with Garrad Hassan, BS2 0QD Bristol, U.K.

Color versions of one or more of the figures in this paper are available online at http://ieeexplore.ieee.org.

Digital Object Identifier 10.1109/TIE.2009.2032202

I. INTRODUCTION

OVER THE last 40 years, there has been an increased application of wind turbines (WTs) around the world, with growth in rating from 30 kW to > 5 MW and, more recently, their application offshore [1]. To reduce the cost of energy from WTs, there is a pressing need to improve the WT availability and reduce the operational and maintenance (O&M)

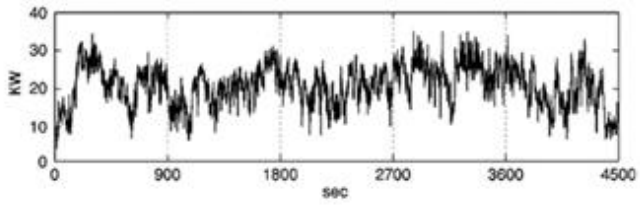

Fig. 1. Variation in power output from a 33-kW fixed-speed WT over five successive periods of 900 s, each showing the large variation in the signal due to wind turbulence (taken from [7]).

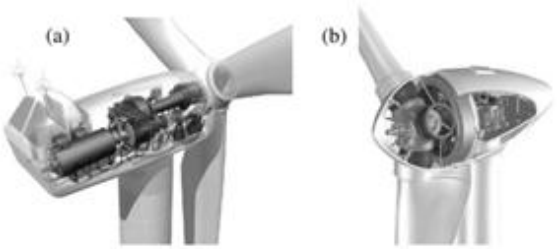

Fig. 2. Structures of real large WTs. (a) Geared. (b) Direct drive.

costs. Aside from developing more advanced machine designs [2] to improve the availability, an effective way to achieve this improvement would be to apply reliable and cost-effective condition monitoring [3], which is why this subject is attracting industrial and academic attention.

The wind industry currently uses condition monitoring systems (CMSs), such as vibration, temperature, lubrication oil, and generator current analysis, developed from other rotating machine power generation industries [4]–[6], where they have achieved success. However, despite their application in the wind industry [7], they have not yet proven their effectiveness due to the peculiarities of a WT, which has a slow speed and rapidly varying torque. Commercial WT CMSs mostly employ vibration-based techniques, which are sophisticated, and the sensors and cabling are costly. The technique is also not ideally suited to all WT types and faults. Lubrication oil analysis is becoming more popular for detecting gearbox tooth and bearing wear but cannot detect failures outside the gearbox. More advanced techniques, such as optical strain measurement, have been developed for monitoring WT blade integrity. However, these are expensive, and recent reliability surveys [8] have shown that WT electrical systems have a higher failure rate than the mechanical systems. For these reasons, an electrically based WT CMS would be beneficial and could be more comprehensive, simpler, and cheaper than other techniques. This paper will propose such a technique.

Instantaneous electric power measurement has been demonstrated on induction machines for detecting motor faults [9]. Three-phase total power monitoring has also been applied to WTs as a condition monitoring and fault diagnosis signal [10] but has not achieved commercial application. This research will be based entirely on the use of this signal and the generator speed for condition monitoring. Power output measurement was considered for condition monitoring in [7] and [10], but Fig. 1, taken from [7], shows how the WT power output signal experiences continuous and rapid variations during operation.

The work reported in this paper is an enhancement of the research described in [11], now including the following:

1) a more comprehensive description of the background technology and the state of the art of the proposed technique;
2) an improved mathematical presentation;
3) additional figures to enhance the description of the technique;
4) more substantial experimental results;
5) an amended conclusion.

The novelties of the proposed technique are summarized as follows:

1) a technique for WT condition monitoring based on measuring the generator total power signal rather than more conventional measurements validated by experiments on a test rig with a simple fault setup;
2) a new adaptive continuous-wavelet-transform (CWT)-based energy tracking method, reducing the calculation time for feature extraction when applied to lengthy signals, making possible less time-intensive WT condition monitoring;
3) the successful detection of two types of fault using this method has been demonstrated on two WT arrangements, including both electrical and mechanical faults;
4) the proposed method is more efficient for the detection of faults in variable-speed WTs than other more conventional techniques;
5) the technique used in this paper can be applied to any WT generator for tracking any characteristic, fault-related frequency component, so it is general and could be applied to detect a variety of faults depending on the choice of frequency selected.

Wavelet transforms have been successfully used in condition monitoring and diagnosis of rotating electrical machine faults [1], [12]–[14]. However, most used the discrete wavelet transform (DWT) rather than the CWT, although the latter is superior to the former in multiresolution signal analysis. However, the CWT involves more intensive convolution calculations than the DWT, making it more difficult to process lengthy online data, such as WT monitoring signals. Moreover, it is inconvenient to apply the traditional time–frequency–amplitude CWT image to machine condition monitoring, as was done in [15]. Wavelets have been proposed for WT condition monitoring [16], [17] but have not yet received commercial application.

II. Applying Generator Power Monitoring to WTs

A WT converts the kinetic energy of the wind into electrical energy, utilizing mechanical and electrical conversion, control, and transmission systems. The architectures of two commonly used large WTs are shown in Fig. 2.

The application of vibration, temperature, and lubrication oil techniques to monitoring WTs should improve their availability but, to date, is not being widely used for the following reasons:

1) lack of practical industry experience with condition monitoring in the wind environment;
2) difficulties collecting and interpreting the data, including the risk of false or missed alarms;

3) the fact that present techniques may not be suited to all types of WTs such as shown in Fig. 2;
4) the fact that developing reliable WT condition monitoring techniques requires complex and lengthy collaboration between WT operators and manufacturers in the field.

WT power flows are disturbed by both mechanical and electrical faults [16], [17]. To measure the WT shaft torque is costly and usually impractical for a real WT. In contrast, shaft speed and electrical power output are routinely monitored for WTs, but, to date, commercial CMSs do not use these signals.

In comparison with conventional stator current analysis, widely adopted for condition monitoring motors [4], [6], power monitoring could have the following disadvantages.

1) The error in the total power signal depends not only on the voltage and current transducer error ε but also on the measurement method. In the three-wattmeter method, the error will be 6ε, but, in the two-wattmeter method, the error is limited to 4ε, whereas the current signal error would be only ε. Therefore, the signal-to-noise ratio for basic analysis should be better for current than power analysis.

On the other hand, monitoring based on power analysis could have the following advantages.

1) The power signal is already available from the generator terminal voltage and current signals for the control of the WT and can conveniently be accessed.
2) Fewer cheaper transducers than accelerometers and oil debris probes are required for power monitoring.
3) Mechanical and electrical faults both disturb the generator power output, so power monitoring could detect both types of faults.
4) Single line current analysis contains the mains frequency carrier, whereas this is absent in the power signal. Therefore, the signal-to-noise ratio for faulty feature analysis should be better for power than current analysis, balancing the aforementioned transducer error effect.
5) In the power signal, the fault-related frequency sidebands, around the mains frequency, are folded down around dc, limiting the bandwidth needed to monitor the signal.

An example of the current, voltage, and power signals measured under faulty conditions on an induction generator, fitted to the test rig described in the following, is shown in Fig. 3, where the signals were collected when a periodic rotor electrical asymmetry was applied in the presence of serious noise due to power system imbalance.

The fault in Fig. 3 was applied at the time intervals of 20–40 s and 60–80 s and was absent in the other time intervals. It can be seen that the amplitudes of both the current–time and voltage–time waveforms gave no indication of abnormal conditions, whereas the total three-phase power signal P changes significantly during the abnormality due to the presence of $2f_{se}$ and $2sf_{se}$ components. The total power $P(t)$ was calculated using

$$P(t) = \sum_{i=1}^{3} I_i(t) \cdot V_i(t). \tag{1}$$

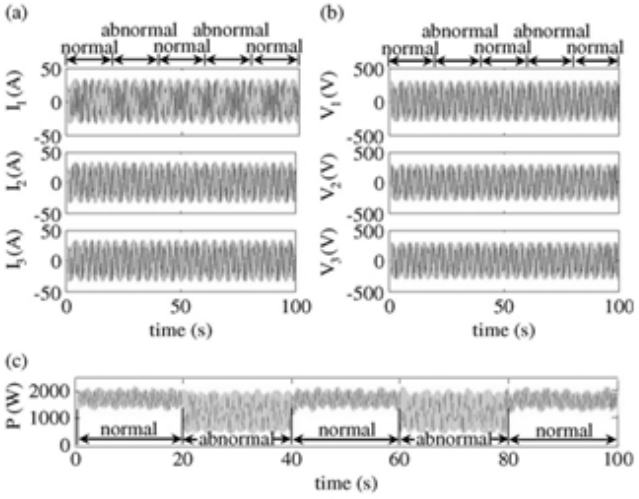

Fig. 3. Comparison of current, voltage, and total power signal in the presence of a rotor asymmetry fault. (a) Line currents. (b) Phase voltages. (c) Total power.

III. Design of Wavelet-Based Adaptive Filter

In this paper, a CWT-based adaptive filter has been designed to track the energy in the power signal in the prescribed fault-related frequency bands rather than at all frequencies of the monitoring signal. In this way, the wavelet calculation can significantly be reduced, and the results can be displayed graphically rather than as a screen dump image, making the technique attractive for online application. Details of the technique are described as follows.

The CWT of a real-time signal $x(t)$ can be defined as

$$\mathrm{CWT}(b,a) = \frac{1}{\sqrt{|a|}} \int_{-\infty}^{\infty} x(t)\psi^* \left(\frac{t-b}{a}\right) dt \tag{2}$$

where the asterisk "$*$" indicates the complex conjugate.

Traditionally, the wavelet function $\psi(t)$ is dilated or compressed by changing the scale parameter a so that all signal components ranging from frequency 0 to half the sampling frequency can be projected onto an appropriate time-scale map, as shown in Fig. 4. The bottom figure shows the time waveform of a sample signal of increasing frequency being inspected; the top figure shows the wavelet coefficients of this signal obtained at different wavelet scales and times.

Many of the calculations shown in Fig. 4 are unnecessary for WT condition monitoring because the fault-related frequencies are few in number and the energy extracted at nonfault-related frequencies is not helpful to assess the machine condition.

Therefore, an adaptive CWT-based filter has been designed, which only extracts energy at known fault frequencies, while frequencies unrelated to the fault are left unprocessed. The calculation time for the new technique will be much shorter than that for a conventional CWT applied to a broad bandwidth signal. Therefore, the proposed CWT-based energy tracking technique should prove more efficient for online processing of WT monitoring signals than conventional CWT processing.

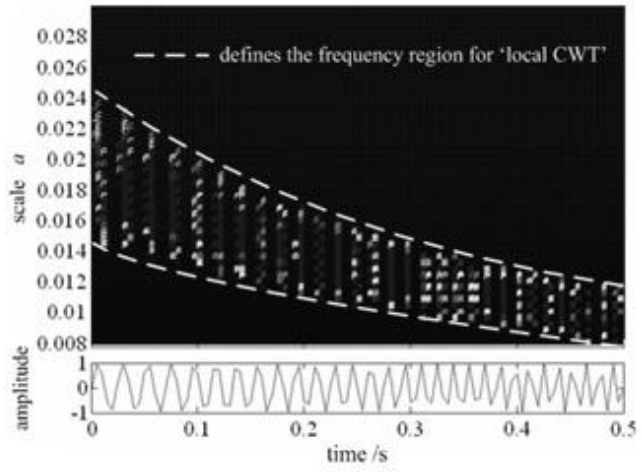

Fig. 4. Illustrative example of the conventional CWT.

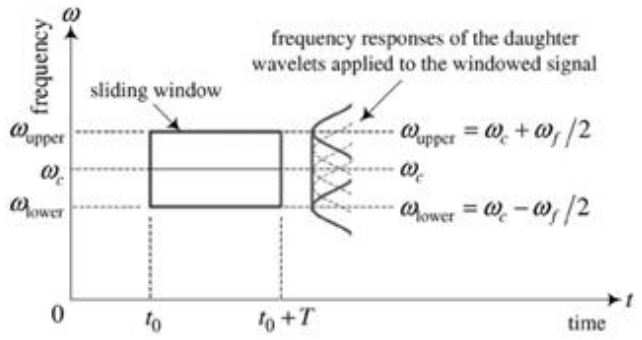

Fig. 5. Two-dimensional sliding window.

A time–frequency sliding window has been designed for this task, as shown in Fig. 5. Its central frequency ω_c is the mean frequency during the time interval T of the prescribed fault-related frequency band. The upper and lower cutoff frequencies ω_{upper} and ω_{lower} are adapted to the fluctuation of the generator rotational speed ω_{fg} in that interval, i.e.,

$$\begin{cases} \omega_{\text{upper}} = \omega_c + \omega_f/2 \\ \omega_{\text{lower}} = \omega_c - \omega_f/2 \\ \omega_f = \eta\omega_{\text{fg}}. \end{cases} \tag{3}$$

From Fig. 4, it is noticed that ω_f could also be a time-varying parameter, intrinsically dependent on the turbulence of the wind. Experience has shown that onshore wind turbulence varies between 12% and 20%, whereas offshore turbulence approximates to ~6%.

The relationship between any prescribed frequency ω and its corresponding wavelet scale a is

$$a = \frac{\omega_0}{\omega}. \tag{4}$$

With the aid of (3) and (4), the range of the wavelet scales for conducting bandpass filtering can be determined by

$$a \in [a_{\min} \quad a_{\max}] \tag{5}$$

$$\begin{cases} a_{\min} = \frac{\omega_0}{\omega_{\text{upper}}} \\ a_{\max} = \frac{\omega_0}{\omega_{\text{lower}}}. \end{cases} \tag{6}$$

TABLE I
COMPUTATIONAL EFFICIENCY COMPARISON BETWEEN CWT, DWT, AND PROPOSED APPROACH

Method	Time cost	Operation manner	Accuracy
CWT	18.91s	All frequencies between zero and half sampling frequency are calculated.	Good
DWT	0.31s	Interested frequency band is determined in a rigid dyadic step way.	Not good
Energy tracking	0.16s	Interested frequency band is determined intelligently.	As good as CWT

Subsequently, by performing the CWT locally in the scale range defined by (5), a matrix of wavelet coefficients is obtained

$$\text{CWT}_{\text{local}}(b,a) = \frac{1}{\sqrt{|a|}} \int_{-\infty}^{\infty} x(t)\psi^*\left(\frac{t-b}{a}\right) dt. \tag{7}$$

The energy A of the frequency component of interest in the time interval T is estimated by

$$A(t_0 + T/2) = \max\left(|\text{CWT}_{\text{local}}(b,a)|\right) \quad \begin{cases} a \in [a_{\min} \quad a_{\max}] \\ b \in [t_0 \quad t_0 + T]. \end{cases} \tag{8}$$

The sliding window is moved forward along the signal; the maximum and minimum wavelet scales in (5) being redefined within each time interval according to the generator rotational speed ω_{fg}. Then, using the aforementioned technique, the energy A in the fault-related frequency band is calculated in each time interval using (7) and (8). These calculations are repeated until the whole signal has been processed. Finally, a curve of the energy variation in the fault-related frequency band is obtained, and changes in the running condition of the WT can be assessed.

This task could have been accomplished using a series of conventional bandpass filters set up to cover the expected speed range of the turbine. However, such an analysis would not have the advantages of the CWT in processing nonstationary signals shown in Fig. 1 and [18].

To verify the computational efficiency of the proposed technique compared to the traditional CWT and DWT, a calculation was performed to extract the 50-Hz energy component from 1 s of line current signal, sampled at a frequency of 2 kHz. The time taken by each approach is listed in Table I. The calculations were done in a computer with 1.4 GHz of Intel Pentium processor and 512 MB of RAM.

From Table I, it can be concluded that the proposed energy tracking technique is the most computationally efficient of the three approaches.

IV. WT CONDITION MONITORING BY POWER SIGNAL ANALYSIS

In view of the proposed advantages of generator power signal analysis for detecting both mechanical and electrical faults in a variety of designs of WT drive train, it has been applied in this paper, in combination with the energy tracking method described previously, to develop a new WT condition monitoring technique.

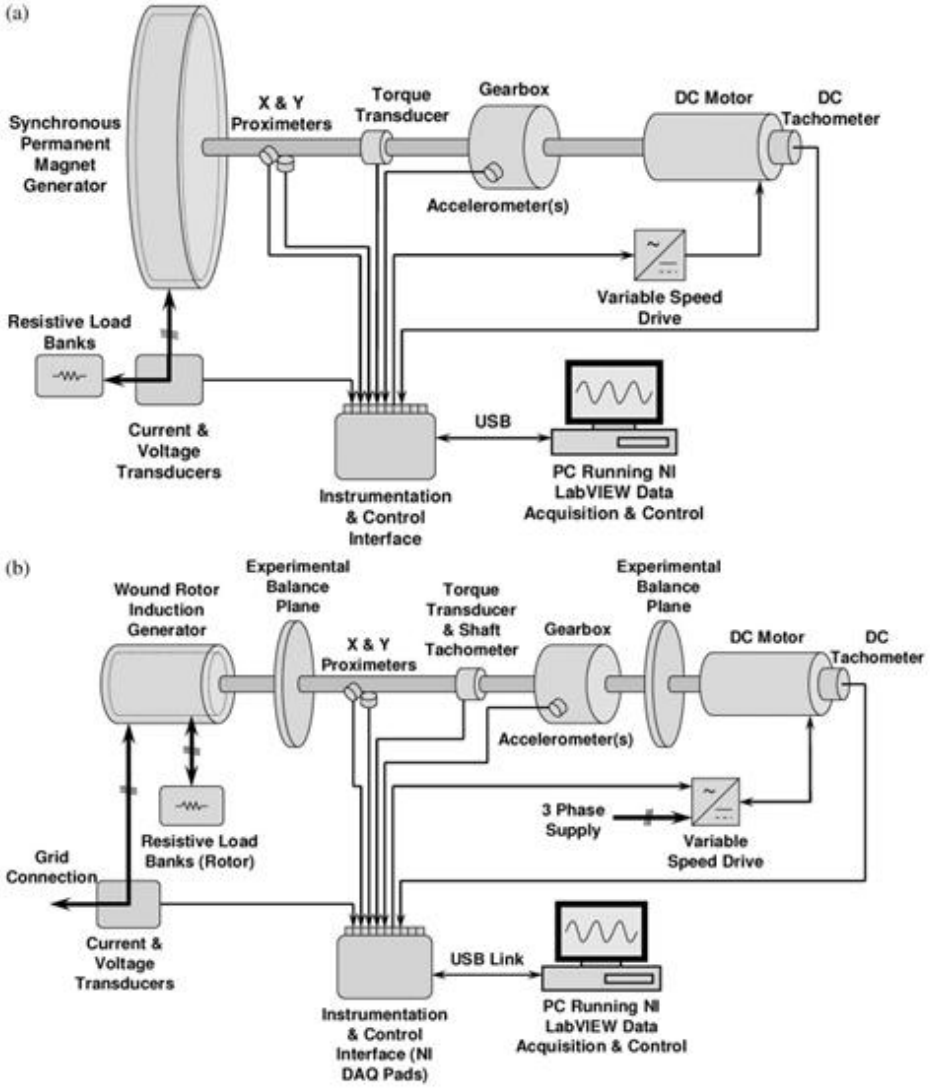

Fig. 6. Schematic diagrams of the WT drive train test rig. (a) With permanent-magnet synchronous generator installed. (b) With induction generator installed.

A. WT Drive Train Test Rig

One of the difficulties in gaining practical industry experience of condition monitoring on real WTs is the lack of collaboration needed with WT operators and manufacturers, due to data confidentiality, particularly when faults are present. This can be avoided by gaining condition monitoring experience using a controllable experimental test rig to which defined faults can be applied. Therefore, the technique proposed in this paper has been validated experimentally on a WT drive train test rig designed to investigate condition monitoring signals in the laboratory. This test rig was described in detail in [16] and was equipped first with a permanent-magnet synchronous generator and, subsequently, with an induction generator, both as shown in Fig. 6.

The synchronous generator [Fig. 6(a)], such as might be used in a direct-drive WT, was rated for the experiment at 10 kW, three-phase 54-pole permanent-magnet machine with a rectified output feeding a resistive load bank.

The induction generator [Fig. 6(b)], such as might be used in a geared-drive WT, was rated for the experiment at 30 kW, three-phase four-pole wound-rotor machine, with the rotor circuit coupled via slip rings to a three-phase resistive load bank, so that rotor electrical imbalance could be applied, and the generator stator fed the three-phase mains.

The test rig comprises a 54-kW dc variable-speed motor and a two-stage gearbox, instrumented and controlled using LabVIEW. In the experiments, a variety of wind speed inputs could be applied to the test rig via the dc motor, the speed of which is controlled by an external model incorporating the properties of natural wind at a variety of speeds and turbulences and the mechanical behavior of a 2-MW WT operating under closed-loop conditions. Relevant signals were collected from the terminals of the generator and the drive train when subjected to this driving speed.

A number of electrical and mechanical drive train faults could be applied to the test rig. Because they are not necessarily

precise replicas of WT faults, they have been called "fault-like perturbations" but contain similarities with faults on real WTs.

In this paper, to verify the efficacy of the proposed condition monitoring technique for WTs, two "faultlike perturbations" were applied to two different generator configurations as follows.

1) In the first configuration, with the synchronous generator representing a direct-drive WT, the "faultlike perturbation" applied was mechanically unbalanced on the generator rotor, representing the effect of a mechanical unbalance fault on the WT generator drive train.
2) In the second configuration, with the slip-ring induction generator representing a geared-drive WT, the "fault-like perturbation" applied was electrically asymmetric on the generator rotor, representing the effect of a rotor winding fault, brush imbalance, or air gap eccentricity in the WT generator.

Details of both experimental arrangements are described as follows.

B. Mechanical Unbalance Fault Simulated on Rotor of Synchronous Generator

The mechanical unbalance fault was simulated by attaching a 1-kg mass to the generator rotor with an equivalent rotating mass of 290.7 kg, which is ~0.3%. This represents a balance quality grade of G 7.8 (7.8 mm/s), within the limit of G 16 (16 mm/s) prescribed in ISO1940-1:2003 for a low-speed propeller shaft, applicable to a direct-drive WT shaft. The details of this estimation are given in Appendix A. The peak-to-peak measured displacement of the generator shaft changed a little before and after the placement of the unbalanced mass, varying in the range 90–140 μm. The equivalent vibration velocity would have been 0.13–0.21 mm/s, with the generator running at the maximum rotational speed of 28 r/min well within the 0.71-mm/s limit that is acceptable for machines $\leq$ 15 kW prescribed in ISO2372:1974.

When the synchronous generator ran at varying speed representing the wind driving situation, the speed, torque, and total power were measured using a sampling frequency of 1 kHz, and the "fault-like perturbation" was periodically applied to the rotor. The time waveforms of the signals before and after the application are shown in Fig. 7(a).

From Fig. 7(a), it can be seen that, in the presence of the mass unbalance fault, the driving shaft torque signal gave a response at the shaft rotational frequency f_{rm}, as expected, fluctuating by 8% range due to the combined effects of mass unbalance fault and wind driving turbulence, which can be compared to fluctuating by 4% due to the wind driving turbulence alone. By contrast, the generator power showed only a slight change in the presence of the fault. In this case, the fault-related frequency is f_{rm}, and the CWT-based energy tracking technique was applied to extract energy at this frequency, as shown in Fig. 7(b). This provided a clear indication of the presence or absence of the mechanical unbalance fault despite the fact that the shaft speed was varying continuously throughout the experiment and the effect could not be observed in the unprocessed total power signal shown in Fig. 7(a).

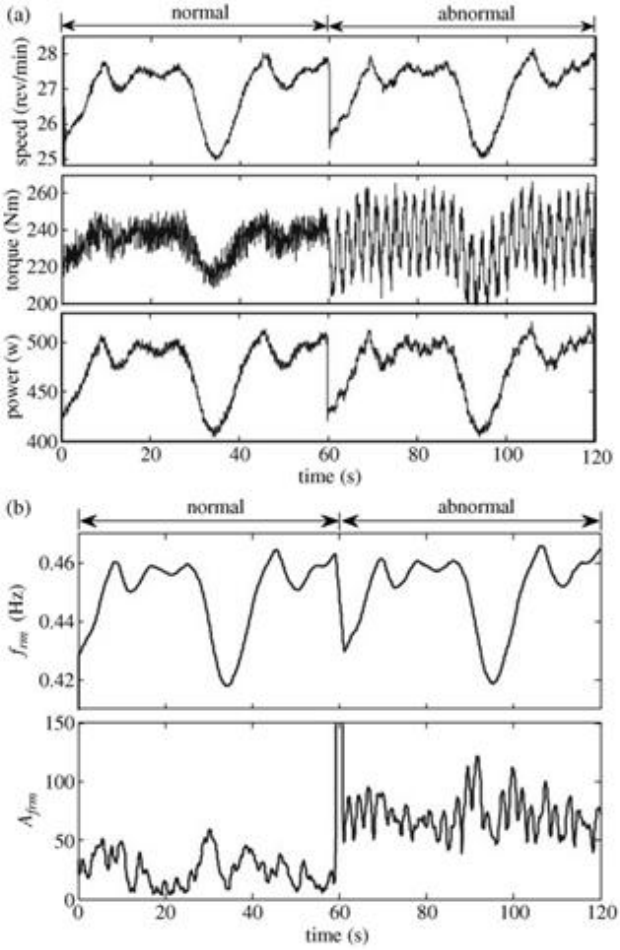

Fig. 7. Mass unbalance fault applied to a synchronous generator rotor on the WT test rig, representing a direct-drive WT. (a) Signals when a mass unbalance fault was simulated on a synchronous generator rotor. (b) Detecting a mass unbalance fault from the power signal.

TABLE II
PARAMETERS USED FOR CALCULATION RESULTS IN FIG. 7

ω_c	ω_f	T
ω_{rm}	$0.03\omega_{rm}$	$0.2s$

It can be seen from Fig. 7(b) that a 0.3% or G 7.8 unbalance fault was easily detectable. This shows that the proposed technique has the potential to detect an incipient mechanical unbalance fault of 0.3% or G 7.8 on a direct-drive WT. The parameters used for this calculation are given in Table II.

C. Electrical Asymmetry on Rotor of Induction Generator

The electrical asymmetry was simulated on the induction generator by adjusting the phase resistances in the load bank externally connected to the rotor. Two levels of rotor asymmetry were applied to investigate the effect of an incipient fault. These were an electrical asymmetry of $U_e = 4.7\%$ and, then, a larger asymmetry of 9.2%. The details of the rotor circuit and the estimation of asymmetry are described in Appendix B and in Table IV.

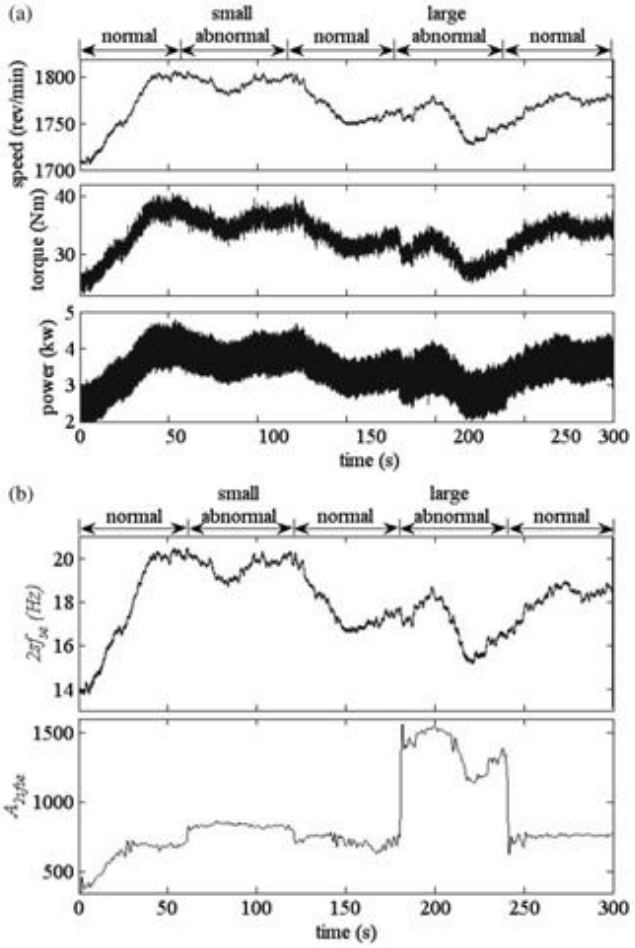

Fig. 8. Electrical asymmetry applied to an induction generator rotor on the test rig, representing a geared-drive WT. (a) Signals when an electrical asymmetry fault was simulated on an induction generator rotor. (b) Detecting an electrical asymmetry fault from the power signal.

As in the mechanical unbalance experiment, the rotational speed, mechanical drive shaft torque, and generator total power signals were measured when the "faultlike perturbation" was periodically applied to the rotor. A smaller fault was applied in the period 60–120 s and a larger fault between 180 and 240 s, with the rotor circuits being balanced in the periods 0–60 s, 120–180 s, and 240–300 s. The time waveforms of the signals collected in this experiment are shown in Fig. 8(a), and it can be seen that, due to the effect of the varying generator speed, the fault symptom cannot be observed clearly from either the generator shaft torque or total power.

When the rotor phase resistances are imbalanced, the generator current, voltage, and power are modulated twice by the slip frequency as the rotor asymmetry moves through the air gap magnetic field twice for every pole pair cycle [4]. Therefore, in this case, the fault-related frequency is $2sf_{se}$, and the CWT-based energy tracking technique was applied to extract the energy at that frequency, as shown in Fig. 8(b).

From Fig. 8(b), it can be seen that the smaller, 4.7%, fault was not clear although it is still visible, so the condition monitoring algorithm had limited detectability in this case. This lack of detectability was due to the residual imbalances present in the rotor windings, brush gear, and connections, as well as the negative influence of the timely varying generator rotational speed which partially hid the faulty feature. However, the larger 9.2% fault was clearly visible in the figure and, therefore, readily detectable despite the fact that the $2sf_{se}$ frequency signal was varying during the experimental processes.

This shows that the proposed technique has the potential to detect an incipient 9.2% electrical asymmetry fault on a geared-drive WT generator. The parameters used for this calculation are given in Table III.

TABLE III
PARAMETERS USED FOR CALCULATION RESULTS IN FIG. 8

ω_c	ω_f	T
$2sf_{se}$	$0.4sf_{se}$	$0.12s$

V. CONCLUSION

To improve the WT availability and reduce the O&M costs, a new WT condition monitoring technique has been proposed. From this research, the following conclusions can be reached.

1) In comparison with the conventional vibration, temperature measurement, and lubrication oil analysis, the technique proposed shows the following potential advantages:
   a) reduced capital cost;
   b) ability to detect both electrical and mechanical faults;
   c) applicable to both geared and direct-drive WTs.
2) The proposed CWT-based energy tracking method not only reduces the calculation needed to extract features from lengthy online data but also provides a feasible condition monitoring approach that is applicable to WTs operating at either fixed or variable speed.
3) Experiments have shown that the proposed technique is capable of detecting both mechanical and electrical faults in WT drive trains of different types.
4) The technique is a feasible way to establish a simple, cheap, but potentially global cost-effective CMS for a WT.

The technique now needs to be applied to the power signals obtained from real WTs during real mechanical and electrical faults to determine the detectability of the algorithm and its ability to detect incipient faults in both cases.

Further work will also be needed to establish the ability of this technique for a wider range of faults and for a variable-speed WT under closed-loop control.

APPENDIX A
GENERATOR ROTOR MECHANICAL UNBALANCE

Based on BS ISO1940-1:2003, the balance quality grade G may be calculated by

$$G = e \cdot 2\pi f_{rm} \tag{A1}$$

where

$$e = mr/M_{eq} \tag{A2}$$

$$U_m = (m/M_{eq}) \times 100. \tag{A3}$$

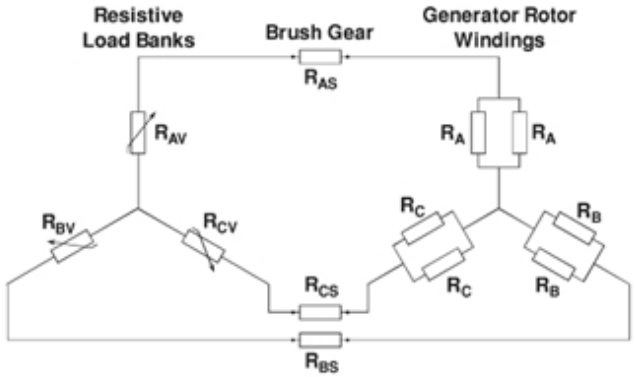

Fig. 9. Rotor circuit diagram, including a resistive load bank.

TABLE IV
ELECTRICAL ASYMMETRY APPLIED TO TEST RIG IN FIG. 8

Time (s)	Description	U_e (%)
0 – 60s	Balanced	0.0
60 – 120s	Low asymmetry	4.7
120 – 180s	Balanced	0.0
180 – 240s	High asymmetry	9.2
240 – 300s	Balanced	0.0

For the test rig shown in Fig. 6(a), the unbalance mass $m = 1.0$ kg, the effective radius $r = 865$ mm, and the equivalent rotating mass of the test rig $M_{eq} = 290.7$ kg. The average rotational speed of the generator rotor is 25 r/min. This gives a balance quality grade and mechanical unbalance for Fig. 7 of G 7.8 ($G = 7.8$ mm/s) and $U_m = 0.3\%$, respectively.

APPENDIX B
GENERATOR ROTOR ELECTRICAL ASYMMETRY

The details of the generator rotor circuit shown in Fig. 6(b) taking into account the external resistive load bank are shown in Fig. 9.

The balanced circuit resistances were given by

$$\begin{cases} R_{AB} = R_{AV} + R_{BV} + R_{AS} + R_{BS} + (R_A + R_B)/2 \\ R_{BC} = R_{BV} + R_{CV} + R_{BS} + R_{CS} + (R_B + R_C)/2 \\ R_{CA} = R_{CV} + R_{AV} + R_{CS} + R_{AS} + (R_C + R_A)/2. \end{cases} \quad \text{(B1)}$$

The circuits are balanced, giving

$$R_{AB} = R_{BC} = R_{CA} = \overline{R} = 7.60\,\Omega \quad \text{(B2)}$$

where $\overline{R} = (R_{AB} + R_{BC} + R_{CA})/3$.

Then, the electrical imbalance can be estimated through calculating the residual circuit resistance δR, i.e.,

$$\delta R = |R_{AB}e^{i\theta_1} + R_{BC}e^{i\theta_2} + R_{CA}e^{i\theta_3}| \quad \text{(B3)}$$

where $i = \sqrt{-1}$, $\theta_1 = 0$, $\theta_2 = 2\pi/3$, and $\theta_3 = 4\pi/3$.

The percentage fault can be described by

$$U_e = (\delta R/\overline{R}) \times 100. \quad \text{(B4)}$$

The larger the value of U_e, the more serious the electrical asymmetry. The electrical asymmetries applied in Fig. 8 are listed in Table IV.

ACKNOWLEDGMENT

The authors would like to thank the New and Renewable Energy Centre, Blyth, for the assistance for the original provision of the test rig.

REFERENCES

[1] J. F. Manwell, A. L. Rogers, and J. G. McGowan, "Status of offshore wind energy in the United States," in *Proc. IEEE Power Eng. Soc. Summer Meeting*, Jul. 15–19, 2001, vol. 1, pp. 10–13.
[2] H. Polinder, F. F. A. van der Pijl, G. J. de Vilder, and P. J. Tavner, "Comparison of direct-drive and geared generator concepts for wind turbines," *IEEE Trans. Energy Convers.*, vol. 21, no. 3, pp. 725–733, Sep. 2006.
[3] J. Nilsson and L. Bertling, "Maintenance management of wind power systems using condition monitoring systems—Life cycle cost analysis for two case studies," *IEEE Trans. Energy Convers.*, vol. 22, no. 1, pp. 223–229, Mar. 2007.
[4] P. J. Tavner, "Review of condition monitoring of rotating electrical machines," *IET Elect. Power Appl.*, vol. 2, no. 4, pp. 215–247, Jul. 2008.
[5] D. Casadei, F. Filippetti, A. Yazidi, C. Rossi, and G. A. Capolino, "Diagnostic technique based on rotor modulating signals signature analysis for doubly fed induction machines in wind generator systems," in *Conf. Rec. IEEE IAS Annu. Meeting*, Oct. 8–12, 2006, vol. 3, pp. 1525–1532.
[6] A. Bellini, F. Filippetti, C. Tassoni, and G. A. Capolino, "Advances in diagnostic techniques for induction machines," *IEEE Trans. Ind. Electron.*, vol. 55, no. 12, pp. 4109–4126, Dec. 2008.
[7] P. Caselitz and J. Giebhardt, "Rotor condition monitoring for improved operational safety of offshore wind energy converters," *Trans. ASME, J. Sol. Energy Eng.*, vol. 127, no. 2, pp. 253–261, May 2005.
[8] F. Spinato, P. J. Tavner, G. J. W. van Bussel, and E. Koutoulakos, "Reliability of wind turbine subassemblies," *IET Renew. Power Gener.*, vol. 3, no. 4, pp. 1–15, 2009.
[9] S. F. Legowski, A. H. M. Sadrul Ula, and A. M. Trzynadlowski, "Instantaneous power as a medium for the signature analysis of induction motors," *IEEE Trans. Ind. Appl.*, vol. 32, no. 4, pp. 904–909, Jul./Aug. 1996.
[10] W. Q. Jeffries, J. A. Chambers, and D. G. Infield, "Experience with bicoherence of electrical power for condition monitoring of wind turbine blades," *Proc. Inst. Elect. Eng.—Vis. Image Signal Process.*, vol. 145, no. 3, pp. 141–148, Jun. 1998.
[11] W. Yang, P. J. Tavner, C. J. Crabtree, and M. Wilkinson, "Research on a simple, cheap but globally effective condition monitoring technique for wind turbines," presented at the XVIII Int. Conf. Electrical Machines (ICEM), Vilamoura, Portugal, Sep. 2008, Paper ID 1053.
[12] J. Cusido, L. Romeral, J. A. Ortega, J. A. Rosero, and A. E. Garcia, "Fault detection in induction machines using power spectral density in wavelet decomposition," *IEEE Trans. Ind. Electron.*, vol. 55, no. 2, pp. 633–643, Feb. 2008.
[13] A. Ordaz-Moreno, R. de Jesus Romero-Troncoso, J. A. Vite-Frias, J. R. Rivera-Gillen, and A. Garcia-Perez, "Automatic online diagnosis algorithm for broken-bar detection on induction motors based on discrete wavelet transform for FPGA implementation," *IEEE Trans. Ind. Electron.*, vol. 55, no. 5, pp. 2193–2202, May 2008.
[14] M. Riera-Guasp, J. A. Antonino-Daviu, M. Pineda-Sanchez, R. Puche-Panadero, and J. Perez-Cruz, "A general approach for the transient detection of slip-dependent fault components based on the discrete wavelet transform," *IEEE Trans. Ind. Electron.*, vol. 55, no. 12, pp. 4167–4180, Dec. 2008.
[15] S. S. Tsai, C. T. Hsieh, and S. J. Huang, "Enhancement of damage-detection of wind turbine blades via CWT-based approaches," *IEEE Trans. Energy Convers.*, vol. 21, no. 3, pp. 776–781, Sep. 2006.
[16] W. Yang, P. J. Tavner, and M. Wilkinson, "Condition monitoring and fault diagnosis of a wind turbine synchronous generator drive train," *IET Renew. Power Gener.*, vol. 3, no. 1, pp. 1–11, Mar. 2009.
[17] E. Wiggelinkhuizen, T. Verbruggen, H. Braam, L. Rademakers, J. Xiang, and S. Watson, "Assessment of condition monitoring techniques for offshore wind farms," *Trans. ASME, J. Sol. Energy Eng.*, vol. 130, no. 3, pp. 1–9, Aug. 2008.
[18] S. K. Lee, "An acoustic decay measurement based on time–frequency analysis using wavelet transform," *J. Sound Vib.*, vol. 252, no. 1, pp. 141–153, Apr. 2002.

Wenxian Yang received the Ph.D. degree in mechanical engineering from Xi'an Jiaotong University, Xi'an, China, in 1999. He completed his postdoctoral research in Northwestern Polytechnical University, Xi'an, in 2001.

He was with the City University of Hong Kong, Kowloon, Hong Kong; Nottingham Trent University, Nottingham, U.K.; Cranfield University, Cranfield, U.K.; and Durham University, Durham, U.K. He is currently a Technical Specialist with the New and Renewable Energy Centre, Blyth, U.K. He has worked in the areas of new and renewable energy, signal processing, machine condition monitoring and fault diagnosis, nondestructive testing and nondestructive evaluation, and artificial intelligence in both industry and academia.

Peter J. Tavner (SM'08) received the M.A. degree from Cambridge University, Cambridge, U.K., in 1969 and the Ph.D. degree from Southampton University, Southampton, U.K., in 1978.

He held research and technical positions in the industry, including being a Group Technical Director with FKI Energy Technology, Loughborough, U.K. He is currently a Professor of new and renewable energy and the Head of the School of Engineering and Computing Sciences, Durham University, Durham, U.K. His research interest includes machines for renewable energy, condition monitoring, and reliability.

Dr. Tavner was the recipient of the Institution Premium of the Institution of Electrical Engineers, U.K.

Christopher J. Crabtree received the M.Eng. degree in engineering from Durham University, Durham, U.K., in 2007, having studied new and renewable energy as an electrical engineer, where he is currently working toward the Ph.D. degree in condition monitoring of offshore wind turbines.

His research interests include the development of condition monitoring techniques using industrial data and a test rig.

Michael Wilkinson received the M.Sc. degree in electromagnetic sensing from Durham University, Durham, U.K., in 2003 and the Eng.D. degree with a thesis on condition monitoring for offshore wind turbines from Newcastle University, Newcastle upon Tyne, U.K., in 2007, in a collaborative project with Durham University and FKI Energy Technology.

In 2007, he joined Garrad Hassan, Bristol, U.K., as part of the operational projects team, where he has been monitoring wind farms worldwide on behalf of owners. His research interests include condition monitoring and reliability of wind turbines.

Condition Monitoring of Wind Turbine Induction Generators by Current or Power Analysis

Post-ICEM 2010 paper

Abstract— **This paper investigates the condition monitoring of wound rotor or doubly fed induction generators for wind turbines by analysis of stator current or total power spectra. The research is verified using measured data compared against data from a time-stepped numerical model. A steady-state study of healthy and faulty current and power spectra was performed using measured data from two test rigs. This led to a number of fault-specific signal changes and consistent slip-dependent fault indicators being identified using both test rigs. In order to enable real-time fault frequency tracking, a set of concise analytic expressions, describing these fault frequencies, were defined and validated by measurement. A variable speed study, representative of real wind turbine operation, of healthy and faulty current and power frequency components was then performed on one test rig. Identified current and power frequency tracking of faults achieved reliable fault detection for two realistic wind turbine generator fault scenarios of differing severity. Conclusions are drawn on the relative merits of current and power signal analysis as a medium for fault detection and diagnosis.**

I. Introduction

Wind power is at the forefront of contemporary sustainable power generation with increasing global wind generating capacity. A large proportion of today's wind turbines (WT) employ induction generators (IG) for energy conversion [1,2]. The dominant market concepts for high power (1MW to 3MW) variable speed WTs typically employ IGs in two topologies [2], with a grid-connected stator and either a power electronic converter, (DFIG), or an electronically-controlled variable resistance in the rotor circuit, Wound Rotor Induction Generator (WRIG).

An undetected generator fault may have a catastrophic effect on the turbine drive train resulting in costly and lengthy repairs. Prompt fault detection, or ideally detection of a developing fault, is essential for planned preventative maintenance and correct system operation. As modern turbines increase in capacity and move to windier, less accessible and off-shore environments, condition monitoring (CM) of WTs and their generators has become essential to reduce downtime and improve capacity factors. Generator CM is significant as generator defects have been shown to be a major contributor to WT downtime [3-5]. Indeed [4] showed that 30% of annual downtime was due to converter power module failures, 30% of which resulted directly from the generator. Two dominant locations of failure in rotating AC machinery are identified as the windings and bearings [6,7]. In addition, recent industrial surveys on commercial wind turbine generator failure rates [8] highlight brush-gear/slip-ring failures in WRIGs, which make up *16 %* of failures, while *50%* of failures originate from rotor unbalance in up to 2MW range generators.

An important requirement in CM systems is to use non-invasive monitoring methods. Established induction machine monitoring techniques, including Motor Current Signal Analysis (MCSA), typically use non-invasive, spectral-based machine terminal quantity analysis. Previous work [9,10] has shown that induction motor cage faults can be detected by either current or power analysis and [11] has demonstrated power signal analysis for WT fault detection. Consequently, a number of authors have turned to analysis and detection of winding faults in WRIGs [12-22] using current or power analysis since this is non-invasive and signals are readily available. The reported and previous works were partly based on analysis of experimental data only [12,13], with winding fault-induced changes in stator/rotor current frequency spectra identified in [12] and Park vector monitoring method for winding unbalance detection during transient operation proposed in [13].

[14-19] provided extensive winding fault analysis based on both simulation and experimental data. The WRIG modelling techniques ranged from two-axis models [14,15] to models accounting for a limited number of higher order air-gap field space harmonics [16] or all of them [17-19]. Fault modelling in the majority of reported work has been based on connecting resistive and/or inductive elements to machine windings [12-16,20,21]. Actual short and open circuit faults were also simulated by short or open circuiting machine phase windings sections in [17,19,22]. Changes in WRIG stator and rotor current spectral content, originating from stator and rotor winding faults, were identified in [12,14-22]. Theoretical and/or analytic explanations of identified fault frequencies and their generation were provided in [15-17,19,22]. The analysis and fault frequencies outlined in [15,16] considered only fundamental field effects, whereas the work in [17] focused on rotor current spectral content originating from stator inter-turn faults and [22] focused on rotor inter-turn fault detection using specific stator current spectral components. In [19] an extensive study of WRIG stator current spectral content provided a concise set of analytical expressions defining current frequencies for a range of healthy and faulty operating conditions. The analyses in [12,14-19,22] focused on steady-state stator and rotor current signals to identify winding fault spectral indicators.

This paper will build on the research in [20,21] to present an in-depth investigation of the influence of rotor electrical unbalance on the stator line current and total instantaneous power signals spectra of WT IGs, in DFIG or WRIG configurations. The analysis is performed first under steady-state, constant speed operating conditions, and second for transient, variable speed operation such as encountered in the modern WTs. Experimental research uses measured data from two different grid-connected WRIG test rigs. In addition, calculated current and power signal data from a time-stepped DFIG model [18] are analysed for simulated steady-state operation. Analytical expressions that describe the healthy and faulty current and power signals spectral content and enable real-time prediction of fault frequencies of interest are defined and verified against measured data from the two test rigs. Finally, this work examines and evaluates the potential of the

outlined fault-specific spectral components for fault detection use during transient WRIG operation. A fault-frequency tracking algorithm was designed for this purpose to track measured and calculated frequencies in the WRIG variable speed current and power signals. The potential of each tracked spectral component to become a reliable CM fault indicator is evaluated and conclusions drawn on the relative merits of current or power signal analysis for generator fault detection.

II. Experimental and Simulation Tools

A. Time-stepped Model

The model used in this work is based on harmonic conductor distributions and a coupled-circuit modelling approach [18]. Higher order air-gap field space harmonics are included in the calculations when evaluating machine parameters, thus making the model competent for frequency domain analysis of machine electrical quantities. The model validity in both time and frequency domains was verified by comparison with experimental data [18-20], and a detailed model description can be found in [18]. Machine geometry and design data used as model inputs for the purpose of this research match the specifications of the commercial WRIG used in the tests.

B. Experimental Test Rigs

Experimental research was performed on two specially constructed WRIG test rigs; one at University of Manchester and the other at Durham University. The Manchester rig operates as either a DFIG or WRIG at constant speed. The Durham test rig features a WRIG with resistive rotor, driven at either constant speed or with transient, variable speed conditions. The rigs are described in detail in the Appendix and simplified test rig schematics are shown in Figure 1. Both test machines operated synchronised with the grid and their stator and rotor windings were star connected.

C. Fault Modelling

Rotor electrical or brush-gear faults manifest themselves as uneven rotor current distribution. In addition, despite brush resistance being low in comparison with that of machine windings, the sliding-brush/collector-ring contact drop constitutes the dominant brush-gear resistive component [24].

Healthy brush contact resistance is reported to range from 0.01Ω at 100A to > 0.2Ω at low current, dependant on operating current magnitude [24-26]. In addition, brush-wear or brush pressure irregularity, material defect or high current density can lead to a high-resistance contact and cause uneven current distribution between brushes [25-27].

Rotor electrical or brush-gear fault-like conditions were emulated in this work by introducing additional resistance in one of the rotor phase windings. The Manchester and Durham test generator rated rotor phase resistance was 0.07Ω. To model experimentally a DFIG fault on Manchester test rig an additional 0.05Ω was introduced in one rotor phase winding. WRIG rotor unbalance was experimentally modelled at a slightly higher additional resistance of 0.12Ω on Manchester test rig due to different machine operating conditions. To

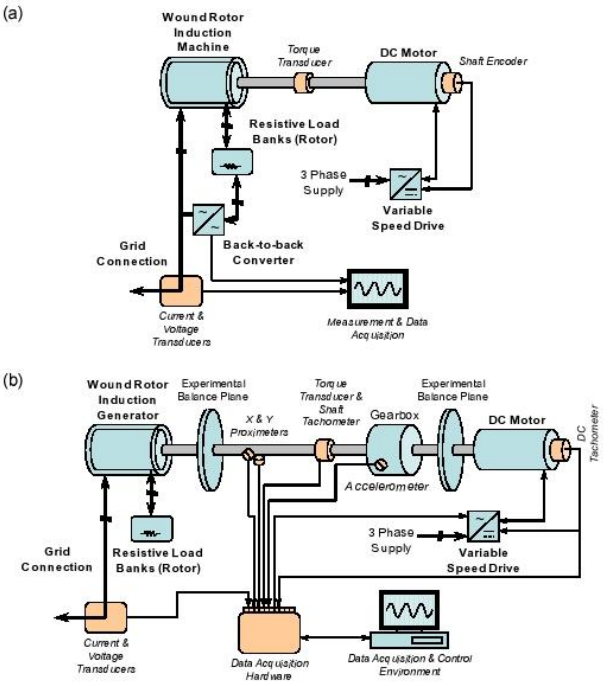

Fig. 1: Test rig configurations: (a) Manchester; (b) Durham

achieve the same speed range at Durham the 'healthy' phase resistance was increased to 0.9Ω per phase with an additional 0.4Ω added to one phase, to create the unbalanced condition. In order to clearly identify fault spectral signatures a slightly increased additional resistance levels were used in steady-state analysis. Once the fault indicators have been established it was demonstrated that reduced fault levels are detectable by considering lower resistance levels for transient analysis. The change of resistance investigated was therefore reasonable and is similar to the additional resistance levels used in previous work for modelling rotor electrical unbalance or brush-gear damage [14,15,28].

III. Steady-state Current and Power Signal Spectra

A. Analytical Expressions

Analysis of contents and origins of WRIG stator current spectrum when used in DFIG configuration is given in [19]. Building on [19] this work utilises equations for possible spectral frequencies in WRIG primary current spectrum that are generalised and include the effects of supply time-harmonic voltages [29]. From [19] healthy (1) and faulty (2) machine stator current spectra can be described by:

$$f_{ind}^{k} = \left|6k(1-s) \pm l\right| f \qquad (1)$$

$$f_{ind}^{k} = \left|\frac{k}{p}(1-s) \pm l\right| f \qquad (2)$$

where f is the fundamental supply frequency, s is the fractional slip, p is the number of pole pairs, $k=0,1,2,3...$ and $l=0,1,2,3...$ Here k relates to the air-gap field pole numbers

and l refers to the order of the current time-harmonics that originate from the supply harmonic voltages. (1)-(2) yield a range of frequencies that may exist in the current signal, however not all will be clear as their magnitudes may be attenuated or highlighted by machine design artefacts or operating conditions. Expressions that define the spectral content of the total stator instantaneous power signal for healthy and faulty machine are obtained by modulating the corresponding current signal spectra with that of a three-phase voltage supply [29]. Healthy (3) and faulty (4) machine stator total power spectra are then described by:

$$f_{ind}^{k} = \left| j \pm 6k(1-s) \pm l \right| f \tag{3}$$

$$f_{ind}^{k} = \left| j \pm \frac{k}{p}(1-s) \pm l \right| f \tag{4}$$

where $j=0,1,2,3\ldots$ and all other parameters are as previously defined. The additional integer constant j relates to supply voltage time-harmonic orders and equations (1-4) in general assume an unbalanced stator voltage supply system.

The generalised faulty current and power spectra expressions assume a secondary mmf pattern, due to the unbalanced rotor disturbances, that could result in air-gap fields with any number of poles and a stator winding layout capable of coupling with that disturbance. However, the fundamental effect of rotor electrical/brush-gear unbalance, investigated here, will give rise to reverse rotating fields at slip frequency. The current and power signal fault components can then be shown to be a subset of the possible fault specific spectral frequencies series identified by the relations above. Derivations are omitted for brevity and the detailed principles of the analysis are given in [19,29].

B. DFIG Current and Power Spectra

The effect of rotor unbalance on DFIG steady-state current and power signal spectra was investigated at Manchester. Tests were first performed for a typical on-line operating point of 1572rpm, with balanced stator and rotor windings and a load torque of 20Nm. Additional resistance of 0.05Ω was introduced in one rotor phase to emulate fault conditions and stator line current and total instantaneous power signals were recorded. Measured DFIG load torque and stator and rotor fundamental rms voltages were used as inputs to the numerical model to recreate the test conditions. Fault conditions were simulated by adding 0.05Ω to one rotor phase in the calculations. Stator and rotor excitation were represented in the model as single-frequency sine waves.

In Fig. 2 measured healthy and faulty current spectra, Figs 2(a) and (b), are compared with the calculated spectra, Figs 2(c) and (d). The measured spectra are seen to be component rich and a number of frequencies of interest are identified in the graphs. Many of the harmonic frequency components found in the current signal arise largely from grid supply harmonic voltages [29,30] while inter-harmonic frequency components are slip dependant and characteristic of WRIGs [16,18,19,22]. Fig. 2(c) and 2(d) show the predicted current spectra ignoring the supply time-harmonic frequencies.

Measured faulty current spectra indicate that the presence of rotor unbalance induces a considerable magnitude change in a number of current frequencies. These are the *2sf* sidebands on dominant spectral components, and are most pronounced at 54.8, 259.6 and 369.2 Hz. An increase is also present in 154.8 Hz component, which roughly doubles in magnitude with fault, but this is less obvious on the graph due to logarithmic scaling. The observed frequencies can be obtained directly from (2) and are discussed in more detail in the following sections. A

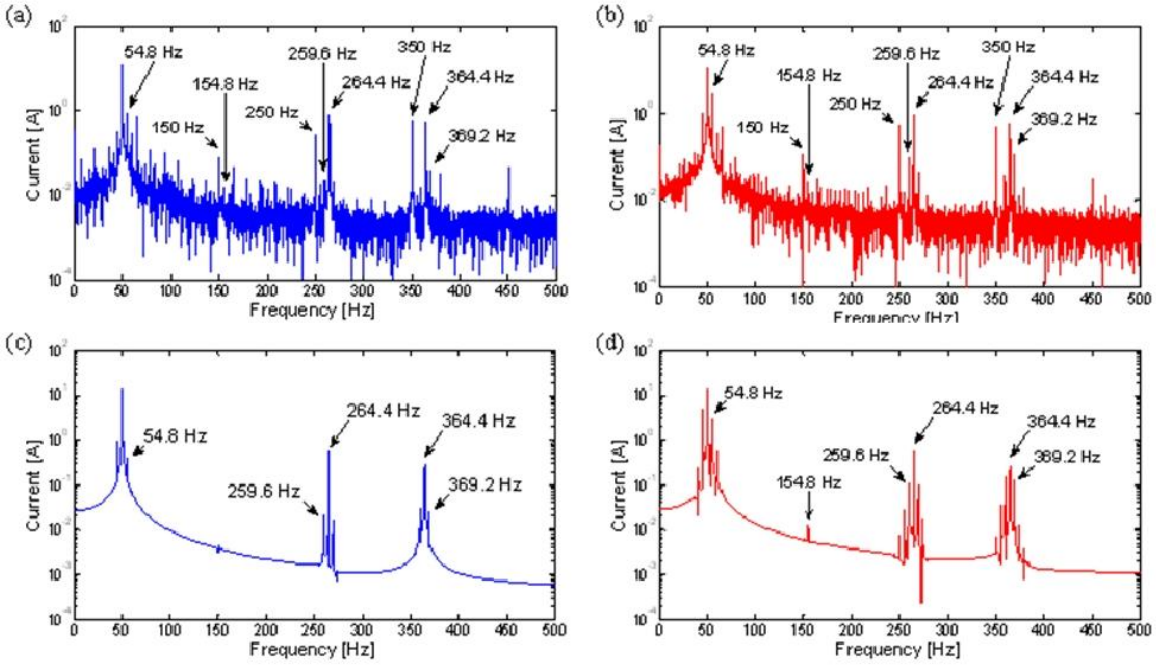

Fig. 2: Line Current spectra at 1572rpm: (a) healthy measured data, (b) faulty measured data, (c) healthy calculated data, (d) faulty calculated data

clearer indication of fault spectral signature is obtained from comparison of calculated healthy and faulty DFIG current spectra given in Fig. 2(c) and 2(d), respectively. These outline the dominant effect of rotor faults on the current spectrum as a strong increase in the magnitude of the sideband components at 54.8, 259.8 and 369.2 Hz, and an increase in the 154.8 Hz component.

Predictions and measurements are in good agreement when current spectral content originating from the fundamental excitation is concerned. The data differ however in the general noise levels, with measurements exhibiting a much higher presence of noise compared to simulation. Another obvious difference is the presence of higher order harmonic components in the current spectrum and resulting inter-harmonic frequencies [29]. These are a consequence of supply time-harmonics and are not accounted for in the model for the purpose of this research.

Data in Fig. 2 demonstrate that the identified fault-specific components are also present in healthy machine current spectrum, but at a significantly lower magnitude level. For healthy machine operation these originate from existing rotor excitation unbalance and/or inherent rotor manufacturing imperfections [18,19].

Measured and calculated stator total power signal spectra are shown in Fig. 3. The data are presented for identical measured and simulated operating conditions as the current signals in Fig. 2. The measured power spectra are noticeably noisier than the current spectra due to the effects of voltage and current multiplication. Each current spectral component is modulated by a series of harmonic voltage frequencies, resulting in component rich measured power spectra in Fig.3(a) and 3(b). A range of frequencies of interest are labelled in the graphs: the harmonic components originate from interaction of current and voltage harmonic frequencies, while the inter-harmonic frequencies result from modulation of current inter-harmonic spectral content with supply harmonic voltages. More importantly, the comparison of healthy and faulty measured data indicates a significant rise in magnitude of a number of spectral components. These are directly related to fault induced changes previously observed in the current signal, but reflected at different spectral frequencies in the power signal. The fault related change of magnitude is most obvious at 4.8, 104.8, 309.6 and 319.2 Hz. The power signal fault frequencies follow a similar spectral pattern to that identified for current and are manifested as an increased magnitude in the 2sf frequency sidebands of dominant spectral frequencies present in the healthy and faulty spectra, as well as a single 2sf frequency component.

Corresponding calculated healthy and faulty power spectra are shown in Fig. 3(c) and 3(d), respectively. The difference between predictions and measurements is consistent with what was observed and commented upon for current signal data. As before, model predictions are seen to be in good agreement with measurements where content originating from fundamental excitation is concerned. In addition, and consistently to what was observed in the current signal, the unbalance-specific frequencies can also be found in the healthy machine power signal, however they are of considerably lower magnitudes in comparison to faulty operation. Simulation and experimental data in Figs. 2 and 3 provide a detailed illustration of the spectral signature of fault for steady-state DFIG stator current and power signals. The presented analysis indicates that there are a number of frequency components in the current and power spectra that have potential to be employed as fault indicators.

C. WRIG Current and Power Spectra

The spectral signature of a rotor fault in WRIG steady-state signals was investigated by comparing the data measured on

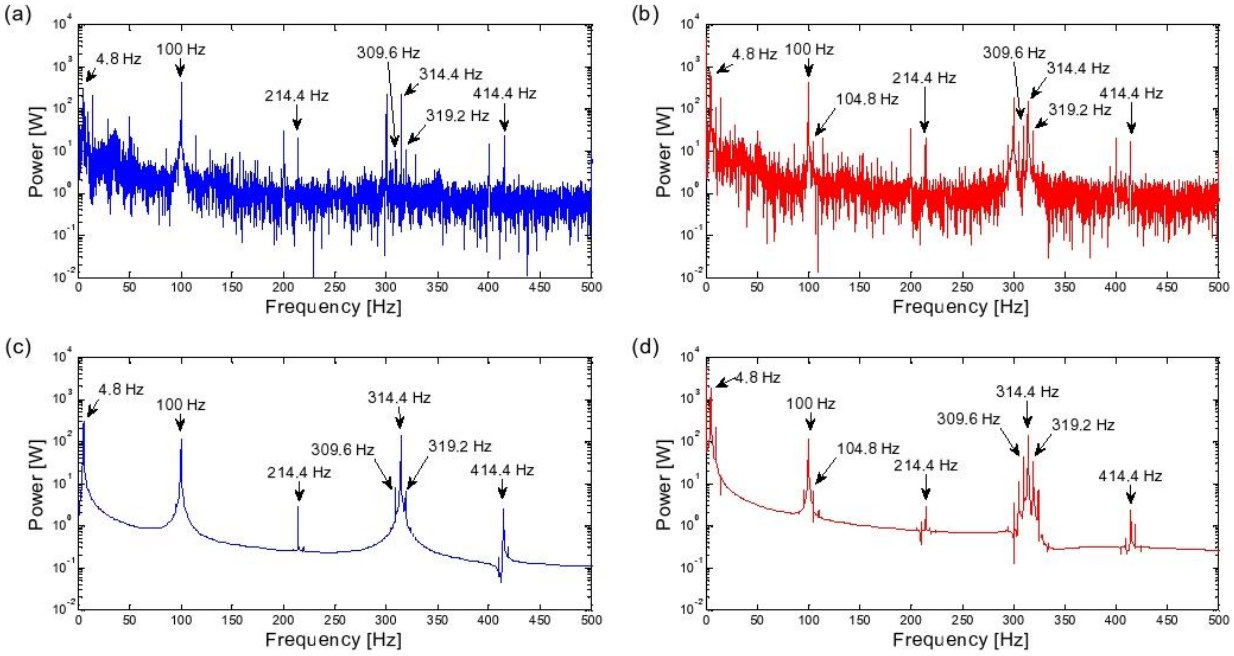

Fig. 3: Total power spectra at 1572rpm: (a) healthy measured data, (b) faulty measured data, (c) healthy calculated data, (d) faulty calculated data

the two test rigs for similar operating conditions. A typical set of healthy and faulty current and power traces for an arbitrarily chosen operating speed of ≈1560rpm achieved on both test rigs are shown in Figs. 4 and 5. In terms of spectral content, the measured spectra are seen to be consistent with those observed for DFIG signals in section III.B. The absence of the rotor converter is not seen to induce a significant change in noise or spectral content in the relatively low signal bandwidth examined in this work. Frequencies of interest are labelled throughout the spectra.

The two healthy machine current signals in Figs. 4(a) and (b) show a comparable spectral content despite different levels of rotor resistance between the Manchester and Durham machines. The harmonic content is seen to differ between the two test rigs and is indicative of different supply conditions in Manchester and Durham laboratory environments. The Durham test rig spectrum, for example, indicates an increased level of supply unbalance through a greater number of supply time harmonics, notably the 100Hz and 450Hz components which are not as pronounced in the Manchester data. However the inter-harmonic spectral content is seen to be in good agreement between the rigs. The dominant inter-harmonic components are labelled 'a' and 'b' and these are seen to be consistent between the two

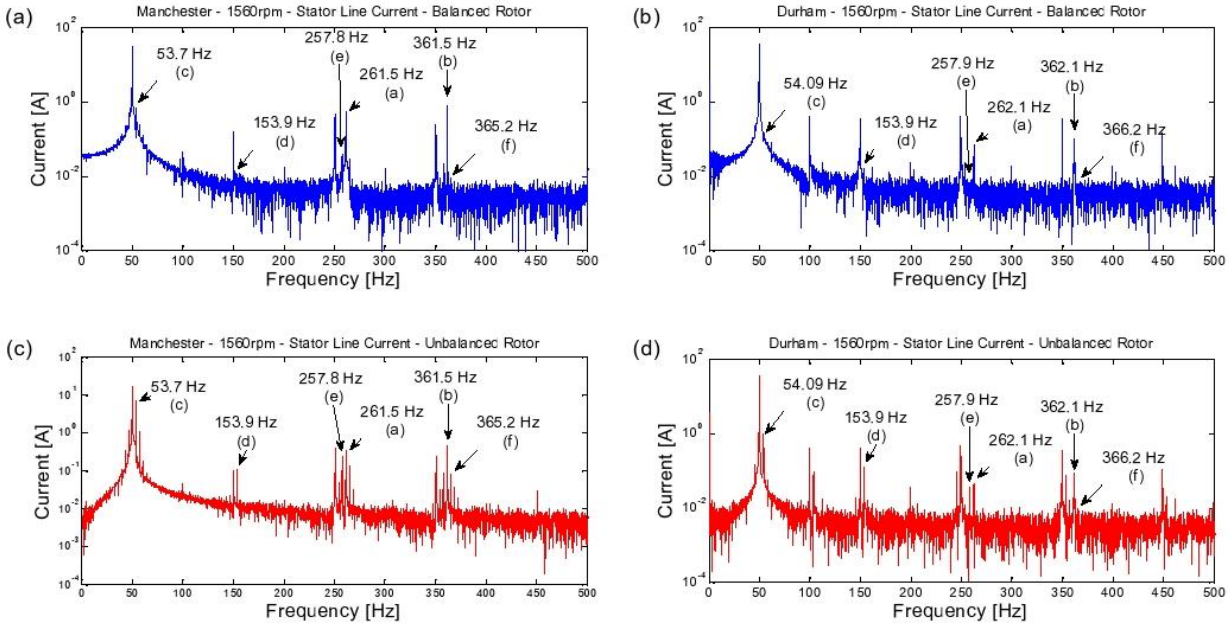

Fig. 4: Measured line current spectra: (a) Manchester, healthy, (b) Durham healthy, (c) Manchester faulty, (d) Durham faulty

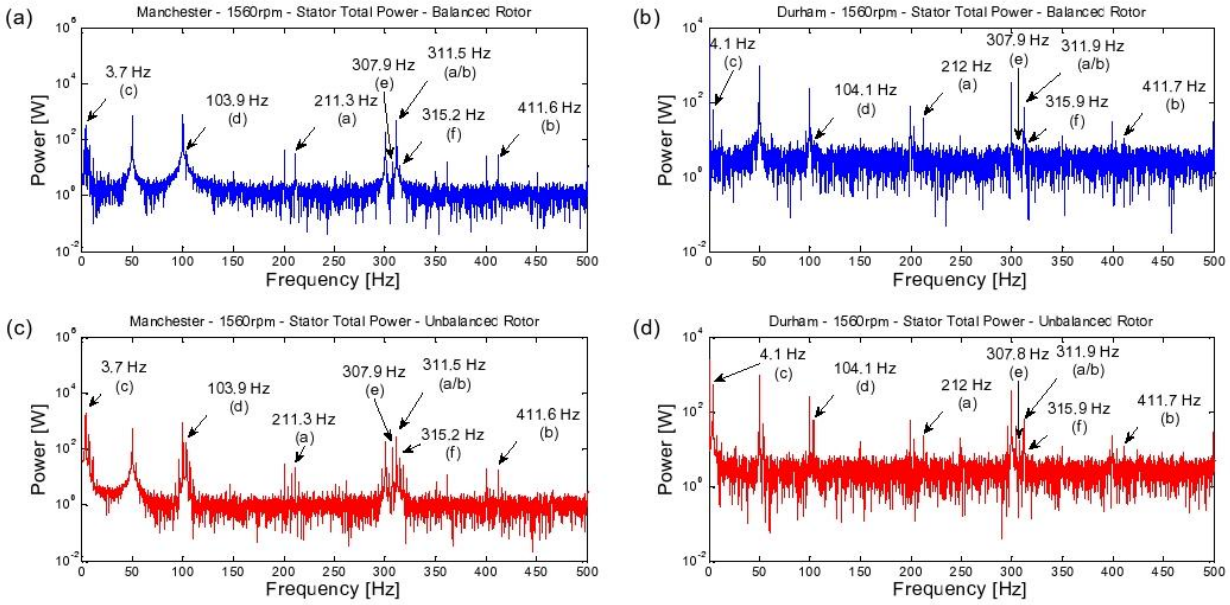

Fig. 5: Measured total power spectra: (a) Manchester, healthy, (b) Durham healthy, (c) Manchester faulty, (d) Durham faulty

test rigs.

The line current spectra, after the rotor unbalance was applied, are shown in Figs. 4(c) and (d). Frequencies 'a' and 'b' are seen to remain consistent in the faulty machines, as are the supply harmonics. There is, however, a clear increase in spectral content in both current data sets. The rotor fault is manifested as an increase in the magnitude of components 'c' to 'f' in the graphs: as before, these are directly related to the *2sf* frequencies around the dominant spectral components. There is also a much greater increase in component 'f' in the Manchester data, resulting from a lower rotor resistance compared to the Durham test rig and therefore greater speed ripple in the presence of fault.

Similar consistency is seen in the healthy and faulty power signal data from Fig. 5. Frequencies 'a', 'a/b' and 'b' in the power signals originate from the interaction of supply voltage harmonic content with 'a' and 'b' current signal frequencies. The presence of the fault results in a significant magnitude increase in components 'c' to 'f', where again the Manchester data demonstrate a higher fault induced magnitude increase of 'f' due to the rotor resistance effects previously commented on.

D. Frequency Selection

Sections III.B-C establish an understanding of the fault influence on the machine current and power signals and identify consistent spectral content patterns and frequencies of interest for WRIG current and power signals. For CM it would be impractical to observe all frequencies given by equations (1-4). As demonstrated in the results, this would not always be necessary either as not all frequencies given by the equations are significant in the current or power spectra. In addition, the frequency components produced by supply time-harmonic frequencies or supply unbalance would also be disregarded in this respect because of the random nature of their presence. This is the reason why they are omitted from the simulated frequency spectra presented in Figures 2 and 3. The performed steady-state analysis enables a reduced set of frequencies of interest to be defined and corresponding equation constants to be identified. Values for current frequencies 'a' to 'f' and their respective equations are listed in Table I. It is clear from Table I that fault frequencies 'c' to 'f' are found by a systematic increase in the integer constant k.

Values of equation parameters that define numerically the frequencies found in the total power spectrum are given in Table II. It is clear that these are highly consistent with those for line current, which is to be expected. Parameter values identified in Tables I and II establish simple expressions that enable real-time prediction of fault frequencies of interest for variable-speed generator operation.

TABLE I
CONSTANTS FOR HEALTHY AND FAULTY LINE CURRENT SPECTRA

Frequency Label	Equation	*k*	*l*
50Hz Multiples	$f_{ind}^{k} = \lvert 6k(1-s) \pm l \rvert f$	0	1,2,3,..
a, b (Healthy)	$f_{ind}^{k} = \lvert 6k(1-s) \pm l \rvert f$	1	1
a, b (Faulty)	$f_{ind}^{k} = \left\lvert \frac{k}{p}(1-s) \pm l \right\rvert f$	12	1
c, d	$f_{ind}^{k} = \left\lvert \frac{k}{p}(1-s) \pm l \right\rvert f$	4	1
e	$f_{ind}^{k} = \left\lvert \frac{k}{p}(1-s) + l \right\rvert f$	8	1
f	$f_{ind}^{k} = \left\lvert \frac{k}{p}(1-s) - l \right\rvert f$	16	1

TABLE II
CONSTANTS FOR HEALTHY AND FAULTY TOTAL POWER SPECTRA

Frequency Label	Equation	*j*	*k*	*l*
50Hz Multiples	$f_{ind}^{k} = \lvert j \pm 6k(1-s) \pm l \rvert f$	1,2, ...	0	1,2 ...
a, b (Healthy)	$f_{ind}^{k} = \lvert j \pm 6k(1-s) \pm l \rvert f$	1	1	1
a, b (Faulty)	$f_{ind}^{k} = \left\lvert j \pm \frac{k}{p}(1-s) \pm l \right\rvert f$	1	12	1
c, d	$f_{ind}^{k} = \left\lvert j \pm \frac{k}{p}(1-s) \pm l \right\rvert f$	1	4	1
e	$f_{ind}^{k} = \left\lvert j + \frac{k}{p}(1-s) + l \right\rvert f$	1	8	1
f	$f_{ind}^{k} = \left\lvert j - \frac{k}{p}(1-s) + l \right\rvert f$	1	16	1

IV. Frequency Tracking for Fault Detection

A. Frequency Tracking

WTs of DFIG or WRIG configuration are variable speed, variable load systems resulting in monitoring signals that are highly variable in both magnitude and spectral content. This means that analysis techniques such as the standard Fourier transform are unsuitable in their raw forms as time information is lost during analysis. Successful WT fault detection relies on the knowledge of how a particular fault-related spectral component varies with time so analysis techniques must adapt to take this into account.

The simple answer would be to decrease the duration of analysis time windows such that signals are stationary over a short period. However, this would lead to an overwhelming number of spectra being produced with different spectral content and all in need of manual interpretation. Consequently, WT CM would quickly become an unmanageable task for operators with large WT populations.

To counter this, [23] proposes a frequency tracking algorithm where the energy of a variable but calculable fault-related component is extracted over time. In [23] a localised

continuous wavelet transform (CWT_{local}) is deployed. The CWT was selected as a result of its popularity in the analysis of non-stationary signals as demonstrated by the analysis of machine starting currents in [31]. The algorithm in [23] proved capable of detecting a rotor electrical asymmetry although with some significant variability in the result.

An algorithm was developed based on the principles of the Fourier transform and the frequency tracking concept. The stages of analysis are summarised as:

- Calculate the required sample length of both the analysis signals and machine speed signal;
- Calculate the fault-related frequency of interest from the mean speed signal within the time window;
- Apply Fourier analysis across a narrow frequency band around the frequency of interest;
- Extract the peak amplitude (peak finding) within the frequency window;
- Repeat the process until the entire signal has been analysed;
- Plot the peak amplitudes from each iteration against time.

The advantage of this analysis is that at each iteration only the frequency of interest has been analysed rather than the entire spectrum, producing a simplified figure indicating the change in a fault-related component's magnitude with time. Importantly, this reduces the amount of manual interpretation required in terms of interpreting spectra and obtaining comprehensible results. Furthermore, the sample time length is adapted to analyse a fixed number of rotations rather than a fixed time length. This removes much of the variability in results seen in [23], caused by variable speed operation.

The full algorithm is described and discussed in [32].

B. Results

The spectral components given in III.D were selected based on the results of the steady-state analysis of two different test rig machines and a detailed model. However, they can only be demonstrated as suitable for monitoring if they are valid under variable, non-stationary conditions.

The frequency tracking algorithm was applied to the stator current and power signals recorded from the Durham test rig. The test rig was driven using conditions derived from a detailed 2MW WT model constructed by the University of Strathclyde, UK, as part of the Supergen Wind Energy Technologies Consortium. The resulting generator speed signal used here is shown in Fig. 6(a).

The fault-like conditions here are lower in magnitude than used for the steady-state operation such that the rotor phase resistance is 1.2Ω per phase when balanced, with 0.25Ω and 0.5Ω added in one phase to create 23% and 46% fault-like conditions respectively. Figs. 6(b) and (c) show the line current and total instantaneous power signals recorded from the test rig.

1) Analysis of the Line Current Signal

Firstly, the algorithm was applied to each frequency component of interest in the stator line current, as given in Table I.

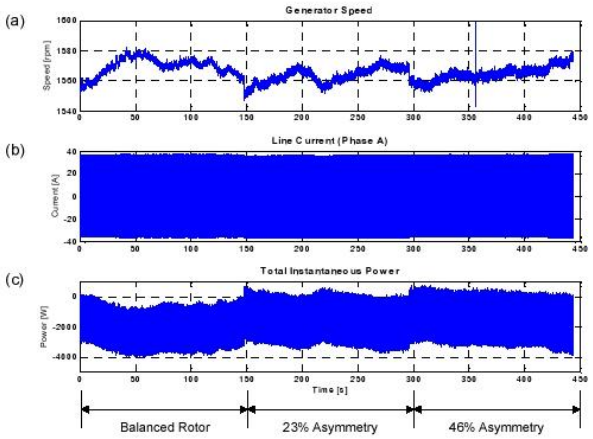

Fig. 6: Raw signals for analysis using the frequency tracking algorithm: (a) speed, (b) line current, (c), total instantaneous power

Fig. 7(a) shows the instantaneous frequency of component 'a', the *(1-2s)f* sideband, calculated from the measured generator speed signal. The amplitude of this component with time was extracted and is plotted in Fig. 7(b). There is a clear step seen for both the 23% and 46% fault-like conditions suggesting successful detection under variable conditions. This also confirms that this component shows a strong correlation with fault severity, as would be expected. The instantaneous frequency on component 'd', the *(3-2s)f* component, is shown in Fig. 7(c). This also shows a clear step change in amplitude when the two fault-like conditions were applied, Fig 7(d). The higher frequency component 'e' was analysed and a similar trend was observed however the result is not included here for conciseness. The step changes were lower in magnitude but remained clearly visible for the 46% fault. Current component 'f' is not plotted here as it did not show a significant change with fault-like conditions. This was expected as this component did not show clearly in the Durham steady-state results and appears to be heavily attenuated for the machine with the larger balanced phase resistance.

These results suggest that the selected spectral components remain valid as fault indicators under variable speed, variable load conditions. Results also suggest that fault severity could be derived from the amplitude of a particular spectral component.

2) Analysis of the Total Instantaneous Power Signal

Secondly, the instantaneous power signal was processed using the frequency tracking algorithm. The results proved similar to those for corresponding frequencies in line current and are presented in Fig. 8.

Figs. 8(a) and (b) show the instantaneous frequency of component 'c' of power, the *2sf* component, with time and its amplitude respectively. Again, a pronounced step change is visible although there is significant variability when compared to the corresponding result from line current, Fig. 8(b). However, a much improved result is found from analysing component 'd', the *(2-2s)f* component, Fig. 8(c).

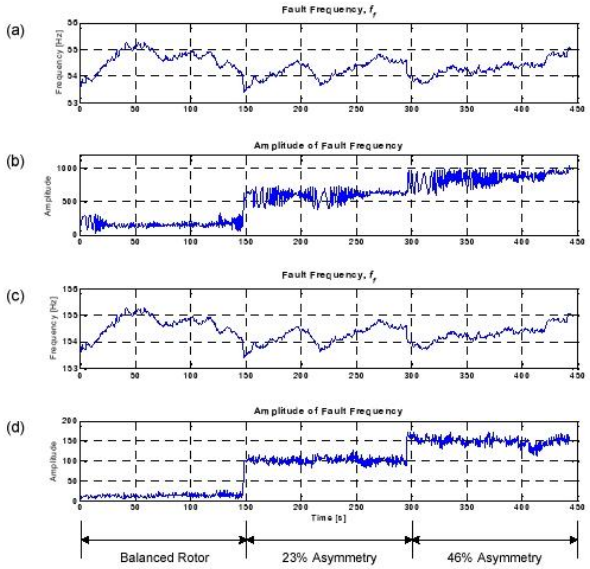

Fig 7: Frequency tracking of line current harmonic components

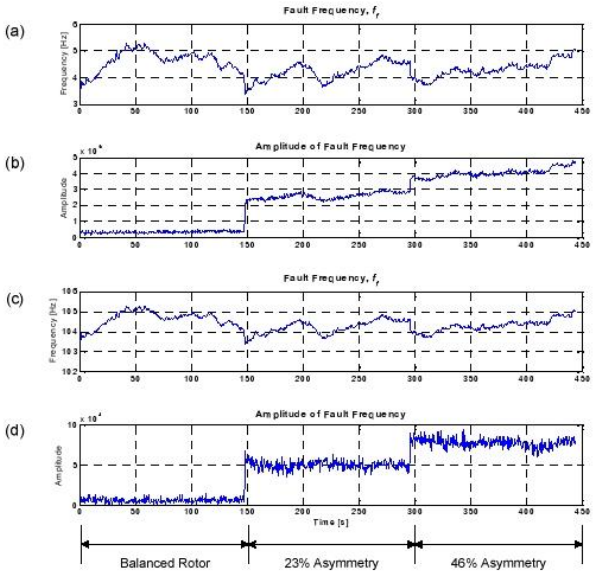

Fig 8: Frequency tracking of total power harmonic components

This component's amplitude is given in Fig. 8(d). Results for component 'e' in power were improved on those for current although they are not included for conciseness. A step change was visible for both the 23% and 46% faults in the power signal as opposed to current where only the 46% fault gave a clear response. In line current, component 'f' did not show a marked change when fault-like conditions were applied. In power, this component gave a response at the higher fault level, suggesting it may be a useful indicator of fault severity. It is apparent that for a machine of lower phase resistance, this component would give a measureable response, as shown in the Manchester steady-state results.

V. Conclusions

This paper has demonstrated that realistic and common wind turbine wound rotor and doubly fed induction generator faults can be detected reliably by analysis of identified fault frequencies in the machine stator current or total power spectrum. The following specific conclusions arise:

- Frequencies from these common faults have been identified from an already published predictive high order air-gap field space harmonic model.
- These fault frequencies have been verified on two independent test rigs at various fixed speed conditions.
- A fault frequency tracking algorithm has been developed to allow these fault frequencies to be detected reliably under variable speed conditions, as would be found in a modern wind turbine.
- A number of these fault frequencies have been selected and using the tracking algorithm have been applied to both the stator current and total power spectra to reliably detect mechanical or electrical unbalance in an induction generator rotor on one of the test rigs under variable speed, wind-driving conditions.
- The results demonstrate that this approach would be valid for application on a full-size wind turbine generator.
- The results show that both stator current and total power spectra are valid for fault detection. The current spectrum has some benefit from the point of view of simplicity and lower noise while the total power spectrum has some benefit from the point of view of globality and lower fault frequencies.

Appendix

The Manchester rig comprises a four-pole, three-phase 30kW Marelli WRIG driven directly by a 40kW DC motor. The prime mover torque and speed are controlled by a DC speed drive. The WRIG rotor circuit is excited from a back-to-back converter switching at 8 kHz. The WRIG stator circuit is connected to the grid. The rotor converter ensures excitation of appropriate frequency and magnitude is achieved. The test rig is designed for on-line steady-state operation and can achieve a range of sub- and super-synchronous operating points. The test rig can also be run as a WRIG with the rotor converter removed and windings shorted, and stator windings grid connected via a three phase variac. Current and voltage probes were installed in the stator circuit and their outputs sampled synchronously by a precision digital oscilloscope. The two wattmeter method was used to calculate the total instantaneous power signal to minimise noise. Machine fundamental rms voltage and current values were measured by three-phase watt meters in the primary and secondary circuits. An in-line torque transducer was installed in the driving shaft and the machine speed obtained from a stub shaft-mounted encoder.

The Durham rig comprises a similar four-pole, 30kW WRIG with altered winding arrangement, driven through a two-stage helical, parallel shaft gearbox by a 54kW DC motor. A variable speed drive allowed the test rig to achieve similar steady-state operating points as used with the Manchester WRIG configuration. The test rig can be driven

using shaft speed data from a detailed wind turbine model, allowing realistic variable speed operation [23]. A speed signal was recorded from an in-line torque transducer. To allow variable speed driving, additional resistance was added to the WRIG rotor circuit, allowing a speed variation of 7% slip above synchronous before the DC motor armature limit. Steady state measurements were made using a precision oscilloscope to record two phase voltages and line currents at 2kHz sampling frequency. The power signal was calculated using the two-wattmeter method. Spectra were calculated using MATLAB's proprietary FFT with 2^{14} points. Results are presented for a bandwidth of 0-500 Hz. Transient signals from the Durham test rig were sampled at 5kHz using a LabVIEW control and data acquisition system. The three-wattmeter method was used to calculate the power signal.

REFERENCES

[1] Y. Amirat, M.E.H. Benbouzid, B. Bensaker, R. Waumkee, "Generators for Wind Energy Conversion Systems: State of the Art and Coming Attractions", *Journal of Electrical Systems*, Vol. 3, Iss. 1, pp 26-38, 2007.

[2] H. Li, Z. Chen, "Overview of different wind generator systems and their comparisons", *IET Ren. Pow. Gen.*, Vol. 2, Iss. 2. pp. 123-128, 2008.

[3] F. Ciamberlano, J. Nitschke, N. Kragelund, J. Thiede, M. Fusselbaugh, M. Johst, F.V. Velde, "Engineering Insurance of Offshore Wind Turbines", *39th IMIA Annual Conf.*, Boston, USA, September. 2006.

[4] M. Wilkinson, B. Hendriks, F. Spinato, E. Gomez, H. Bulacio, J. Roca, P. Tavner, Y. Feng, H. Long, "Methodology and Results of the Reliawind Reliability Field Study", *Scientific Proc. European Wind Energy Conf. (EWEC)*, Warsaw, Poland, March 2010.

[5] F. Spinato, P. J. Tavner, G. J. W. Van Bussel, E. Koutoulakos, "Reliability of Wind Turbine Subassemblies", *IET Renewable Power Generation*, Vol. 3, Iss. 4, pp. 1-15, 2009.

[6] "Improved motors for utility applications, Vol. 1: Industry assessment study: Update and Analysis", Electric Power Research Institute, Palo Alto, Cal, EPRI EL-4286, Project 1763-2, September 1985.

[7] Motor Reliability Working Group, "Report of large motor reliability survey of industrial and commercial installations, Part I", *IEEE Trans. Industry Applications*, Vol. IA-21, No 4, July/August 1985.

[8] K. Alewine, W. Chen, "Wind Turbine Generator Failure Modes Analysis and Occurrence," *Windpower 2010*, Dallas, Texas, May, 2010.

[9] P. J. Tavner, "Review of condition monitoring of rotating electrical machines," *IET Elect. Power Appl.*, vol. 2, no. 4, pp. 215–247, 2008.

[10] J. S. Nandi, H.A. Toliyat and L. Xiaodong, "Condition monitoring and fault diagnosis of electrical motors-a review", *IEEE Trans. Energy Conversion*, Vol. 20, No. 4, pp 719-729, 2005.

[11] W. Q. Jeffries, J. A. Chambers, D. G. Infield, "Experience with Bicoherence of Electrical Power for Condition Monitoring of Wind Turbine Blades", *IEE Proc. Vision, Image and Signal Processing*, Vol. 145, No. 3, pp. 141-148, 1998.

[12] I. Boldea, L.M. Popa, B. Jensen, E. Ritchie, "Condition monitoring of wind generators", *Industry Applications Conference*, Conference record of the 38th IAS Annual Meeting, Vol. 3, pp 1839-1846, October 2003.

[13] H. Douglas, P. Pillay, P. Barendse, "The Detection of Inter-turn Stator Faults in Doubly-Fed Induction Generators", *IEEE Industry Applications Conf.*, Vol. 2, pp 1097-1102, October 2005.

[14] A. Stefani, A. Yazidi, C. Rossi, F. Fillipeti, D. Casadei, G.A. Capolino, "Doubly fed induction machines diagnosis based on signature analysis of rotor modulating signals", *IEEE Trans. Industry Applications*, Vol. 44, No 6, 2008.

[15] Y. Gritli, Y.A. Stefani, A. Chatti, C. Rossi and F. Filippetti, The combined use of the instantaneous fault frequency evolution and frequency sliding for advanced rotor fault diagnosis in DFIM under time-varying condition, *Proc. IEEE Industrial Electronics Conference*, IECON'09, pp. 3471–3476, 2009.

[16] Q.F. Lu, Z.T. Cao, E. Ritchie, "Model of Stator Inter-turn Short Circuit Fault in Doubly-Fed Induction Generators for Wind Turbine", *35th Annual IEEE Power Electronics Specialists Conf.*, Vol. 2, pp 932-937, June 2004.

[17] D. Shah, S. Nandi, P. Neti, "Stator Inter-Turn Fault |Detection Of Doubly-Fed Induction Generators Using Rotor Current and Search Coil Voltage Signature Analysis", *IEEE Trans. Industry Applications*, Vol. 45, Iss. 5, pp 1831-1842, 2009.

[18] S. Djurović, S. Williamson, A. Renfrew, "Dynamic Model for Doubly-fed Induction Generators with Unbalanced Excitation, both With and Without Faults", *IET Electric Power Applications*, Vol. 3, Iss. 3, pp. 171-177, 2009.

[19] S. Williamson, S. Djurovic, "Origins of Stator Current Spectra in DFIGs with Winding Faults and Excitation Asymmetries", *Proc. IEEE IEMDC 2009*, pp.563-570, Miami, USA, 2009.

[20] C. J. Crabtree, S. Djurovic, P. J. Tavner, A. C. Smith, "Condition Monitoring of a Wind Turbine DFIG by Current or Power Analysis", *Proc. IET PEMD*, pp. 1-6, Brighton, UK, 2010.

[21] C. J. Crabtree, S. Djurovic, P. J. Tavner, A. C. Smith, "Fault Frequency Tracking During Transient Operation of Wind Turbine Generators", *Presented at the XIX Int. Conf. Electrical Machines (ICEM)*, Rome, Italy, pp. 1-6, Sep. 2010, Paper ID 4782.

[22] A. Yazidi, H. Henao, G.A. Capolino, F. Betin, "Rotor Inter-turn Short Circuit Fault Detection in Wound Rotor Induction Machines", *Presented at the XIX Int. Conf. Electrical Machines (ICEM)*, Rome, Italy, pp. 1-6, Sep. 2010, Paper ID 12297.

[23] W. Yang, P. J. Tavner, C. J. Crabtree, M. Wilkinson, "Cost-Effective Condition Monitoring for Wind Turbines", *IEEE Trans. Industrial Electronics*, Vol. 57, No. 1, pp. 263-271, 2010.

[24] R. D. Hall, R. P. Roberge, "Carbon Brush Performance on Slip Rings", *Record of 2010 Pulp and Paper Industry Technical Conference (PPIC)*, pp. 1-6, San Antonio, Texas, June 2010.

[25] D. Betz, "Relationship between contact resistance and wear in sliding contacts," *IEEE Trans. Parts, Hybrids and Packaging*, Vol. 10, Iss. 1, pp. 32-37, 1974.

[26] N. Morita, T. Ueno, M. Takanezawa, T. Otaka, D. Hiramatsu, "A study for heavily saturated V-I characteristics at carbon brush/steel collector ring sliding contact, on the view point of parallel connected brush current sharing unbalance", *Proc. 56th IEEE HOLM Conf.*, pp. 1-7, 2010.

[27] J. K. Skjlberg, H. F. Ohma, M. Runde, , "Wear Rates and Current Distribution of Carbon Brushes on Slip Rings", *IEEE Trans. Energy Conversion*, Vol. 24, Iss. 4, pp. 835-840, 2009.

[28] X. Q. Liu , H. Y. Zhang , J. Liu and J. Yang "Fault detection and diagnosis of permanent magnet DC motor based on parameter estimation and neural network", *IEEE Trans. Industrial Electronics*, Vol. 47, pp. 1021-1030, 2000.

[29] S. Djurovic, S. Williamson, "Influence of Supply Harmonic Voltages on DFIG Current and Power Spectrum", *Presented at the XIX Int. Conf. Electrical Machines (ICEM)*, Rome, Italy, pp. 1-6, Sep. 2010, Paper ID 5908.

[30] Voltage Characteristics of the Electricity Supplied by Public Distribution Systems, European/British Standard EN 50160:2007.

[31] R. Yacamini, K. S. Smith, L. Ran, "Monitoring Torsional Vibrations of Electro-mechanical Systems Using Stator Currents", *Trans. ASME*, Vol. 120, pp. 72-78, 1998.

[32] C. J. Crabtree, "Condition Monitoring Techniques for Wind Turbines", *PhD Thesis*, Durham University, UK, 2011.